Uncertainty Quantification for Ocean Biogeochemical Models

Nabir Mamnun

March 2024
Bremerhaven

Image: NASA Earth Observatory images by Joshua Stevens, using Landsat data from the U.S. Geological Survey and MODIS data from LANCE/EOSDIS Rapid Response.

Universität Bremen

Uncertainty Quantification for Ocean Biogeochemical Models

Nabir Mamnun

Dissertation submitted to the Faculty 5 Geosciences of the University of Bremen
in partial fulfillment of the requirements for the degree of

Doctor of Natural Sciences (Dr. rer. nat.) in Geosciences

Supervised by:

Prof. Dr. Thomas Laepple
Dr. Lars Nerger
Dr. Christoph Völker
Prof. Dr. Michail Vrekousis

March 2024
Bremerhaven, Germany

Date of Doctoral Colloquim: 07 February 2024

Keywords: Ensemble Data Assimilation, Parameter Estimation, Regulated Ecosystem Model Version 2, Ocean Color, Marine Primary Production

Cover Image Credits: *NASA Earth Observatory*

Nabir Mamnun

Uncertainty Quantification for Ocean Biogeochemical Models

Doctoral Dissertation, Fachbereich 5: Geosciences

Universität Bremen, Bremen, Germany

Date of Doctoral Colloquim (Promotionskolloquium): 07.02.2024

Declarations

(DECLARATION IN LIEU OF AN OATH)

I, Nabir Mamnun, declare in lieu of an oath by my signature that I have completed the thesis above myself and without any third-party assistance, and have identified as such all parts I have cited in letter or spirit from publications, and that I have not used any literature or any other aids other than those stated.

I declare in lieu of an oath that I have provided the information above to the best of my knowledge and belief and that the information provided is the truth and that I have not withheld anything.

I am aware that making a false declaration in lieu of an oath is a punishable offence, namely the punitive sanction pursuant to §156 StGB (German Penal Code) of up to three years' imprisonment or a fine, when the commission was intentional, or up to one year's imprisonment or a fine pursuant to §161 Para. 1 StGB when it was negligent.

Bremerhaven, 10. October 2023

Nabir Mamnun

Acknowledgments

I acknowledge the funding support from the Helmholtz Initiative and Networking Fund pilot project *Uncertainty Quantification – From Data to Reliable Knowledge (Helmholtz-UQ)*.

I thank Dr. Lars Nerger for welcoming me to the Data Assimilation Research Group at the Alfred Wegener Institute (AWI) and for his help and mentorship. I sincerely thank Prof. Dr. Mihalis Vrekoussis for taking me under his wing and supervising my Ph.D. research. Being a part of his lab, the Laboratory for Modeling and Observation of the Earth System (LAMOS), has been an honor and an exceptional learning experience. I sincerely thank Dr. Christoph Völker and Prof. Dr. Thomas Laepple for their support and guidance. I sincerely thank Dr. Özgör Gürses for being a valuable member of my Thesis Advisory Committee.

I thank colleagues from the Data Assimilation Research Group and LAMOS, whose various insights and feedback have greatly enriched my research. I want to appreciate the collaborative spirit of my colleagues from the Helmholtz-UQ Project. The diverse perspectives I received from them inspired me to think differently. Interacting with the Helmholtz-UQ Project's Ph.D. students was enlightening and fun.

I must thank my darling wife, Umme Salma, for her unwavering support and encouragement. I extend my heartfelt appreciation to my colleagues and friends from AWI for their companionship and support, which made the difficult period of COVID-19 more manageable.

This thesis would not have been possible without the collective support, guidance, and encouragement of all those mentioned above and the many others who have touched my life during this remarkable journey. Thank you all for being part of this meaningful chapter in my life.

Abstract

The oceans play a central role in regulating climate by absorbing carbon dioxide from the atmosphere and sequestering heat through ocean biogeochemical (BGC) processes. Predicting climate change necessitates a thorough understanding of these BGC processes and the coupling between marine ecosystems and the global carbon cycle. Ocean BGC models are tools employed for this purpose. However, current ocean models used to simulate and thus better understand the ocean BGC processes are highly uncertain in their parameterization. For example, zooplankton grazing on phytoplankton is a function of available phytoplankton and zooplankton population and is parameterized, assuming the grazing rate increases linearly with the phytoplankton concentration until a maximum grazing rate is reached. However, the value of this maximum grazing rate is not precisely known. BGC models encompass a variety of processes, each characterized by multiple such kinds of process parameters. The values of these parameters are often poorly constrained by laboratory experiments or the limited availability of observations. Uncertainty in the parameter values results in significant uncertainty in the model outputs.

This work delves into research to quantify uncertainties that arise in ocean BGC models and obtain improved parameters to reduce those uncertainties utilizing the BGC ocean model RecoM2 (Regulated Ecosystem Model Version 2). It involves two procedures for the specification uncertainties in model parameterization: i) sensitivity analysis to determine relatively important parameters for estimation in data assimilation simulations and ii) parameter estimation to obtain optimized parameter values using data assimilation.

A Global Sensitivity Analysis (GSA) is performed to identify which parameters influence the uncertainty of model outputs the most in a one-dimensional (1-D) configuration at two ocean sites in the North Atlantic (BATS) and the Mediterranean Sea (DYFAMED), respectively. The study provided a detailed analysis of parameter sensitivities under two distinct environmental conditions by computing variance-based sensitivity indices on key model outputs.

This dissertation uses the Parallel Data Assimilation Framework – PDAF to implement ensemble data assimilation for estimating BGC state variables and parameters, focusing predominantly on assimilating satellite ocean color data. First, data assimilation ex-

periments are carried out in a 1-D model using an ensemble Kalman Filter to estimate preselected BGC parameters at BATS and DYFAMED stations. These stations were specifically chosen because they are distinct enough from each other and possess long-term time series data, thereby facilitating a deeper understanding of the BGC processes under varying environmental conditions. Subsequently, the scope and application of experiments are broadened to a global scale 3-D model by incorporating spatial variations in parameter values. By assimilating ocean color-derived surface chlorophyll-a concentration, this work estimates spatially temporally varying values of the most influential parameters provided by the GSA in a global model set up for improved model prediction. The effects of estimated spatially varying parameters on the BGC fields and dynamics are assessed for insights into BGC modeling.

This work finds that the grazing parameter, the maximum chlorophyll-to-nitrogen ratio, the photosynthesis–irradiance parameters, and the chlorophyll degradation rate are particularly important for BGC simulation. Replacing the default parameter values with the optimal values obtained in this work improves the model outcomes in both 1-D and 3-D configurations, with a notable reduction of model data root mean squared errors relative to assimilated and independent data. The estimated parameters compensate for model deficiencies not attributed to parameter uncertainties, a finding supported by data assimilation literature. The spatial variations of the obtained parameter values are similar to those reported from observation, indicating that ocean color data can adequately constrain spatially varying BGC simulations. Moreover, the dynamical variations of model simulation using the estimated set of parameter values are closer to the satellite observations than that of using the uniform default parameter values.

The methodologies in this work are applied to the REcoM2 model. While the obtained parameter values may not be directly transferable to other BGC models, the methods used are applicable to other ocean models. This work underscores the importance of spatially varying parameter optimization and highlights the potential benefits of incorporating spatially varying BGC parameters in regional and global 3-D BGC models. Through such rigorous scientific endeavors, we inch closer to a more coherent understanding of the complex interplay between the ocean BGC processes and the carbon cycle, paramount in the era of escalating climate change.

Zusammenfassung

Die Ozeane spielen eine zentrale Rolle bei der Regulierung des Klimas, indem sie Wärme speichern und Kohlendioxid durch biogeochemische Prozesse aus der Atmosphäre aufnehmen. Um den Klimawandel vorherzusagen, ist ein tiefes Verständnis der biogeochemischen Prozesse und der Kopplung zwischen marinen Ökosystemen und dem globalen Kohlenstoffkreislauf erforderlich. Ozeanische Biogeochemie-Modelle sind Werkzeuge, die zu diesem Zweck eingesetzt werden. Die derzeitigen Ozeanmodelle zur Simulation biogeochemischer Prozesse sind jedoch in ihrer Parametrisierung sehr unsicher. Zum Beispiel ist das Abweiden von Phytoplankton durch Zooplankton eine Funktion des verfügbaren Phytoplanktons und der Zooplanktonpopulation und wird parametrisiert, indem angenommen wird, dass die Abweidungsrate mit der Phytoplanktonkonzentration ansteigt, bis eine maximale Abweidungsrate erreicht ist. Der Wert dieser maximalen Abweidungsrate ist jedoch nicht genau bekannt. BGC-Modelle umfassen eine Vielzahl von Prozessen, die jeweils durch mehrere solcher Prozessparameter charakterisiert sind. Die Werte der biologischen Prozessparameter sind oft nur unzureichend durch Laborexperimente oder begrenzt verfügbare Beobachtungen eingeschränkt. Unsicherheit in den Parameterwerten führt zu erheblicher Unsicherheit in den Modellergebnissen.

Diese Arbeit geht der Fragestellung nach, Unsicherheiten zu quantifizieren, die in ozeanischen biogeochemischen Modellen auftreten, und verbesserte Parameter zu erhalten, um diese Unsicherheiten mit dem biogeochemischen Ozeanmodell RecoM2 (Regulated Ecosystem Model Version 2) zu reduzieren. Es beinhaltet zwei Verfahren zur Spezifikation von Unsicherheiten in der Modellparametrisierung: i) Eine Sensitivitätsanalyse zur Bestimmung relativ wichtiger Parameter für die Schätzung in Datenassimilationssimulationen und ii) eine Parameterschätzung zur Erlangung optimierter Parameterwerte durch Datenassimilation.

Eine Globale Sensitivitätsanalyse (GSA) wird durchgeführt, um zu identifizieren, welche Parameter den Unsicherheitsgrad der Modellausgaben am meisten in einer eindimensionalen (1-D) Konfiguration an zwei Ozeanstandorten im Nordatlantik (Bermuda Atlantic Timeseries Station, BATS) und im Mittelmeer (Dynamique des Flux Atmosphériques en MEDiterranée, DYFAMED) beeinflussen. Die Studie lieferte eine detaillierte Analyse

der Parametersensitivitäten unter zwei unterschiedlichen Umweltbedingungen, indem varianzbasierte Sensitivitätsindizes für Schlüsselmodellausgaben berechnet wurden.

Diese Dissertation verwendet das Parallel Data Assimilation Framework - PDAF, um eine Ensemble-Datenassimilation zur Schätzung von BGC-Zustandsvariablen und -parametern zu implementieren, wobei der Schwerpunkt hauptsächlich auf der Assimilation von Satelliten-Ozeanfarbdaten liegt. Zunächst werden Datenassimilationsexperimente in einem eindimensionalen Modell mit einem Ensemble Kalman Filter durchgeführt, um vorausgewählte biologische Parameter an den BATS- und DYFAMED-Stationen zu schätzen. Diese Stationen wurden speziell ausgewählt, weil sie sich deutlich voneinander unterscheiden und Langzeit-Zeitreihendaten besitzen, wodurch ein tieferes Verständnis der Prozesse unter verschiedenen Umweltbedingungen ermöglicht wird. Anschließend werden der Umfang und die Anwendung von Experimenten auf ein globales dreidimensionales Modell erweitert, wobei mögliche räumliche Variationen in den Parameterwerten berücksichtigt werden. Durch die Assimilation der aus Ozeanfarben abgeleiteten Oberflächen-Chlorophyll-a-Konzentration schätzt diese Arbeit raumzeitlich variierende Werte der einflussreichsten Parameter, die von der GSA in einer globalen Modellkonfiguration für eine verbesserte Modellvorhersage bereitgestellt werden. Die Auswirkungen der geschätzten räumlich variierenden Parameter auf die biogeochemischen Felder und Dynamiken werden zur Einsicht in dieModellierung bewertet.

Diese Arbeit stellt fest, dass die maximale Abweiderate, das maximale Chlorophyll-zu-Stickstoff-Verhältnis, die Photosynthese-Irradianz-Parameter und die Chlorophyll-Abbaugeschwindigkeit besonders wichtig für die Simulation sind. Das Ersetzen der Standardparameterwerte durch die in dieser Arbeit erhaltenen optimalen Werte verbessert die Modellergebnisse sowohl in 1-D- als auch in 3-D-Konfigurationen, wobei ein bemerkenswerter Rückgang der mittleren quadrierten Modell-Daten-Diskrepanzen im Verhältnis zu assimilierten und unabhängigen Daten zu verzeichnen ist. Die geschätzten Parameter kompensieren Modellmängel, die nicht auf Parameterunsicherheiten zurückzuführen sind, ein Befund, der durch die Datenassimilationsliteratur unterstützt wird. Die räumlichen Variationen der erhaltenen Parameterwerte ähneln denen, die aus Beobachtungen berichtet werden, was darauf hindeutet, dass Ozeanfarbdaten räumlich variierende biogeochemische Simulationen angemessen einschränken können. Darüber hinaus sind die dynamischen Variationen der Modellsimulation mit dem geschätzten Parametersatz den Satellitenbeobachtungen näher als die Verwendung der einheitlichen Standardparameterwerte.

Die in dieser Arbeit verwendeten Methoden werden auf das REcoM2-Modell angewendet. Während die erhaltenen Parameterwerte möglicherweise nicht direkt auf andere biogeochemische Modelle übertragbar sind, sind die verwendeten Methoden auf andere Ozeanmodelle anwendbar. Diese Arbeit unterstreicht die Bedeutung der räumlich variierenden Parameteroptimierung und hebt die potenziellen Vorteile der Einbeziehung von räumlich variierenden Parametern in regionalen und globalen 3-D-biogeochemischen

Modellen hervor. Durch solche rigorosen wissenschaftlichen Bemühungen nähern wir uns einem kohärenteren Verständnis des komplexen Zusammenspiels zwischen ozeanischen biogeochemischen Prozessen und dem Kohlenstoffkreislauf, das im Zeitalter des eskalierenden Klimawandels von größter Bedeutung ist.

Contents

Abstract i
Zusammenfassung iii
Contents vi
List of Figures x
List of Tables xiii
List of Abbreviations xv

1 Introduction **1**
1.1 Application of Ocean BGC Models 2
1.2 Model Uncertainties 3
1.3 Parameter estimation 7
1.4 Objectives of the thesis 10
1.5 Outline 11
1.6 Contributions to Co-authored Publications 13

2 Global sensitivity analysis of a one-dimensional ocean biogeochemical model **15**
2.1 Introduction 16
2.2 Biogeochemical Models 19
2.2.1 Regulated Ecosystem Model 2 23
2.3 Global sensitivity analysis 24
2.3.1 Uncertainty Propagation 25
2.3.2 Derivative-based Global Sensitivity Measure (DGSM) 25
2.3.3 Variance-based sensitivity measures 26
2.3.4 Computing of Sobol' indices 28
2.3.5 Implementation in this study 28
2.3.6 Quantities of interest 31
2.4 Results 32
2.4.1 Screening step 32
2.4.2 Parameter sensitivity 34
2.5 Discussion 40
2.5.1 Parameter sensitivity across locations 40

2.5.2 First-order vs. total-order Sobol' indices . . . 45
2.5.3 Implications of our study . . . 46
2.6 Conclusion . . . 47

3 Uncertainties in ocean biogeochemical simulations: Application of ensemble data assimilation to a one-dimensional model 49
3.1 Introduction . . . 50
3.2 Materials and Methods . . . 52
3.2.1 Model description . . . 52
3.2.2 Data Assimilation (DA) . . . 55
3.2.2.1 Observational data . . . 55
3.2.2.2 DA method . . . 55
3.2.2.3 DA Experiment . . . 59
3.3 Results . . . 59
3.3.1 Joint state-parameter estimation (EXP_{Joint_DP}) . . . 60
3.3.1.1 Evaluation of parameter estimates . . . 60
3.3.1.2 Correlation among the parameters . . . 66
3.3.2 Model performance with estimated parameters . . . 67
3.3.2.1 Surface chlorophyll-a and NPP . . . 67
3.3.2.2 Phytoplankton phenology indices . . . 69
3.4 Discussions . . . 70
3.4.1 Parameter estimation . . . 70
3.4.2 Usefulness of estimated parameters . . . 76
3.4.3 Discrepancies of bottle NPP data at BATS . . . 77
3.5 Conclusions . . . 80

4 Spatially varying biogeochemical parameter estimation in a global ocean model 83
4.1 Introduction . . . 84
4.2 Materials and Methods . . . 87
4.2.1 The Coupled Hydrodynamic -Biogeochemical Model . . . 87
4.2.2 Model setup . . . 88
4.2.3 Data Assimilation Methods . . . 89
4.2.4 Experiments design . . . 92
4.2.5 Observational data . . . 93
4.3 Joint state-parameter estimation . . . 94
4.3.1 Impact of the joint estimation on the state variables . . . 94
4.3.2 Parameter Estimation . . . 96
4.3.3 Temporal evaluation along the Atlantic Ocean . . . 100
4.3.4 Model Run with Estimated Parameters . . . 102
4.4 Discussion . . . 104

4.4.1 Subset of Parameters 104
4.4.2 Spatial variation of estimated parameters 105
4.4.3 Parameter compensation for other model deficiencies 110
4.5 Conclusion 112

5 Conclusion and Outlook **113**
5.1 Conclusion 113
5.2 Outlook 118

Bibliography **121**

A Appendices **151**
Appendices 151
A.1 List of tracers simulated by the Regulated Ecosystem Model 2 (REcoM2) 151
A.2 List of Parameters in the Regulated Ecosystem Model 2 (REcoM2) . . . 153
A.3 Figures of first-order Sobol' indices 157
A.4 Figures of ensemble evaluation of parameter estimates 161
A.4.1 Satellite chlorophyll-a only assimilation 161
A.4.2 Simultaneous assimilation of satellite chlorophyll-a and in-situ NPP 164

List of Figures

1.1 Depiction of the O'Neill conjecture. 4
1.2 Projections of marine biomass changes in future climate scenarios. . . . 5

2.1 Schematic of a typical NPZD model with its compartments of nutrients, phytoplankton, zooplankton, and detritus. 21
2.2 Schematic diagram of the BGC model REcoM2. 24
2.3 First-order Sobol' indices and DGSMs and their 95% confidence interval of 62 parameters for mean surface chlorophyll-a. 33
2.4 Number of QoIs for which the estimate of the first-order index and the DGSM exceed a threshold value. 35
2.5 Total-order Sobol' indices of the 26 shortlisted parameters regarding mean surface chlorophyll-a 37
2.6 First- and total-order Sobol' sensitivity indices of the short-listed parameters regarding all included QoIs at both stations. 41
2.7 Scatterplot of first-order and total-order Sobol' indices of the short-listed parameters for NPP. 45

3.1 Observational data during the study period at BATS. 56
3.2 The ensemble evaluation of log-transformed surface chlorophyll-a concentration and NPP at BATS and DYFAMED of joint state-parameter estimation. 61
3.3 Evaluation of α_{Nano} and μ_{Nano}^{max} at BATS and DYFAMED station for combined assimilation of satellite surface chlorophyll-a and in situ NPP. 63
3.4 Evaluation of d_{Nano}^{CHL} rate analogous to Figure 3.3. 64
3.5 Evaluation of ξ and γ analogous to Figure 3.3. 65
3.6 Evaluation of Φ_{Phy} analogous to Figure 3.3. 66
3.7 The Pearson correlation coefficients between each pair of the ten biogeochemical parameters at BATS and DYFAMED. 68
3.8 Comparison of log-transformed surface chlorophyll-a concentration of combined assimilation of satellite chlorophyll-a and in situ NPP simulations with default and estimated parameters. 70
3.9 Phytoplankton phenology metrics bloom initiation, peak time, termination, duration and peak value at BATS and DYFAMED. 71
3.10 Simulated log-transformed surface chlorophyll-a and NPP in the parameter estimation experiments for free-run, satellite chlorophyll-a only assimilation and simultaneous assimilation of satellite chlorophyll-a and in situ NPP. 74
3.11 Comparison of monthly mean simulated NPP, satellite-derived NPP based on SeaWiFS satellite and in situ bottle data. 78

3.12 Simulations of chlorophyll-a concentration of at BATS. 79

4.1 Lat-Lon-Cap (LLC) Grid and the horizontal resolution of the LLC90 grid. 88
4.2 Comparison of area-weighted RMSE of log-transformed surface chlorophyll-a concentration relative to the OC-CCI data. 95
4.3 Monthly mean log-transformed surface chlorophyll-a concentrations for April 2020 and September 2020. 96
4.4 Estimated parameters values for initial slope of the Photosynthesis-irradiance curve of nanophytoplankton and diatoms; maximum photosynthesis rate of nanophytoplankton and diatoms; maximum chlorophyll to nitrogen ratio of nanophytoplankton diatoms; Chl degradation rate nanophytoplankton and diatoms; and maximum grazing rate. 99
4.5 Temporal evaluation of average estimated parameter values across the 12 Longhurst provinces. 102
4.6 Taylor diagrams illustrating the comparison of surface chlorophyll-a concentration from model simulations with default parameters and estimated parameters against satellite observations for the period 2019-2021. . . . 103
4.7 Monthly mean vertically Integrated NPP for April and October 2020. . 104
4.8 Annual maximum mixed layer depth (MLD) and the month of the year when maximum MLDs of MITgcm were found in 2020. 107

A.1 First-order Sobol' indices regarding mean surface total chlorophyll-a. . . 157
A.2 First-order Sobol' indices regarding mean surface nanophytoplankton chlorophyll-a. 157
A.3 First-order Sobol' indices regarding mean surface diatom chlorophyll-a. . 157
A.4 First-order Sobol' indices regarding annual peak surface total chlorophyll-a. 158
A.5 First-order Sobol' indices regarding annual peak surface nanophytoplankton chlorophyll-a. 158
A.6 First-order Sobol' indices regarding annual peak surface diatom chlorophyll-a. 158
A.7 First-order Sobol' indices regarding mean NPP. 159
A.8 First-order Sobol' indices regarding mean nanophytoplankton NPP. . . . 159
A.9 First-order Sobol' indices regarding the mean diatom NPP 159
A.10 First-order Sobol' indices regarding the mean export production of carbon. 160
A.11 First-order Sobol' indices regarding the mean surface flux of CO_2. . . . 160
A.12 First-order Sobol' indices regarding the mean partial pressure of CO_2 . . 160
A.13 Evaluation of α_{Nano} at BATS and DYFAMED for chlorophyll-a only assimilation 161
A.14 Evaluation of α_{Dia} at BATS and DYFAMED for chlorophyll-a only assimilation 161

A.15 Evaluation of μ_{Nano}^{max} at BATS and DYFAMED for chlorophyll-a only assimilation . . . 161
A.16 Evaluation of μ_{Dia}^{max} at BATS and DYFAMED for chlorophyll-a only assimilation . . . 162
A.17 Evaluation of d_{Nano}^{CHL} at BATS and DYFAMED for chlorophyll-a only assimilation . . . 162
A.18 Evaluation of d_{Dia}^{CHL} at BATS and DYFAMED for chlorophyll-a only assimilation . . . 162
A.19 Evaluation of ξ at BATS and DYFAMED for chlorophyll-a only assimilation 162
A.20 Evaluation of γ at BATS and DYFAMED for chlorophyll-a only assimilation . . . 163
A.21 Evaluation of Φ_{Phy} at BATS and DYFAMED for chlorophyll-a only assimilation . . . 163
A.22 Evaluation of Φ_{Det} at BATS and DYFAMED for chlorophyll-a only assimilation . . . 163
A.23 Evaluation of α_{Nano} at BATS and DYFAMED simultaneous assimilation of chlorophyll-a and in-situ NPP . . . 164
A.24 Evaluation of α_{Dia} at BATS and DYFAMED simultaneous assimilation of chlorophyll-a and in-situ NPP . . . 164
A.25 Evaluation of μ_{Nano}^{max} at BATS and DYFAMED simultaneous assimilation of chlorophyll-a and in-situ NPP . . . 164
A.26 Evaluation of μ_{Dia}^{max} at BATS and DYFAMED simultaneous assimilation of chlorophyll-a and in-situ NPP . . . 165
A.27 Evaluation of d_{Nano}^{CHL} at BATS and DYFAMED simultaneous assimilation of chlorophyll-a and in-situ NPP . . . 165
A.28 Evaluation of d_{Dia}^{CHL} at BATS and DYFAMED simultaneous assimilation of chlorophyll-a and in-situ NPP . . . 165
A.29 Evaluation of ξ at BATS and DYFAMED simultaneous assimilation of chlorophyll-a and in-situ NPP . . . 165
A.30 Evaluation of γ at BATS and DYFAMED simultaneous assimilation of chlorophyll-a and in-situ NPP . . . 166
A.31 Evaluation of Φ_{Phy} at BATS and DYFAMED simultaneous assimilation of chlorophyll-a and in-situ NPP . . . 166
A.32 Evaluation of Φ_{Det} at BATS and DYFAMED simultaneous assimilation of chlorophyll-a and in-situ NPP . . . 166

List of Tables

2.1 Quantities of interest chosen for the present study. 32
2.2 Shortlisted parameters after scrrening step. 36
2.3 Ranking of the seven most influential model parameters for on mean surface chlorophyll-a, annual peak surface chlorophyll-a, mean NPP, mean carbon export production, mean pCO_2 from the first- and total-order Sobol' indices. 39

3.1 The ten BGC parameters that are estimated in this study: the default and the estimated values. 62
3.2 RMSE of log-transformed surface chlorophyll-a concentration from combined assimilation of satellite chlorophyll-a and in situ NPP against satellite and bottle data. 68

4.1 The nine selected BGC parameters with their symbol, unit and default value. 91
4.2 The experiments performed in this study. 94
4.3 The default value, global average, minimum, maximum and standard deviation (percentage relative to global average) of spatially varying estimated parameters. 100
4.4 Code corresponding to Longhurst province, as defined by Longhurst (2007). 101

A.1 Tracers simulated by REcoM2 151
A.2 REcoM2 parameters, their Symbol, unit, and default value 153

List of Abbreviations

1–D	One-Dimensional
2–D	Two-Dimensional
3–D	Three-Dimensional
ALK	Total Alkalinity
BATS	Bermuda Atlantic Time-Series Study
BGC	Biogeochemical
CAFE	Carbon, Absorption, and Fluorescence Euphotic-Resolving
CbPM	Carbon-Based Productivity Model
CO_2	Carbon Dioxide
COREv2	Coordinated Ocean Research Experiments Version 2
DA	Data Assimilation
DCM	Deep Chlorophyll Maximum
DCML	Deep Chlorophyll Maximum Layer
DFe	Dissolved Iron
DIC	Dissolved Inorganic Carbon
DIN	Dissolved Inorganic Nitrogen
DON	Dissolved Organic Nitrogen
DO_2	Dissolved Oxygen
DGSM	Derivative Based Global Sensitivity Measures
DYFAMED	Dynamique des Flux Atmosphériques en Méditerranée
EnKF	Ensemble Kalman Filter

ESA	European Space Agency
ESM	Earth System Model
ESTKF	Error Subspace Transform Kalman Filter
GLODAPv2	Global Ocean Data Analysis Project
GSA	Global Sensitivity Analysis
GSM	Garver-Siegel-Maritorena
JGOFS	US Joint Global Ocean Flux Study
LLC	Lat-Lon-Cap
LLC90	Lat-Lon-Cap 90
LSA	Local Sensitivity Analysis
MLE	Maximum Likelihood Estimation
MITgcm	Massachusetts Institute of Technology General Circulation Model
MLD	Mixed Layer Depth
NPP	Net Primary Production
NPZD	Nutrient-Phytoplankton-Zooplankton-Detritus
OC-CCI	Ocean Color Climate Change Initiative
OAT	One-at-a-time
PDAF	Parallel Data Assimilation Framework
PFT	Plankton Functional Type
P-I curve	Photosynthesis-Irradiance Curve
pCO_2	Partial Pressure of Carbon Dioxide
PON	Particulate Organic Nitrogen
POC	Particulate Organic Carbon
qMC	Quasi-Monte Carlo
QoI	Quantities of Interest
RCP	Representative Concentration Pathway
REcoM2	Regulated Ecosystem Model 2

RMSD	Root Mean Squared Deviation
RMSE	Root Mean Squared Error
SA	Sensitivity Analysis
SCDA	Strongly Coupled Data Assimilation
SMS	Sources Minus Sinks
SST	Sea Surface Temperature
SSS	Sea Surface Salinity
UQ	Uncertainty Quantification
WCDA	Weakly Coupled Data Assimilation

Chapter 1

Introduction

The oceans play a central role in shaping our climate by absorbing atmospheric carbon dioxide (CO_2) and sequestering heat. As the largest carbon reservoir, oceans control the atmospheric CO_2 concentration on decadal or longer scales (Khatiwala et al., 2013; McKinley et al., 2016). The seasonal dynamics of carbon and nutrient cycles in the upper ocean determine the productivity of ecosystems, the net exchange of CO_2 between the atmosphere and the ocean, and the distribution of many elements in the sea. Ocean biogeochemical (BGC) processes directly regulate the changes and variability in marine ecosystems and the overall balance, distribution, and cycling of these elements. Thus, BGC processes are ultimately tied to larger-scale climates, potentially modifying the global climate (Hatje et al., 2022). Improving our ability to predict the effects of climate change on ecosystems and vice-versa requires a comprehensive understanding of ocean biogeochemical (BGC) processes and how they relate to climate processes.

Traditional laboratory experiments are limited in exploring the large-scale effects of climate change on ocean BGC dynamics and how they lead to changes in global fluxes. Hence, scientists use numerical models to understand ocean BGC processes and their effects on the global carbon cycle and to project their potential changes with changing climate. Ocean BGC model outputs are increasingly used by the scientific community and environmental managers to inform policy (see Bindoff et al., 2019) and to develop marine environmental applications and services (Fennel et al., 2019). However, the current BGC models, used to simulate the ocean BGC cycle and thus better understand the marine ecosystem processes, are highly uncertain (see Rohr et al., 2023) and sensitive to BGC parameter choice (see Brett et al., 2021). The uncertainties are unavoidable, but uncertainty quantification (UQ) of the ocean BGC models can make the models more useful and mitigate the discrepancies in the model outputs. This thesis aims to i) quantify the uncertainties arising in an ocean BGC model and ii) to reduce those uncertainties for improved model predictions.

This chapter provides the basis that motivates the research aim of the thesis by first discussing the background and identifying current research gaps, followed by the research objectives and provides an overview of the thesis structure, highlighting the intercon-

nections between the chapters.

1.1 Application of Ocean BGC Models

Ocean BGC models are a primary tool for investigating ocean biogeochemistry, marine ecosystem functioning, and the global carbon cycle. They are essential to Earth system models utilized to generate climate projections (Orr et al., 2017). Approximately one-fourth of the CO_2 emitted by human activities is absorbed by the global ocean (Friedlingstein et al., 2022). Ocean BGC models are central in quantifying the patterns and rates of ocean anthropogenic CO_2 uptake (see Crisp et al., 2022) and estimating the global carbon budget (e.g., Friedlingstein et al., 2022; Hauck et al., 2020). Furthermore, they are pivotal in understanding future ocean CO_2 uptake and predicting the atmosphere-ocean CO_2 flux on a global scale, which is crucial for assessing carbon policy and management strategies (Ilyina et al., 2021).

Given the substantial CO_2 uptake capacity of the ocean, various deliberate CO_2 removal or negative emissions approaches have been proposed to mitigate climate change (Gattuso et al., 2018). However, there are significant knowledge gaps concerning these ocean-based CO_2 removal methods. These uncertainties encompass the effectiveness of CO_2 uptake, long-term carbon storage, verification and accounting of the methods, scalability, and potential environmental impacts (National Academies of Sciences, Engineering and Medicine, 2022). In addressing these critical questions, Ocean BGC models assume a crucial role, facilitating the verification of CO_2 removal techniques and ensuring accurate carbon accounting.

The ocean's uptake of anthropogenic CO_2, which mitigates atmospheric CO_2 accumulation and climate change, leads to aqueous CO_2 and lower the pH of seawater, a phenomenon called ocean acidification (Feely et al., 2009). In addition, the oxygen content of the global ocean declines because of reduced ventilation of the deep ocean from global warming (see Levin, 2018; Oschlies et al., 2018), resulting in deoxygenation. Ocean BGC models serve as valuable tools for exploring ocean acidification (e.g., Gehlen et al., 2007; Ilyina et al., 2009; Krumhardt et al., 2019) and deoxygenation (e.g., Andrews et al., 2017; Bopp et al., 2017). In coastal ecosystems, acidification is compounded by additional factors such as eutrophication, acidic freshwater discharge, and terrestrial organic carbon inputs. Regional Ocean BGC models are used to analyze the synergy between acidification and eutrophication (Laurent et al., 2017) and to characterize the highly variable physical and biogeochemical conditions (Hauri et al., 2020; Rutherford et al., 2021). Ocean BGC models have proven instrumental in quantifying the time of emergence when anthropogenic changes exceed natural variability (Hauri et al., 2013). Further applications include investigating how anthropogenic CO_2 trends amplify the frequency of extreme acidification events (Hauri et al., 2021) and compound events with

overlapping extremes of acidification, marine heatwaves, and deoxygenation (Gruber et al., 2021). These insights are essential for comprehending the complexities and potential impacts of ongoing changes in the ocean ecosystem and the associated environmental consequences.

Further, ocean BGC models play a crucial role in studying the economic implications of climate change on fisheries (e.g., Loukos et al., 2003). Researchers have utilized these models to explore the potential impact of climate change on fish catch and global fishery revenues (Cheung et al., 2010; Lam et al., 2016). However, such projections are accompanied by large uncertainties, particularly concerning the lower trophic level biomasses and production as projected by ocean BGC models (Lotze et al., 2019). Recent advancements have led to the direct integration of ocean BGC models with higher trophic level models, enabling the examination of top-down control exerted by higher trophic levels on planktonic ecosystems and marine biogeochemical cycles in general (e.g., Archibald et al., 2019; Aumont et al., 2018).

Ocean BGC models have emerged as a powerful and indispensable tool for developing marine environmental applications and ecological forecasting (Fennel et al., 2019; Gehlen et al., 2015). By optimally integrating models and observations, data assimilative ocean BGC models offer short-term ecological forecasts in diverse coastal systems and at the global scale (see Fennel et al., 2019; Gehlen et al., 2015). Furthermore, these data assimilative models enable the generation of reanalysis datasets (e.g., Carroll et al., 2020; Ciavatta et al., 2016), which facilitates the reconstruction of historical marine conditions and provides a comprehensive view of past ecological trends. These reanalysis datasets further serve to model validation and enhance our understanding of long-term ecosystem changes.

1.2 Model Uncertainties

Similar to any geoscientific model, the objective of ocean BGC models is predominantly to replicate the state and dynamics of real-world systems in the oceans as accurately as possible, or at the very least, to the extent that provides pertinent insight into the targeted problem or region of interest. Replicating the state and dynamics of a real-world system requires the model to incorporate an adequately accurate description of the system, as the model is an abstract representation of a system and related processes (Turner & Gardner, 2015).

The process of geoscientific modeling always demands a degree of concession within the facets of model design and implementation. It is essential to realize that models are not true or false, not even in the sense of being closer to the real-world system of interest. They are simply less uncertain (better) or more (worse) concerning how

closely they resemble all the data we have of the target system. Thus, model quality is primarily contingent on their degree of uncertainty. Complex models are seen as more accurate, and simple ones as more general. A lack of detail may lead to systematic bias in predictions - but adding detail to a model only guarantees an increase in reliability if the added processes are essential, well-understood, and reliably estimated (Turner & Gardner, 2015).

"O'Neill's Conjecture" was that there may be an optimal balance between model complexity and model uncertainty (O'Neill, 1973, Figure 1.1). Systematic bias caused by the lack of details in simplistic models can be diminished by enhancing their complexity, for instance, by increasing the number of plankton function types. However, beyond a certain threshold, the increased complexity inadvertently amplifies model uncertainty, primarily due to the uncertainty stemming from model parameter values or 'parameter uncertainty'. Because ocean BGC processes are diverse and complex, a more complex model will require a large amount of data for estimating all model parameters reliably, which would be very difficult, if not impossible, to measure.

The systematic point here is that model utility depends on the uncertainty trade-offs in their construction. Uncertainties are built up from collecting data onwards via deciding what the model should focus on (scale and scope) and boundaries of target systems to parameter selection and design functionality of the model (how it should work). When sharing these models with potential users, communicating these trade-offs and uncertainties is a moral imperative (Kaiser et al., 2022). This is especially important when using models to predict future events. In very complex systems, or those we do not fully understand, even a model accurately depicting current processes might not accurately predict a future outcome. Because ocean BGC processes are diverse and complex, a model that can reasonably mimic observed dynamics will be complex with the optimal balance towed toward complexity.

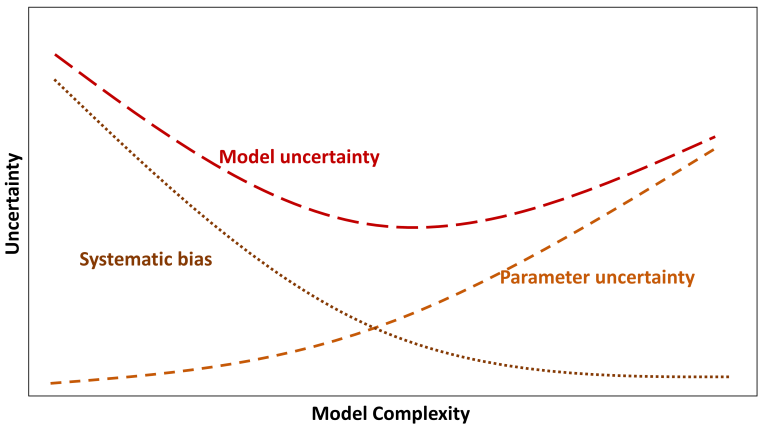

Figure 1.1 Depiction of the O'Neill conjecture; drawn after Turner and Gardner (2015).

Current ocean BGC models that are used to generate climate projections are associated with substantial uncertainties. In state-of-the-art Earth System Models (ESMs), the inorganic chemistry is regulated by well-defined chemical and thermodynamic formulations (G. Flato et al., 2014). Conversely, the representations of biological processes, such as marine productions, are highly uncertain (Bopp et al., 2013; Kwiatkowski et al., 2020; Löptien & Dietze, 2019; Tagliabue et al., 2021). Despite advances in climate science achieved through global collaborative efforts, future climatic change projections remain significantly uncertain, particularly in ecosystem projection (Bopp et al., 2013; Laufkötter et al., 2015; Lotze et al., 2019; Rohr et al., 2023). Figure 1.2 shows the decline in global marine biomass in 2090–2099 relative to 1990–1999 under different climate scenarios coupled with large uncertainties. The latter is derived from a multimodal ensemble; however, the uncertainty of individual models remains unspecified. The uncertainty of ocean BGC models becomes more pronounced at regional scales compared to global estimates (Tagliabue et al., 2021; Vancoppenolle et al., 2013), posing significant challenges for BGC models' application in regional impact studies.

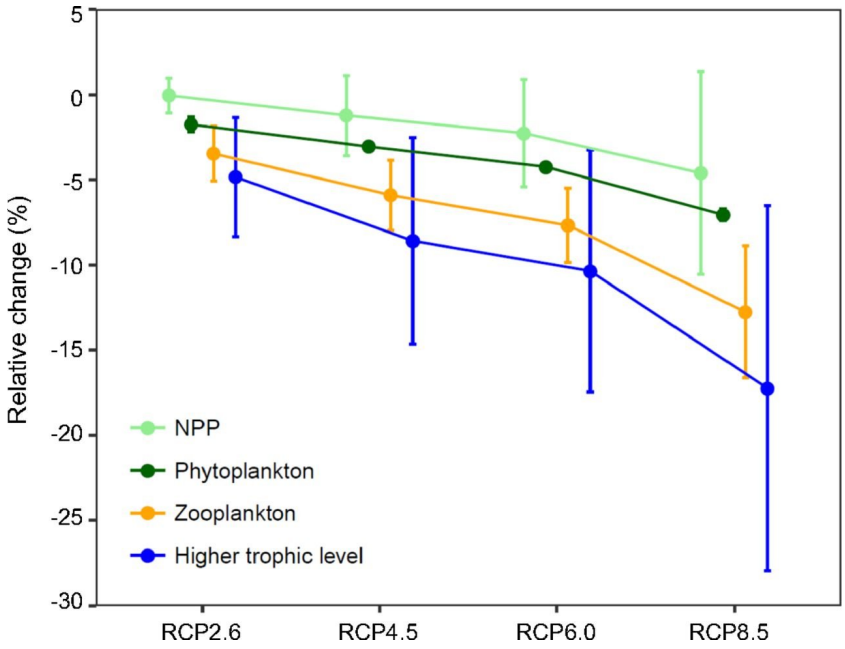

Figure 1.2 Projections of marine biomass changes in future climate scenarios are highly uncertain. The figure shows the projected mean changes in percent of magnitude and their standard deviations in 2090-2099 relative to 1990-1999 for net primary production (NPP), phytoplankton, and zooplankton biomass in four Representative Concentration Pathways (RCP2.6, RCP4.5, RCP6.0, and RCP8.5). Figure from Lotze et al. (2019).

To enhance the meaningful interpretation and application of ocean BGC simulations, it is imperative to accurately quantify the uncertainty present in the model outputs. This step is crucial for ensuring accurate and reliable interpretation of scientific findings. Assessment of the current state and development of new strategies for mitigation,

adaptation, and protection of socio-ecological systems require adequate uncertainty information of BGC analysis and predictions that provide decision-makers and the public with the necessary information to assess the impact of policy decisions.

Ocean BGC models are spatially explicit models that describe the transformations of BGC constituents, including nutrients, functional plankton groups, non-living organic matter, dissolved gases, and variables of the inorganic carbon system contained in seawater by ecosystem growth and interactions. The representation of growth and ecosystem interactions in BGC models is based on, besides the conservation of mass, a large part of heuristic mathematical descriptions of observed processes, e.g., between prey density of zooplankton and their grazing rates. Either through choice or necessity, each BGC transformation in the model is described by simplified schemes known as parameterizations (Hourdin et al., 2017) which require closure parameters.

Ocean BGC models include a wide variety of bio-physical processes – each represented by a parameterization (Franks, 2009; Geider et al., 1998) that requires at least one, but typically more, BGC model parameter (see Fennel et al., 2022). Therefore, they involve many input parameters, usually several times more than the state variables. The values of these numerous input parameters are not precisely known. The uncertainty of these parameter values is quite large (see Schartau et al., 2017) and potentially translates into significant uncertainties in model outputs. To accurately determine the uncertainty in model predictions, it is essential to quantify the uncertainty related to parameter values rigorously.

Specifying these parameter values rests upon the assumption that optimal parameter values exist if the underlying model can adequately replicate the real world, not just for one particular state but for the full spectrum of system states the model is designed to explore. In addition, if optimal parameter values exist, they can be determined, and a means must exist to estimate them. As ocean BGC models are highly uncertain in their parametrization (see Fennel et al., 2022; Schartau et al., 2017) and the larger portion of uncertainties in the ocean BGC model outputs source from imprecision parameter values (Friedrichs et al., 2007; Ilyina et al., 2013; Kwiatkowski & Orr, 2018), we see the uncertainty quantification of these ocean BGC models as a parameter estimation problem.

Ocean BGC models can be computationally expensive in terms of the number of processors required to run the model, the amount of memory needed to run the model, and the amount of time necessary to complete a simulation. Due to the increasing availability of computing resources, more processes are incorporated into BGC models. Thus, the state-of-art ocean BGC models have become more and more complex (see Mignot et al., 2023). However, more complex does not necessarily imply more realistic (T. R. Anderson, 2005; Friedrichs et al., 2007; Ward et al., 2013) unless the added processes and related parameters are well known (Denman, 2003).

In modeling practice, modelers frequently rely on previously published parameter values. This preference is driven mainly by the substantial time and effort associated with parameter estimation. The reliance on reference values persists even if the referenced values were derived from a different model configuration or an entirely different model. This practice may lead to inappropriate parameter selection and, consequently, significant uncertainties within model experiments. Employing fixed parameter values within model ensembles implies that the resultant uncertainties in model predictions will not encompass variations from uncertainties in the parameter values themselves. Neglecting parameter uncertainty consequently underestimates the overall uncertainty inherent in the model predictions. Therefore, despite the challenges, it was recommended that parameter estimation should be a routine part of ocean BGC modeling and be documented as part of the scientific publishing of results (see Schartau et al., 2017).

In this context, to mitigate model uncertainty, sensitivity analysis (SA) plays a pivotal role. SA aims to determine the relative influence of the inputs on some given outputs in a complex system, like an ocean BGC model. Indeed, SA can help better understand the model's behavior and identify the most influential model parameters that should be studied carefully. SA helps to focus parameter estimation efforts on these parameters. However, despite being a critical step for any ocean BGC modeling study, SA is often overlooked or not reported – the study of Shimoda and Arhonditsis (2016) revealed that less than half of the BGC modeling studies performed quantitative parameter sensitivity analyses.

1.3 Parameter estimation

Parameter values can either be rooted in laboratory experiments or require sufficient observational data to drive the model and evaluate the model simulations. The model needs to maintain a stable reference state and be able to reproduce climatological phenomena. However, specific models, such as ocean BGC models, may not consistently achieve this stability. These models are susceptible to drift (A. S. Gupta et al., 2012) and might display multiple stable states (Hawkins et al., 2011). Additionally, computational limitations can come into play. It is crucial to ensure that there is capacity to conduct a vast number of simulations and that these simulations can run long enough to explore the parameter space thoroughly.

Parameter estimation is often termed as "tuning" (e.g., Hourdin et al., 2017). In general, tuning a model involves bringing the model to an equilibrium state under specific boundary conditions, mainly sourced from observations. Subsequently, these simulations are evaluated against observational datasets, with the extent of deviation between the model and observations being quantified using a predetermined statistical algorithm.

However, it is noteworthy that tuning itself can refer to the manual adjustment of parameter values (e.g., Samuelsen et al., 2015), distinct from parameter estimation. The approaches used for parameter estimation of ocean BGC models can be grouped into the following broad categories:

- *Bayesian estimation:* This approach consists of running the model forward multiple times with different combinations of parameter values where parameters are treated as random variables, and values are chosen based on their "posterior probability". The parameter can be varied individually or multiple parameters simultaneously (e.g., Chien et al., 2020; V. Jones et al., 2013; Mattern & Edwards, 2017; Oliver et al., 2022). However, utilizing Bayesian estimation necessitates knowledge of the prior distributions of parameter values, which are often unknown. Furthermore, this approach may demand a large number of ensemble simulations even when dealing with a relatively low dimensionality parameter space (Guillas et al., 2009), which is computationally infeasible with global three-dimensional (3–D) simulations.
- *Maximum likelihood estimation (MLE):* In this approach, the values of parameters are not treated as random variables but rather as fixed, unknown constants. MLE seeks the parameter values that maximize the probability of the data given the parameter set (Casella & Berger, 2002). Therefore, in a non-Bayesian context, the likelihood is not a conditional probability because one set of random variables depends on another.
- *Data Assimilation (DA):* Ocean BGC parameter estimation is greatly aided by DA (see Ford et al., 2018), which infers parameter values from optimal match between simulated output and observational data (Asch et al., 2016; Eknes & Evensen, 2002). A variety of DA techniques have been successfully applied to BGC models for state estimation, parameter estimation, and joint (state and parameter) estimation. Ensemble-based sequential DA techniques like the Ensemble Kalman Filter (EnKF, see Vetra-Carvalho et al., 2018, for a review) offer a simple but efficient framework for joint state and parameter estimation by augmenting them in the "state vector" and treating them as time-varying (J. L. Anderson, 2001). Note that the sequential DA is usually also a Bayesian approach. The sequential DA consists of two primary steps executed consecutively: a forecast and analysis steps. If the sequential algorithm is accurate, it should approximate the posterior parameter distribution according to Bayes' theorem when observational data becomes available.
- *Machine learning:* Machine learning techniques are designed to identify and quantify unspecified associations between input and output datasets independent of understanding the intrinsic physical processes (Y. Kim & Nakata, 2018). This approach facilitates the exploration and exploitation of previously unrecognized relationships. However, it simultaneously raises questions concerning the validity and applicability of these relationships in states that extend beyond the scope encompassed by the training datasets.

Given the potential advantages of DA over the alternatives (see Schartau et al., 2017), we adopt the approach in this dissertation. DA aids in estimating the values for BGC parameters that are difficult (if not impossible) to measure. In the broadest sense, DA techniques can be categorized as either sequential approaches or variational approaches, each with its distinct advantages and disadvantages. Variational algorithms minimize a cost function of the weighted sum of squared model-data differences. Sequential methods, on the other hand, rely on approximating the probability distribution generated from an ensemble of model initial states at a particular time based on observations of the state until that time.

The variational DA approaches have been applied to parameter estimation applications in one-dimensional (1–D) BGC models (Bagniewski et al., 2011; Fiechter et al., 2011, 2013; Friedrichs et al., 2006, 2007; Laiolo et al., 2018; Pelc et al., 2012; Song et al., 2016; Ward et al., 2010; Xiao & Friedrichs, 2014a, 2014b; Zhao et al., 2005) but have shown limited success in constraining parameters for 3–D models (see Mattern & Edwards, 2017).

On the other hand, sequential DA approaches applied to BGC models (Ciavatta et al., 2014, 2016, 2018; Gharamti, Samuelsen, et al., 2017; Gharamti, Tjiputra, et al., 2017; Goodliff et al., 2019; J. T. Hu et al., 2012; E. M. Jones et al., 2016; Natvik & Evensen, 2003; Nerger & Gregg, 2007, 2008; Pradhan et al., 2019, 2020; Simon et al., 2012, 2015; Triantafyllou et al., 2007) showed promising performance to improve the BGC simulation. The method also provides an efficient way for parameter estimation by the state augmentation approach (J. L. Anderson, 2001), where the state variables and parameters are combined in an augmented state vector, and the parameters are treated as time-varying variables with small artificial evolution noise. The most common sequential methods used in these studies are different variants of EnKF.

The values of the parameters depend on the physical and biogeochemical (see Follows et al., 2007) context, thus varying spatially and temporally, while in practice, they are used as constant values across space and time in the model simulations. Studies that estimated BGC parameters in multiple locations (e.g., Friedrichs et al., 2007; Gharamti, Tjiputra, et al., 2017; Losa et al., 2004; Mamnun et al., 2022; Schartau & Oschlies, 2003) found different estimated parameter values across locations. Sometimes parameter values estimated from a 1–D assimilative application are used in a 3–D implementation (e.g., McDonald et al., 2012; Oschlies & Schartau, 2005; St-Laurent et al., 2017).

Losa et al. (2004) estimated 6 BGC parameters into a simple box model (0-D) in the North Atlantic by varying the parameters values in different cells. Tjiputra et al. (2007) estimated spatially varying BGC parameters using an adjoint method by assimilating satellite chlorophyll-a concentration. They showed that using estimated spatially variable parameters improved the global simulation of NPP. Doron et al. (2013) estimated five spatially varying biogeochemical parameters by assimilating ocean color derived

chlorophyll-a into a 3–D regional model and found better model-data agreement using spatially varying estimated parameters than the reference simulation using uniform parameters' values. They found that using spatially varying parameter values reduced the RMSD between the model output and the observations compared to the simulation with uniform parameters. Simon et al. (2015) estimated four spatially varying BGC parameters in the North Atlantic and the Arctic Ocean and found that regional patterns of estimated parameters can be associated with Longhurst provinces in regions where the model performs well but not in the region of model deficit. Simon et al. (2015) also demonstrated that BGC predictions generally benefit spatially varying parameter estimation. Xu et al. (2022) estimated spatially varying BGC parameters in the Bohai, Yellow, and East China Seas assimilating satellite chlorophyll-a data using an adjoint method and found that variational data assimilation can also determine reasonable parameter values of ocean BGC model. Using an idealized twin experiment, Singh et al. (2022) showed that estimating spatially varying ocean BGC parameters is feasible using ensemble-based data assimilation techniques in global-scale models.

Incorporating temporally varying parameters can significantly improve the agreement between models and observations (e.g., Mattern et al., 2012, 2014; Roy et al., 2012; Simon et al., 2015). Simon et al. (2015) specifically identified seasonal patterns in estimated parameters and advocated using time-dependent parameters in ocean BGC models. However, they also highlighted that in regions with substantial model errors, the parameter values either converge to extreme values resulting in larger model errors, or may diverge toward a high ensemble spread. Singh et al. (2022) also noted that even in an ideal model setting, certain BGC parameters fail to converge to their true values when significant model errors occur.

1.4 Objectives of the thesis

The aim of the thesis is to study the uncertainties that arise in ocean BGC models, and to obtain improved parameters to reduce those uncertainties and improve model predictions. We utilize the BGC model Regulated Ecosystem Model 2 (REcoM2, Hauck et al., 2013, see section 2.3 in Chapter 2) in this dissertation. REcoM2 is recognized as an intermediate-complexity model extensively utilized by the scientific community to investigate marine BGC dynamics (e.g., Álvarez et al., 2018; Hauck et al., 2020; Laufkötter et al., 2015; Völker & Tagliabue, 2015). Its judicious balance of complexity ensures its suitability for representative uncertainty analyses.

The specific objectives of this dissertation are:

1. To identify the model parameters controlling the processes in the biogeochemical model REcoM2 and are the most influential on the variability of model outputs.

2. To estimate uncertain parameters of REcoM2 by applying ensemble data assimilation and to assess their uncertainty in BGC simulations.
3. To study the effect of estimated spatially and temporally varying parameters on the biogeochemical fields and dynamics.

1.5 Outline

This dissertation comprises five distinct yet interrelated chapters. While each chapter delves into its unique focus, its themes are intertwined and not mutually exclusive. However, the chapters have been structured to stand alone and can be read independently. There may be textual overlap, which serves as a bridge to ensure this independent readability. The subsequent chapters are structured as follows.

Chapter 2: Global sensitivity analysis of a one-dimensional ocean biogeochemical model

Chapter 2 presents the results of a global sensitivity analysis (GSA) of the BGC model REcoM2 with regard to the sensitivity of its input parameters. REcoM2 model involves many process parameters as inputs which are not precisely known. This study aims to identify the parameters whose value significantly impacts the uncertainty of model outputs of interest. This is achieved by computing variance-based sensitivity indices, which measure the relative contribution of individual input parameters on the overall variability of a chosen model output. This study utilized a 1–D configuration of REcoM2 at two ocean sites in the North Atlantic (BATS) and the Mediterranean Sea (DYFAMED). The first and total order Sobol' indices were estimated for 12 model outputs of interest commonly considered for the calibration and validation of BGC models.

This study i) offers a comprehensive list of the most important BGC parameters that should be emphasized in future BGC modeling case studies, parameter estimation and optimization, and for further development of BGC models and ii) helps us select parameters for estimation with data assimilation. Likewise, the parameter estimation experiment study of Chapter 3 provides essential information about error margins and possible ambiguities of parameter estimates and complements this study.

This chapter reproduces a manuscript (Mamnun et al., 2023) accepted for publication in the peer-reviewed journal *Socio-Environmental Systems Modelling*.

Chapter 3: Uncertainties in ocean biogeochemical simulations: Application of ensemble data assimilation to a one-dimensional model

Chapter 3 reports the uncertainty quantification of model fields and parameters within a 1–D configuration of the REcoM2 model at two BGC time-series stations – BATS and DYFAMED. This study utilized the identical model setup of the study in Chapter 2. By assimilating 5-day satellite chlorophyll-a concentration and monthly in situ NPP

data for three years applying an ensemble Kalman filter, the values of ten preselected parameters were estimated at both sites. The study further evaluated the effectiveness of the estimated parameter values on the model's predictive performance. It is found that the estimated set of parameters improved the model prediction up to 66% for the surface chlorophyll-a and 56% for NPP. The chapter presents a detailed assessment of the differences between the two stations, which exhibit distinct environmental conditions.

This study obtained different parameter values in the two stations. As mentioned above, BGC parameters can vary substantially across space, depending on physical and ecosystem context. Consequently, regional and global 3–D models should benefit from spatially varying parameter values. The insights from this study serves as an essential base for conducting spatially and temporally varying ocean BGC parameter estimation studies at the global level in Chapter 4.

This chapter replicates the peer-reviewed article Mamnun et al. (2022), published in *Frontiers in Marine Science*.

Chapter 4: Estimation of spatially and temporally varying biogeochemical parameters in a global ocean model

Chapter 4 estimates spatially and temporally varying parameters in a global ocean BGC model. Nine selected BGC process parameters of REcoM2 are estimated with heterogeneity in parameter values across space and over time using ensemble data assimilation techniques. The parameters were selected based on the GSA presented in 2. The methods used in the 1–D model configuration, as presented in Chapter 3, were extended in this study to estimate spatially varying parameter values in a 3–D global ocean model. For estimating spatially varying parameters, each parameter is defined as a two-dimensional (2–D) field, which is then updated utilizing the cross covariances with the observation. In this study, satellite ocean color data are assimilated to simultaneously estimate the BGC model states and parameters.

This study further assessed the improvement in model predictions with space and time-dependent parameters compared to the simulation with globally constant parameters against assimilative and independent data. The model simulations with this set of estimated parameters are closer to the observations than the reference simulations using uniform values of the parameters. The spatial variabilities of the parameter estimates and the effect of estimated spatially varying parameter values on model fields and dynamics are discussed in this chapter.

Chapter 4 draws from a manuscript in preparation titled "Spatially Varying Biogeochemical Parameter Estimation in a Global Ocean Model" to be submitted to a peer-reviewed journal.

Chapter 5 makes concluding remarks and outlook for future work.

1.6 Contributions to Co-authored Publications

This dissertation follows the format of a "cumulative thesis," comprising three co-authored articles, in addition to introduction and conclusion chapters. The Author Contributions to these articles are as follow:

Article 1 Mamnun, N., Völker, C., Krumscheid, S., Vrekoussis, M., & Nerger, L. (2023). Global sensitivity analysis of a one-dimensional ocean biogeochemical model. *Socio–Environmental Systems Modelling, 5, 18613.* https://doi.org/10.18174/sesmo.18613.

Mamnun, N., Völker, C., Krumscheid, S., Vrekoussis, M., and Nerger, L. contributed to conceptualizing and defining experiments. Mamnun, N. carried out the experiments, analyzed data and wrote the manuscript. Völker, C., Krumscheid, S., Vrekoussis, M., and Nerger, L. contributed to improving the manuscript draft. Völker, C., Vrekoussis, M., and Nerger, L supervised the overall research.

Article 2 Mamnun, N., Völker, C., Vrekoussis, M., & Nerger, L. (2022). Uncertainties in ocean biogeochemical simulations: Application of ensemble data assimilation to a one-dimensional model. *Frontiers in Marine Science,* 9. https://doi.org/10.3389/fmars.2022.984236.

Mamnun, N., Völker, C., Vrekoussis, M., and Nerger, L. contributed to conceptualizing and defining experiments. Mamnun, N. carried out the experiments, analyzed data and wrote the manuscript. Völker, C., Vrekoussis, M., and Nerger, L. contributed to improving the manuscript draft. Völker, C., Vrekoussis, M., and Nerger, L supervised the overall research.

Article 3 Mamnun, N., Völker, C., Vrekoussis, M., & Nerger, L. (in preparation). Spatially Varying Biogeochemical Parameter Estimation in a Global Ocean Model. *Journal of Geophysical Research: Oceans*

Mamnun, N., Völker, C., Vrekoussis, M., and Nerger, L. contributed to conceptualizing and defining experiments. Mamnun, N. carried out the experiments, analyzed data and wrote the manuscript. Völker, C., Vrekoussis, M., and Nerger, L. contributed to improving the manuscript draft. Völker, C., Vrekoussis, M., and Nerger, L supervised the overall research.

Chapter 2

Global sensitivity analysis of a one-dimensional ocean biogeochemical model

This chapter presents a varience-based global sensitivity analysis (GSA) of a one-dimensional ocean biogeochemical (BGC) model, the Regulated Ecosystem Model 2 (REcoM2), regarding important model outputs that are commonly considered for calibration and validation of BGC models. The GSA is performed by computing Sobol' sensitivity indices at two ocean biogeochemical time series stations – the Bermuda Atlantic Time-series Study station in the North Atlantic Ocean and the Dynamique des Flux Atmosphériques en Méditerranée (DYFAMED) station in the Mediterranean Sea to identify the parameters whose uncertainty has the largest impact on the uncertainty of the selected model outputs. These stations with distinct environmental conditions are chosen to better understand parameter uncertainty under varying environmental conditions. This study finds that model predictions are most sensitive to photosynthesis parameters, the maximum chlorophyll to nitrogen ratio, the chlorophyll degradation rate, grazing parameters, and remineralization parameters. The GSA lists relatively important BGC parameters for data assimilative experiments to estimate optimal parameter values. This chapter replicates the peer-reviewed manuscript of the same title accepted for publication in the Socio-Environmental Systems Modelling.

Citation: Mamnun, N., Völker, C., Krumscheid, S., Vrekoussis, M., & Nerger, L. (2023). Global sensitivity analysis of a one-dimensional ocean biogeochemical model. *Socio–Environmental Systems Modelling, 5, 18613.* https://doi.org/10.18174/sesmo.18613.

abstract

Ocean biogeochemical (BGC) models are a powerful tool for investigating ocean biogeochemistry and the global carbon cycle. The potential benefits emanating from BGC simulations and predictions are broad, with significant societal impacts from fisheries management to carbon dioxide removal and policy-making. These models contain numerous parameters, each coupled with large uncertainties, leading to significant uncertainty in the model outputs. This study performs a global sensitivity analysis of an ocean BGC model to identify the uncertain parameters that impact the variability of model outputs most. The BGC model Regulated Ecosystem Model 2 is used in a one-dimensional configuration at two ocean sites in the North Atlantic (BATS) and the Mediterranean Sea (DYFAMED). Variance-based Sobol' indices are computed to identify the most influential parameters for each site for the quantities of interest (QoIs) commonly considered for the calibration and validation of BGC models. The most sensitive parameters are the maximum chlorophyll to nitrogen ratio, chlorophyll degradation rate, zooplankton grazing and excretion parameters, photosynthesis parameters, and nitrogen and carbon remineralization rate. Overall, the sensitivities of most QoIs were similar across the two sites; however, some differences emerged because of different mixed layer depths. The results suggest that implementing multiple zooplankton function types in BGC models can improve BGC predictions. Further, explicitly implementing heterotrophic bacteria in the model can better simulate the carbon export production and CO_2 fluxes. The study offers a comprehensive list of the most important BGC parameters that need to be quantified for future modeling applications and insights for BGC model developments.

2.1 Introduction

Ocean biogeochemical (BGC) processes play a central role in shaping our climate by absorbing and sequestering atmospheric carbon dioxide (CO_2). Improving our ability to predict the climate and assess the impacts of climate change on the ecosystems requires a comprehensive understanding of the ocean BGC processes and how they relate to the global climate. Numerical Ocean BGC models are, in addition to measurements, the primary tools for investigating ocean BGC processes and their effects on the carbon cycle and marine ecosystem functioning. BGC models are essential to earth system models used to generate climate projections (Orr et al., 2017) and estimate the global carbon budget (e.g., Hauck et al., 2020). Ocean BGC model outputs also support management decisions and policy-making, such as end-to-end models of the marine environment and fisheries (e.g., Fennel et al., 2019; Lavoie et al., 2021) and for assessing the economic impacts of climate change, for example, on fisheries (Tommasi et al., 2017), thereby providing information on how to mitigate the future effects. BGC models have been used to forecast marine ecosystems operationally (e.g., Gutknecht et al., 2019) and

generate reanalysis datasets (e.g., Carroll et al., 2020).

The evaluation of these models involves a wide variety of complex biological and chemical processes described by often simplified schemes in models known as parameterizations. Hence, ocean BGC models include numerous parameters. The values of these parameters are often poorly constrained by theory or observation and are not precisely known. The uncertainty of these parameter values is substantial (Schartau et al., 2017) and, in turn, translates into possibly significant uncertainty in the model outputs. The values of these parameters are usually constrained only from the limited field data or laboratory experiments but usually not in the ocean basin of interest. Therefore, modelers must adjust and tailor model parameters and configuration in each application case (Wagener & Pianosi, 2019) to calibrate the BGC model using observational data, either manually or through optimization algorithms that minimize the misfit between simulations and available data. Focusing on the most influential parameters for the model outputs of interest is crucial to ensure robust and high-quality model prediction. Quantifying the uncertainty caused by these parameters is essential to improve the reliability of the models. Identifying the most relevant input parameters using a computationally cheap one-dimensional (1–D) setup permits significant computational savings compared to a three-dimensional (3–D) global-scale one by putting numerical effort into the appropriate parameters.

Further developments and improvements of these models are essential to advance our understanding of ocean BGC processes and ensure greater model realism. Sensitivity analysis (SA) is a well-established tool to identify the most influential model parameters and critical relationships within a system, to guide model assessments, and navigate model development (Razavi et al., 2021; Wagener & Pianosi, 2019), especially in a policy context (Saltelli & Funtowicz, 2014). BGC simulations and predictions are used to assess the current state and develop new strategies for mitigating, adapting, and protecting socio-ecological systems. These require adequate uncertainty assessment that provides decision-makers and the public with the necessary information to assess the impact of policy decisions. In turn, uncertainty assessment in model predictions and analysis requires proper uncertainty quantification of model parameters.

SA methods have commonly been divided into two broad categories, namely local sensitivity analysis (LSA), where input factors are varied one-at-a-time (OAT) around the reference values, and global sensitivity analysis (GSA), which assesses the behavior of model outputs by perturbing the entire space of input parameters. In developing and applying the marine BGC models, SA has seldom been performed and reported (e.g., Chien et al., 2020; Leles et al., 2018) and is usually not an integral part of a new modeling application (Prieur et al., 2019). The most common approach in BGC modeling is to conduct a local analysis with a few experiments by varying the parameter values OAT or simultaneously (e.g., Baklouti et al., 2006; Kriest et al., 2012; Kvale & Meissner, 2017).

Some studies assessed the adjoint sensitivity (e.g., Fennel et al., 2001; Ji et al., 2015; Tjiputra & Winguth, 2008) of model output to its inputs by computing gradients. However, it is important to understand that gradient-based SA is a local method because the gradient is a local notion computed in the vicinity of the parameter's current value. Therefore, this gradient, which is a way to quantify the influence of a parameter on model outputs, can be quite different depending on the chosen value of the parameters. To address this, Sobol' and Kucherenko (2009) introduced derivative based global sensitivity measures (DGSM).

Variance-based sensitivity indicators, in particular so-called Sobol' indices (Saltelli et al., 2004; Sobol', 2001) are widely recognized and popular GSA measures (see Razavi et al., 2021) which provide comprehensive insight into a system's behavior by quantifying each input's contribution to output variance (first-order indices), including their interactions (total-order indices), across the entire parameter space (Saltelli et al., 2008). The computation of Sobol' indices requires a massive number of model evaluations to explore the entire parameter space, which increases exponentially with the number of parameters for grid-based approaches.

As indicated above, ocean BGC models involve numerous parameters, usually several times more than the state variables, ranging from half a hundred to a few hundred. The high number of parameters in the ocean BGC models make GSA computationally very expensive. Therefore, a preliminary screening analysis, such as the OAT screening approach introduced by Morris (1991), is usually carried out to reduce the number of input dimensions before a GSA based on Monte Carlo sampling is performed (e.g., Sankar et al., 2018; Wang et al., 2018). DGSMs, regarded as extensions of the Morris method (Morris, 1991) and related to Sobol' total-order indices (Sobol' & Kucherenko, 2009, 2010), have been widely employed for screening across various fields. However, the application of DGSM in ocean BGC models remains unexplored. Another way to limit the number of model evaluations to a few thousand is to implement a gradient-informed sampling to compute Sobol' indices (e.g., Andersen et al., 2021; Leles et al., 2018). Nonetheless, Prieur et al. (2019) showed that implementing a direct Monte Carlo sampling-based GSA is feasible for ocean BGC models. Some studies used additional techniques of GSA, such as Gaussian emulators or machine learning approaches (e.g., Scott et al., 2011).

The high demand for computational resources of GSA is why LSA is typically preferred over GSA in ocean BGC models. However, LSA can lead to misleading conclusions and, thus, to a misunderstanding of the influence of every individual process on the simulation results (Prieur et al., 2019). On the other hand, most of the GSA studies for ocean BGC models considered a small set of input parameters due to being computationally expensive. With the increasing availability of computational resources and advances in the GSA algorithms, it is now possible for the scientific community to make GSA the first choice, mainly when dealing with highly parameterized models (Prieur et al., 2019).

This study uses a high-performance computer to make the GSA of an ocean BGC model with a large set of parameters feasible. The GSA focused on computing the sensitivity measures of its input parameters. We consider the BGC model Regulated Ecosystem Model 2 (REcoM2, Hauck et al., 2013) in a one-dimensional configuration at two ocean sites for which observational time series data are available: 1) the Bermuda Atlantic Time-series Study (BATS, Steinberg et al., 2001) in the North Atlantic; and 2) the DYFAMED station (J. C. Marty, 2002) in the Mediterranean Sea. The GSA aims to identify the parameters whose uncertainty impacts the variability of BGC model outputs. We compute variance-based Sobol' indices (Saltelli et al., 2004; Sobol', 2001) to assess the most influential parameters for each location for different model outputs that are commonly considered for calibration and validation of BGC models.

2.2 Biogeochemical Models

Biogeochemistry deals with the exchange and transformations of chemical matter mediated by biological activity within and between reservoirs of the Earth system. In the marine environment, biogeochemistry focuses on the uptake and cycling of carbon and nutrients, e.g., nitrogen, phosphorus, silicon, and iron, between the ocean's organic and inorganic compartments. Therefore, ocean BGC models represent how these chemical species are converted from inorganic matter into organic matter and vice-versa. They are spatially explicit models consisting of components that describe the ocean's physical environment (e.g., temperature and salinity), the marine ecosystem (e.g., phytoplankton, zooplankton), the cycling of inorganic and detrital matter, and air-sea interactions and gas transfer.

Ocean BGC models are generally a set of nonlinear equations of marine physical, biogeochemical, and ecological processes (see Fennel et al., 2022; Franks, 2002) that are translated into computer code, with each equation expressing how each component of the model (e.g., the biomass of phytoplankton) changes with time due to the hydrodynamical effects (e.g., ocean circulation and mixing) and to fluxes between the various components of the marine ecosystem. The common form of these equations is:

$$\frac{\partial C}{\partial t} = dynamics + SMS(C) \tag{2.1}$$

Here C represents the concentration of a given biological state variable for instant nutrients or the biomass of phytoplankton groups; *dynamics* includes the advection and transport processes affecting the concentration of C. The term $SMS(C)$, where SMS stands for sources minus sinks, represents the changes of C due to biological processes, air-sea gas exchange, atmospheric deposition, sediment-water exchange, river input, and

any transport not arising from ocean circulation, such as the vertical sinking of organic matter.

The SMS components of BGC models describe how ocean biology converts inorganic into organic matters and vice-versa. Phytoplankton takes up inorganic elements, i.e., carbon, nitrogen, silicate, phosphorus, and iron, as nutrients. They gain energy from the sunlight using photosynthesis and convert the inorganic elements into organic ones when they grow. In turn, zooplankton consumes phytoplankton. When phytoplankton and zooplankton die, they sink as part of the detrital matter to the depth where most parts are remineralized back to inorganic form, and the rest are consumed by benthos - organisms that live at or near the bottom of the ocean.

One of the simplest forms of ocean BGC models is the nutrient-phytoplankton-zooplankton-detritus (NPZD) model (see Franks, 2002). It represents how the elements (commonly nitrogen) flow from inorganic nutrients (N) to phytoplankton (P), to zooplankton (Z), how organic matter ends up in a non-living organic pool (detritus, D), and how it is remineralized back to the inorganic pool (Figure 2.1).

In NPZD models, only nitrogen is typically processed as it is either available as an inorganic nutrient or present in phytoplankton, zooplankton, or detritus in organic form. Carbon and phosphorus are assumed to be in the Redfield ratios (Carbon:Nitrogen:Phosphorus = 106:16:1, Redfield, 1934) with nitrogen. The NPZD model describes the concentration of the four variables (N, P, Z, D) in a homogeneous volume or box by ignoring the physical term *dynamics*. Consequently, the equations are simplified to rate equations for the four state variables. Assuming a closed system, the terms on the right-hand side of the equation reflect transformations between the state variables.

$$\frac{dN}{dt} = \text{remineralization} - \text{uptake} \tag{2.2}$$

$$\frac{dP}{dt} = \text{uptake} - (\text{assimilated grazing}^1 + \text{sloppy feeding}^2 + \text{phyto. mortality}) \tag{2.3}$$

$$\frac{dZ}{dt} = \text{assimilated grazing} - (\text{excretion} + \text{zoo. mortality}) \tag{2.4}$$

$$\frac{dD}{dt} = \text{sloppy feeding} + \text{phyto. mortality} + \text{excretion} + \text{zoo. mortality} - \text{remineralization} \tag{2.5}$$

The conversions of variables are mass conserving, with gain in one component to another balanced by a corresponding loss. Also, the four equations make a coupled system of equations because the terms on the right-hand side depend on multiple state vari-

[1] Marine zooplankton consume a portion of phytoplankton, which refers to *assimilated grazing*.
[2] The unconsumed parts are released as dissolved or particulate organic matter, which refers to *sloppy feeding*.

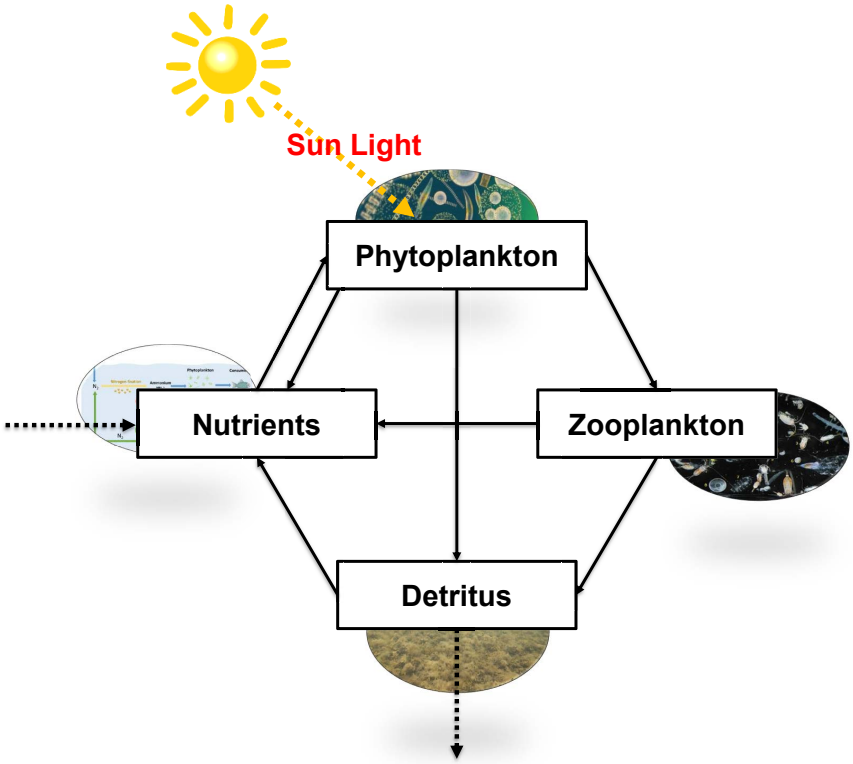

Figure 2.1 Schematic of a typical NPZD model with its compartments of nutrients, phytoplankton, zooplankton, and detritus. The elements (e.g., N) flow from the inorganic nutrients to phytoplankton, to zooplankton, produce nonliving organic matter detritus, and remineralize back to the inorganic pool. Arrows between compartments indicate the fluxes between them. The dotted arrows imply boundary interactions with the atmosphere and the ocean floor.

ables. A simplified scheme describes each BGC transformation, referred to as parameterization. The parameters are defined using conceptual understanding from laboratory experiments, field studies, and biological theory (Franks, 2002).

Most current ocean BGC models are extensions of the basic NPZD framework, including more complex BGC model components. Additional state variables include multiple nutrients such as nitrate, ammonium, phosphate, silicate, and dissolved iron; dissolved organic matters, e.g., dissolved organic carbon and nitrogen; numerous phytoplankton and zooplankton functional groups; dissolved gases, for example, oxygen; dissolved inorganic carbon and related properties such as alkalinity.

Ocean BGC models often employ simplified plankton grouping, often referred to as plankton functional types (PFTs, Baretta et al., 1995), for example, diatoms (silicifying phytoplankton), diazotrophs (nitrogen fixers), etc. Organism size is frequently used to differentiate between different PFTs, such as micro-, meso- and macrozooplankton. Multiple PFTs are included to account for the biogeochemically distinct roles played by

different functional groups.

Multiple nutrients are needed to address spatial and temporal switches between limiting nutrients and unique requirements by some functional phytoplankton groups, such as diatoms. Many ocean BGC models use the standard Redfield ratios of organisms and fluxes within the marine food web. This simplification allows models to use a single element (e.g., carbon, nitrogen, or phosphorus) as "currency", which reduces computational costs substantially. However, there are significant deviations around this Redfield stoichiometry (Martiny et al., 2013). A deeper understanding of the drivers of these deviations has enabled the development of a growing number of models with dynamic stoichiometry (Daines et al., 2014; Ward et al., 2012). This dynamism comes with a computational cost; each element within each PFT needs a variable rather than tracking a single nutrient currency for each. Chlorophyll is usually included within the models to compare the output to satellite ocean color data. Chlorophyll concentrations are often represented in the model by dynamic chlorophyll to carbon ratios (Geider et al., 1998). Due to photoacclimation, the chlorophyll to carbon ratio can vary by one order of magnitude (Fennel & Boss, 2003). Many, but not all, BGC models account for variations in the chlorophyll to carbon ratio using a parameterization of photoacclimation (Geider et al., 1997).

Including the inorganic carbon cycle is crucial for any ocean BGC model used for climate studies (Orr et al., 2017), which requires state variables presenting for dissolved inorganic carbon and alkalinity unless alkalinity can be inferred from other state variables, typically salinity. Including these two properties enables the calculation of other carbonate system properties, such as the partial pressure of carbon dioxide (pCO_2), which is required to parameterize air-sea gas exchange and pH. The latter is of considerable interest, given concerns about ongoing ocean acidification. Another standard state variable in ocean BGC models is oxygen because of its relevance for ecosystem health and functioning.

Ocean circulation and mixing are essential for redistributing the inorganic and organic tracers and plankton (phytoplankton and zooplankton). As such, these models must include a representation of ocean currents, mixing, temperature, salinity, and density. Vertical mixing is particularly important as it controls the supply of nutrients from deep waters to the euphotic zone where phytoplankton grow. The transformations between BGC state variables are connected to their advective and dispersive transport arising from ocean circulation by partial differential equations of the general form given by Equation 2.1, which can be rewritten for each state variable C:

$$\frac{\partial C}{\partial t} = -u \cdot \nabla_3 C + \nabla_2 \cdot k_H \nabla_2 C + \frac{\partial}{\partial z}\left(k_V \frac{\partial C}{\partial z}\right) + SMS\,(C) \tag{2.6}$$

Here, $u \cdot \nabla_3 C$ represents the advective transport of the constituent C (u is the fluid veloc-

ity vector), the terms $\nabla_2 \cdot k_H \nabla_2 C$ and $\frac{\partial}{\partial z}\left(k_v \frac{\partial C}{\partial z}\right)$ represent dispersion in the horizontal and vertical directions, respectively. The parameters k_H and k_V are the horizontal and vertical dispersion coefficients, respectively, while $\nabla_3 = \left(\frac{\partial}{\partial x}, \frac{\partial}{\partial y}, \frac{\partial}{\partial z}\right)$ and $\nabla_2 = \left(\frac{\partial}{\partial x}, \frac{\partial}{\partial y}\right)$ are three-dimensional and two-dimensional operators, respectively. The combination of the first three terms on the right-hand side is referred to simply as *dynamics* in Equation 2.1. As physical transport processes operate in all three spatial directions, Equation 2.6 is three-dimensional in space and includes partial derivatives to time, t, and the three spatial dimensions, x , y, and z. In addition to the equation of this form for each BGC state variable, ocean BGC models include partial differential equations for the physical state variables, including temperature, salinity, and velocity, and parameterizations for horizontal and vertical dispersion coefficients, which can vary in space and time.

Except for a few highly idealized cases — for example, when considering only one spatial dimension or a circular or rectangular two-dimensional domain with homogeneous initial conditions and constant forcing — the solution to these equations cannot be obtained analytically and must be approximated numerically (Glover et al., 2011). The equations are discretized using finite differences in time with time steps Δt on a three-dimensional grid representing the model domain. In the finite-difference methods, the derivatives in the differential equations are replaced by finite difference approximations; for instance, $\frac{\partial C}{\partial t}$ and $\frac{\partial C}{\partial x}$ become $\frac{\Delta C}{\Delta t}$ and $\frac{\Delta C}{\Delta x}$, respectively. Replacing the differential equations leads to a system of prognostic equations, which include only basic arithmetic operations on defined quantities that can be carried out on a computer (Glover et al., 2011).

2.2.1 Regulated Ecosystem Model 2

In this study, we consider the BGC model Regulated Ecosystem Model 2 (REcoM2, Hauck et al., 2013). REcoM2 describes two phytoplankton classes, diatoms, and nanophytoplankton, with an implicit representation of calcifiers and a generic heterotrophic zooplankton class (Figure 2.2). It has one class of organic sinking particles whose sinking speed increases with depth and a class of organic matters.

REcoM2 simulates 22 passive tracers (see Figure 2.2 and Appendix A.1). The intracellular stoichiometry of carbon, nitrogen, calcite and chlorophyll (Carbon:Nitrogen: Chlorophyll) pools for nanophytoplankton and carbon, nitrogen, silicate, and chlorophyll (Carbon:Nitrogen:Silica:Chlorophyll) pools for diatoms are allowed to respond dynamically to environmental conditions following Geider et al. (1998) and Hohn (2009) for the silicate quota. The intracellular iron pool is a function of the intracellular nitrogen concentration (fixed Iron:Nitrogen), as iron is physiologically mainly linked to nitrogen metabolism and the photosynthetic electron transport chain (Behrenfeld & Milligan, 2013; Geider & La Roche, 1994). Dead organic matter is transferred to detritus by aggregation and grazing by one zooplankton class, and the sinking and advection of de-

tritus are represented explicitly. The model has two external iron sources: atmospheric dust deposition and sedimentary input. The iron cycle in the model is driven by biological uptake, remineralization, and scavenging onto biogenic and lithogenic particles. There are 68 BGC parameters in REcoM2 which are summarized in Appendix A.2.

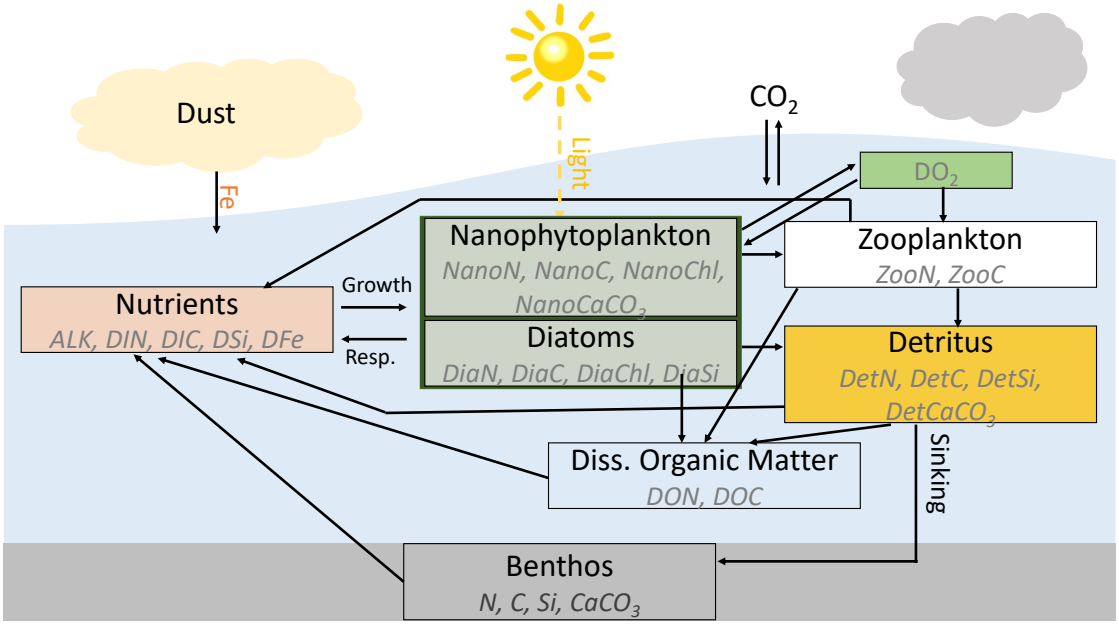

Figure 2.2 Schematic diagram of the BGC model REcoM2. The abbreviations are for the 22 passive tracers – dissolved inorganic carbon (DIC) and alkalinity (ALK) for the carbonate system; the macro-nutrients dissolved inorganic nitrogen (DIN) and silicic acid (DSi); the trace metal dissolved iron (DFe), nanophytoplankton biomass content of carbon (NanoC), nitrogen (NanoN), calcium carbonate ($NanoCaCO_3$) and chlorophyll (NanoChl); diatoms biomass content of carbon (DiaC), nitrogen (DiaN), silica (DiaSi) and chlorophyll (DiaChl); zooplankton biomass content of carbon (ZooC), nitrogen (ZooN); detritus content of carbon (DetC), nitrogen (DetN), silicate (DetSi) and calcium carbonate ($DetCaCO_3$); extra-cellular dissolved organic carbon (DOC) and nitrogen (DON); and dissolved oxygen (DO_2). Arrows depict source and sink terms.

2.3 Global sensitivity analysis

Many mathematical models involve input parameters that are not precisely known. GSA aims to identify the parameters whose uncertainty influences the variability of a Quantity of Interest (QoI) most - for instance, by computing Sobol' indices. Let our model output of interest be Y, which is, in abstract terms, a function of the vector of the distributed parameters, $\vec{X} = \{X_1, X_2, X_3, \cdots, X_n\}$ with $n = |\vec{X}|$, i.e.,

$$Y = f\left(\vec{X}\right) = f\left(X_1, X_2, X_3, \cdots, X_n\right) \tag{2.7}$$

2.3.1 Uncertainty Propagation

Sources of uncertainties in a mathematical model can be multifold, especially for complex models like ocean BGC. Since the scope of GSA is to identify which model parameters are most influential in the variability of QoIs, we project all uncertainties onto the model input parameters. The main idea is to propagate uncertainties through the model by perturbing the parameters to determine the QoI's sensitivities with respect to these uncertainties. We use the Monte Carlo method, where distribution functions determine the range and probability of parameter values for uncertain parameters.

Deterministic numerical integration encounters problems if the underlying function has many variables. The number of function evaluations required increases exponentially with the number of dimensions, sometimes called the 'curse of dimensionality.' The Monte Carlo method breaks out of this dimensional constraint by solving the definite multidimensional integral for a QoI probabilistically. Such modification will turn the inherently deterministic model into a stochastic one.

In order to describe the domain of uncertainty, we define a probability space for the parameters of $\vec{X}$ by assigning suitable probability density functions $r(\vec{X})$. The respective probability functions $r(\vec{X})$ enable us to formulate the expected value of Y, $\mathbb{E}[Y]$ which can be written mathematically as:

$$\mathbb{E}[Y] \equiv \int_{\Omega_n} f\left(\vec{X}\right) r\left(\vec{X}\right) d\vec{X} \tag{2.8}$$

where $\Omega_n \subseteq \mathbb{R}^n$ is the parameter domain in the n–dimensional hypercube. However, without loss of generality we assume that $\Omega_n \subseteq [0,1]^n$ instead of $\mathbb{R}^n$ since all parameters can be, in theory, mapped to the n-dimensional unit hypercube thanks to the inverse transformation method.

2.3.2 Derivative-based Global Sensitivity Measure (DGSM)

DGSM is a model independent GSA approach that examines the relative influence of different model parameters on a given QoI by calculating the expected value of the square of the derivative of the function f with respect to that parameter.

Let $f : \mathbb{R}^n \to \mathbb{R}$ and denoted by $\frac{\partial f(\vec{X})}{\partial X_i}$ its partial derivative with respect to the input parameter X_i evaluated at $\vec{X} = (X_1, X_2, \cdots, X_n)^T \in \mathbb{R}^n$. The DGSM, as defined by

Sobol' and Kucherenko (2009), with respect to the i-th input can be written as

$$DGSM_i \equiv \mathbb{E}\left(\frac{\partial f}{\partial X_i}\left(\vec{X}\right)\right)^2 = \int \left(\frac{\partial f}{\partial X_i}\left(\vec{X}\right)\right)^2 r\left(\vec{X}\right) d\vec{X} \tag{2.9}$$

Here, $\mathbb{E}$ denotes the expected value of the squared partial derivative with respect to the input X_i and $r(\vec{X})$ is the probability density functions of $\vec{X}$.

The principle underlying this approach is that the parameters that cause larger variations in the model output will have larger derivatives, and hence, will have larger DGSM values. Therefore, the DGSM value provides an indication of the relative influence of the input parameters on the output.

For simple and differentiable models the derivative may be directly calculated using calculus. However, for more complex models, particularly those involving non-differentiable functions, or many input parameters like ocean BGC, one needs to resort to numerical methods to approximate the derivative. The most common approach is the finite difference method, which involves calculating the change in the model output for a small perturbation in the parameter of interest:

$$\frac{df}{dX_i} \approx \frac{f\left(X_1, \cdots, X_i, X_i + \Delta X_i, \cdots, X_n\right) - f\left(X_1, \cdots, X_i, X_i - \Delta X_i, \cdots, X_n\right)}{2\Delta X_i} \tag{2.10}$$

where, ΔX_i is a small increment to the parameter X_i while the other input parameters remain unchanged.

2.3.3 Variance-based sensitivity measures

Since we treat the input parameters $\vec{X} = \{X_1, X_2, \cdots, X_n\}$ as random variables, the model response Y is turned into stochastic due to the uncertainty in $\vec{X}$, although the integral is deterministic. The overall uncertainty in the sense of variability (or spread) in Y caused by $\vec{X}$ is the variance of Y, $Var[Y]$. We are interested in variance-based sensitivity measures that quantify how much of $Var[Y]$ can be attributed to each X_i, for $i \in \{1, 2, \cdots, n\}$.

The Sobol' indices (Sobol, 1993) were first introduced to measure the sensitivity of the output to each of the inputs X_i. Under the assumption of independent inputs, $Var[Y]$ is decomposed as a sum of variance components attributable to each X_i. Homma and Saltelli (1996) define the first-order Sobol' index, S_i of X_i as

$$S_i \equiv Var\left[\mathbb{E}\left[Y|X_i\right]\right] = Var\left[Y\right] - \mathbb{E}\left[Var\left[Y|X_i\right]\right] \tag{2.11}$$

By definition, S_i leaves out the variability of Y caused by interactions of X_i with other

inputs. The right-hand side of Equation 2.11 can be interpreted as the expected reduction in $Var[Y]$ when we fix the value of X_i to a constant. To complement the first-order Sobol' index (Homma & Saltelli, 1996) define the total-order Sobol' index T_i of X_i as

$$T_i \equiv Var\left[Y\right] - Var\left[\mathbb{E}\left[Y|X_{\sim i}\right]\right] = \mathbb{E}\left[Var\left[Y|X_{\sim i}\right]\right] \tag{2.12}$$

where $X_{\sim i}$ denotes the vector of all input parameters $\vec{X}$ except X_i. Here, T_i is the expected variance that remains in Y when the values of every parameter except X_i could be fixed to a constant.

These two Sobol' indices are widely used and are a robust measure of parameter sensitivity. The first- and total-order sensitivity indices can be related to the objectives of GSA (Saltelli et al., 2004, 2008). The first-order Sobol' index, also known as the main effect (Homma & Saltelli, 1996), tells us how much variance of model output Y, $Var[Y]$, can be reduced when we fix the respective parameter. The sum of the first-order Sobol' indices can not exceed 1 (Glen & Isaacs, 2012). Therefore, in the case of a large set of input parameters, the first-order Sobol' indices of many input parameters are close to 0, and the corresponding parameters have low main effects. The main effects or total-order Sobol' indices are relevant to parameter prioritization in identifying the most influential parameter since fixing a parameter to a constant with the highest index value would, on average, lead to the most significant reduction in the output variation. However, a low first-order Sobol' sensitivity index value does not imply that the model output is independent of the input parameter X_i as it does not capture the interaction with other parameters (Plischke et al., 2013; Saltelli et al., 2008).

The total-order Sobol' indices, also known as the total effects (Homma & Saltelli, 1996), provide us with the sensitivity due to interactions among a given parameter X_i and all other parameters. The total-order index is relevant in identifying the least influential parameters since fixing any parameter with a minimal total effect would not significantly reduce output variation. Therefore, using the total-order Sobol' index to identify which parameter can be excluded for surrogate modeling would be more exact, though computationally expensive.

GSA sometimes includes a screening step to reduce the computational burden, as Saltelli et al. (2008) recommended. The screening step aims to identify all non-influential parameters conditional on the chosen QoI and concentrate the detailed GSA on influential parameters. We also applied this approach in this study. After screening, we deal with uncertainty propagation, where some values of $\vec{X}$ are considered to be uncertain while others are not. We thus split the input into a vector $\vec{\chi}$ of undisturbed parameters and a vector $\vec{x}$ of parameters screened as uncertain, i.e., $\vec{X} = (\vec{\chi}, \vec{x})$, which enable us to reformulate $\mathbb{E}[Y]$ with regard to $\vec{X}$:

$$\mathbb{E}\left[f\left(\vec{\chi},\vec{x}\right)\right] \equiv \int_{\Omega_d} f\left(\vec{\chi},\vec{x}\right) r\left(\vec{x}\right) d\vec{x} \tag{2.13}$$

in contrast to Equation 2.8 we integrate over the function of vector $\vec{x} = (x_1, x_2, \cdots, x_d)$. The integral bounds are, therefore, only d–dimensional here.

2.3.4 Computing of Sobol' indices

For simple models, SA can be done analytically by directly computing the first- and total-order effects according to Equations 2.11 and 2.12. However, this is generally prohibitive for complex models like ocean BGC. In those cases, one evaluates the model with perturbed input parameter values and then uses the resulting output values to estimate sensitivity indices of interest using suitable sample averages. Many different estimation procedures of the Sobol' indices have been proposed and studied. However, the traditional method has two big drawbacks. First, it relies on a particular experimental design that may be unavailable in practice. Second, its computational cost may be prohibitive when estimating several indices. Naturally, the cost of an estimator depends on the cost of each evaluation of the computational model and the number of evaluations. For the traditional estimator, the number of model calls for all the first-order Sobol' indices grows linearly with the number of input parameters. For most of the traditional estimators, the number of required model evaluations is $(n + 2) \times N$, where n is the number of input parameters and N is the sample size (i.e., the number of perturbed input parameter replica).

In recent years a few estimators have been developed to estimate the first-order global sensitivity indices with only N number of model evaluations, for example, the random balance designs method (Tarantola et al., 2006) or double loop reordering approaches proposed by Kucherenko and Song (2017). Gamboa et al. (2022) presented an estimator based on rank statistics using an empirical correlation coefficient introduced by Chatterjee (2020), which can estimate the first-order Sobol' indices with a unique N-sample, thus, N model evaluations. We applied the estimator developed by Gamboa et al. (2022) to compute first-order Sobol' indices in this study. For total-order Sobol' indices, we utilized the nearest neighbor search proposed in Broto et al. (2020), which needs only N model evaluations.

2.3.5 Implementation in this study

In this study, we used a one-dimensional (1–D) coupled hydrodynamic-biogeochemical model. In the coupled model, the Massachusetts Institute of Technology General Circulation Model (MITgcm, Marshall, Adcroft, et al., 1997) simulates ocean dynamics

and tracer transport, while REcoM2 (see Section 2.2.1) handles ocean BGC processes and transformation. MITgcm is a finite volume, general circulation model with a non-hydrostatic capability that allows the model to be used for describing small-scale to global-scale processes. REcoM2 is coupled with MITgcm as a combined model system.

We used the identical model set-up of Mamnun et al. (2022). A 1–D configuration of the coupled MITgcm-REcoM2 was set up at two ocean sites, BATS in the North Atlantic Ocean and DYFAMED in the Mediterranean Sea, for which observational time series data are available. Both stations are in an oligotrophic environment, i.e., exhibiting low primary production.

The 1–D water column model consists of 30 vertical layers. The vertical grid intervals increase as the depth increases, starting at 10 meters near the surface and reaching 100 meters near the lowermost layer, encompassing a total model depth of 1188 meters. Since we focus on ecosystem processes within the euphotic zone and their connection to vertical nutrient transport from the mesopelagic, we have restricted our model configuration to slightly over the upper 1000 meters, ensuring ample distance from the seabed at both sites. The model time step was 1 hour (3600 seconds).

The model temperature, salinity, DO_2, DIN, and DSi fields were initialized with in situ bottle data. We obtained in situ data for BATS from its website (`https://bats.bios.edu/`) and for DYFAMED from Coppola et al. (2021). We initialized the ALK and DIC fields of the model from the mapped climatology of the GLobal Ocean Data Analysis Project (GLODAPv2, Lauvset et al., 2016) at both sites, and DFe with data from the U.S. GEOTRACES North Atlantic Transect (GA-03, Boyle et al., 2015) at BATS and from the data reported in Guieu and Blain (2013) at DYFAMED. We initialized all other passive tracers with small uniform values. We force the model with inter-annually varying atmospheric forcing data from the Coordinated Ocean Research Experiments version 2 (COREv2, Large & Yeager, 2008) for BATS and ERA5 (Hersbach et al., 2020) single levels data for DYFAMED. We used the monthly dust deposition field from the present-day simulation of Albani et al. (2014) to compute DFe input flux from the atmosphere, assuming 3.5% iron content in dust particles and 2% solubility.

As mentioned above, REcoM2 includes 68 uncertain input parameters. Our model does not touch the ocean bottom; therefore, we excluded the five parameters related to the benthic layer. In REcoM2, the linear slope of Arrhenius function is fixed to 4500, therefore, we also excluded this parameter from our analysis. We considered the remaining 62 parameters for the GSA.

The first step to implement a GSA was to propagate uncertainties into the model by perturbing the input parameters applying the Monte Carlo method. We assume that each parameter has some predefined reference value. The uncertainties address relatively small deviations. It is plausible to employ a probability density function where the statistical properties of mean, median, or mode lie close to the reference value and

where values are more improbable the more they diverge from the reference value. Such intuition naturally excludes uniform or exponential distributions, for example. A commonly used distribution for this purpose is the normal distribution. With a normal distribution $N(1, \sigma^2)$ for some standard deviation, we would center its bell curve to 1 such that uncertainties are realized by a factor multiplication of the reference value with a normally distributed variable. However, a normal distribution may not be suitable for BGC parameters. Campbell (1995) demonstrated that log-normal statistics reasonably describe many BGC variables (e.g., chlorophyll-a concentrations) in the ocean. Therefore, a common distribution used for BGC parameters is the log-normal distribution. Furthermore, BGC parameters are always positive quantities. Utilizing the log-normal parameter guarantees the positiveness of parameter values. Notably, some BGC parameters are ratio of quantities and constrained between 0 and 1, thus assumed to follow a beta distribution.

The Monte Carlo approach samples points uniformly at random on a unit hypercube Ω_n. In this study, we employ the pseudo-random number generator, `random`, embedded in the core Python library (van Rossum & the Python development team, 2022) for generating random numbers. We transformed the random values onto a probability density function in the interval $[0; 1)$. For the transformation, we specified a probability distribution for each input parameter with the following assumption.

1. The uncertainties of the various parameters are independent.
2. The ratio parameters constraining value between 0 and 1 follow a beta distribution.
3. The parameter "reference temperature" follows a normal distribution.
4. Other parameters follow a log-normal distribution.
5. The standard deviation of the distribution is 50% of their reference value.

We used a sample size of one hundred thousand (10^5). Therefore, the Monte Carlo method gave 10^5 sets of parameter values. The sample size 10^5 was chosen, guided by a convergence test.

Application of a quasi-Monte Carlo (qMC) method based on low discrepancy sequences (e.g., Sobol' sequences) often surpasses the performance of standard Monte Carlo methods by several orders of magnitude, which manifests a noteworthy decrease in the number of necessary model evaluations (Kucherenko & Song, 2017; Kucherenko et al., 2011; Ökten & Liu, 2021). However, a preceding study (Thelen, 2021) has demonstrated that despite the better convergence rate of qMC compared to the standard Monte Carlo, the qMC based Sobol' sequences sometimes give negative or unreasonably high values of Sobol' indices for REcoM2 model parameters. Although demanding in computation resources, a standard Monte Carlo method-based sampling for GSA has become affordable, thanks to the advancements of high-performing computers.

The next step was to evaluate the model for each parameter set. We performed model simulations for ten years (1990–1999) at both stations and saved time-average output

values every five days. To minimize the effects of model initialization, we excluded the first five years of simulations as a spin-up period (1990–1994). The output values were processed across the analysis period of the later five years (1995–1999).

Running the ocean BGC model several thousand times is computationally very costly despite using a 1–D column model. The high demand for computational resources is why LSA is typically preferred in practice over GSA for ocean BGC models. For computationally expensive ocean BGC models with many parameters, applying a standard Monte Carlo method-based sampling for GSA is often not feasible due to the necessity for a substantial sample size. In this study, we make GSA tractable with a large set of parameters using a high-performance computer. A single model simulation took around 5 minutes using one processor core. Using 960 cores (10 compute nodes) of the computer we were able to perform 100,000 simulations in about 9 hours.

We computed Sobol' indices using the `R` package `sensitivity` (Iooss et al., 2022). Though, the estimator used in this study allows us to compute the total-order Sobol' indices with $N = 10^5$ model evaluations, with all 62 model parameters, the estimator needs a very large matrix for computing the total-order Sobol' indices. This makes it impractical to compute the total-order Sobol' indices for all 62 parameters, even in a high-performance computer.

To reduce the computational burden, we carried out a screening step using first-order Sobol' indices and DGSM. The screening step aims to identify all influential and non-influential parameters on the chosen QoIs and concentrate the detailed GSA on influential parameters Saltelli et al. (2008).

We computed DGSMs utilizing the Python library Sensitivity Analysis Library (SALib, Herman & Usher, 2017; Iwanaga et al., 2022). We drew samples using the qMC (Sobol') sequence combined with the finite difference approach with small increment, as implemented in the SALib for each input parameter. The abovementioned probability distribution with a 50% standard deviation determined the bounds of parameter values. The sample size was 1000.

The screening step identified 28 uncertain parameters (see section 4.1) for which we computed both first- and total-order Sobol' indices. Note that the screening step is essential for a traditional method as it reduces the number of input parameters, thus reducing the requirements of high number $N \times (n+2)$ of model runs, where n is number of input parameters.

2.3.6 Quantities of interest

One defines the QoIs according to the primary scientific objectives of the sensitivity study. We considered QoIs that are commonly used for the calibration and validation

of BGC models as our QoIs. GSA applies to scalar output quantities. Therefore, to apply the GSA method, we reduced the time variations of QoIs to scalar indicators by time-averaging. The QoIs considered in the study are listed in Table 2.1.

Table 2.1 Quantities of interest chosen for the present study.

QoI	**Description**
SURF_TOTCHL	Mean surface total chlorophyll-a
SURF_NANOCHL	Mean surface nanophytoplankton chlorophyll-a
SURF_DIACHL	Mean surface diatom chlorophyll-a
MBP_TOTCHL	Annual peak surface total chlorophyll-a
MBP_NANOCHL	Annual peak surface nanophytoplankton chlorophyll-a
MBP_DIACHL	Annual peak surface diatom chlorophyll-a
TOTNPP	Mean net primary production (NPP)
NANONPP	Mean nanophytoplankton NPP
DIANPP	Mean of Annual diatom NPP
EXPORTC	Annual mean export production of carbon
pCO_2	Mean partial pressure of CO_2
CO_2FLUX	Mean surface flux of CO_2

2.4 Results

2.4.1 Screening step

In the screening step, we estimated the first-order Sobol' indices and their 95% confidence interval for all 62 parameters regarding each QoI at both locations. The first-order Sobol' indices for mean surface chlorophyll-a at both stations are presented in Figure 2.3A. As we used a large sample size ($N = 10^5$), the 95% confidence intervals are close to zero and not visible in a plot therefore not shown in Figure 2.3B. A threshold value of 0.02 clearly separates the high and low first-order indices (Figure 2.3A).

Only ten parameters have a first-order index greater than the threshold value of 0.02 against mean surface chlorophyll-a at least one station (Figure 2.3A). We obtained similar results for the other QoIs (see Appendix A.3). 26 model parameters have a first Sobol' index greater than 0.02 for at least one of the QoIs and for at least one station.

However, employing first-order Sobol' indices to screen out non-influential parameters has certain limitations. Specifically, it can result in erroneous conclusions (Sobol' et al., 2007) as the first-order index of a parameter does not account for its interaction with

other parameters. A parameter with a negligible estimated first-order Sobol' index may still have a high total-order index due to significant interactions with other parameters, and thereby the parameter remains influential to the variability of model outputs. To address this concern, we supplemented the screening using first-order indices with DGSM, given its global nature and relation with Sobol' total order indices (Sobol' & Kucherenko, 2009). We computed DGSMs and their 95% confidence interval of all 62 parameters for each of the QoIs. Figure 2.3B shows DGSMs and their 95% confidence interval for mean surface chlorophyll-a (SURF_TOTCHL).

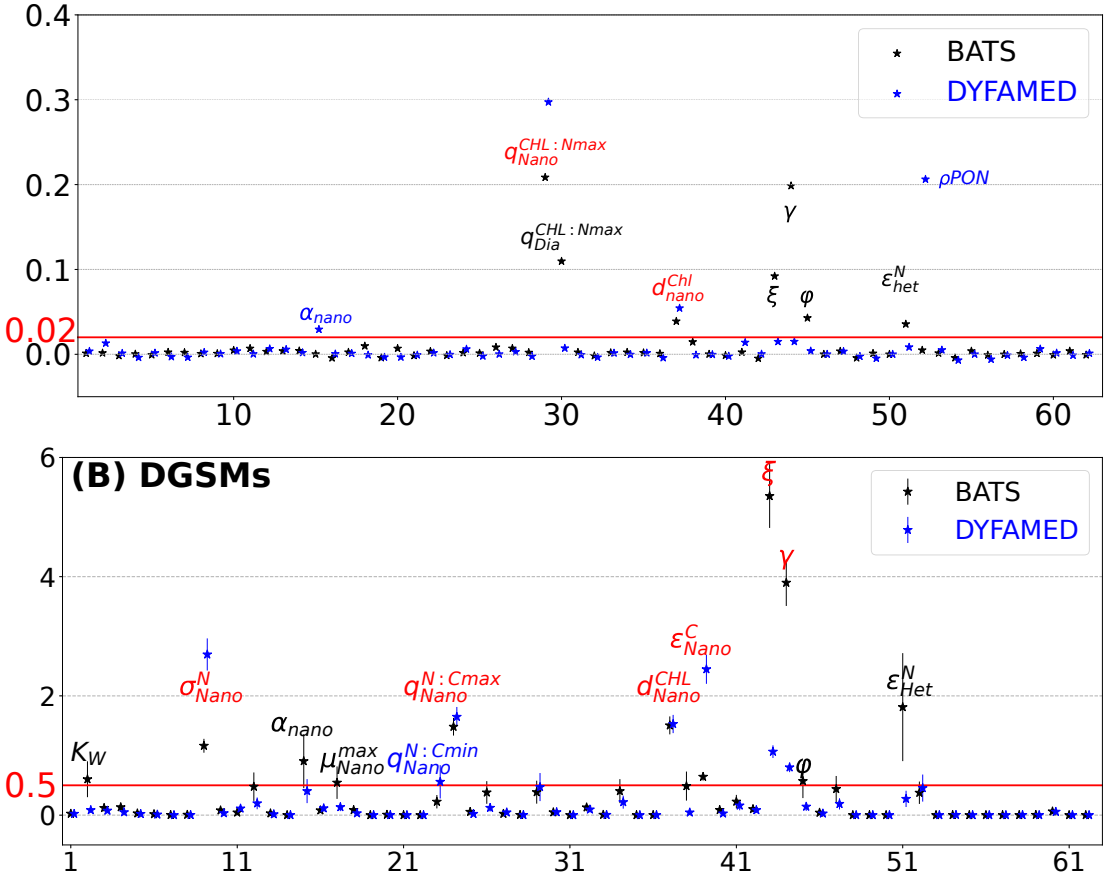

Figure 2.3 A) First-order Sobol' indices and B) DGSMs and their 95% confidence interval of 62 parameters for mean surface chlorophyll-a (SURF_TOTCHL). In both plots, parameters for which the sensitivity measures are greater than the threshold value at both stations are written in red, at only BATS in black, and at only DYFAMED in blue. The x-axis labels are the serial number of parameters in Appendix A.2.

Similar to Sobol' first-order indices we can identify a threshold value that clearly separates the high and low DGSM. In case of DGSM the threshold value is 0.5, much higher than the one for first-order indices because of their interaction effects. Overall, the important parameters are the same except for nitrogen uptake ratio (σ^{N}_{Dia}) and the

minimum cell quota of nitrogen for nanophytoplankton, which have high DGSMs but low Sobol' first-order indices at both stations. On the other hand, nanophytoplankton maximum chlorophyll to nitrogen ratio ($q_{Nano}^{CHL:Nmax}$) has high first-order indices but low DGSMs.

We applied an approach analogous to the one previously employed for screening parameters through the utilization of Sobol' first-order indices to DGSMs. Similar to Sobol' first order indices only 12 parameters exhibit high DGSM values for SURF_TOTCHL and can be distinctly separated by a threshold value of 0.5 (see Figure 2.3B). Through the utilization of DGSM, we shortlisted 26 parameters. It is noteworthy that each approach shortlisted two uncommon parameters to each other. Figure 2.4 summarizes the number of QoI for which the estimate of the first-order Sobol' index and DGSMs exceeded the threshold value. We merged both approaches and shortlisted 28 parameters based on the fact that they are influential for at least one chosen QoI at least at one station. The shortlisted parameters are presented in Table 2.2.

2.4.2 Parameter sensitivity

We computed first- and total-order Sobol' indices of those 26 influential shortlisted parameters for each of the QoIs at both locations. The first-order Sobol' indices of the shortlisted parameters corroborated with the first-order Sobol' indices of the screening step. The relative ranking of the most influential parameters was consistent for all the QoIs at both locations.

Figure 2.5 shows the total-order Sobol' indices of the short-listed parameters for mean surface chlorophyll-a at both stations. The total-order indices are far larger than the first-order indices. This shows that the parameters contribute to the total variance primarily through their interactions with other parameters. However, it is not possible to define a threshold value for the total-order Sobol' indices. Nonetheless, total-order Sobol' indices provide us with the rank of the most critical parameters and bring important information since input parameters with a very low value for both first-order and total-order Sobol' index can be fixed to a reference value in a calibration procedure. The seven most influential parameters for mean surface chlorophyll-a, annual peak surface chlorophyll-a, mean NPP, mean carbon export production and mean pCO_2 with their ranking according to the first- and total-order Sobol' indices are presented in Table 2.3 for both stations. Though the ranking order differs in the two locations, the top seven influential parameters are more or less similar across both stations.

Figure 2.6 shows the first- and total-order Sobol' indices regarding all of the QoIs for each of two stations. As total-order indices are large and not on a similar scale across the two stations, we normalized them for better visibility and comparison; and plotted the normalized values. Overall, the most sensitive parameters are the maximum chloro-

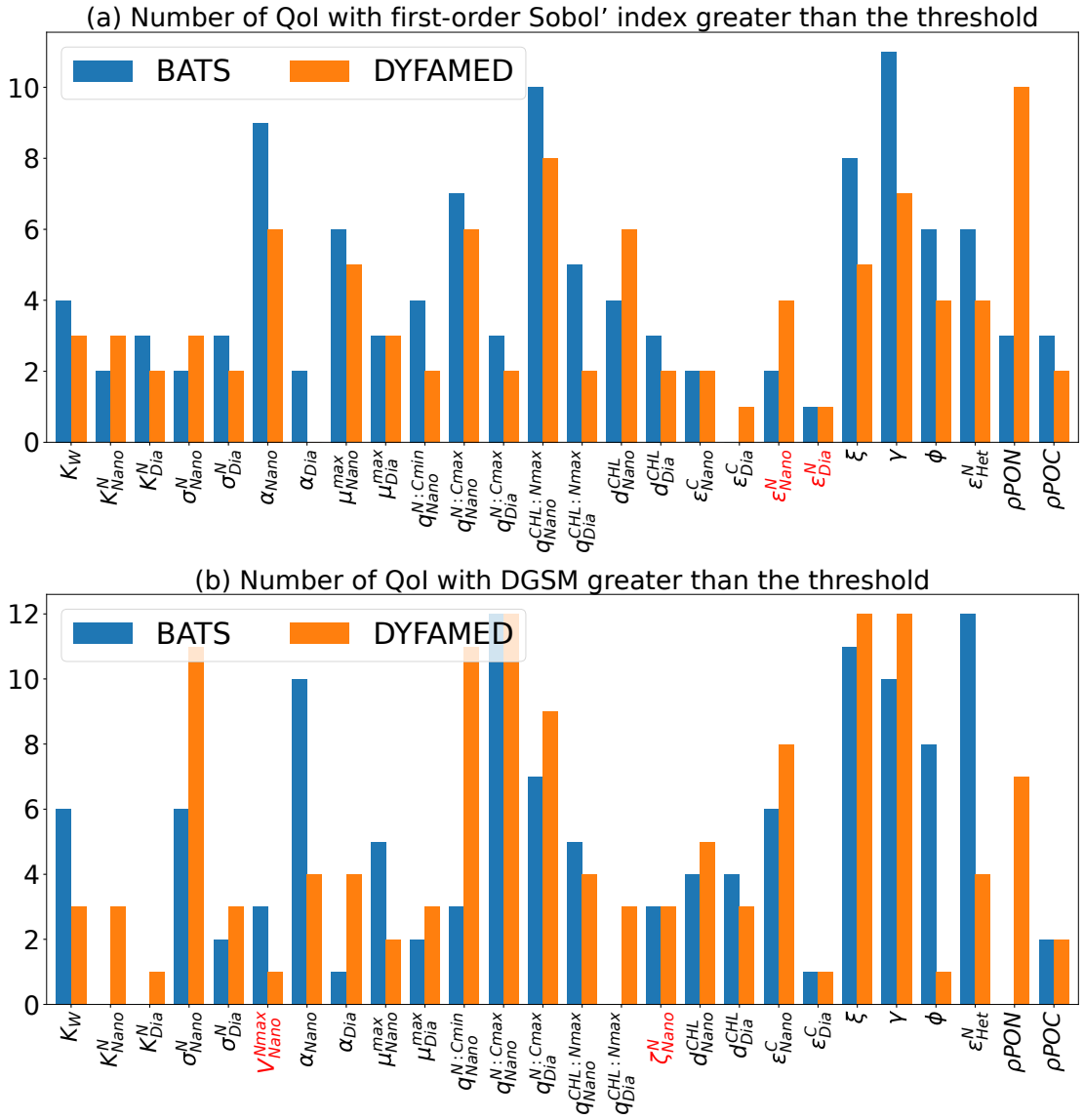

Figure 2.4 Number (count) of QoIs (y-axis) for which the estimate of; A) the first-order index and B) the DGSM exceed a threshold value. Here, for each of the screening approaches, the parameters whose sensitivity measures are larger than the threshold for at least one QoI at any one station are plotted and rest of the parameters whose sensitivity measures stayed within the threshold value for all QoIs at both locations are not shown. The symbol of uncommon parameters in each group is written in red.

phyll to nitrogen ratio, chlorophyll degradation rate, zooplankton grazing and excretion parameters, photosynthesis parameters, and nitrogen and carbon remineralization rate.

For the mean surface chlorophyll-a (SURF_TOTCHL) simulation, the maximum chlorophyll-a to nitrogen ratio of nanophytoplankton ($q_{Nano}^{CHL:Nmax}$) and two grazing parameters, the maximum grazing rate (ξ) and grazing efficiency (γ) are the most influential parameters

Table 2.2 Shortlisted parameters for which the first-order Sobol' indices and DGSMs are greater than the threshold values for at least one QoI at any one station.

Parameter	Description
K_W	Light attenuation coefficient
K^N_{Nano}	Nanophytoplankton half-saturation constant for nitrogen uptake
K^N_{Dia}	Diatom half-saturation constant for nitrogen uptake
σ^N_{Nano}	Nanophytoplankton nitrogen to carbon uptake ratio
σ^N_{Dia}	Diatom nitrogen to carbon uptake ratio
V^{Nmax}_{Nano}	Nanophytoplankton maximum nitrogen uptake
α_{Nano}	Nanophytoplankton initial slope of P-I curve
α_{Dia}	Diatom initial slope of P-I curve
μ^{max}_{Nano}	Nanophytoplankton maximum photosynthesis rate
μ^{max}_{Dia}	Diatom maximum photosynthesis rate
$q^{N:Cmin}_{Nano}$	Nanophytoplankton minimum cell quota of nitrogen (N:C)
$q^{N:Cmax}_{Nano}$	Nanophytoplankton Maximum cell quota of nitrogen (N:C)
$q^{N:Cmax}_{Dia}$	Diatom Maximum cell quota of nitrogen (N:C)
$q^{CHL:Nmax}_{Nano}$	Nanophytoplankton maximum of chlorophyll to nitrogen ratio
$q^{CHL:Nmax}_{Dia}$	Diatom maximum of chlorophyll to nitrogen ratio
ζ^N_{Nano}	Nanophytoplankton cost of nitrogen biosynthesis
d^{CHL}_{Nano}	Nanophytoplankton chlorophyll degradation rate
d^{CHL}_{Dia}	Diatom chlorophyll degradation rate
ϵ^C_{Nano}	Nanophytoplankton excretion rate of carbon
ϵ^C_{Dia}	Diatom excretion rate of carbon
ϵ^N_{Nano}	Nanophytoplankton excretion rate of nitrogen
ϵ^N_{Dia}	Diatom excretion rate of nitrogen
ξ	Maximum grazing rate by zooplankton
γ	Grazing efficiency of zooplankton
φ	Half-saturation constant for grazing
ϵ^N_{Het}	Zooplankton nitrogen excretion rate
ρ_{PON}	Particulate organic nitrogen degradation rate of detritus
ρ_{POC}	Particulate organic carbon degradation rate of detritus

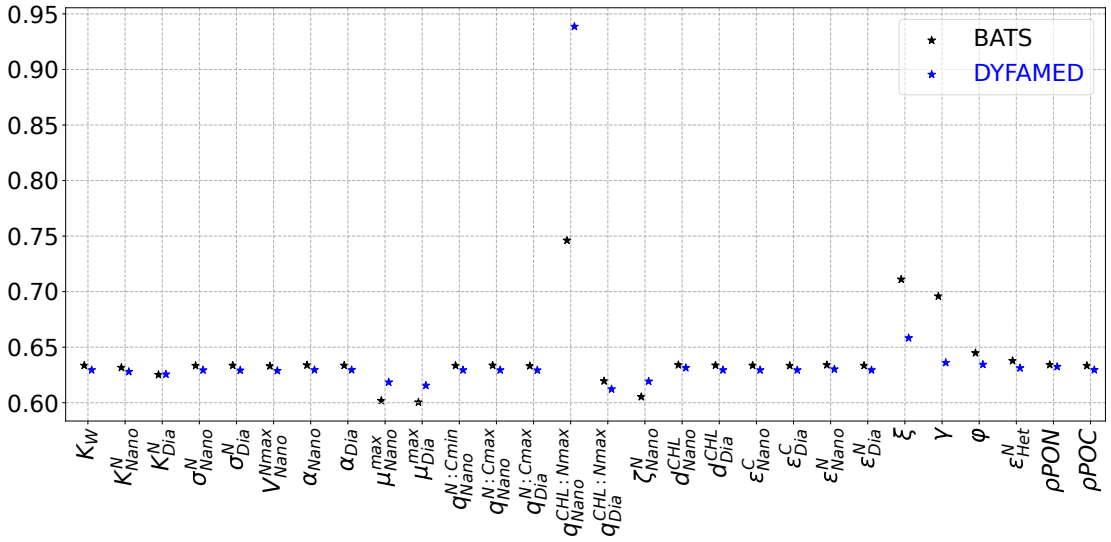

Figure 2.5 Total-order Sobol' indices of the 26 shortlisted parameters regarding mean surface chlorophyll-a (SURF_TOTCHL). For a description of the parameters, see Table 2.2.

at both stations (Table 2.3 and Figure 2.6). At DYFAMED, ξ and γ show less sensitivity for first-order Sobol' indices but are highly influenced by their interactions with other parameters. Other sensitive parameters at BATS are the zooplankton nitrogen excretion rate (ϵ^N_{Het}), the nanophytoplankton chlorophyll degradation rate (d^{CHL}_{Nano}), the half-saturation constant for grazing (φ), the nanophytoplankton excretion rate of nitrogen (ϵ^N_{Nano}), the maximum chlorophyll to nitrogen ratio of diatoms ($q^{CHL:Nmax}_{Dia}$), the initial slope of photosynthesis-irradiance curve of nanoplankton (α_{Nano}), diatom chlorophyll degradation rate (d^{CHL}_{Dia}), and the maximum photosynthesis rate of nanophytoplankton (μ^{max}_{Nano}). These parameters are also sensitive at DYFAMED except for two diatom-related parameters, d^{CHL}_{Nano} and d^{CHL}_{Dia}. In addition, the particulate organic nitrogen degradation rate of detritus (ρPON) is also sensitive at DYFAMED (Figure 2.6).

The sensitive parameters for nanophytoplankton surface chlorophyll-a (SURF_NANOCHL) are similar to SURF_TOTCHL except for diatom-related parameters. From the model outputs, we found that the diatoms had less than a 10% contribution to the annual mean surface chlorophyll-a concentration; therefore, it is apparent that the diatom parameters are not sensitive to SURF_NANOCHL. Similar to SURF_NANOCHL, the maximum chlorophyll-a to nitrogen ratio of diatom is the most influential parameter for the diatom surface chlorophyll-a (SURF_DIACHL). However, the other sensitive parameters for this QoI vary from SURF_TOTCHL and SURF_NANOCHL at both stations. The grazing parameters show less sensitivity to SURF_DIACHL compared to SURF_NANOCHL. For SURF_DIACHL, some of the nanophytoplankton parameters e.g., α_{Nano}, μ^{max}_{Nano}, $q^{CHL:Nmax}_{Nano}$ and $q^{N:Cmax}_{Nano}$ (nanoplankton maximum cell quota of nitrogen) are also influential at both locations (Figure 2.6).

$q_{Nano}^{CHL:Nmax}$ was the most influential parameter in determining the annual peak surface chlorophyll-a (MBP_TOTCHL) at both stations with its main- and total-effects. The other sensitive parameters for MBP_TOTCHL at BATS are $q_{Dia}^{CHL:Nmax}$, the grazing parameters γ, ξ and ϕ, zooplankton excretion parameter ϵ_{Het}^{N}, and CHL loss parameter d_{Nano}^{CHL}. At DYFAMED, $q_{Dia}^{CHL:Nmax}$ is not sensitive regarding MBP_TOTCHL. The remineralization parameter ρPON shows high sensitivity at BATS. In addition to the abovementioned parameters α_{Nano}, μ_{Nano}^{max} and $q_{Nano}^{N:Cmax}$ were sensitive for MBP_TOTCHL at both stations. The sensitive parameters for the annual peak nanophytoplankton surface chlorophyll-a (MBP_NANOCHL) are analogous to MBP_TOTCHL, except for the diatom parameters and slight shifts in ranking. For annual peak surface diatom chlorophyll-a (MBP_DIACHL), two nanophytoplankton parameters, μ_{Nano}^{max} and α_{Nano} were also sensitive, which highlights the interaction between the two phytoplankton groups (Figure 2.6). The nanophytoplankton maximum nitrogen uptake (V_{Nano}^{Nmax}) shows sensitivity to MBP_NANOCHL and MBP_TOTCHL when interacting with other parameters at both locations.

For simulating NPP (totnpp in Table 2.1), the grazing parameters γ, ξ, and φ, photosynthetic parameter α_{Nano} and μ_{Nano}^{max}, the zooplankton respiration parameters ϵ_{Het}^{N}, the nanophytoplankton excretion rate of carbon (ϵ_{Nano}^{C}), the light attenuation coefficient K_W, and the cell quota $q_{Nano}^{CHL:Nmax}$ and $q_{Nano}^{C:Nmax}$ were sensitive at both locations (Table 2.3 and Figure 2.6). In addition d_{Nano}^{CHL} and ρPON were sensitive at DYFAMED. At BATS, γ and ξ had their highest values for both first- and total-order Sobol' indices, whereas at DYFAMED, they have the highest values for total-order Sobol' indices but relatively lower value for first-order indices. Overall, zooplankton parameters are more sensitive at BATS compared to DYFAMED. The influential parameters for total NPP (TOTNPP) and nanophytoplankton NPP (NANONPP) are the same, except for the ranking difference. Comparably, a higher number of parameters showed sensitivity for diatom NPP than other quantities of interest at both stations with the initial slope of photosynthesis–irradiance curve of diatom (α_{Nano}), the diatom maximum photosynthesis rate (μ_{Dia}^{max}) and $q_{Dia}^{CHL:Nmax}$ the most sensitive parameters for diatom NPP (DIANPP). (V_{Nano}^{Nmax}) has a small main effect but a high total effect on NANONPP and TOTNPP at BATS. Similar effects of nanophytoplankton cost of nitrogen biosynthesis (ζ_{Nano}^{N}) were found at DYFAMED.

The remineralization parameters ρPON and ρPOC are the most influential parameters for the simulation of export production of carbon (EXPORTC) at BATS followed by the photosynthesis parameter α_{Nano}, the cell quota $q_{Nano}^{C:Nmin}$, $q_{Nano}^{C:Nmax}$ and $q_{Nano}^{CHL:Nmax}$, photosynthesis parameter μ_{Nano}^{max} and grazing parameter γ. At DYFAMED, ρPON, γ, $q_{Nano}^{C:Nmin}$ and ξ are the most influential parameters for export production simulation.

The most influential parameters for the simulation of the partial pressure of carbon dioxide (pCO_2) and surface flux of carbon dioxide (CO_2FLUX) are the remineralization rate of nitrogen ρPON and carbon ρPOC, and the light attenuation coefficient (K_W)

at BATS. At DYFAMED the most influential parameters are ρPON, ρPOC, $q_{Nano}^{C:Nmax}$ and the grazing parameter γ.

Table 2.3 Ranking of the seven most influential model parameters on mean surface chlorophyll-a (SURF_TOTCHL), annual peak surface chlorophyll-a (MBP_TOTCHL), mean NPP (TOTNPP), mean carbon export production (EXPORTC) and mean pCO_2 from the first- and total-order Sobol' indices.

QoI	**Rank**	**BATS**		**DYFAMED**	
		first-order	total-order	first-order	total-order
	1	γ	$q_{Nano}^{CHL:Nmax}$	$q_{Nano}^{CHL:Nmax}$	$q_{Nano}^{CHL:Nmax}$
	2	$q_{Nano}^{CHL:Nmax}$	γ	d_{Nano}^{CHL}	ξ
	3	ξ	ξ	ϵ_{Nano}^{N}	γ
SURF_TOTCHL	4	ϵ_{Het}^{N}	φ	ρPON	φ
	5	d_{Nano}^{CHL}	ϵ_{Nano}^{N}	ϵ_{Het}^{N}	ρPON
	6	φ	ρPON	ξ	d_{Nano}^{CHL}
	7	ϵ_{Nano}^{N}	α_{Nano}	γ	ϵ_{Nano}^{N}
	1	$q_{Nano}^{CHL:Nmax}$	$q_{Nano}^{CHL:Nmax}$	$q_{Nano}^{CHL:Nmax}$	$q_{Nano}^{CHL:Nmax}$
	2	γ	$q_{Dia}^{CHL:Nmax}$	ρPON	ρPON
	3	$q_{Dia}^{CHL:Nmax}$	ξ	d_{Nano}^{CHL}	ξ
MBP_TOTCHL	4	ξ	γ	α_{Nano}	d_{Nano}^{CHL}
	5	φ	φ	φ	φ
	6	ϵ_{Het}^{N}	V_{Nano}^{Nmax}	ϵ_{Nano}^{N}	α_{Nano}
	7	d_{Nano}^{CHL}	ϵ_{Nano}^{N}	γ	V_{Nano}^{Nmax}
	1	γ	γ	α_{Nano}	ξ
	2	ξ	ξ	ϵ_{Nano}^{C}	γ
	3	α_{Nano}	φ	ρPON	μ_{Nano}^{max}
TOTNPP	4	μ_{Nano}^{max}	ϵ_{Het}^{N}	ξ	φ
	5	ϵ_{Nano}^{C}	α_{Nano}	ϵ_{Het}^{N}	$q_{Nano}^{CHL:Nmax}$
	6	φ	μ_{Nano}^{max}	$q_{Nano}^{CHL:Nmax}$	α_{Nano}
	7	ϵ_{Het}^{N}	V_{Nano}^{Nmax}	γ	ζ_{Nano}^{N}
	1	ρPON	ρPON	ρPON	ρPON
	2	ρPOC	$q_{Nano}^{CHL:Nmax}$	γ	γ

	3	$q_{Nano}^{N:Cmin}$	ρPOC	$q_{Nano}^{N:Cmax}$	$q_{Nano}^{N:Cmax}$
EXPORTC	4	$q_{Nano}^{N:Cmax}$	μ_{Nano}^{max}	ξ	ρPOC
	5	$q_{Nano}^{CHL:Nmax}$	α_{Nano}	ρPOC	σ_{Nano}^{N}
	6	μ_{Nano}^{max}	$q_{Nano}^{N:Cmax}$	ϵ_{Het}^{N}	ϵ_{Nano}^{N}
	7	γ	γ	φ	ϵ_{Dia}^{N}
	1	ρPOC	ρPOC	ρPON	ρPON
	2	γ	ρPON	ρPOC	ρPOC
	3	ρPON	γ	$q_{Nano}^{N:Cmax}$	$q_{Nano}^{N:Cmax}$
pCO_2	4	$q_{Nano}^{N:Cmax}$	φ	$q_{Nano}^{N:Cmin}$	σ_{Nano}^{N}
	5	$q_{Nano}^{N:Cmin}$	α_{Nano}	γ	ϵ_{Nano}^{N}
	6	ξ	α_{Dia}	φ	ϵ_{Dia}^{N}
	7	α_{Nano}	ϵ_{Het}^{N}	ϵ_{Het}^{N}	ϵ_{Het}^{N}

2.5 Discussion

2.5.1 Parameter sensitivity across locations

We undertook a GSA with variance-based sensitivity methods to analyze the sensitivity of model outputs in a 1–D configuration of the ocean BGC model MITgcm-REcoM2 for two ocean locations. Overall, the sensitivity responses of most of the QoIs were similar between the two locations. However, some differences emerged, which can be attributed to the availability of nutrients and, specifically, continuous upwelling and strong convective mixing differing mixed layer depth.

Surface chlorophyll-a is often the first choice of model output for calibration and validation of ocean BGC models, as it can be compared to satellite ocean color products that are widely available and have good spatial coverage. In REcoM2, chlorophyll-a synthesis is coupled with nitrogen uptake, with its rate being proportional to nitrogen uptake by phytoplankton (Hauck et al., 2013). The chlorophyll-a synthesis is represented by the cell quota, the maximum chlorophyll-a to nitrogen ratio for the respective phytoplankton group ($q_{Nano}^{CHL:Nmax}$ for nanophytoplankton and $q_{Dia}^{CHL:Nmax}$ for diatoms). Therefore, the maximum chlorophyll-a to nitrogen ratios significantly contribute to the variability of surface CHL. At both locations, $q_{Nano}^{CHL:Nmax}$ has the highest value in both first- and total-order indices. In contrast, $q_{Dia}^{CHL:Nmax}$ has little influence on the total surface chlorophyll-a simulations because of low diatom contributions to the annual total phytoplankton population in oligotrophic environments. The contribution of diatoms to total

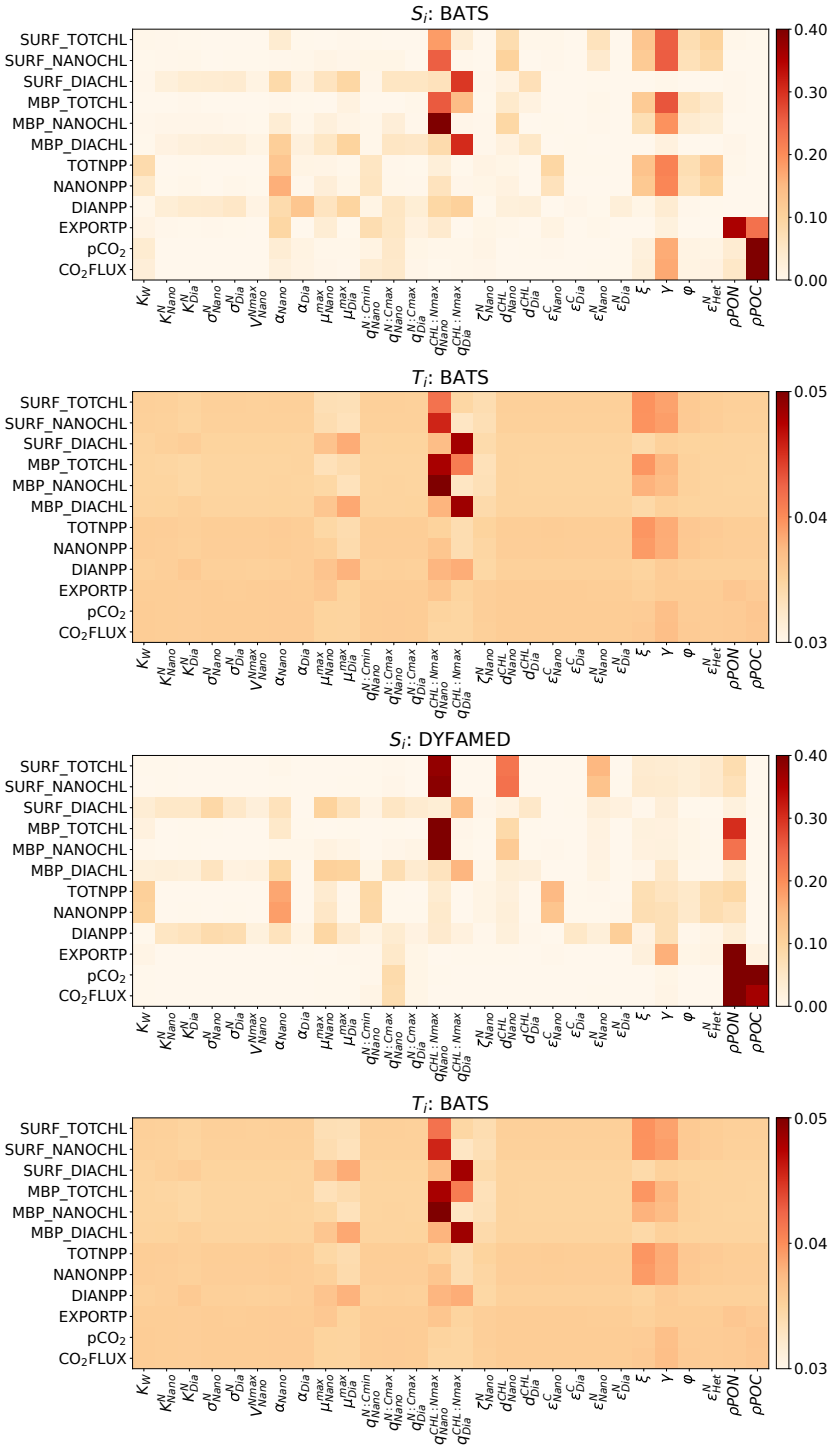

Figure 2.6 First- and total-order Sobol' sensitivity indices of the short-listed parameters regarding all included QoIs at both stations. For better visibility, the total-order Sobol' indices were normalized. For a description of QoI and parameters, see Table 2.1 and Table 2.2, respectively.

surface chlorophyll-a concentration is generally less than 10% at both stations, which agrees with data from in situ observations from Steinberg et al. (2001) for BATS and J.-C. Marty et al. (2008) for DYFAMED.

The annual peak surface chlorophyll-a concentration at BATS is sensitive to $q_{Dia}^{CHL:Nmax}$. Diatom contribution to the total phytoplankton biomass can exceed 30% during the bloom period at this station (Nelson & Brzezinski, 1997). Albeit their low abundance and biomass, diatoms grow actively during the spring bloom period at BATS and have a higher contribution to NPP. REcoM2 chlorophyll-a production is computed as a function of irradiance and nitrogen uptake. The uptake of nitrogen by the phytoplankton is converted to chlorophyll-a using the parameters maximum chlorophyll to nitrogen ratio ($q_{Nano}^{CHL:Nmax}$ and $q_{Dia}^{CHL:Nmax}$) . The highest possible chlorophyll-a synthesis is down-regulated by this ratio, which depends on photosynthesis and light absorption. It increases under low irradiance and decreases as photosynthesis becomes light-saturated. Therefore, during the bloom period, when photosynthesis is significant, changes in this ratio produce a large variability in the chlorophyll-a synthesis. As diatom photosynthesis is high during bloom peak at BATS, changes in $q_{Dia}^{CHL:Nmax}$ lead to considerable variability in the chlorophyll-a synthesis. On the other hand, unlike BATS, diatoms are less abundant during the spring bloom at DYFAMED. REcoM2 underestimates diatom production at the station, hence, $q_{Dia}^{CHL:Nmax}$ is not important for the phytoplankton bloom at DYFAMED in our analysis.

As the chlorophyll-a concentration products derived from satellite ocean color are widely available, chlorophyll-a is often included in the model as a proxy for living phytoplankton biomass so that the chlorophyll-a simulation can be used for model validation. Photoinduced and microbial processes lessen chlorophyll-a before the phytoplankton are grazed or die. The overall chlorophyll-a loss, in turn, contributes to phytoplanktonic carbon loss. Therefore, loss of chlorophyll from functional cells is necessary in REcoM2, and is parameterized by a fixed chlorophyll degradation rate (d_{Nano}^{CHL} for nanophytoplankton and d_{Dia}^{CHL} for diatom). These parameters are highly influential for the simulation of surface chlorophyll-a concentration (Figure 2.6), which are difficult to constrain by observations (Mamnun et al., 2022). They become even more important during low-growth conditions in winter. The latter is supported by the higher sensitivities computed for the annual mean surface chlorophyll-a compared to the mean peak surface chlorophyll-a. The chlorophyll-a loss term, in reality, describes processes in senescent or photo-stressed cells, thus playing a pivotal role in phytoplankton carbon to chlorophyll ratios (Álvarez et al., 2018). Our results suggest that replacing the simple chlorophyll degradation model with a more process-based description of the degradation of photosystem functionality can lead to improved modeled carbon to chlorophyll ratios and should be pursued further, as also indicated in Álvarez et al. (2018).

Our study emphasizes the importance of the parameters describing the zooplankton grazing process, such as ξ, γ and φ for BGC simulations (Figure 2.6). Zooplankton grazing is vital in the ocean food web and biogeochemical cycles (see Steinberg & Landry,

2017). The grazing parameters in ocean BGC models strongly impact the phytoplankton dynamics and nutrient cycling processes (T. R. Anderson et al., 2013; Karakuş et al., 2022; Le Quéré et al., 2016). They regulate the phytoplankton biomass in the photic zone, thus controlling the biological production and the carbon and nutrients uptake by photosynthesis. Previous sensitivity studies of ocean BGC models (e.g., Bracis et al., 2020; Chien et al., 2020; Prieur et al., 2019; Tjiputra et al., 2007) indicated that zooplankton grazing parameters are very sensitive BGC parameters for simulated variables related to phytoplankton dynamics. (Chenillat et al., 2021) showed that small changes in grazing rate greatly affect the plankton ecosystem model. (Makler-Pick et al., 2011) performed a GSA study by including three zooplankton groups in a BGC model and did not find zooplankton grazing parameters as the most influential sloppy feeding and grazing rate of zooplankton was overall sensitive, though. REcoM2 parameterized only one zooplankton group to represent the entire zooplankton community and its impact on the marine ecosystem. As most zooplankton communities vary across space and time, a single zooplankton group might provide a too limited description of the grazing process of an entire ecosystem. Increasing the number of zooplankton groups would likely weaken the sensitivity of grazing parameters, which suggests that implementing multiple zooplankton function types in BGC models would likely improve chlorophyll-a and NPP simulation, provided that efforts are invested in estimating parameters characterizing the grazing in marine ecosystems. It has been shown (Karakuş et al., 2022) that representing multiple zooplankton groups in an ocean BGC model strongly impacts the seasonal dynamics of phytoplankton, food web structure, and elemental cycles.
The grazing parameters show stronger sensitivity at BATS compared to DYFAMED. In addition to being grazed by zooplankton, in REcoM2, phytoplankton mortality is represented by non-physiological terms such as aggregation. The aggregation is assumed to be proportional to phytoplankton abundance, becoming more important during the spring bloom period. In REcoM2, mortality dominates the loss process compared to grazing in nutrient-abundant areas (Laufkötter et al., 2016). The grazing parameters strongly influence BGC simulations at BATS because zooplankton consumes most of the primary production at this location, consistent with in situ measurements reported by Evelyn and Michael (1998). At BATS, reduced ξ increases phytoplankton biomass in the euphotic zone, thus increasing nutrient uptake by photosynthesis. As grazing parameters are less sensitive at DYFAMED compared to BATS, the aggregation parameters should have some sensitivity (Laufkötter et al., 2016) at DYFAMED. However, our sensitivity analysis shows that aggregation parameters do not have much influence on the phytoplankton dynamics at DYFAMED. This suggests that the aggregation parameterization does not properly represent the phytoplankton mortality process at the station. It is likely that explicitly representing phytoplankton mortality as physiological mortality can improve the simulation in oligotrophic regions. The effect of grazing parameters at DYFAMED increases when they interact with other parameters. Increasing influence because of interaction indicates strong co-dependencies of zooplankton grazing on phytoplankton

dynamics and nutrient cycling.

The GSA shows that the zooplankton nitrogen excretion rate, ϵ^N_{Het} is sensitive to BGC simulations. The rate ϵ^N_{Het} mainly controls the DON released by zooplankton. In addition, DON concentration is reduced when ϵ^N_{Het} is small, reducing the amount of organic matter that is immediately recycled into nutrients in the euphotic zone. Hence, the parameter influences the balance between new and regenerated nitrogen, which affects the BGC cycle. An increase in ϵ^N_{Het} reduces zooplankton biogenic concentration. It thus increases the flux of regenerated nitrogen, which leads to an increase in primary production, chlorophyll-a concentration and nitrogen assimilation. However, the zooplankton excretion rate of carbon ϵ^C_{Het}, did not show sensitivity in our analysis. In the oligotrophic regions, the zooplankton excretion of carbon regulates primary production by supplying regenerated nutrients, especially when the zooplankton concentration is high (Popova et al., 2006). (Druon & Le Fèvre, 1999) found that increasing the zooplankton excretion rate of carbon in a BGC model could enhance primary productivity. Since ϵ^C_{Het} impacts the zooplankton biomass, it would also help control the grazing pressure, hence sloppy feeding, over a more extended period. Over longer time scales, changes in HetC would influence regenerated nutrients, which would change photosynthesis and carbon uptake, but that is not evident in our analysis. One reason is that carbon content loss from zooplankton is dominated by carbon-rich fecal pellets of macrozooplankton (Karakuş et al., 2022), which our model does not represent explicitly. The representation of macrozooplankton fecal pellets and their contribution to sinking particles are significant in ocean BGC models (Laufkötter et al., 2016). Our results highlight the critical role of macrozooplankton in the carbon and nutrient cycles. Thus, representing macrozooplankton in the BGC model would improve future projections of carbon cycling.

The photosynthesis parameters maximum growth rate (μ^{max}) and initial slope of photosynthesis-irradiance curve (α) show sensitivity at both stations. Annual upwelling and intense convective mixing maintain a seasonal supply of essential nutrients to the surface for phytoplankton growth at both locations (Sweeney et al. (2003) for BATS; J.-C. Marty et al. (2008) for DYFAMED). Because of atmospheric dust input, iron availability does not limit phytoplankton growth either at BATS (Nelson & Brzezinski, 1997) or at DYFAMED (Mayot et al., 2020). Therefore, the increasing growth rate increases photosynthesis. However, the GSA suggests that photosynthesis parameters have a low sensitivity on export production at the two sites investigated here, though these processes are essential for DIC in general (Olsen et al., 2008). In our study, the parameters related to phytoplankton growth had relatively low importance for BGC simulations. The low sensitivity of phytoplankton growth parameters can be because the model was implemented in two oligotrophic areas with a fully stratified water column and relatively low primary production. Therefore, the mass of organic matter exported from the surface to the depth is low. In our simulation, the weak connection between the euphotic (productive) zone and the lower layers makes the export production less dependent on phytoplankton growth.

Our study indicates that the surface CO_2 fluxes and pCO_2 are mostly sensitive to the remineralization parameters ρ_{PON} and ρ_{POC}, the grazing parameter γ, and cell quota $q_{Nano}^{N:Cmax}$ and $q_{Nano}^{N:Cmin}$. Remineralization parameters control the dissolved organic matter. An increase in remineralization rate decreases dissolved organic matter concentration at the surface and enhances regenerated nutrients, increasing photosynthesis and carbon uptake. In REcoM2, the remineralization is not regulated by biological processes. It is likely that implementing heterotrophic bacteria explicitly in the model has the potential for an improved simulation of export production and CO_2 fluxes. Reducing γ would substantially increase the uptake of atmospheric CO_2. The results agree with previous sensitivity studies, which indicated that the sea-to-air CO_2 flux and surface pCO_2 are sensitive to grazing parameters.

2.5.2 First-order vs. total-order Sobol' indices

Figure 2.7 shows a scatter plot of first-order and total-order indices. The relation between first-order and total indices is not linear. More precisely, the parameters with a high first-order Sobol' index generally have a larger total-order Sobol' index value than those with a low first-order Sobol' index. Nevertheless, this generalization may vary significantly for some parameters. For example, the maximum growth rate corresponds to the largest first-order Sobol' index, which has a total-order index smaller than several other parameters with much smaller first-order indices at BATS. On the other hand, some parameters with a small first-order Sobol' index have a high total-order index.

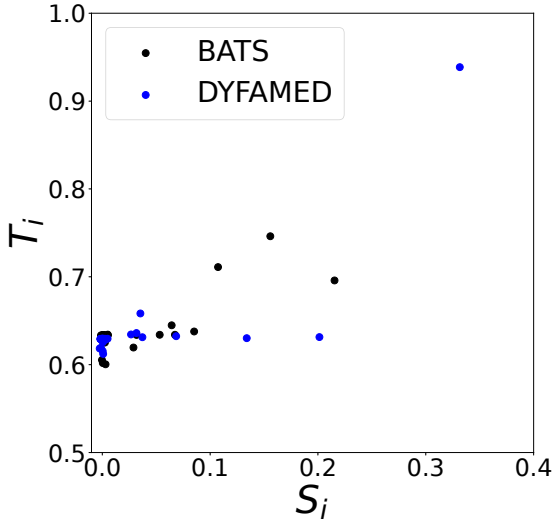

Figure 2.7 Scatterplot of first-order (x-axis) and total-order (y-axis) Sobol' indices of the short-listed parameters for NPP.

Note that the sum of first-order Sobol' indices is less than 1 and the sum of total-order Sobol' indices equals far more than 1. This indicates that the BGC models are not

additive models of the form of Equation 2.7. This is due to correlations between different BGC parameters (Mamnun et al., 2022). Co-dependencies between parameters make any simple interpretation of Sobol' indices non-trivial. As mentioned above, computing total-order Sobol' indices may not always be affordable, depending on the computational resources available. However, they bring essential information since input parameters with a minimal value for their total Sobol' index can be fixed to a nominal value in a calibration procedure.
The hypothesis of uncorrelated input parameters is common in GSA regardless of the method used (see Razavi et al., 2021). This assumption, however, faces challenges in real-world problems, where it becomes a rare exception to find models without correlated input parameters, particularly in models representing highly complex systems or systems with numerous parameters like those used in earth system modeling. The correlation effect is distinct from the 'total effect', which denotes the non-additive influence of individual parameters on the QoI (Razavi & Gupta, 2015). The presence of dependent input parameters might indeed induce errors and bias in the GSA outcomes. Yet, they are used to identify the most uncertain parameters and provide vital insights that enhance our understanding of the modeled system which our results also demonstrated. Researchers in various fields frequently utilize Sobol' indices in their models, even when dealing with dependent inputs (e.g., Islam & Karadogan, 2019; Kalra et al., 2017; Prieur et al., 2019). They recognize, however, that overlooking the correlation effects can introduce biases into the results of GSA. This understanding underscores the need for careful consideration and potential adjustment when interpreting the outcomes of such analyses. Recently, some methods have emerged to accommodate correlated inputs, including but not limited to copula-based techniques (e.g., Kucherenko et al., 2012; Sheikholeslami et al., 2021) and applications of game-theory concepts (e.g., Iooss & Prieur, 2019; Owen & Prieur, 2017; Owen et al., 2014). However, these novel methods' applications are still on the horizon for ocean BGC models.

2.5.3 Implications of our study

Modelers usually rely on previous SA studies for targeted parameters to be tuned during calibration for a new modeling application (see Wagener & Pianosi, 2019). However, most previous SA studies are conducted on a single location, mainly because of computational constraints. The conventional LSA can result in misleading conclusions and, thus, a misinterpretation of the influence of process parameters on the critical model outputs (Prieur et al., 2019). Ocean BGC models contain many parameters, so conducting a GSA for the output of these models is computationally expensive. Therefore, ocean BGC modelers prefer the LSA to GSA. With the availability of high-performing computing technologies and recent advances in computation algorithms, BGC researchers can apply the GSA methods presented in this study with little effort before any new modeling application. The methods set here can be applied to analyze the sensitivity

of other ocean BGC model outputs or QoIs (e.g., dissolved oxygen in surface layers) as well as other locations of the world ocean.
As indicated above, the main aim of GSA is to identify the parameters that have the most impact on a QoI. Thus, GSA helps prioritize the parameters for estimation with data assimilation (see Dowd et al., 2014, for a review of data assimilation into ocean BGC models) which we apply in an ongoing study. In model tuning, it prioritizes the most influential parameters for the model outputs to focus on optimization efforts, that minimize the misfit between simulations and available data, on these few parameters. Before starting with parameter estimation, a preceding GSA could provide helpful information, e.g., selecting only parameters to which the observed variables are sensitive. Likewise, an identifiability analysis could complement the SA by furnishing information on parameter range and possible ambiguities of parameter estimates (Schartau et al., 2017).
GSA could also serve as an additional tool for model evaluation during the calibration of an ocean BGC model. It can provide a system-level assessment (e.g., Leles et al., 2018), assuming that the influential parameters identified by the GSA reflect the most critical processes of interest. Any dissimilarity between observed data and the outcomes of GSA in terms of the most significant process parameters would require an examination into the parameterization and the cause of the discrepancy (see H. V. Gupta & Razavi, 2018) and thereby help parameter identification in the ocean BGC model. If the discrepancies come from parameter values, this deserves a new round of calibration. On the other hand, if the discrepancies do not match the current knowledge of the modeled systems, this demands investigation of the model structure and parameterization to better reflect the knowledge of essential processes in the marine ecosystem. For example, at both locations, the aggregation parameters are not influential for any of the QoIs. REcoM2 describes the loss process of phytoplankton by grazing and aggregation, where aggregation dominates grazing (Laufkötter et al., 2016). A recent study by Mamnun et al. (2022) found that aggregation parameters influence the surface chlorophyll-a concentration at DYFAMED - an increase in the specific aggregation rate of both phytoplankton and detritus decreases surface chlorophyll-a concentration significantly. Therefore, the absence of influence of aggregation parameters does not correspond with current knowledge of the systems modeled and needs investigations into these parameterizations and maybe changes in the model structure.

2.6 Conclusion

We performed a GSA of an ocean BGC model concerning the sensitivity of its input parameters. The GSA aimed to understand which model parameters contribute the most to the model uncertainty. We consider the BGC model REcoM2 in a one-dimensional configuration at two ocean sites. We estimated variance-based Sobol' indices for each

parameter at both stations. For mean chlorophyll-a simulations, we found that the maximum chlorophyll to nitrogen ratio, chlorophyll degradation rate, and parameters related to zooplankton grazing and excretion were sensitive at both stations. For predictions of net primary production, the most influential parameters are those related to photosynthesis, zooplankton grazing, and the excretion of organic matter by phytoplankton and zooplankton. Export production of carbon, pCO_2 and surface CO_2 flux are sensitive to mainly the remineralization of nutrients and grazing by zooplankton. The parameters related to diatoms were not significant because the contribution of the phytoplankton group to the overall phytoplankton community was low at both locations.

Our results suggest that implementing multiple zooplankton functional types in BGC models will likely improve chlorophyll-a and NPP prediction, provided that efforts are invested in estimating parameters characterizing the grazing in marine ecosystems. The GSA indicates that explicitly representing phytoplankton mortality as physiological mortality, currently not used in REcoM2, can improve simulation in oligotrophic regions. Our results also indicate that the explicit representation of heterotrophic bacteria in the model can potentially improve the simulation of carbon export production and CO_2 fluxes.

Despite the limitation of the one-dimensional model configuration, our application offers a comprehensive list of the most important biogeochemical parameters that need to be quantified for future applications of a global configuration. The insight gained from the GSA will be broadly applicable in future BGC modeling case studies, parameter estimation and optimization, and for further development of BGC models. Stakeholders, policies, and society need reliable information for decision-making, not only in the current state but also in space and time. This study's insight will help increase the reliability of BGC models and predictions to society.

Chapter 3

Uncertainties in ocean biogeochemical simulations: Application of ensemble data assimilation to a one-dimensional model

In this chapter, an ensemble data assimilation approach is applied to the same one-dimensional model configuration from Chapter 2 at two ocean cites, BATS in the Atlantic Ocean and DYFAMED in the Mediterranean Sea, where observational time series data exist to quantify the uncertainty arising from the parameterization within REcoM2 at these stations. Using the Parallel Data Assimilation Framework – PDAF, an ensemble Kalman filter is applied to assimilate satellite ocean color data and in situ net primary production data to estimate ten selected biogeochemical parameters and eight model state variables. This chapter presents interdependence features of the estimated parameters in relation to the significant biological processes and delves into the nuanced differences at the two specified stations, each with its unique environmental conditions. In general, the estimated parameter values result in improved model prediction and reduced prediction uncertainty. The method applied here was successful and served as an essential base for conducting spatially and temporally varying ocean BGC parameter estimation studies at the global level. Estimation of spatially and temporally varying parameter values in a 3–D global ocean setup REcoM2 is presented in Chapter 4.
This chapter is a reproduction of a peer-reviewed journal article with the same title.

Citation: Mamnun, N., Völker, C., Vrekoussis, M., & Nerger, L. (2022). Uncertainties in ocean biogeochemical simulations: Application of ensemble data assimilation to a one-dimensional model. *Frontiers in Marine Science, 9.* https://doi.org/10.3389/fmars.2022.984236

Abstract

Marine biogeochemical (BGC) models are highly uncertain in their parameterization. The value of the BGC parameters are poorly known and lead to large uncertainties in the model outputs. This study focuses on the uncertainty quantification of model fields and parameters within a one-dimensional (1–D) ocean BGC model applying ensemble data assimilation. We applied an ensemble Kalman filter provided by the Parallel Data Assimilation Framework (PDAF) into a 1–D vertical configuration of the biogeochemical model Regulated Ecosystem Model 2 (REcoM2) at two BGC time-series stations: the Bermuda Atlantic Time-series Study (BATS) and the Dynamique des Flux Atmosphériques en Méditerranée (DYFAMED). We assimilated 5-days satellite chlorophyll-a concentration and monthly in situ net primary production (NPP) data for three years to jointly estimate ten preselected key biogeochemical parameters and the model state. The estimated set of parameters resulted in improvements in the model prediction up to 66% for the surface chlorophyll-a and 56% for NPP. Results show that assimilating satellite chlorophyll-a concentration data alone degraded the prediction of NPP. Simultaneous assimilation of the satellite chlorophyll-a data and in situ NPP data improved both surface chlorophyll-a and NPP simulations. We found that correlations between parameters preclude estimating parameters independently. Co-dependencies between parameters also indicate that there is not a unique set of optimal parameters. Incorporation of proper uncertainty estimation in BGC predictions, therefore, requires ensemble simulations with varying parameter values.

3.1 Introduction

Outputs from marine biogeochemical (BGC) models are increasingly used for scientific purposes (e.g., Carroll et al., 2020; Ciavatta et al., 2016; Goodliff et al., 2019; Pradhan et al., 2020), environmental management (e.g., Fennel et al., 2019; E. M. Jones et al., 2016) and to inform policy (Brown & Caldeira, 2017). Including an ocean BGC component in Earth System Models is essential for climate simulation and prediction (see G. M. Flato, 2011; Orr et al., 2017). Ocean BCG model outputs and reanalysis data are key requirements for developing marine environmental applications and services (Gehlen et al., 2015), monitoring and predicting algal blooms (Flynn & McGillicuddy, 2018) and monitoring the movement of fish populations (Tommasi et al., 2017).

Ocean BGC models are composed of different components of the marine systems, including the marine ecosystem (e.g., phytoplankton, zooplankton), physical environment processes (e.g., ocean circulation and mixing), the cycling of inorganic and detrital matter, and air-sea interactions and gas transfer. These models aim at replicating the state and dynamics of the ecosystem components (flow of matter and energy between inorganic nutrients and marine plankton) as close as possible to the real world, or at least

with reasonable accuracy to generate useful insights into the problem being studied. To achieve the latter, the model needs to incorporate a sufficiently accurate description of the representation of the real processes.

The description of growth and ecosystem interactions in BGC models is based, besides the conservation of mass, largely on heuristic mathematical descriptions of observed processes, such as the relation between prey density of zooplankton and their grazing rates. The numerous parameters involved in these descriptions are often taken from laboratory experiments on single species, while in the model, they are applied in a more general sense as describing whole classes of organisms. BGC models are thus highly uncertain regarding these parameters (see Schartau et al., 2017). Uncertainty in the parameter values translates into uncertainty in the model prediction. Thus, neglecting parameter uncertainty will result in underestimating the uncertainty in the model outputs. Therefore, the parameter uncertainties must be properly quantified to improve model predictions and the quality of reanalysis data.

Data assimilation (DA) techniques allow us to estimate model parameters and their uncertainty using observational data (see Wikle and Berliner, 2007). DA combines models and observations in an effort to obtain an accurate estimation of the state of the modelled system. DA approaches can be categorized as either variational or sequential. Both have been applied to BGC models for state estimation, parameter optimization and/or both in a broader sense. Variational algorithms minimize a cost function of the weighted sum of squared model-data differences. Sequential methods, on the other hand, rely on approximating the probability distribution generated from an ensemble of model initial states at a particular time based on observations of the state until that time.

The variational DA approaches have been applied to parameter optimization applications in one-dimensional (1–D) BGC models (e.g., Friedrichs, 2001; Friedrichs et al., 2006, 2007; Laiolo et al., 2018; Pelc et al., 2012; Song et al., 2016; Xiao & Friedrichs, 2014a, 2014b; Zhao et al., 2005) but have shown limited success in constraining parameters (see Mattern & Edwards, 2017). Parameter estimation applications of the variational approach to three-dimensional (3–D) problems have not yet been demonstrated. On the other hand, sequential DA approaches applied to BGC models (Ciavatta et al., 2014, 2016, 2018; Gharamti, Samuelsen, et al., 2017; Gharamti, Tjiputra, et al., 2017; J. T. Hu et al., 2012; E. M. Jones et al., 2016; Natvik & Evensen, 2003; Nerger & Gregg, 2007, 2008; Pradhan et al., 2019, 2020; Simon et al., 2012, 2015; Triantafyllou et al., 2007) showed promising performance to improve the BGC simulation. The method also provides an efficient way for parameter estimation by the state augmentation approach (J. L. Anderson, 2001), where the state variables and parameters are combined in an augmented state vector, and the parameters are treated as time-varying variables with small artificial evolution noise. The most common sequential methods used in these studies are different variants of the Ensemble Kalman Filter (EnKF, see Vetra-Carvalho et al., 2018 for a review) that is also used in this study.

Running a BGC model multiple times over a large 3–D domain for sequential assimilation

is computationally very expensive. Therefore, often parameter optimization is performed in a 1–D model and then used in a 3–D model (e.g., Hoshiba et al., 2018; Kane et al., 2011; McDonald et al., 2012; St-Laurent et al., 2017; Wang et al., 2018). Recently, Singh et al. (2022) have implemented biogeochemical parameter estimation in a 3–D global model by assimilating synthetic observations. However, the study could only afford assimilation of monthly mean data because of the high computational cost.

Fennel et al. (2001) found poor results in a parameter optimization study using data assimilation to a simplified marine BGC model. They suggested that any parameter optimization study requires proper uncertainty analysis. Over time, BGC DA has improved through substantial developments of DA techniques, utilization of satellite data (e.g., ocean color) and deployment of new measurement platforms (e.g., ARGO). Despite the progress made, most of the BGC DA literature acknowledges that the structure and equations of BGC models are uncertain, and the quality, sparsity, and relationship between BGC observations and the BGC model state variables is challenging (see Schartau et al., 2017). Only a few studies have partially assessed the uncertainties in the BGC models, including uncertainty in the model parameters and DA itself. The ensemble DA algorithms can improve model state and parameter estimation with uncertainty quantification, as demonstrated in other scientific fields (e.g., L. Y. Hu et al., 2013; Moradkhani et al., 2005; Pathiraja et al., 2018).

Towards the direction of improving model predictions, this study focuses on the quantification of the uncertainty of model fields and parameters within a 1–D ocean BGC model. We used ensemble DA as a method of uncertainty quantification applied to the BGC model Regulated Ecosystem Model 2 (REcoM2, Hauck et al., 2013; Schourup–Kristensen et al., 2014). The analysis was performed at two BGC time-series stations - the Bermuda Atlantic Time-series Study (BATS, Steinberg et al., 2001) in the North Atlantic and the Dynamique des Flux Atmosphériques en Méditerranée (DYFAMED, J. C. Marty, 2002) at the North-west Mediterranean Sea. We estimated ten selected BGC parameters controlling the source and sink of phytoplankton and assessed the interdependency of the estimated parameters in these two stations to get insights into BGC processes. We further assessed how useful the estimated parameters are to improve the prediction capability of REcoM2.

3.2 Materials and Methods

3.2.1 Model description

The BGC model REcoM2 is a so-called quota model (Droop, 1983). It simulates 22 tracers including, among others, dissolved inorganic carbon and alkalinity for the carbonate system, the macro-nutrients dissolved inorganic nitrogen (DIN) and silicic acid, biomass content of carbon (C), nitrogen (N), silicate (Si), calcium carbonate (CaCO3)

and chlorophyll-a, and the trace metal iron (Fe) (see Appendix A.1 for a list of all 22 tracers). REcoM2 has two phytoplankton classes, nanophytoplankton, with an implicit representation of calcifiers and diatoms. The intracellular stoichiometry of carbon, nitrogen, calcite and chlorophyll (C:N:Chl) pools for nanophytoplankton, and carbon, nitrogen, silicate and chlorophyll (C:N:Si:Chl) pools for diatoms are allowed to respond dynamically to environmental conditions following Geider et al. (1998) and Hohn (2009) for the Si quota. The intracellular iron pool is a function of the intracellular nitrogen concentration (fixed Fe:N), as iron is physiologically mainly linked to nitrogen metabolism and the photosynthetic electron transport chain (Geider & La Roche, 1994). Dead organic matter is transferred to detritus by aggregation and grazing by one zooplankton class, and the sinking and advection of detritus are represented explicitly. See Figure 2.2 for a schematic of REcoM2 model pathways.

We used the Massachusetts Institute of Technology General Circulation Model (MITgcm, Marshall, Adcroft, et al., 1997) to simulate ocean circulation and mixing. MITgcm solves the time-dependent, Boussinesq-approximated Navier-Stokes equations with or without hydrostatic approximation and conservation equations for salinity and energy. REcoM2 is coupled with MITgcm online at every time step, set up to 1 hour (3600s). The total depth of the model setup is 1188 meters. The model has 30 vertical layers. The vertical grid spacing increases with depth from 10m near the surface to 100m near the bottom layer. As we are interested in ecosystem processes in the euphotic zone, and their coupling to vertical nutrient transports from the mesopelagic, we have limited our model setup to a bit more than the upper 1000 m, well above the sea-floor for both sites. Thus, the total depth of the model setup is independent of location and bathymetry. The coupled MITgcm-REcoM2 model is configured in a 1–D vertical configuration at the geolocations of BATS (31°40′N, 64°10′W) located in the subtropical gyre of the North Atlantic (Sargasso Sea) and DYFAMED (43°25′N, 7°52′E) located in the Liguro-Provencal current of the Ligurian Sea at the north-western Mediterranean Sea. Both stations have long-term time series records with a wide variety of BGC variables. The choice of using two different stations in this study is to gain a better insight into the same BGC processes under different environmental conditions.

BATS and DYFAMED, provide contrasting sampling schemes and environments. At BATS, the mesoscale eddies are a significant feature in the Sargasso Sea and impart an additional level of biogeochemical variability (Sweeney et al., 2003). On the other hand, the biogeochemical variability at DYFAMED is mainly induced by the seasonal succession of hydrological conditions (de Fommervault et al., 2015). DYFAMED has a shallower mixed layer compared to BATS in summer and fall (off-peak period) because it is highly saline (>38 psu) with a very shallow thermocline (J. C. Marty & Chiaverini, 2010). Another distinct feature of DYFAMED is that it receives significant atmospheric input from the deserts of North Africa and the industrialized countries bordering the Mediterranean Sea (J. C. Marty, 2002), which allows phytoplankton to grow at the surface even in the oligotrophic period. As a result of shallower mixed layer depth and

large atmospheric nutrient deposition, DYFAMED has higher surface chlorophyll-a and lower vertically integrated net primary production (NPP) during the off-peak period compared to BATS. Notably, despite being close to the coast, DYFAMED is protected from lateral inputs by a coastal current, acting as a barrier to exchanges with the coastal zone.

We initialized the temperature, salinity, dissolved oxygen, nitrate and silicate fields of the model at both stations with in situ bottle data – obtained for BATS from its website (BATS Team, Last access: June 2022) and for DYFAMED from Coppola et al. (2021). The total alkalinity and dissolved inorganic carbon fields at BATS were initialized with data from the mapped climatology of the GLobal Ocean Data Analysis Project (GLODAPv2, Lauvset et al., 2016). At DYFAMED these fields were initialized from bottle data (Coppola et al., 2021). The dissolved iron is initialized with data from the U.S. GEOTRACES North Atlantic Transect (GA-03, Boyle et al., 2015) at BATS and from the data reported in Guieu and Blain (2013) at DYFAMED. All other passive tracers were initialized with small uniform values. We use inter-annually varying atmospheric forcing – the Coordinated Ocean Research Experiments version 2 (COREv2, Large & Yeager, 2008) for BATS and ERA5 hourly data on single levels (Hersbach et al., 2018; Hersbach et al., 2020) for DYFAMED. Iron deposition was estimated from the monthly present-day simulation of Albani et al. (2014) at both stations.

To prevent long-term drifting and to avoid compensating for hydrographic errors caused by the 1–D setup, which ignores lateral advection, we apply a relaxation of temperature and salinity at every time step from the surface down to 400 m depth at BATS and from the surface down to 250 m at DYFAMED. The relaxation depth was determined as no clear seasonal temperature variability can be observed below this depth according to the long-term bottle data.

We additionally applied restoring sea surface salinity (SSS) to the monthly climatology with a timescale of ten days at BATS and two days at DYFAMED. The monthly climatology of SSS was calculated from the in situ bottle data at both stations. At DYFAMED, while the vertical processes dominate in setting water properties, the lateral advection still plays a major role (Béthoux et al., 1998). However, the cyclonic circulation of the Ligurian Sea is not represented in the 1–D framework at this site. During the phase of intense and dry winds associated with surface buoyancy loss, the advection of homogeneous water columns becomes dominant and drives a doming of isopycnals which drift away from the 1–D model SSS from its climatology more frequently than BATS. This drifting of model SSS leads to a deeper mixed layer at DYFAMED in the winter. This required us to restore SSS more frequently at DYFAMED than BATS.

3.2.2 Data Assimilation (DA)

3.2.2.1 Observational data

We assimilate two sets of observations: i) satellite chlorophyll-a concentration, and ii) in situ vertically integrated NPP.
We obtained the satellite chlorophyll-a concentration data from the ESA (European Space Agency) Ocean Color Climate Change Initiative (OC-CCI, Sathyendranath et al., 2019) time-series data product. It is a daily merged product of MODIS-Aqua, MERIS, SeaWiFS, and VIIRS on a sinusoidal grid at 4 km resolution. We downloaded the 5-days average dataset via FTP from the OC-CCI website (European Space Agency, Last access: March 2023). We take an area of a one-degree square at each site and average all available values in the area as the representative data value for the station.
The chlorophyll-a concentrations provided in the OC-CCI dataset are not bias corrected. However, the dataset provides per pixel biases and root mean squared deviation (RMSD). We calculate the unbiased chlorophyll-a concentration and its variance based on Appendix A of Ciavatta et al. (2016). The variances were used as observation errors in the DA. Figure 3.1A shows the average chlorophyll-a concentration (green dots) in 5-day intervals and its standard deviation as error bars at BATS. From the error bars, large uncertainty is evident in the data. As the chlorophyll-a concentration is lognormally distributed (Campbell, 1995), we used logarithmically transformed (log-transformed) concentrations in the DA implementation.
We obtained the ^{14}C primary production data for BATS from the BATS website (BATS Team, Last access: June 2022) and for DYFAMED from Coppola et al. (2021). The methods for the sample collection and the calculation of 14C primary production are described in the US Joint Global Ocean Flux Study (JGOFS) protocol (JGOFS, 1997; Laws et al., 2002) for BATS and J.-C. Marty et al. (2008) for DYFAMED. We calculated the water column integrated NPP in mgC m^{-2} d^{-1} from the measurements at individual depths by trapezoidal integration, assuming that the rate from the surface to the nearest measure is constant and the rate after 200m is zero (see JGOFS, 1997). Figure 3.1B shows the integrated NPP at BATS from October 1999 to December 2002. For all DA runs, we assume a Gaussian error distribution with a relative error of 0.25 for NPP at both stations.

3.2.2.2 DA method

The DA was performed using the Parallel Data Assimilation Framework (PDAF, Nerger & Hiller, 2013) – a free and open-source software designed to implement ensemble data assimilation with existing numerical models. PDAF provides fully implemented and optimized data assimilation algorithms, in particular, ensemble-based Kalman filters. We applied the ensemble-based Error-Subspace Transform Kalman Filter (ESTKF, Nerger et al., 2012b) in this study. The ESTKF is an ensemble square root filter that

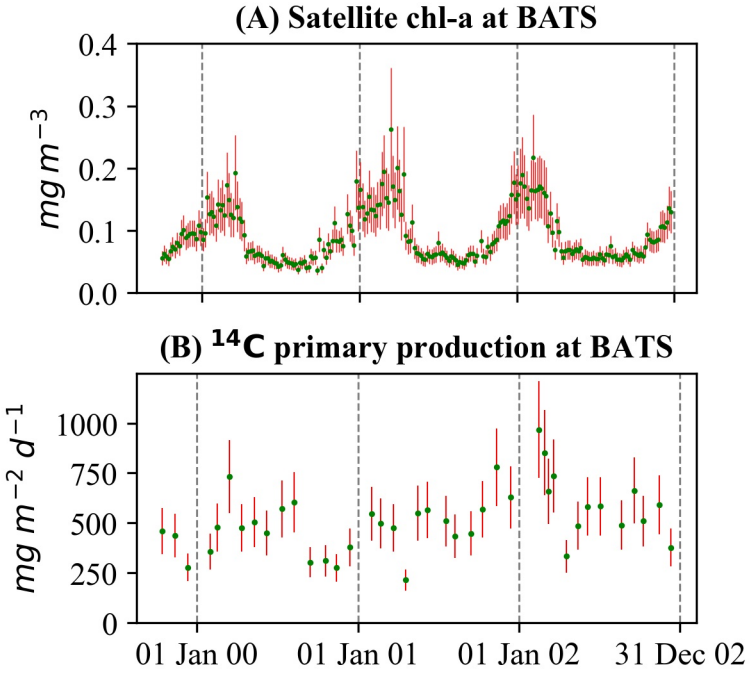

Figure 3.1 Observational data during the study period at BATS. (A) OC-CCI satellite chlorophyll-a concentration. The green dots depict data values and the red lines standard deviations. (B) Vertically integrated NPP (green) and assumed errors (red).

computes the weights for the ensemble transformation directly in the error-subspace represented by the ensemble.

We used a 108-member ensemble. To make the BGC processes slightly different in each ensemble member and generate varying model states (ensemble members), we randomly perturbed ten parameters. The parameters are chosen following earlier studies (e.g., Ciavatta et al., 2016; Doron et al., 2013; J. T. Hu et al., 2012; Pradhan et al., 2019, 2020) and model descriptions (e.i., Hauck et al., 2013; Schourup–Kristensen et al., 2014) that they control the key BGC processes of the model and that their values are poorly constrained. As we assimilated chlorophyll-a concentration and NPP data, we focused on the parameters related to phytoplankton production, and to those that directly influence phytoplankton mortality. Four of the selected parameters are related to phytoplankton sources, while the remaining six are related to the phytoplankton sinks.

A brief description of the ten selected parameters is provided below. A list of all REcoM2 parameters can be found in the Appendix A.1.

Maximum photosynthesis rate of nanophytoplanktons (μ^{max}_{Nano}) and diatoms (μ^{max}_{Dia}): Phytoplankton takes up nutrients from the inorganic nutrient pool and energy from the sunlight to produce biomass to grow. The process is known as photosynthesis. REcoM2 calculates the C-specific photosynthesis (P) based on the maximum photosynthesis rate P^{max} which has an intrinsic maximum growth rate of μ^{max} (time^{-1}) and is limited

($0 < f_{lim} < 1$) by either physical conditions (e.g., temperature, turbulence) or resources such as light, nutrients and dissolved inorganic carbon.

$$P^{max} = \mu^{max} \cdot f_T \cdot \left(f_{lim}^{Fe}, f_{lim}^{N:C_{min}}, f_{lim}^{Si:C_{min}} \right) \tag{3.1}$$

where, f_T is an Arrhenius function of temperature dependency. f_{lim}^{Fe}, $f_{lim}^{N:C_{min}}$ and $f_{lim}^{Si:C_{min}}$ are growth-limitation by iron, nitrogen and silicon and are calculated using the Liebig law of the minimum, in which the most limiting nutrient limits production (O'Neill et al., 1989).

Initial slope of the photosynthesis-irradiation (P-I) curve of nanophytoplankton (α_{Nano}) and diatoms (α_{Dia}): P depends on how much photosynthetically available radiation (PAR) the cell can harvest. This is controlled by the initial slope of the P-I curve (α), which represents the photosynthetic efficiency under light levels close to zero and is obtained by multiplication of the light-harvesting efficiency per chlorophyll with the intracellular chlorophyll to carbon ratio ($q^{Chl:C}$). α is used to model P as a saturating function of PAR.

$$P = P^{max} \left(1 - \exp \left(\frac{-\alpha \cdot q^{Chl:C} \cdot PAR}{P^{max}} \right) \right) \tag{3.2}$$

The C-specific photosynthesis rate, P, is calculated for both nanophytoplankton (P_{Nano}) and diatoms P_{Dia}) with α_{Nano} and α_{Dia}, respectively.

Chlorophyll degradation rate of nanophytoplanktons (d_{Nano}^{CHL}) and diatons (d_{Dia}^{CHL}): Chlorophyll concentrations are used as a proxy for living phytoplankton biomass. Photoinduced and microbial processes can degrade chlorophyll before the phytoplankton dies or is eaten by the zooplankton. In REcoM2, chlorophyll is degraded with a fixed rate d^{CHL} which contributes to the overall chlorophyll loss, in turn phytoplanktonic carbon loss. As phytoplanktonic carbon loss is calculated for both nanoplankton and diatom REcoM2 uses two chlorophyll degradation rate parameters d_{Nano}^{CHL} and d_{Dia}^{CHL}

Maximum grazing rate (ξ) and grazing efficiency (γ): Zooplanktons consume phytoplankton in a process known as grazing. The grazing function describes a rectangular hyperbolic relationship between phytoplankton nitrogen (N) abundance, with a sigmoidal dependency of nutritional intake to resource density with an N-specific maximum grazing rate (ξ). It depends on temperature following the same relationship as for phytoplankton growth (f_T). The grazing G on nanophytoplankton and diatoms is defined as:

$$G = \xi \cdot \frac{(N_{Nano} + N'_{Nano})}{\varphi_1 + \left(N_{Dia} + N'_{Dia}\right)} \cdot f_T \cdot N_{het} \tag{3.3}$$

N'_{Dia} encompasses a preference term for grazing on diatoms, relative to that on nanophytoplankton:

$$N'_{Dia} = \tau \cdot \frac{N_{Dia}^2}{\varphi_2 + N'_{Dia}} \tag{3.4}$$

Here, τ is the maximum diatom preference and is smaller than 1, which implies that zooplankton grazes preferably on nanophytoplankton; the effective grazing preference is allowed to vary with diatom biomass, with φ_2 being the half-saturation parameters for grazing preference of diatoms. $\varphi_2 = 0$ implies a constant preference.
The phytoplankton biomass that enters the zooplankton may be incorporated into new biomass, voided through defecation to Pellets assuming a fixed grazing efficiency (γ) which determines how much of the grazed phytoplankton is built into heterotrophic biomass.
Specific aggregation rate of phytoplankton (Φ_{Phy}) and detritus (Φ_{Det}): A non-physiological mortality term denoted as aggregation loss describes a part from the grazing loss of phytoplankton to sinking detritus. The removal of material from oceanic surface waters and its subsequent transport to the ocean interior is driven by the formation and sinking of particles. However, only larger particles with high settling rates significantly contribute to the vertical flux reaching the sea floor (Mccave, 1984). The collection of smaller particles into larger ones is called aggregation. The aggregation rate g is assumed to be proportional to the abundance of phytoplankton and detritus:

$$g = \Phi_{Phy} \cdot N_{Nano} + \Phi_{Phy} \cdot N_{Dia} + \Phi_{Det} \cdot N_{Det} \tag{3.5}$$

Where the phytoplankton-specific aggregation rate (Φ_{Phy}) and detritus-specific aggregation rate (Φ_{Det}) reflect the roles of phytoplankton and detritus in the aggregation process. Phytoplankton-specific aggregation rate, Φ_{Phy} is assumed to be the same for nanoplanktons and diatoms.
We keep the reference values, hereafter referred to as the default values, of the parameters as used in Hauck et al. (2013). We perturbed the parameters assuming a lognormal distribution with a relative variance of 0.25 for all the selected parameters. Hence, each ensemble member was started from the same initial condition but with different values for the perturbed parameters. The DA process was initialized from the ensemble of model states at the end of the spin-up period (see section 3.2.2.3).
We estimated eight BGC model state variables, total chlorophyll-a, and vertically integrated NPP using the ESTKF in all DA simulations. The eight model state variables are:

1. Nanophytoplankton content of carbon
2. Diatom content of carbon
3. Nanophytoplankton content of nitrogen
4. Diatom content of nitrogen
5. Nanophytoplankton calcium carbonate
6. Biogenic silica for diatoms
7. Nanophytoplankton chlorophyll-a
8. Diatom chlorophyll-a

Note that total chlorophyll-a and vertically integrated NPP are diagnostic model variables. For these two diagnostic variables, the observation operator selects the corre-

sponding values from the state vector. The eight model state variables are updated through the ensemble-estimated cross covariances to total chlorophyll-a and vertically integrated NPP when observations are available. The total chlorophyll-a and the vertically integrated NPP estimated by the DA process are not distributed to the model, but stored as diagnostic variables.
One issue of parameter estimation through DA is that in the analysis step, the value of parameters in each ensemble member changes toward the optimal values. As a result, the ensemble spread decreases, and the parameter ensemble may collapse before an optimal parameter value is found. To avoid this, we inflated the variance of the parameter ensemble in every assimilation cycle by 2.56%.

3.2.2.3 DA Experiment

DA experiments were performed from October 1999 to December 2002 for BATS and from October 1997 to December 2000 for DYFAMED. The difference in the chosen period was caused by the availability of the in situ bottle NPP data. The model was first run with 108 ensemble members using the perturbed parameters from January 1990 as a spin-up for both stations. We conducted three types of DA experiments.

- EXP_{State_DP} – *State estimation with the default parameters:* We performed state estimation experiments with the default parameters as the reference simulations.
- EXP_{Joint_DP} – *Joint state-parameter estimation:* In these experiments, we augmented the state vector by the ten selected BGC parameters and updated them in each assimilation cycle together with the state variables. Therefore, the selected parameters vary over time in this experiment.
- EXP_{State_EP} – *State estimation with estimated parameters:* To assess the effect of the estimated parameters on model prediction, we performed state estimation experiments (DA runs for model state) with the estimated parameters.

For each type of experiment, we implemented four simulations: i) Free-run (ensemble run without DA), ii) satellite chlorophyll-a only assimilation, iii) vertically integrated NPP only assimilation, and iv) combined assimilation of satellite chlorophyll-a and vertically integrated NPP. The free-run simulation of EXP_{Joint_DP} is identical to the free-run simulation of EXP_{State_DP}. Therefore, we did not repeat the free-run simulation in the EXP_{State_DP}.

3.3 Results

In this section, we first present the results of the joint state-parameter estimation from the EXP_{Joint_DP} (section 3.3.1), particularly the estimation of ten model parameters. Then, we assess the performance of the estimated parameters (EXP_{State_EP}) compared

to the reference simulations (EXP_{State_DP}), state estimation with the default parameters) and the prediction capabilities of DA in general for both stations (section 3.3.2).

3.3.1 Joint state-parameter estimation (EXP_{Joint_DP})

The ensemble evaluation of surface chlorophyll-a concentration and vertically integrated NPP shows that the free-run with default parameters (EXP_{Joint_DP}) performs poorly at both stations (Figure 3.2). At BATS, the free-run overestimates the surface chlorophyll-a concentration compared to satellite data (Figure 3.2A) and underestimates the NPP compared to bottle data (Figure 3.2B). The free-run performs better at DYFAMED than at BATS for surface chlorophyll-a concentration. At DYFAMED, the model produces realistic surface chlorophyll-a concentrations during the bloom period but overestimates them during the oligotrophic periods (Figure 3.2C). NPP is overestimated at DYFAMED for both free-run and combined assimilation of EXP_{Joint_DP} (Figure 3.2D). The simulation with combined assimilation of satellite chlorophyll-a and vertically integrated NPP of EXP_{Joint_DP} performs better because the filter brought the model state close to the observations during the first bloom period for both stations.
NPP shows larger discrepancies at BATS. The filter even pushed the NPP simulation away from the observations at the station to compensate for the correction in the surface chlorophyll-a concentration. In the DA process, satellite chlorophyll-a data had a stronger influence than the in situ $_{14}$C primary production data on the overall change of the states.

3.3.1.1 Evaluation of parameter estimates

We estimate values of the same ten parameters Section 3.2.2.2 that were perturbed to generate the ensembles at both stations. The objective was to get an optimized set of parameters to improve the model prediction, from which we can gain insight into the interaction between phytoplankton growth and decay. The minimization of the model-data misfit in the assimilation run compared to the free-run presented above is mostly due to the simultaneous update of the selected parameters. The value of parameters obtained at the final DA cycle (time step) is the estimated parameter value. Table 3.1 shows the default values and estimated values at the end of the experiment of the 10 selected parameters for both stations.
The initial slope of the photosynthesis-irradiance (P-I) curve of nanoplankton (α_{Nano}), and diatom (α_{Dia}), maximum photosynthesis rate of nanoplankton (μ^{max}_{Nano}), and maximum grazing rate (ξ) were changed the most at both stations. The maximum photosynthesis rate of diatoms (μ^{max}_{Dia}), nanoplankton chlorophyll degradation rate (d^{CHL}_{Nano}), and grazing efficiency (γ) were changed significantly at BATS but not much at DYFAMED. The two aggregation parameters, the phytoplankton-specific aggregation rate

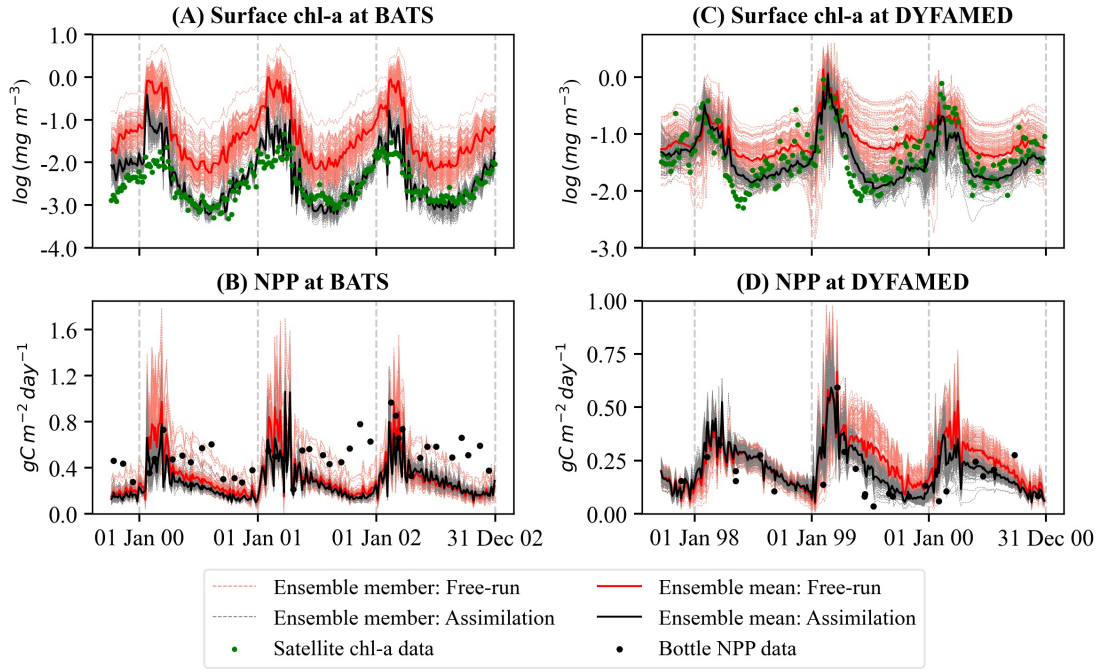

Figure 3.2 The ensemble evaluation of log-transformed surface chlorophyll-a concentration at (A) BATS and (C) DYFAMED, and NPP at (B) BATS and (D) DYFAMED for joint state-parameter estimation (EXP_{Joint_DP}). The red dashed lines show ensemble members for the free-run, and the solid red line shows their mean. Gray dashed lines are ensemble members of the simulation with combined assimilation of satellite surface chlorophyll-a and in situ NPP data, and the solid black line is their mean. The green dots represent observations (satellite data for surface chlorophyll-a and bottle data for NPP).

(Φ_{Phy}) and the detritus-specific aggregation rate (Φ_{Det}) were changed significantly only at DYFAMED. Significant change refers to more than one-third (36%) of change after the final DA time step.

The ensemble evaluations of all ten parameters for satellite chlorophyll-a only assimilation and combined assimilation of satellite chlorophyll-a and vertically integrated NPP resulting from the EXP_{Joint_DP} for both stations are presented in Appendix A.4. Here we focus on the parameters that changed significantly at one or both stations when assimilating both datasets in the experiment EXP_{Joint_DP} and examine their temporal evolution and variability at the two stations.

The evolution of the assimilated values of α_{Nano} and μ^{max}_{Nano} for both stations is shown in Figure 3.3. At BATS, α_{Nano} reached a final value of 0.45 and had much larger updates (increased more than 200% than its initial value) than at DYFAMED where the parameter increased 50% from the initial value (Figure 3.3A and C, Table 1). The large change at BATS is related to the large bias of surface chlorophyll-a compared to observations (see Figure 3.2). At DYFAMED, on the other hand, the model without DA represented the surface chlorophyll-a much better (see Figure 3.2). The value of α_{Nano}

Table 3.1 The ten BGC parameters that are estimated in this study: the default and the estimated values. The estimated values are the parameter values achieved at the end of the experiment (EXP_{Joint_DP}).

Parameter	Unit	Default Value	Estimated Value at BATS	Estimated Value at DYFAMED
α_{Nano}	$mmolC(mgChl)^{-1}$ $(Wm^{-2}d)^{-1}$	0.15	0.45	0.21
α_{Dia}	$mmolC(mgChl)^{-1}$ $(Wm^{-2}d)^{-1}$	0.19	0.09	0.26
μ^{max}_{Nano}	d^{-1}	3.00	1.98	1.59
μ^{max}_{Dia}	d^{-1}	3.50	0.96	4.10
d^{CHL}_{Nano}	d^{-1}	0.10	0.11	0.10
d^{CHL}_{Dia}	d^{-1}	0.10	0.11	0.10
ξ	$mmolNm^{-3}d^{-1}$	2.40	3.52	3.37
γ	dimensionless	0.40	0.91	0.49
Φ_{Phy}	$(mmolNm^{-3})^{-1}d^{-1}$	0.015	0.013	0.021
Φ_{Det}	$(mmolNm^{-3})^{-1}d^{-1}$	0.165	0.181	0.23

at DYFAMED was increased from the default value of 0.15 by around 50% in the first year and stabilized after that for the rest of the assimilation period with a final value of 0.21 (Figures 3.3B and D, Table 1). This change could relate to the overestimation of surface chlorophyll-a during the off-peak period at this site.

At both stations the reduction of surface chlorophyll-a concentration led to a decrease in μ^{max}_{Nano} which is partly compensated by an increase in α_{Nano}. The value of μ^{max}_{Nano} decreased around one-third after the first spring bloom at BATS (Figure 3.3B). Approximately the same value is reached after the later blooms, while it is slightly higher during the off-peak periods. At DYFAMED, updates to μ^{max}_{Nano} occurred only during the second bloom period with a decrease of around 45% (Figure 3.3D).

The change in α_{Nano} and μ^{max}_{Nano} were induced by the correlation between the observations and the model resulting from the ensemble. At both stations, α_{Nano} is negatively correlated with surface chlorophyll-a concentration during off-peak periods, while the correlation coefficient becomes positive at the beginning of the bloom periods (Figure 3.3A and C, bottom panels). For μ^{max}_{Nano} the correlation is also positive around the beginning of blooms. However, it does not show extended periods of negative values (Figure 3.3B and D, bottom panels). These correlations also denote that a varying dependence between the photosynthesis parameters and the seasonal ecosystem variability exists. Lower values of correlation coefficients between surface chlorophyll-a concentration and α_{Nano} during the bloom period indicate that this parameter is difficult to

constrain with surface chlorophyll-a and uncertainty increases during a bloom period.

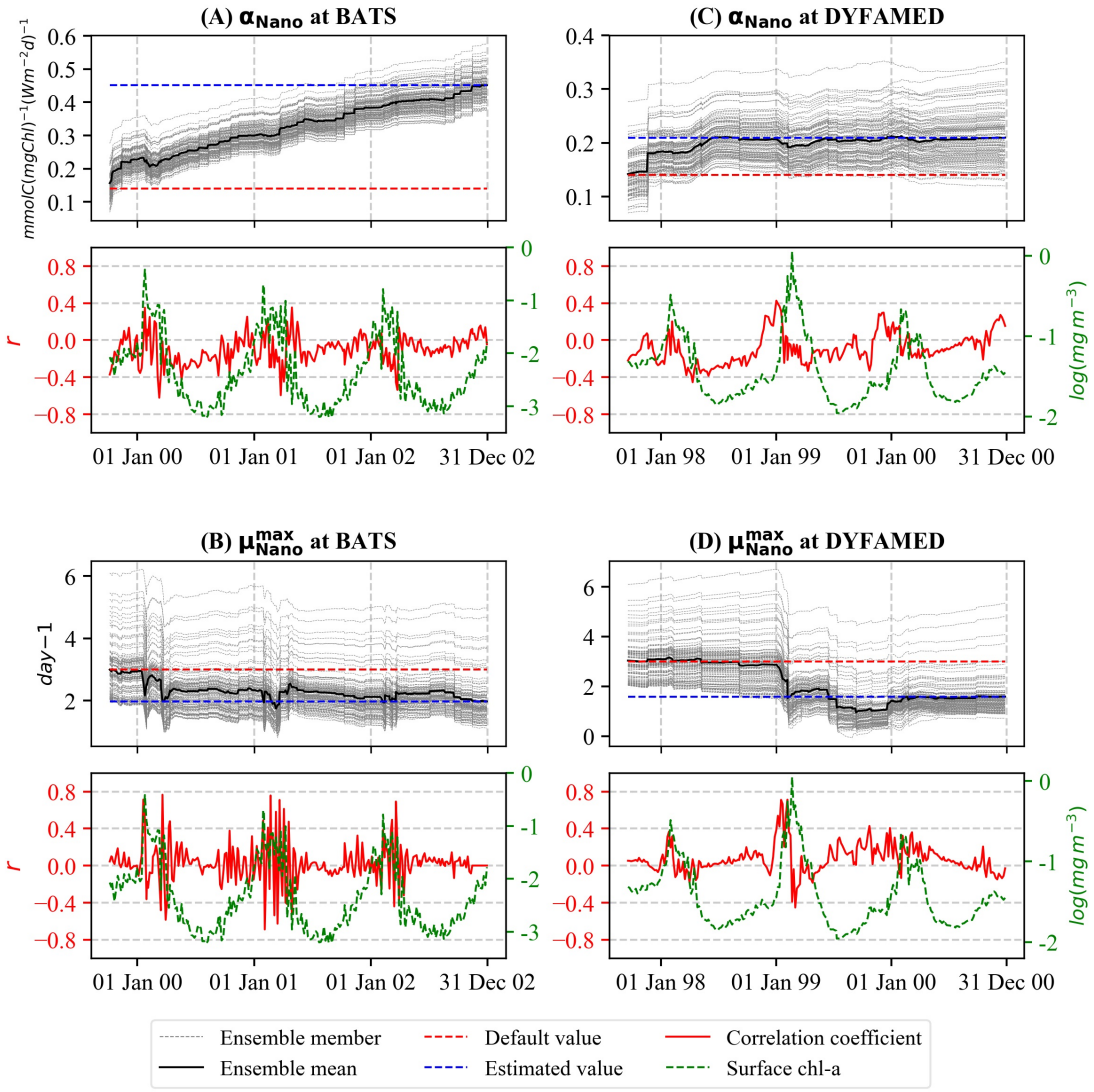

Figure 3.3 Evaluation of α_{Nano} for (A) BATS and (C) DYFAMED and μ^{max}_{Nano} for (B) BATS and (D) DYFAMED for combined assimilation of satellite surface chlorophyll-a and in situ NPP simulations of EXP_{Joint_DP}. Top panels show the ensemble evaluation (gray dashed line) and the associated ensemble means (black solid line). The default and estimated values are shown as dashed lines (red for default and blue for estimated). The bottom panels show the correlation of parameter value with the surface chlorophyll-a concentration at each assimilation cycle.

The loss parameter d^{CHL}_{Nano} increased by 60% at BATS and decreased by 10% at DYFAMED from its initial value at the end of the experiment with a final value of 0.16 d-1 and 0.09 d-1, respectively (Figure 3.4). At BATS, d^{CHL}_{Nano} first increased by around 80% after the first bloom period, further increased slightly during the second bloom period,

but then decreased slightly until the third bloom period (Figure 3.4A). This suggests high uncertainty of d_{Nano}^{CHL} at BATS. Similarly, at DYFAMED, the parameter increased first and then decreased after the second bloom period. This indicates that parameter values can have large inter-annual variation (Figure 3.4B).
For both stations, the correlation of $d_{Nano}^{CHL}$with surface chlorophyll-a is significant during the beginning of the bloom and becomes weaker later in the bloom period. One possible explanation for this weak correlation is that during the bloom period, grazing becomes prominent for loss of chlorophyll-a thus, the grazing parameters compensate d_{Nano}^{CHL}. At BATS, the high variability of the correlation coefficient indicates high uncertainty of the parameter at the station.

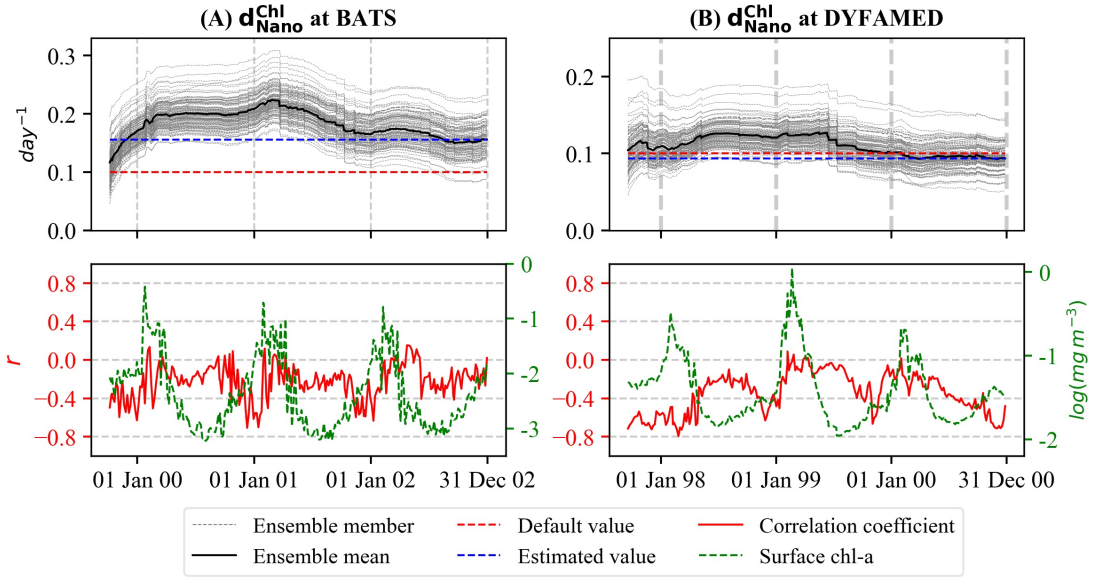

Figure 3.4 Evaluation of d_{Nano}^{CHL} for (A) BATS and (B) DYFAMED analogous to Figure 3.3.

For the grazing parameters ξ and γ, Figure 3.5 shows the ensemble members and their means. The value of ξ is increased from its default value by around 50% in the first spring bloom at BATS (Figure 3.5A). In contrast, it remained nearly unchanged at DYFAMED during the first year but increased by around 40% in the second spring bloom (Figure 3.5B). This behavior could be related to the higher bias of the free-run simulations (overestimation of surface chlorophyll-a) during the second year at DYFAMED. In the first year, the bias was compensated by other parameters e.g., α_{Nano} and d_{Nano}^{CHL}.
While at BATS, γ increased by around 125%, at DYFAMED the increase was smaller which is around 20% (Figure 3.5C and D).γ appears to show a continuously increasing trend at BATS from the beginning of the second bloom period.
Both grazing parameters showed a similar pattern of correlation with surface chlorophyll-a. At BATS, we see a positive correlation to the surface chlorophyll-a, mainly during the off-peak periods (Figure 3.5C). On the contrary, the correlation is mainly positive

during the bloom periods and negative at the other times of the year at DYFAMED (Figure 3.5D).

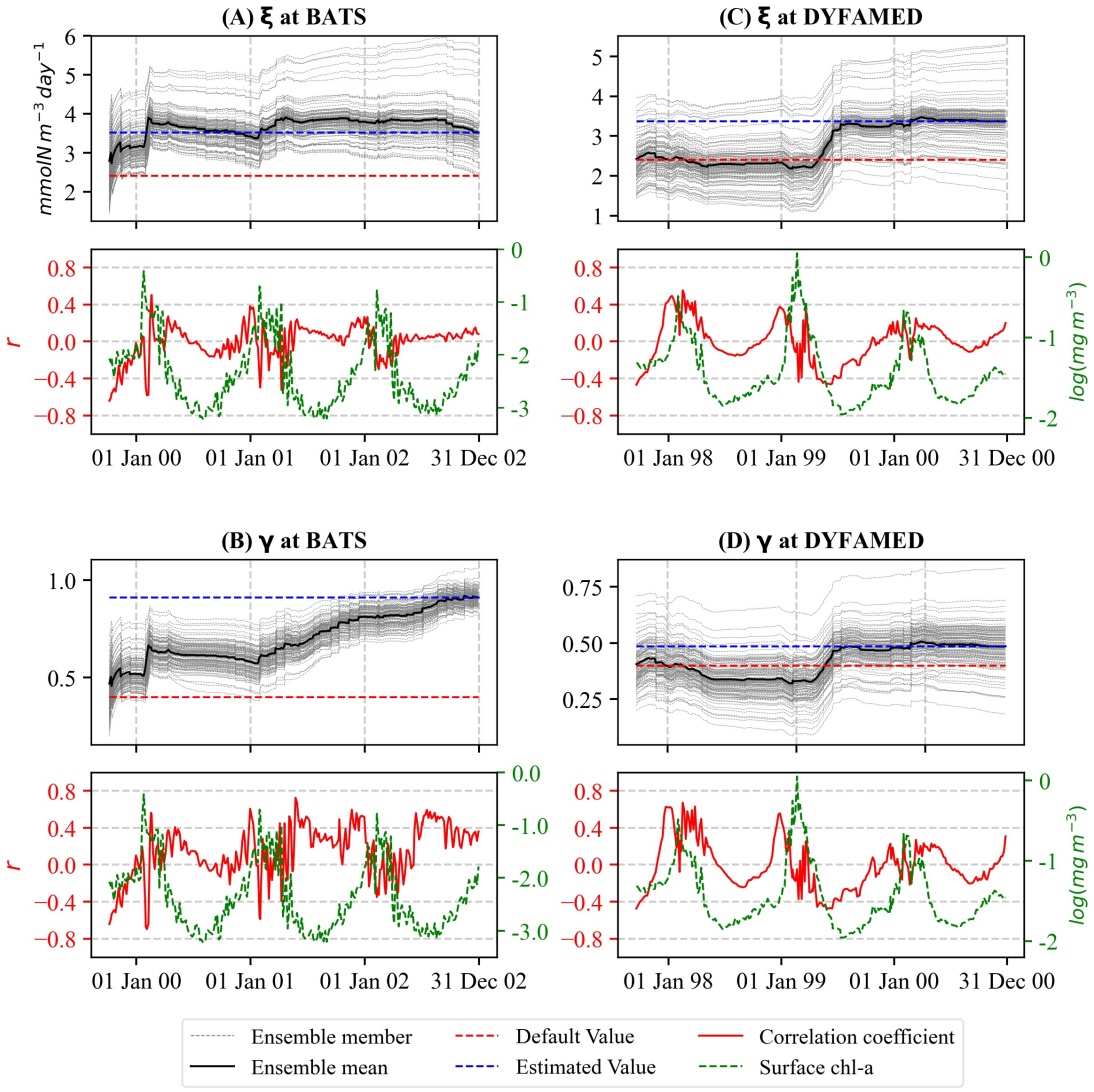

Figure 3.5 Evaluation of ξ for (A) BATS and (C) DYFAMED, and γ for (B) BATS and (D) DYFAMED analogous to Figure 3.3.

The aggregation parameter Φ_{Phy} decreased slightly at BATS (Figure 3.6A) but increased at DYFAMED between the first and second spring bloom with a final value of 0.021, which is about 40% larger than the default value (Figure 3.6B). This change is connected to a negative correlation between the parameter and chlorophyll-a at the station. At DYFAMED, Φ_{Phy} is negatively correlated after the first bloom termination to the next initialization when its values change. From the second bloom the parameter reaches a stable value and shows only a weak correlation. On the other hand, Φ_{Phy} is not well correlated with surface chlorophyll-a at BATS, which explains minor changes in

the parameter in the station (Figure 3.6A). The other aggregation parameter Φ_{Det} also exhibits a similar pattern as Φ_{Phy} (not shown).

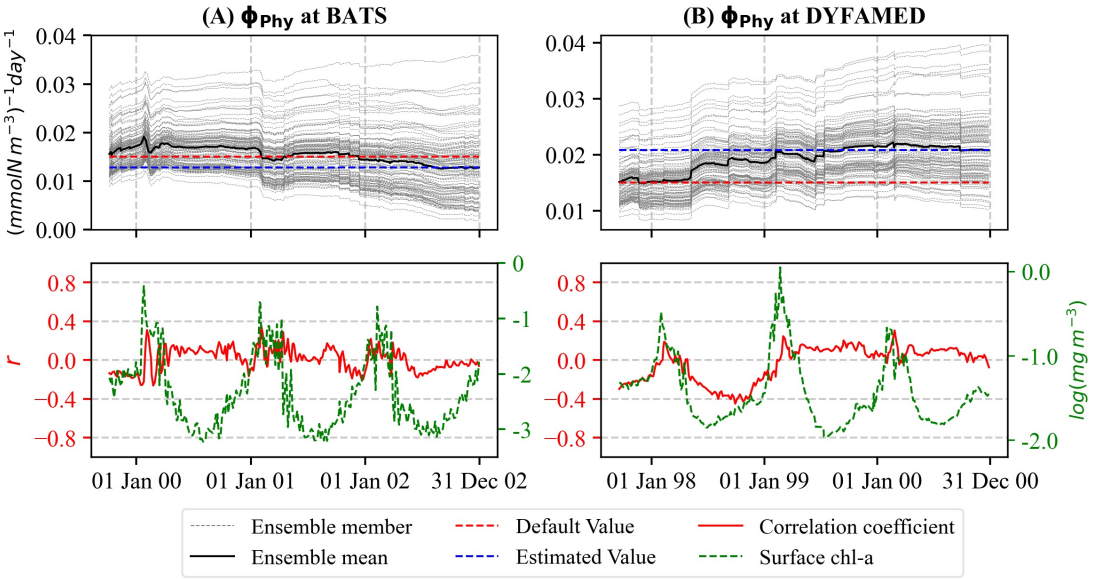

Figure 3.6 Evaluation of Φ_{Phy} for (A) BATS and (B) DYFAMED analogous to Figure 3.3.

3.3.1.2 Correlation among the parameters

To assess how strongly different parameters are correlated, we computed the Pearson correlation coefficients between each possible pair of parameters over time for both stations. The correlations are shown in Figure 3.7. Using T-test to determine statistical significance, there are five parameter pairs at BATS (Figure 3.7A) and three pairs at DYFAMED (Figure 3.7B) for which it is possible to reject the null hypothesis of no correlation at the p=0.01 probability level. The explanation of the computed relationships is the following:

- α_{Nano} *versus* μ^{max}_{Nano}*:* Increases in α_{Nano} mean that less chlorophyll-a is required to achieve the same primary production while increases in μ^{max}_{Nano} result in higher chlorophyll-a production. Therefore, balance among chlorophyll-a concentration and NPP accounts for the negative relationship between these two photosynthesis parameters. The correlation at both sites becomes significant after the first year of parameter estimation, pointing out that the optimal values of these two parameters depend on each other.
- ξ *versus* γ*:* Increases in both grazing parameters ξ and γ reduce the yield of chlorophyll-a concentration, accounting for the positive relationship. The correlations decreased over time and became insignificant when the value of the parameters got optimal. Constraining these two parameters individually may produce

unrealistic values.

- α_{Nano} *versus* d_{Nano}^{CHL}*:* Decreases in α_{Nano} increase chlorophyll-a concentration for the same primary production while increases in d_{Nano}^{CHL} compensate for this by decrementing chlorophyll-a concentration before decease of the phytoplankton, accounting for the negative relationship.
- d_{Nano}^{CHL} *versus* ξ*:* Increase in the chlorophyll degradation rate reduces the abundance of phytoplankton. So, the zooplankton can graze less, which accounts for the negative relationship.
- d_{Nano}^{CHL} *versus* γ*:* Similar to the previous point, a higher chlorophyll degradation rate means less phytoplankton abundance for grazing. d_{Nano}^{CHL} is strongly correlated with both ξ and γ at BATS only because of the large overestimation of the surface chlorophyll-a concentration at the station. This large overestimation is not present at DYFAMED.
- d_{Nano}^{CHL} *versus* Φ_{Phy}*:* Increases in chlorophyll degradation result in decreased aggregations of senescent cells. Aggregation is a significant pathway by which nanoplankton contribute to export production in low biomass environments (Jackson et al., 2005). Therefore, it accounts for negative correlations.

3.3.2 Model performance with estimated parameters

To evaluate the effect of the parameter estimation, we performed state estimation experiments (with perturbed parameters but no parameter estimation) using the default parameter values (EXP_{State_DP}) and the estimated parameter values (EXP_{State_EP}).

3.3.2.1 Surface chlorophyll-a and NPP

The log-transformed surface chlorophyll-a and its uncertainty estimate for both stations using default and estimated parameters over the study period are presented in Figures 3.8A and C. Root mean square errors (RMSE) of simulated log-transformed surface chlorophyll-a against satellite (assimilated) and bottle (independent) data are summarized in Table 3.2. As seen in both Figures 3.8A and C, the estimated parameters improve the model predictions of surface chlorophyll-a concentration substantially at both sites. The RMSE of surface chlorophyll-a concentration simulations was reduced by about 66.67% against satellite data and about 44.78% against bottle data. At DYFAMED, RMSE for log-transformed surface chlorophyll-a concentration was reduced by 28.58% and 11.11% against satellite and in situ bottle data, respectively.
The improvements are larger at BATS with a strong reduction of RMSE for log-transformed surface chlorophyll-a concentration. This large improvement is because the default parameters perform poorly at BATS. Most of the concentrations from satellite and bottle data fall below the ensemble from the simulation with default parameters at

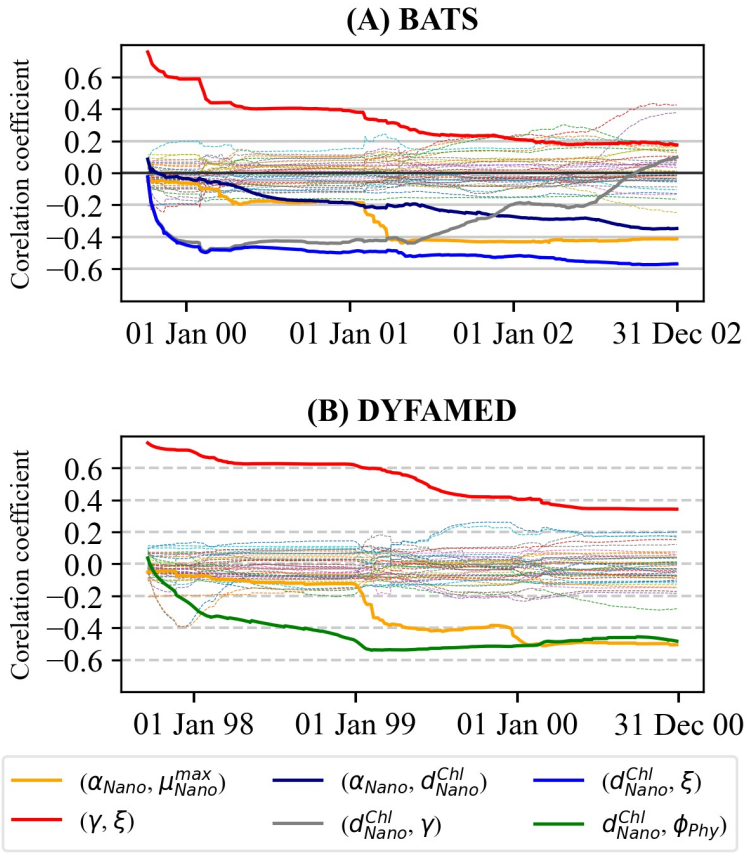

Figure 3.7 The Pearson correlation coefficients between each pair of the ten biogeochemical parameters at (A) BATS and (B) DYFAMED. The solid lines denote significantly correlated pairs.

Table 3.2 RMSE of log-transformed surface chlorophyll-a concentration from combined assimilation of satellite chlorophyll-a and in situ NPP data of EXP_{State_EP} against satellite and bottle data at both stations.

Variable	Experiment	BATS		DYFAME	
		Satellite data	Bottle data	Satellite data	Bottle data
Chl-a	EXP_{State_DP}	0.72	0.67	0.28	0.36
	EXP_{State_EP}	0.24	0.37	0.20	0.32
NPP	EXP_{State_DP}	129.3	248.6	48.5	72.6
	EXP_{State_EP}	56.2	129.8	46.9	66.4

Chl-a = Chlorophyll-a

the station. However, they fall inside the ensemble range when the estimated parameters are used (Figure 3.8A). At DYFAMED some observations fall outside of the ensemble for default parameters and remain outside of the ensemble for estimated parameters (Figure 3.8C). At DYFAMED, satellite data shows brief blooms during autumn, which the model does not reproduce. A possible explanation can be that the model does not represent destratification correctly as the 1–D framework does not capture cyclonic circulation.

The NPP predictions for default (EXP_{State_DP}) and estimated parameters (EXP_{State_EP}) and their uncertainty estimates are shown in Figures 3.8 B and D. We compare NPP simulations with in situ bottle data (assimilated observation) and monthly satellite-derived data (independent observation) obtained from the Ocean Productivity website at the Oregon State University (Ocean Productivity, Last update 2021). The satellite-derived data is NPP computed using the Carbon, Absorption, and Fluorescence Euphotic-resolving (CAFE) model (Silsbe et al., 2016) based on SeaWiFS satellite data. RMSEs of the ensemble mean NPP of combined satellite chlorophyll-a and in situ NPP assimilation of both EXP_{State_DP} and EXP_{State_EP} against in situ bottle and satellite-derived data are presented in Table 2. As can be seen, the estimated parameters largely improve the NPP prediction at BATS and little improvement at DYFAMED. Despite the improvement, there are still large discrepancies at BATS. The RMSE of NPP simulation was reduced by 56.5% against satellite data and 47.78% against in situ bottle data at BATS, and by 3.30% and 8.54% against satellite-derived and bottle data respectively.

At BATS, model simulations agree reasonably with satellite NPP estimations but show large discrepancies with the bottle data. The concentrations in bottle data are much higher, particularly during oligotrophic periods. Notably, the bottle data at BATS shows no apparent seasonality. Due to this behavior, we suspect large uncertainty in the $_{14}C$ NPP measurements. At DYFAMED, the improvements are smaller compared to BATS.

3.3.2.2 Phytoplankton phenology indices

To further assess the influence of the estimated parameters, we examine five phytoplankton bloom phenology indices, namely i) initiation, ii) peak time, iii) termination time, iv) duration, and v) peak value. At both stations, the initiation generally occurs in December/January (Figure 3.9A and F), bloom peaks mostly 4-6 weeks later (Figure 3.9B and G), and the termination is in March/April (Figure 3.9C and H). Differences in the timing of these phenological events between the simulations with default (EXP_{State_DP}) and estimated parameters (EXP_{State_EP}) are relatively small, with the observed timing of these indices falling within the ensemble range.

At BATS, the range for these phenological timings is broader, indicating a large uncertainty of these matrices on the selected BGC parameters, at least the parameters we selected in this study. At both stations, the model-simulated bloom duration is shorter than the satellite observation. At BATS, the bloom duration with estimated parame-

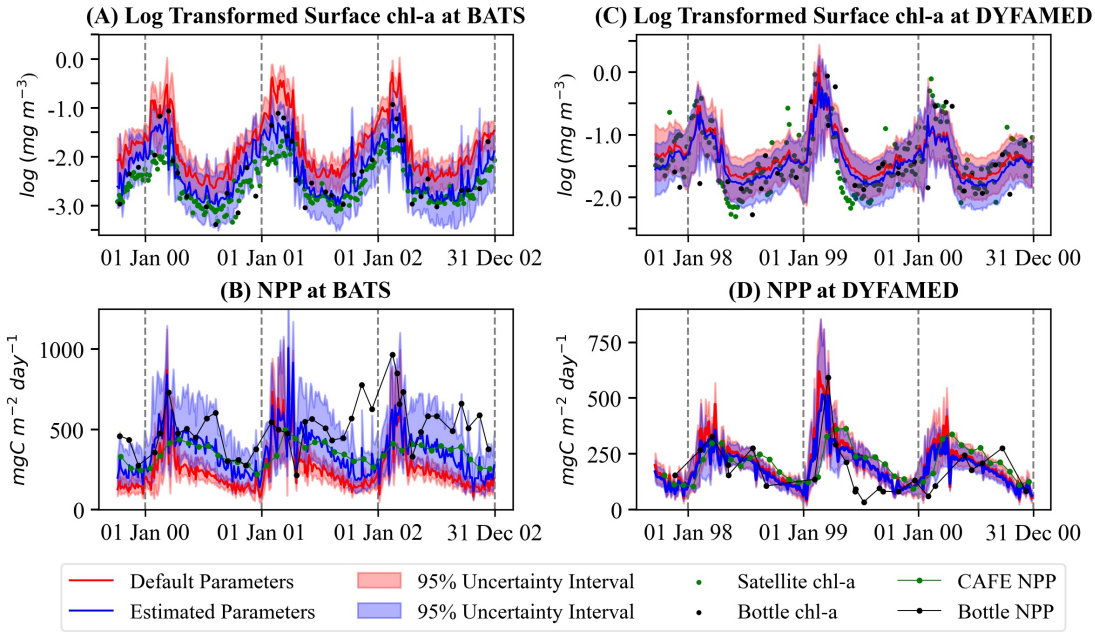

Figure 3.8 Comparison of log-transformed surface chlorophyll-a concentration of combined assimilation of satellite chlorophyll-a and in situ NPP simulations with default (EXP_{State_DP}) and estimated parameters (EXP_{State_EP}) at (A) BATS and (B) DYFAMED, and of NPP simulations with default and estimated parameters at (C) BATS and (D) DYFAMED. The red line shows the ensemble mean with default parameters and the blue line is for estimated parameters. The green dots show satellite data, and the black dots are bottle data.

ter values falls within the ensemble range for the first and second years (Figure 3.9D). However, it gets even shorter in the third year. At DYFAMED, bloom durations with estimated parameter values did not change much compared to default parameter values (Figure 3.9I). The blooms occur earlier at BATS for EXP_{State_EP}, with its peak concentrations being strongly reduced compared to EXP_{State_DP} and coming closer to the observations (Figure 3.9E). Estimated parameter values had less influence on the peak concentration at DYFAMED (Figure 3.9J). At DYFAMED, the bloom peaks in both model and observation have higher chlorophyll-a concentration than at BATS. However, the bloom duration is rather short compared to BATS.

3.4 Discussions

3.4.1 Parameter estimation

Similar to some earlier studies (e.g., Gharamti, Tjiputra, et al., 2017; Mattern et al., 2010), our results show that ensemble DA techniques are generally suitable for param-

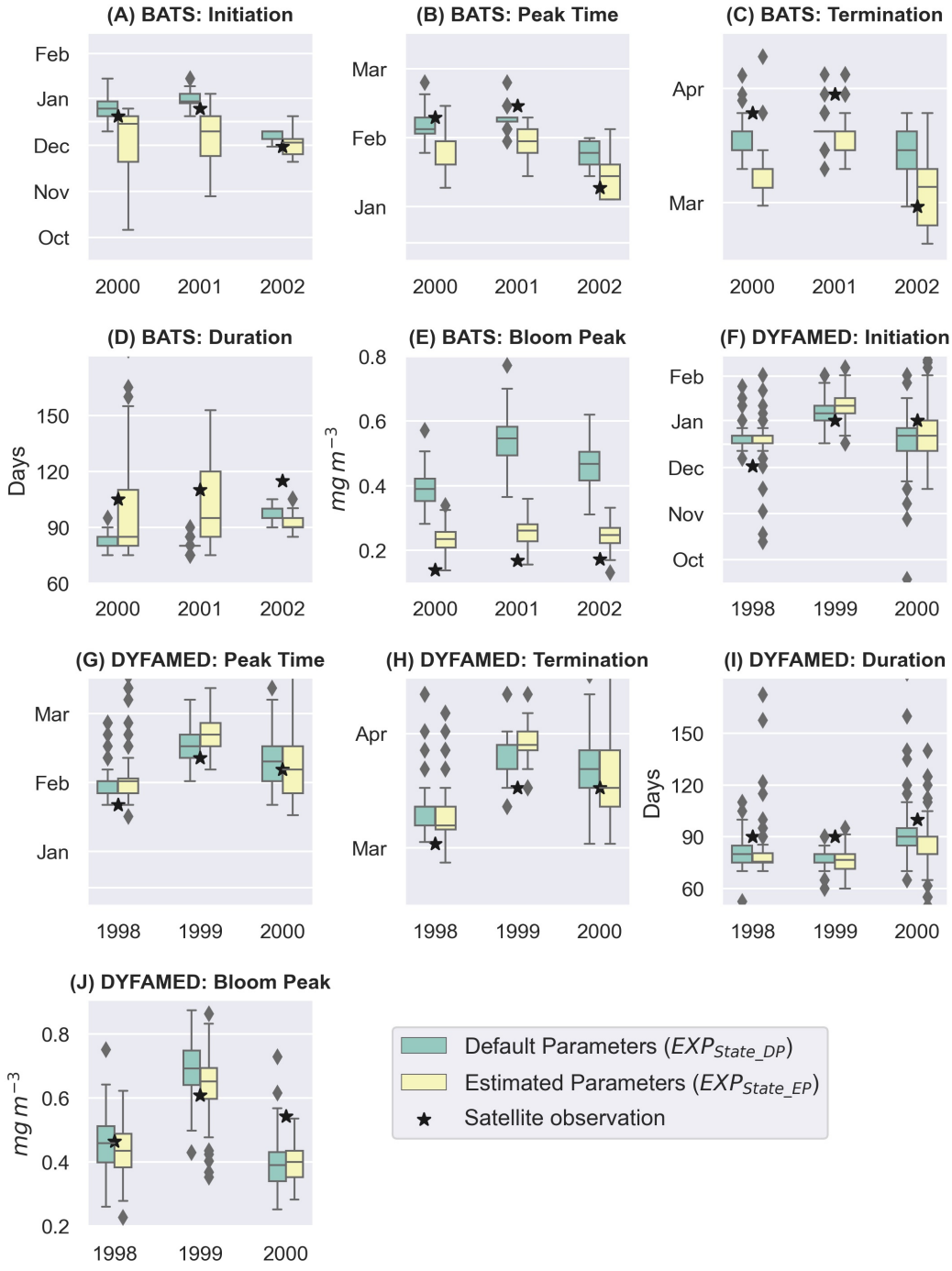

Figure 3.9 Phytoplankton phenology metrics (A–E) bloom initiation, peak time, termination, duration and peak value at BATS and (F–J) = DYFAMED. The black stars are calculated from satellite data; the boxes show the quartiles of the ensemble of the combined chlorophyll-a and NPP assimilation, while the whiskers extend to show the rest of the ensemble members except for points determined to be "outliers" using the inter-quartile ranges.

eter estimation in a 1–D ocean BGC model to decrease the model-data misfit. In the experiments conducted here, a notable reduction of RMSE of surface chlorophyll-a and NPP was achieved compared to simulations using the default parameters. The default parameter values used in this study (Table 3.1) have been optimized for a global model configuration. Therefore, we can expect distinct parameter values as optimal at the two different sites considering the distinct environmental conditions.

The DA process generally decreased the growth parameters and increased the loss parameters to reduce model-data misfit. This behavior corroborates that at the oligotrophic BATS and DYFAMED sites, the production is less than the global average.

At both stations, the parameters describing nanoplankton dynamics had much larger adjustments than those for diatoms. This was because of low diatom contributions to the total phytoplankton population in the oligotrophic environment. At BATS, the contribution of diatoms to total chlorophyll-a biomass is generally less than 10% (Steinberg et al., 2001) and to the annual primary productivity is less than 13% (Nelson & Brzezinski, 1997). In the annual cycle, the phytoplankton biomass and production at DYFAMED are dominated by nanoplankton (J.-C. Marty et al., 2008). Even though diatoms are a small component of the phytoplankton at both sites they grow actively during the spring bloom period and their abundance increases. Specifically, the diatom biomass can exceed 25% at both BATS (Nelson & Brzezinski, 1997) and DYFAMED (Mayot et al., 2020) during the spring bloom. Hence, the changes in diatom parameters are mainly related to bloom period production.

Changes in the photosynthesis-irradiance parameters α and μ^{max} for both phytoplankton groups were crucial in reducing the model-data misfits and thus improving the prediction capability of REcoM2. These parameters express the physiological state of chlorophyll-a or, more generally, are used to characterize phytoplankton production. Under low light conditions, photosynthesis is a linear function of irradiance with the initial slope (MacIntyre et al., 2002), whereas, at light saturation, it proceeds at the maximum rate μ^{max} (Falkowski, 1981). A higher value of α means that under light-limiting conditions less chlorophyll-a concentration is needed to obtain the same primary production. Therefore, the model yields enough nanoplankton production with low chlorophyll-a in winter when light is limiting. On the other hand, decreased μ^{max} leads to less production, when light is not limiting. α_{Nano} changed the most at both stations – increased by 220% at BATS and 50% at DYFAMED.

At BATS, assimilating in situ NPP data together with satellite chlorophyll-a had a large influence on changes in these two photosynthesis parameters. Assimilation of only satellite chlorophyll-a concentration resulted in a value of α_{Nano}=0.22 at the station, which is only about half the value obtained when we assimilate both observation types. Further μ^{max}_{Nano} is reduced strongly to about one quarter ($\mu^{max}_{Nano} = 0.72$) of the default value at BATS when only the satellite chlorophyll-a is assimilated. At DYFAMED, on the other hand, assimilation of in situ NPP together with satellite chlorophyll-a made little difference in the estimate of α_{Nano}. Furthermore, assimilation of satellite

chlorophyll-a did not change the μ^{max}_{Nano} much at the site.
We found an opposite sign in updating these two photosynthesis parameters for diatoms. At BATS, α_{Dia} decreased by about 52%, while the parameter increased by about 37% at DYFAMED. Similarly, μ^{max}_{Dia} decreased around 72% at BATS and increased 17% at DYFAMED. Both α and μ^{max} vary with temperature, ambient inorganic nutrient (nitrate and phosphate) concentrations, and phytoplankton functional type. However, the relations are not linear, and the cause and effects in these relationships are unclear (Richardson et al., 2016). Diatom-dominated communities exhibit higher α and lower μ^{max} (Richardson et al., 2016). At DYFAMED, the discrepancies of surface chlorophyll-a concentration are less during the bloom spring period than the rest of the year. Most of the adjustment in the states and parameters happens during non-bloom periods when the diatom abundance is negligible at DYFAMED. On the other hand, most of the filter updates happen during the bloom period at BATS. This explains the higher value of α_{Dia} and lower value of μ^{max}_{Dia} at DYFAMED than BATS.
At BATS, satellite chlorophyll-a only assimilation reduces the simulated chlorophyll-a concentration to minimize model data misfit, which also reduces phytoplankton production in the model and increases the biases in NPP simulation during the non-bloom season (Figure 3.10). Simultaneous assimilation of satellite chlorophyll-a and in situ NPP data decreases the simulated chlorophyll-a concentration. On the contrary, it increases NPP in the non-bloom period and thus a smaller chlorophyll-a concentration is sufficient for high phytoplankton production. Therefore, to simulate high production with low chlorophyll-a concentration during the light-limiting conditions of the non-bloom period, the filter adjusts α_{Nano} to a high value and μ^{max}_{Nano} to a lower value. However, during the bloom season when diatoms have a larger contribution, the filter has smaller updates in the NPP simulation. Therefore, the estimation of α_{Dia} and μ^{max}_{Dia} do not show much difference between satellite chlorophyll-a only assimilation and simultaneous assimilation of satellite chlorophyll-a and in situ NPP.
The photosynthesis parameters α and μ^{max} have different values at the two stations. Spatial variability of these parameters due to temperature, nutrient availability and phytoplankton composition (H. A. Bouman et al., 2000). In REcoM2, these parameters are based on the mean values of Geider et al. (1998). In our experiment, the estimated values of α and μ^{max} for both phytoplankton groups (nanoplankton and diatoms) are within the range of Geider et al. (1998) and other BGC model literature (e.g., T. R. Anderson, 1993; Fasham et al., 1990). Similar values were reported at BATS from in situ profiles by Kovač et al. (2018) and in the Mediterranean Sea from a BGC-Argo data by Barbieux et al. (2019).
True values of BGC parameters (if available) are not constant over time and change during seasons (Simon et al., 2015) due to species composition. They also show interannual variability, which is also observed in our experiments. For example, d^{CHL}_{Nano} showed large variability during each assimilation cycle for both stations. Though the overall updates are small, the estimates of the parameter hardly stabilized over the course of the

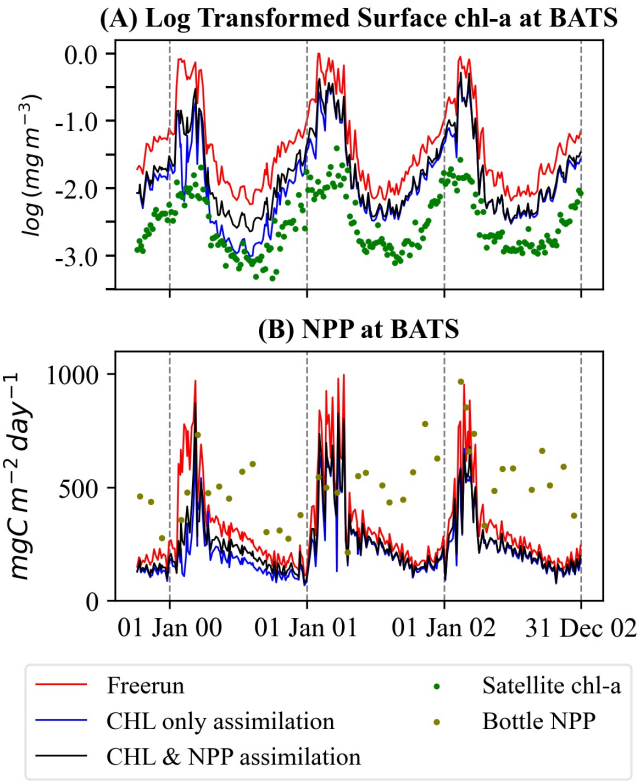

Figure 3.10 Simulated (A) log-transformed surface chlorophyll-a and (B) NPP in the parameter estimation experiments (EXP_{Joint_DP}) for free-run, satellite chlorophyll-a only assimilation and simultaneous assimilation of satellite chlorophyll-a and in situ NPP.

assimilation experiments, indicating a large uncertainty of the parameter with regard to chlorophyll-a concentration and NPP simulation. At DYFAMED, the final estimate of the parameter is close to the default value. However, it is quite variable in between and updated at each assimilation cycle. The parameter is less constrained during bloom peak episodes. Intra and inter-annual variations indicate that time-dependent parameters should be used in ocean BGC models. It also suggests that parameter values resulting from a short period may not be suitable for multi-decadal ecosystem studies or generating long biogeochemical reanalysis.

Though we get similar values of d_{Nano}^{CHL} at BATS, when assimilating only satellite chlorophyll-a and by the simultaneous assimilation of satellite chlorophyll-a and in situ NPP data, the value of d_{Nano}^{CHL} converges after the second bloom period for the earlier case at both sites. In contrast, simultaneous assimilation leads to time-varying parameter estimates. At DYFAMED, we obtain similar variation over time. However, the change in the parameter value is smaller.

Loss of chlorophyll from functional cells, here described by a chlorophyll degradation rate d^{CHL} is a necessary, but hard to constrain process in quota-based ecosystem models.

The original model by Geider et al. (1998) , which primarily describes photoacclimation on timescales of days, contains no such term, which becomes mainly important during low-growth situations in winter and at the lower boundaries of the euphotic zone. Without a chlorophyll loss term, which in reality describes complicated processes in senescent or photostressed cells, phytoplankton C:Chl ratios become unreasonable in such situations. The parameter is therefore usually tuned subjectively until when a reasonable agreement between observation and simulation is found and may not be suitable for biogeochemical models other than those for which they were tuned. A wide range of values of this parameter can led to improvement in the model results as the parameter shows correlation with other parameters (Figure 3.7). The estimated values resulted from all our joint-estimation experiments are below 0.25. It has been shown (Álvarez et al., 2018) that a replacement of the simple chlorophyll degradation model by a more process-based description of the degradation of photosystem functionality can lead to improvements in modeled C:Chl ratios. This should be pursued further.
In REcoM2, phytoplankton mortality is described by grazing and aggregation. The grazing parameters have large updates in both stations. At BATS, changes in the grazing parameters were prominent, while changes in aggregation were prominent at DYFAMED. In REcoM2, the loss process is dominated by aggregation compared to grazing (Laufkötter et al., 2016). However, at BATS, the model overall underestimated NPP compared to the in situ observations but overestimated surface chlorophyll-a (see Figure 3.2). Therefore, to reduce the model-data misfit of NPP and chlorophyll-a, the simulation had to keep the phytoplankton population sufficiently low through enhanced grazing. On the other hand, the model overestimated NPP compared to in situ observations, which compensated for more aggregation rather than grazing.
The durations of the spring blooms reproduced by the model and the filter are too short compared to the satellite data (Figure 3.9). Ensemble members using the default parameters overestimate the chlorophyll-a concentration during the bloom periods at BATS. The model state with estimated parameters displays a better fit to the observations at this site. This is an additional indication justifying the increased grazing at BATS. At DYFAMED, on the other hand, the surface chlorophyll-a concentration exhibits a better fit to the observations during the bloom period justifying the increased aggregation.
At BATS, the estimated maximum grazing rate of zooplankton ξ exceeds what is commonly considered a 'realistic' value in the biogeochemistry literature. Most likely, this parameter compensating for the other grazing parameter, i.e., γ, which indicates large uncertainty of the grazing process at BATS. Including both grazing parameters in the estimation process enabled the model to follow a trajectory that better fits with satellite chlorophyll-a concentration and in situ NPP. Satellite chlorophyll-a assimilation produces a more reasonable value of γ at BATS (0.61) but increases discrepancies in NPP simulation. Anderson et al. (2015) also used similarly high value of γ and found good agreement between simulation and observation of primary production but at different locations. In addition, more realistic values of both grazing parameters could be ob-

tained by representing phytoplankton mortality as physiological mortality in addition to aggregation as is currently used in REcoM2.
Though sparse in time, the assimilation of in situ NPP had a large impact on the parameter estimates at both sites, particularly at BATS. Parameter estimation with only satellite chlorophyll-a assimilation improves the modeled surface chlorophyll-a but deteriorates NPP (Figure 3.10). Assimilation of both satellite chlorophyll-a and bottle NPP data improves the NPP prediction by 25% compared to satellite chlorophyll-a only assimilation without deteriorating the chlorophyll-a prediction. Satellite chlorophyll-a data is insufficient to constrain the BGC parameters even though they are closely related. However, $_{14}$C primary production shows large discrepancies with satellite-based estimations as discussed in section 3.4.3.
We found correlations between some of the parameters which preclude those parameters from being estimated independently. Correlation between parameters can prevent estimating realistic parameter values. Co-dependencies between parameters mean that different sets of parameter values can be optimal. This suggests that BGC models have no single optimal configuration. Therefore, model parameters cannot be meaningfully "tuned" without additional conditions.
Some studies noted that BGC parameters often could not be effectively constrained, especially in high-dimensional cases when many parameters are considered together (Fiechter et al., 2013; Ward et al., 2010, 2013) due to the lack of available observations or specific types of observations. The optimal value of each parameter can depend on other variables that we have not assimilated. While we have reduced the model-data misfit substantially, correlations among parameters and dependence on other state variables lead to uncertainties in the estimated values of some parameters.
By perturbing ten selected parameters and updating them to bring the model close to observations, we assume that the remaining BGC parameters do not contribute to the model uncertainty. However, the existing knowledge of the BGC parameter uncertainties and their covariances is not sufficient to define a subset of parameters that is optimal. In this study, we assessed how uncertainties in a limited set of parameters are related to each other. Some of our results may depend upon the subset of parameters chosen for perturbation. Different combinations of parameters might lead to better model estimates than others. The covariances of BGC parameter uncertainties will need to be further explored.

3.4.2 Usefulness of estimated parameters

In section 3.3.1.1, we presented that the estimated parameters improved the prediction capability of REcoM2 substantially. However, limitations remain depending on the purpose of their use. One limitation is that parameter estimation experiments were conducted for three years. Thus, the improved parameters may not be optimal for long-term climate simulations/projections. Furthermore, the parameters varied over time,

and not all parameters converged to a constant value. Using the values from the end of the parameter estimation experiments as parameters for the subsequent experiments showed improved model skill. Nonetheless, it is not clear whether these values are the optimal choices.
An alternative to the parameter values at the end of the experiments is to take time averaged values over some later part of the experiment as estimated parameters. However, not all BGC parameters converge during the parameter estimation experiment. For example, α_{Nano} and γ do not have any clear convergence at BATS even after three years of data assimilation. We also performed an experiment using the estimated parameters averaged over the entire period of the DA experiment. The parameter values taken at the end of the experiments outperform the time-averaged parameter estimates. This also raises the question of the optimal length of the experiment, which is hard, if not impossible, to define. The three years period used in our experiments repeatedly covers the bloom and non-bloom seasons which should be sufficient for the parameter estimation. In our experiment some parameters did not converge. For these parameters, optimal values might vary in time in order to react to varying growth conditions. We estimated parameters in two different locations and found distinct optimal parameter values. This points to the fact that BGC parameters can vary substantially across space dependent of physical and ecosystem context. This implies that regional and global 3–D models should profit from using spatially varying parameter values. The methods we used here to estimate parameters can be extended to estimate spatially varying parameter values in a 3–D model. For this, each parameter has to be defined as a 3–D field which then can be estimated utilizing the cross covariances with the observation analogous to the 1–D setup.
The existence of correlations between some parameters indicates that there is no single combination of model parameters that can be considered to be optimal. This means that predictions of a single model configuration are likely to underestimate the magnitude of the uncertainty around the best estimates. Using an ensemble with perturbed parameters will help to represent this uncertainty.
In addition, we did not consider the uncertainty of the physical simulations in this study. It is possible that BGC parameters also compensate for uncertainties from model physics. Whereas ensemble-based DA would allow us to quantify uncertainty in model parameters, in the structure and in the forcing data used to compute the model predictions, the experiments implemented here focused only on parameter uncertainty and did not allow for quantification of uncertainty in the physical simulations.

3.4.3 Discrepancies of bottle NPP data at BATS

In situ bottle, NPP has large discrepancies with model predictions (Figure 3.8). At BATS, in situ NPP shows no prominent seasonality, at least for the period of our experiments. We further explored the satellite-derived NPP estimation based on the

CAFE model. We compared the monthly mean satellite-derived NPP with the monthly mean NPP resulting from the state estimation experiment with estimated parameters (EXP_{State_EP}) and in situ bottle data at BATS. Both model and satellite data show a clear seasonal cycle, whereas in situ bottle data is rather erratic (Figure 3.11). Tin et al. (2016) also found that satellite-based estimation captures the strong seasonality. In contrast, in situ data shows more variability due to errors in the measurement. Saba et al. (2010) found that ocean BGC models underestimate the NPP at BATS.

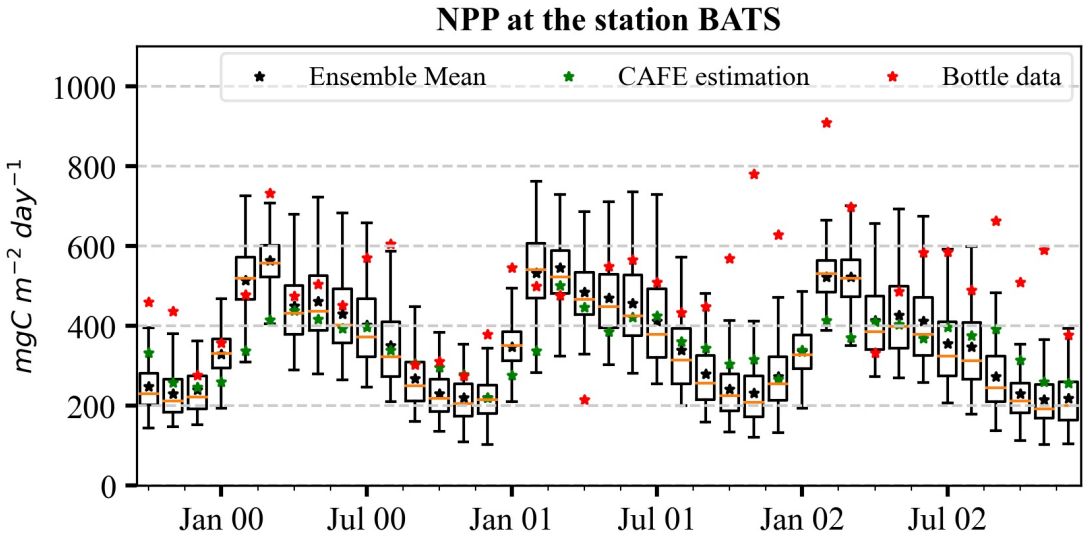

Figure 3.11 Comparison of monthly mean simulated NPP of EXP_{State_EP}, satellite-derived NPP based on SeaWiFS satellite and in situ bottle data. The box denotes the lower to upper quartile values of ensemble members. The horizontal line on the box is the median of the ensemble. The whiskers show the range of the ensemble.

Another explanation for the large model-data misfit at BATS is the absence of picoplankton in REcoM2, which causes the increase in phytoplankton biomass in the summer (White et al., 2015). At BATS picoplankton dominates the phytoplankton community during the off-peak period, becomes abundant in late spring to early winter but is usually scarce during the bloom period (Steinberg et al., 2001). Furthermore, the productivity of picoplankton is higher than other phytoplankton in the western Sargasso Sea (Malone et al., 1993) and is sensitive to nitrogen limitation. In summer and fall, when the thermocline is shallow (deep nitracline), nitrogen levels (Nitrate + Nitrite) go below 80m from the surface. Therefore, picoplankton grows in the deeper part of the euphotic zone (DuRand et al., 2001). Another possibility is that in fall when deep mixing does not occur, the temperature of the euphotic zone rises and picoplankton grows deep in the water column below the euphotic zone (Fawcett et al., 2014). Thus, picoplankton has a greater impact on deep chlorophyll maximum (DCM) during the off-peak period, which is not represented in REcoM2. Therefore, REcoM2 may underestimate the total NPP

in picoplankton-dominated regions.

A DCM is a common feature that occurs below the mixed layer in the oligotrophic ocean. We further investigate the vertical profile of chlorophyll-a concentrations for the existence of a deep chlorophyll maximum layer (DCML) at BATS. As can be seen in Figure 3.12, the simulated depths of DCML are shallower than the observed DCML during the off-peak periods. DA application did not change the DCML and the vertical structure of the chlorophyll-a profile much. Any deepening in DCML should reflect NPP increases. The observed DCML peaks between 60 and 120m (Figure 3.12), indicating active picoplankton production during the off-peak period at BATS, which is absent in the model. High surface chlorophyll-a concentrations in spring are associated with deep convective mixing, which leads to a shallower DCML. At BATS, most of the phytoplankton groups increase during bloom periods rather than any single group (Steinberg et al., 2001). This suggests that the picoplankton grows above the euphotic zone during the bloom period at BATS. However, during the off-peak period, the most important biomass component of the DCML is picoplankton which the model does not represent. This could also explain the underestimation of NPP at BATS by REcoM2.

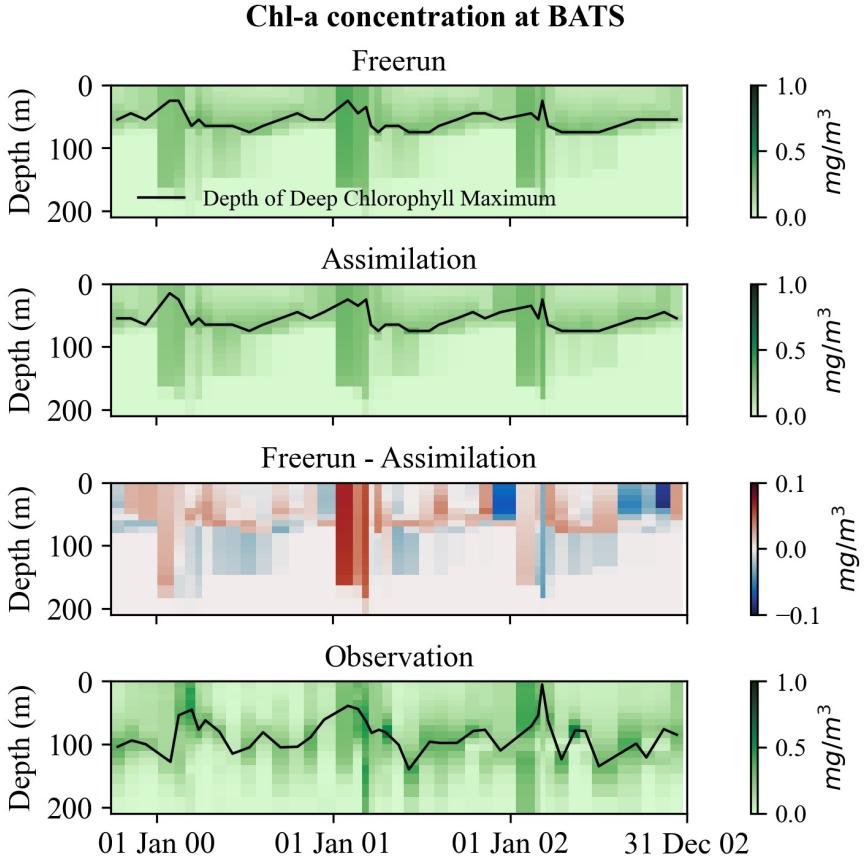

Figure 3.12 Simulations of chlorophyll-a concentration of EXP_{State_EP} at BATS. The black solid lines represent DCML.

3.5 Conclusions

In this study, we estimated the values of ten preselected parameters of the BGC model REcoM2 and evaluated the effectiveness of the estimated parameters on the predictive performance of the model, including the uncertainty quantification of the parameters at two BGC time-series stations – BATS and DYFAMED. The parameters characterize the major processes of phytoplankton sources and sinks, such as photosynthesis, chlorophyll degradation, grazing and aggregation. We used a 1–D configuration of the coupled MITgcm-REcoM2 model and assimilated 5-day satellite chlorophyll-a concentration and monthly in situ NPP for 3 years at both sites applying the ESTKF, an ensemble square root filter. The estimated parameters were assessed and found to improve the prediction capability and the seasonal variability of the model simulations.

The parameter estimation procedure generated improved parameter values when satellite chlorophyll-a and in situ NPP data were simultaneously assimilated. Assimilating satellite chlorophyll-a data alone did not adequately constrain the model. In this case, the filter adjusted the model towards optimal chlorophyll-a simulations. However, it generated parameter values that resulted in larger model-data misfits for NPP. We also found large discrepancies in situ NPP data, which may arise not only from the 14C methodology but also from the distribution of particles and organisms in the highly oligotrophic BATS and DYFAMED waters (Harris et al., 1989).

The strongest updates of the parameters happen during the spring blooms at both stations. As the spring bloom intensity at BATS is lower than at DYFAMED, the pattern of changes in the parameters at BATS is more irregular, not only in one season but throughout the entire assimilation period. As expected, the parameter update is strongly linked to the bias in the estimates of the state variables. Given the large bias in surface chlorophyll-a at BATS, some parameters (e.g., α_{Nano} and γ) may be subject to changes even after three years of assimilation, whereas at DYFAMED, we obtained more stable parameter values. The contribution of diatoms in the phytoplankton community is larger at BATS than at DYFAMED. This complements our finding that grazing parameters are more important than aggregation for describing phytoplankton mortality at BATS. We found that dependences between some parameters exist – a change in one parameter affects the evolution of others. This behavior indicates that multiple different combinations of parameter values are possible, and therefore they cannot be estimated independently. It further suggests that BGC models have no single optimal configuration and predictions from single model configuration are likely to underestimate the magnitude of the uncertainty around the best estimates. The solution is to design ensemble modeling approaches using a sufficiently large ensemble with perturbed parameters.

Given the high parameter uncertainty of BGC models, parameter estimation is essential. However, the model simulations depend on the parameter values in non-linear ways and vary spatially and temporally, which requires a systematic examination of parameters in time and space. Estimating spatial and temporal varying parameter values will allow

for efficient exploration of BGC process and modeling at the basin and global level. We believe that the method and learning from this study will serve as an important base for conducting spatially and temporally varying ocean BGC parameter estimation studies at the global level. Estimation of spatially and temporally varying parameter values in a 3–D global ocean BGC model will be considered in future studies.

Chapter 4

Spatially varying biogeochemical parameter estimation in a global ocean model

This chapter extends the scope and application of data assimilative experiments from location-specific to a global scale by incorporating spatial variations in parameter values within a 3–D model. Using the Parallel Data Assimilation Framework - PDAF, this study employs an ensemble Kalman filter to estimate the optimal parameter values by assimilating satellite ocean color data. The study estimates spatially and temporally varying values of nine parameters selected based on a sensitivity analysis (See Chapter 2) and obtained global parameters maps, allowing more interpretation than the location-specific 1–D analysis. The spatial variations of the obtained parameter values are similar to those reported from observation. The dynamical variations of model simulation using the estimated set of parameter values are closer to the observations than that of using the uniform default parameter values. This chapter presents the effects of estimated spatially and temporally varying parameters on the BGC fields and dynamics for insights into BGC modeling.
This chapter is based on a manuscript in preparation titled 'Spatially Varying Biogeochemical Parameter Estimation in a Global Ocean Model', planned to be submitted to an open-access journal.

Citation: Mamnun, N., Vlker, C., Vrekoussis, M., & Nerger, L. (In preparation). Spatially Varying Biogeochemical Parameter Estimation in a Global Ocean Model.

Abstract

Ocean biogeochemical (BGC) models are a primary tool for investigating ocean biogeochemistry and the global carbon cycle. These models contain many uncertain and often poorly constrained parameters that describe physical and biochemical processes, resulting in large uncertainties in the model outputs. Although these BGC process parameters are often used as constant values in model simulations, in reality they can vary across space and time. This study assimilates satellite ocean color data into the ocean BGC model Regulated Ecosystem Model 2 (REcoM2) to estimate spatially and temporally varying parameters in a global model setup. We apply an ensemble Kalman filter provided by the Parallel Data Assimilation Framework – PDAF to simultaneously estimate selected, selected based on a sensitivity analysis, uncertain parameters and the BGC model states. We then quantify the spatiotemporal uncertainties linked to the estimated parameters and the prediction uncertainties induced by those parameters. We further assess the performance of REcoM2 using the estimated spatially and temporally varying parameters. We show that ocean color-derived surface chlorophyll-a concentration can effectively constrain the uncertainty in the BGC model parameters. The parameters converge in most of the world's oceans in less than a year and reduce the BGC parameter uncertainty. The model simulations with the set of estimated parameters are closer to the observations than the reference simulation using spatially uniform parameter values, with a 52% reduction of root mean square error for surface chlorophyll-a concentration.

4.1 Introduction

Ocean biogeochemical (BGC) models provide an integral tool for studying ocean BGC processes and their effect on the global carbon cycle. They are an essential component of the Earth system models used to simulate climate projections (Orr et al., 2017). These models play a central role in quantifying the patterns and rates of ocean anthropogenic CO_2 uptake (see Crisp et al., 2022) and estimating the global carbon budget (see Hauck et al., 2020). The latter is important because the global ocean absorbs more than a quarter of anthropogenic emissions of CO_2 (Friedlingstein et al., 2022). In this direction, ocean BGC models are pivotal for i) characterizing future ocean CO_2 uptake and its sensitivity to climate change under different policy scenarios (see Crisp et al., 2022), ii) assessing the predictability of global-scale atmosphere-ocean CO_2 flux relevant to carbon policy and management (Ilyina et al., 2021), and iii) investigating deliberate CO_2 removal (see Gattuso et al., 2018).

Ocean BGC models are further used to investigate ocean deoxygenation (e.g., Andrews et al., 2017; Bopp et al., 2017), ocean acidification (e.g., Gehlen et al., 2007; Ilyina et al., 2009; Krumhardt et al., 2019), and to study compound events with overlapping extremes of acidification, marine heatwaves and deoxygenation (e.g., Gruber et al., 2021; Hauri

et al., 2021). They are used to assess the economic impact of climate change on fisheries (e.g., Loukos et al., 2003) and to project changes in fish catch potential (e.g., Cheung et al., 2010; Lam et al., 2016). These models are used to develop marine environmental applications and services (e.g., Gutknecht et al., 2019; E. M. Jones et al., 2016) and to generate reanalysis datasets (e.g., Carroll et al., 2020; Ciavatta et al., 2016).

Ocean BGC models are spatially explicit models that describe the transformations of BGC constituents by ecosystem growth and interactions. BGC constituents include nutrients, functional plankton groups, non-living organic matter, dissolved gases, and variables of the inorganic carbon system contained in seawater. Either through choice or necessity, each BGC transformation in the model is described by simplified process formulation known as parameterizations, which require process parameters. Ocean BGC models include various biophysical processes and involve numerous process parameters (see Fennel et al., 2022). The uncertainty of these parameter values is quite large (see Schartau et al., 2017), leading to possibly significant uncertainty in the model outputs. Ocean BGC models describe numerous plankton species into a handful of functional types - for instance, all the zooplankton are described as a generic class in REcoM2. The available reference parameter values related to these functional classes were usually taken from laboratory experiments targeting single species, while in the model, they are applied broadly to describing whole classes of organisms. The values of the parameters depend on the physical and biogeochemical context (see Follows et al., 2007), which influences the ecosystem species distribution and the acclimation of individual species. Thus, in reality, the parameter values vary spatially and temporally, while in practice, they are used as constant across space and time in the model simulations.

In this context, data assimilation (DA) aids in estimating the values for BGC parameters, which are difficult (if not impossible) to measure. DA infers for parameter values, resulting in an optimal match between simulation output and observations. Due to the high computational expense of running a data assimilative model multiple times over a large three-dimensional (3–D) domain, parameter optimization is often carried out in a one-dimensional (1–D) BGC model. Studies estimated BGC parameters in multiple locations (e.g., Friedrichs et al., 2007; Gharamti, Tjiputra, et al., 2017; Mamnun et al., 2022; Schartau & Oschlies, 2003) and found different estimated parameter values across locations. Sometimes, parameter values estimated from a 1–D assimilative application are then used in a 3–D implementation (e.g., McDonald et al., 2012; Oschlies & Schartau, 2005; St-Laurent et al., 2017).

Losa et al. (2004) estimated six BGC parameters into a simple box model (0-D) at different locations in the North Atlantic and obtained varying parameters in different cells. Tjiputra et al. (2007) estimated spatially varying BGC parameters using an adjoint method by assimilating satellite chlorophyll-a concentration. They showed that using estimated spatially variable parameters improved the global simulation of net primary production (NPP). Doron et al. (2013) estimated five spatially varying BGC parameters by assimilating ocean color-derived chlorophyll-a into a 3–D regional model. They

found better model-data agreement using spatially varying estimated parameters than the reference simulation using uniform ones. Estimating four spatially varying BGC parameters, Simon et al. (2015) found regional patterns of estimated parameters similar to the Longhurst provinces (Longhurst, 2007) in the regions where the model used performs reasonably. They demonstrated that BGC predictions generally benefit from spatially varying parameter estimates. Xu et al. (2022) estimated spatially varying BGC parameters in the Bohai, Yellow, and East China Seas, assimilating satellite chlorophyll-a data using an adjoint method and obtaining reasonable parameter values. Using an idealized twin (identical twin) experiment, Singh et al. (2022) showed that estimating spatially varying ocean BGC parameters is feasible using ensemble-based data assimilation techniques in global-scale models.

Incorporating temporally varying parameters can significantly improve the agreement between models and observations (e.g., Mattern et al., 2013, 2014; Roy et al., 2012; Simon et al., 2015). Simon et al. (2015) specifically identified seasonal patterns in estimated parameters and advocated using time-dependent parameters in ocean BGC models. However, they also highlighted that in regions with substantial model errors, the parameter values either converge to extreme values, resulting in larger model errors or may diverge toward a high ensemble spread. Singh et al. (2022) also noted that even in an ideal model setting, certain BGC parameters fail to converge to their true values when significant model errors occur.

The high parameter uncertainty of BGC models, combined with sparse and error-prone BGC observations, poses significant challenges in establishing relationships among BGC parameters, model state variables, and observations. In a high-dimensional BGC model, the number of unknown model state variables and parameters exceeds the available observations, creating an underdetermined inverse problem that DA seeks to solve by utilizing a small number of observations to estimate a large set of unknowns. Despite the benefits of using satellite-derived surface observations for BGC state estimations (e.g., Ford & Barciela, 2017; Goodliff et al., 2019; Gregg, 2008; Nerger & Gregg, 2007, 2008; Pradhan et al., 2019, 2020), it remains unclear how effectively they can constrain uncertain BGC parameters in a 3–D global ocean model and estimate their spatially varying values. Additionally, the response of the joint state-parameter estimation algorithm to the highly nonlinear relationships and non-Gaussian error statistics inherited from convection is poorly understood.

This study applies DA to estimate nine spatially and temporally varying parameters in a global ocean biogeochemical model. We assimilated ocean color-derived chlorophyll-a concentration into a global setup of the BGC model Regulated Ecosystem Model Version 2 (REcoM2, Hauck et al., 2013; Schourup–Kristensen et al., 2014). We estimated nine spatially and temporally varying REcoM2 parameters, chosen based on a global sensitivity analysis (Mamnun et al., 2023). We further assessed the skill of REcoM2 in a simulation using the estimated spatially and temporally varying parameters. We discuss the effect of estimated spatially and temporally varying parameters on BGC processes

and modeling.

4.2 Materials and Methods

4.2.1 The Coupled Hydrodynamic -Biogeochemical Model

In this study, we used a coupled hydrodynamic-biogeochemical model. The Massachusetts Institute of Technology General Circulation Model (MITgcm, Marshall, Adcroft, et al., 1997; Marshall, Hill, et al., 1997) solves the ocean dynamics and tracers transport, while REcoM2 handles BGC reactions and transformation.

MITgcm is a 3–D, finite-volume, general circulation model. It solves the time-dependent, Boussinesq-approximation Navier-Stokes equations with or without hydrostatic approximation and conservation equations for salinity and energy. The non-hydrostatic capabilities allow the users to use the model to study small-scale and global processes. The open-source MITgcm code (Campin et al., 2023) can be customized to different configurations by modifying its available packages or coupling new packages according to the user's requirements and the design of the numerical experiment. A sea ice model (Losch et al., 2010) is integrated with MITgcm. The BGC model REcoM2 is coupled with MITgcm as an additional package (Losch et al., 2008).

REcoM2, a so-called quota model (Droop, 1983), describes the two phytoplankton groups – nanophytoplankton and diatoms, and a generic heterotrophic zooplankton class. The nanophytoplankton has an implicit representation of calcifiers. REcoM2 has one class of organic sinking particles whose sinking speed increases with depth.

The model describes the carbon cycle, the nutrients nitrogen, silicon and iron, and chlorophyll. The intracellular stoichiometry of carbon, nitrogen, calcite, and chlorophyll ($C\colon N\colon Chl$) pools for nanophytoplankton and carbon, nitrogen, silicate, and chlorophyll ($C\colon N\colon Si\colon Chl$) pools for diatoms are allowed to respond dynamically to the environmental conditions following Geider et al. (1998) and Hohn (2009) for the Si quota. The intracellular iron pool is a function of the intracellular nitrogen concentration (fixed ironto nitrogen ratio), as iron is physiologically mainly linked to nitrogen metabolism and the photosynthetic electron transport chain (Behrenfeld & Milligan, 2013; Geider & La Roche, 1994). Dead organic matter is transferred to detritus by aggregation and grazing by the zooplankton group, and the sinking and advection of detritus are represented explicitly.

The model has two external iron sources: atmospheric dust deposition and sedimentary input. The iron cycle in the model is driven by biological uptake, remineralization, and scavenging onto biogenic and lithogenic particles.

4.2.2 Model setup

This study employs a global model configuration of the so-called Lat-Lon-Cap 90 grid (LLC90, Forget et al., 2015), representing the spherical Earth in a Cartesian curvilinear coordinate system using a cubed-sphere structure in the northern hemisphere and a dipolar grid arrangement in the southern hemisphere. The Cartesian curvilinear coordinate grid system has five faces covering the globe (figure 4.1A). The grid cells are approximately aligned with lines of latitude and longitude between 70°S and ~57°N, and a unique Arctic "cap" is positioned north of ~57°N. Each of the four faces south of ~57°N is partitioned into three tiles, and the Arctic "cap" has a single tile. Thus, the grid consists of 13 tiles. In the case of LLC90, each tile comprises 90×90 horizontal grid cells (hence LLC90). The horizontal model grid resolution varies spatially, ranging from 22km to 110km, with the highest resolutions at high latitudes and the lowest resolution at mid-latitudes (figure 4.1B). There are 50 vertical levels. The vertical grid spacing increases with depth from 10m at the surface layer to 456.5m at the bottom layer.

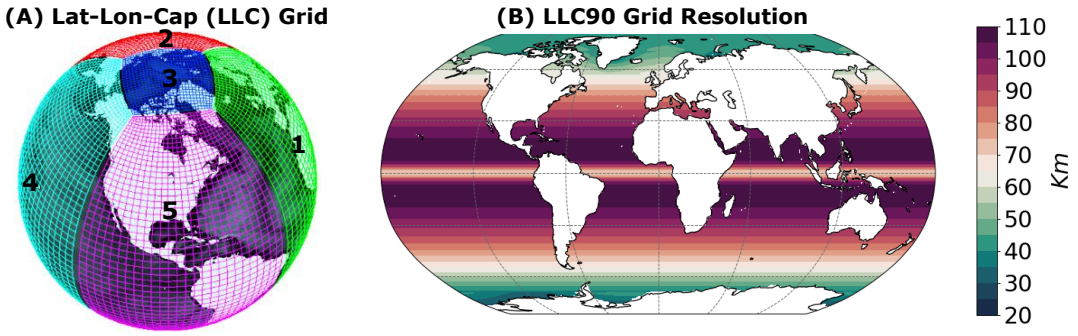

Figure 4.1 Lat-Lon-Cap (LLC) Grid. A) Five faces of the LLC grid. The figure is adopted from Forget et al. (2015); B) The horizontal resolution of the LLC90 grid.

We initialized the temperature, salinity, and dissolved oxygen (DO_2) fields using the winter mean data from the World Ocean Atlas 2018 (WOA-18, Boyer et al., 2018; García et al., 2019a; Locarnini et al., 2019; Zweng et al., 2019). For the dissolved inorganic nitrogen (DIN) and silica (DSi) fields, we used annual climatology from WOA-18 (García et al., 2019b). The total alkalinity (ALK) and the dissolved inorganic carbon (DIC) fields were initialized with mapped climatological data from the GLobal Ocean Data Analysis Project (GLODAPv2, Lauvset et al., 2016). To initialize the dissolved iron (DFe) field, we relied on concentrations obtained from a previous PISCES model run. We used the monthly dust deposition field from the present-day simulation of Albani et al. (2014) to compute DFe input flux from the atmosphere, assuming 3.5% iron content in dust particles and 2% iron solubility. All other passive tracers were initialized with small arbitrary values.

We utilized the inter-annually varying atmospheric forcing (temperature, humidity, downward radiation, and precipitation) from the 6-hourly ERAInterim reanalysis fields

(Dee et al., 2011) from 1992 to 2018 and from ERA-5 hourly reanalysis fields (Hersbach et al., 2020) for 2019 to 2021. For consistency, hourly ERA5 data were interpolated to 6-hourly data. Freshwater runoff is forced using the river and ice-sheet melting runoff data from the JRA55-do dataset (Tsujino et al., 2018).

4.2.3 Data Assimilation Methods

We employ an ensemble-based sequential DA approach, the Ensemble Kalman Filter (EnKF, see review by Vetra-Carvalho et al., 2018), the most common sequential DA method used for BGC models. EnKFs utilize an ensemble of model state realizations to account for model uncertainties. Each realization is represented by a model state vector, which may encompass multiple state variables and process parameters from the coupled physical-biogeochemical system. Subsequently, when observations become available, the ensemble states undergo an update by integrating the observations with the model forecast. A weight matrix is computed based on a covariance matrix of the model forecast ensemble and the observation error to determine the influence of the observations on the model state. The weight matrix assigns relative weights to the forecast and the observations. Upon completing the analysis step, the updated ensemble of state vectors serves as the input for the subsequent forecast phase. This iterative process allows EnKFs to effectively assimilate data and improve the accuracy of the model predictions.

Error Subspace Transform Kalman Filter

We implemented the ensemble DA with the Parallel Data Assimilation Framework (PDAF, Nerger & Hiller, 2013), an open-source software (accessible at http://pdaf.awi.de). PDAF offers comprehensive and parallelized ensemble filter algorithms and support for parallel ensemble integrations and can be implemented within existing model code as a library. PDAF currently contains the ability to implement many variants of EnKF. We used the localized (Nerger et al., 2012a) error subspace transform Kalman filter (ESTKF, Nerger et al., 2012b) for all of our DA experiments in this study. ESTKF is a highly efficient filter for high-dimensional models. As an ensemble square root filter, ESTKF computes the weights for the ensemble transformation directly in the error subspace represented by the ensemble and can be used with a deterministic minimum transformation, allowing the use of small ensembles. Domain localization (Nerger et al., 2012a) is used in this study. In the domain localization approach, each vertical column of the model grid is considered a disjoint local domain. Only observations with a distance smaller than a cut-off radius are used in the analysis step for a given local domain. No ensemble inflation is used in this study.

Ensemble Generation

We apply perturbations to nine process parameters of the REcoM2 model to generate an ensemble of BGC model states. Our goal is to minimize the uncertainty associated with the initial parameter values through stochastic estimations using satellite-derived surface chlorophyll-a concentration data. Accordingly, we targeted the perturbation to parameters showing high sensitivity to the model outputs of surface chlorophyll-a concentration. The selection of these nine parameters was informed by a sensitivity analysis conducted by Mamnun et al. (2023).
Among the nine selected model process parameters, four are phytoplankton photosynthesis-irradiance parameters (H. A. Bouman et al., 2018), two cell quotas - the maximum chlorophyll to nitrogen ratios, two parameters for chlorophyll degradation, and one zooplankton grazing-related parameter. Table 4.1 lists the selected parameters, including their symbols, units, and default values. We adopted the values used by Hauck et al. (2013) as default values.
We utilized a lognormal function to generate random perturbations across all the selected parameters. The respective default values of the parameters were considered the expected value of the distribution, with a standard deviation set at 25% relative to the default value. These perturbations induce subtle differences in the biogeochemical processes across different ensemble members, consequently generating a diverse range of model outcomes. We defined each selected parameter as a two-dimensional (2–D) field within the model and established that each ensemble member has a different set of parameter values. In each ensemble member, the initial values of these parameters were identical across all 2–D grid points.

The (augmented) state vectors

From the BGC model, we included eight model state variables and the total chlorophyll-a concentration of phytoplankton in the state vector. The state variables consist of the following:

1. Biomass content of carbon in nanophytoplankton
2. Biomass content of carbon in diatoms
3. Biomass content of nitrogen in nanophytoplankton
4. Biomass content of nitrogen in diatom
5. Calcium carbonate concentration of nanophytoplankton
6. Biogenic silica concentration of diatoms
7. Chlorophyll-a concentration of nanophytoplankton
8. Chlorophyll-a concentration of diatoms

We assimilate the surface chlorophyll-a concentration of phytoplankton, the surface chlorophyll-a concentration of all phytoplankton available in the ocean. We, therefore, include a variable “total chlorophyll-a concentrations” in the state vector by summing

Table 4.1 The nine selected BGC parameters with their symbol, unit and default value.

	Parameter	Symbol	Unit	Default value
1	Nanophytoplankton Initial slope of the Photosynthesis-irradiance curve	α_{Nano}	mmolC $(\text{mgChl})^{-1}$ $(Wm^{-2}d)^{-1}$ *	0.14
2	Diatom initial slope of the Photosynthesis-irradiance curve	α_{Dia}	mmolC$(\text{mgChl})^{-1}$ $(Wm^{-2}d)^{-1}$	0.19
3	Nanophytoplankton Maximum photosynthesis rate	μ_{Nano}^{max}	d^{-1}	3.00
4	Diatom maximum photosynthesis rate	μ_{Dia}^{max}	d^{-1}	3.50
5	Maximum chlorophyll to nitrogen ration of Nanophytoplankton	$q_{Nano}^{Chl:Nmax}$	mg Chl $(mmolN)^{-1}$	3.15
6	Maximum chlorophyll to nitrogen ration of diatom	$q_{Dia}^{Chl:Nmax}$	mg Chl $(mmolN)^{-1}$	4.2
7	Nanophytoplankton Chl degradation rate	d_{Nano}^{Chl}	d^{-1}	0.10
8	Diatom Chl degradation rate	d_{Dia}^{Chl}	d^{-1}	0.10
9	Maximum grazing rate of zooplankton	ξ	mmol N m^{-3} d^{-1}	2.4

* The unit indicates millimoles of carbon produced per milligram of chlorophyll, adjusted for the amount of light energy received daily per square meter.

up the chlorophyll-a concentration of nanophytoplankton and diatoms. The observation operator for this variable, total chlorophyll-a concentrations, selects corresponding values from the state vector and subsequently updates the eight model state variables through cross-covariances with the total chlorophyll-a concentration.

We applied the state augmentation approach (J. L. Anderson, 2001), which merges state variables and parameters into an augmented state vector, treating the parameters as time-varying variables. This augmented state vector method facilitates the estimation of parameters, given the observation of specific variables and the multivariate covariances between model parameters and model variables.

EnKF's optimality, based on a Gaussian state distribution (Evensen, 2003), is challenged in the ocean BGC model due to non-Gaussian state distribution (Nerger & Gregg, 2007) arising from uncertainty in BGC parameters. To address this challenge, we transformed the chlorophyll-a concentration, both model and observation, to a logarithmic scale,

following the assumption that its distribution is lognormal (Campbell, 1995). This logarithmic transformation was applied also to other BGC state variables, assuming a similar probability distribution as chlorophyll-a concentration. Moreover, since the parameters were perturbed following a lognormal distribution, we also log-transformed their values before each assimilation cycle for analysis.
An advantage of the log-transformation approach is that it prevents estimating unrealistic negative concentrations or parameters during the assimilation process, which could otherwise arise due to the Kalman filter's linear combination of model estimates and observations. By employing this technique, we ensure that the assimilation maintains the integrity of BGC variables and parameters as positive quantities, aligning with their inherent natural constraints.

4.2.4 Experiments design

Three sets of experiments have been performed in this study – (i) reference simulations, (ii) joint state-parameter estimation, and (ii) adjusted simulations. The experiments are as follows, and an overview of all experiments performed is presented in Table 4.2.

Reference Simulations

To assess the effectiveness of our parameter estimation and skills of estimated parameters we conducted four reference simulations using default parameter values (DPVs). We adopted the parameter values used in the study by Hauck et al. (2013) as DPVs. The reference simulations are:

- *Reference single forward run (REF_FOR):* We conducted a single 30-year model run from 1992 to 2021, using the initial conditions specified in Section 2.2 Model setup. This simulation served as the basis for initializing the ensemble reference simulations.
- *Reference ensemble free run (REF_FRE):* We performed a 40-member ensemble simulation spanning three years from 2019 to 2020. The ensemble models were initialized using the restart files from the REF_FOR run. For each ensemble state, perturbations to the DPVs of selected model parameters were applied to generate the BGC ensembles. The hydrodynamic model states were kept identical for each of the ensemble members.
- *Reference Reanalysis (REF_REA):* We conducted a BGC state estimation experiment by assimilating satellite-derived chlorophyll-a concentration data using a 40-member ensemble. The ensemble models were initialized using the same restart files of the experiment REF_FRE at the beginning of 2018 with perturbed parameter values. The REF_ REA experiment was run for three years, from January 2018 to December 2020. During the first year, no DA was performed to allow the model to

undergo a spin-up and reach a stable state. Subsequently, the DA was applied for the years 2019 and 2020.

Joint State-Parameter Estimation (JSPE)

In these experiments, we augmented the state vector by 2–D fields of the selected BGC parameters and updated them in each assimilation cycle together with the state variables. The initial model states were identical to the initial states of REF_REA. Similar to the experiment REF_REA, the year 2018 was considered a spin-up, and in the next year (2019), only state estimations were performed identically to the experiment REF_REA to minimize the model uncertainties sourced from other than parameter perturbation. Subsequently, the BGC state variables and parameters were updated simultaneously by DA analysis in 2020.

Adjusted Simulations

We implemented three experiments with the estimated parameter values (EPVs) resulting from the experiment JSPE. They are similar to the reference simulations, except we utilized the estimated spatially varying parameter values here. The experiments are:

- *Adjusted single forward run (ADJ_FOR):* This is a single 30-year model run identical to the experiment REF_FOR, but using the estimated spatially varying parameter values.
- *Adjusted 40-member ensemble free run (ADJ_FRE):* This experiment is identical to REF_FRE, but uses the estimated spatially varying parameters.
- *Adjusted state estimation of BGC assimilation (ADJ_REA):* This experiment is identical to REF_REA, but using the estimated spatially varying parameters.

4.2.5 Observational data

The DA process utilized remotely sensed surface chlorophyll-a concentration obtained from the European Space Agency's Ocean Colour - Climate Change Initiative project (OC-CCI; Sathyendranath et al., 2019) product, Version 6.0. This product was created by merging satellite data from multiple sensors. The dataset consists of a 5-day mean level-3 binned data presented on a global sinusoidal grid with a resolution of 4 km.
The dataset includes per-pixel error statistics estimated by analyzing match-ups between in situ data and ocean color. We used these error statistics as observation uncertainty in the DA analysis. Specifically, we computed and assimilated unbiased values of chlorophyll-a concentration interpolated on the model grid analogous to Pradhan et al. (2019).

Table 4.2 The experiments performed in this study.

Experiment	Description	Parameter Used	Time period
REF_FOR	Reference single forward run	DPVs	1992-2021
REF_FRE	Reference 40-member ensemble free run	Perturbed DPVs	2019-2020 and one-year prior spin-up
REF_REA	Reference state estimation with BGC assimilation	Perturbed DPVs	2019-2020 and one-year prior spin-up
JSPE	Joint state-parameter estimation with BGC assimilation	Spatiotemporal varying	2020 plus one-year prior state-only estimation and one year spin-up
ADJ_FOR	Adjusted single forward run	Spatially EPVs	1992-2021
ADJ_FRE	Adjusted 40-member ensemble free run	Spatially varying perturbed EPVs	2019-2020 and one year prior spin-up
ADJ_REA	Adjusted state estimation of BGC assimilation	Spatially varying perturbed EPVs	2019-2020 and one-year prior spin-up

4.3 Joint state-parameter estimation

4.3.1 Impact of the joint estimation on the state variables

For accurate parameter estimation, it is essential that the assimilation effectively constrains the uncertainty of state variables. The uncertainty in these state variables, especially at the surface, can significantly impact near-surface BGC processes. In this study, all assimilation experiments improved the simulation of surface chlorophyll-a concentration compared to the free run (REF_FOR), as measured by root mean square errors (RMSE) relative to the assimilative observations. Specifically, the JSPE reduced the RMSE between observations and model output by 51%, compared to the RMSE from the REF_FOR.

Figure 4.2 shows the area-weighted RMSE for surface chlorophyll-a for the experiments REF_FOR and JSPE. During the spring, the concentration of surface chlorophyll-a obtained from each experiment is highly depleted, resulting globally in a large RMSE compared to observations (Figure 4.2A). The model (REF_FOR) is more skillful in the equatorial region (Figure 4.2B) than the higher latitudes. The joint parameter-state estimation was comparatively more effective in mid-latitudes than the low and

high latitudes (Figure 4.2C, D). The model performs poorly during spring in the high latitude of the respective hemisphere, and so does the joint state-parameter estimation (Figure 4.2E, F), most likely because of the low number of observations. JSPE has an enormous influence during the spring bloom in the north. However, the remaining RMSE is still high.

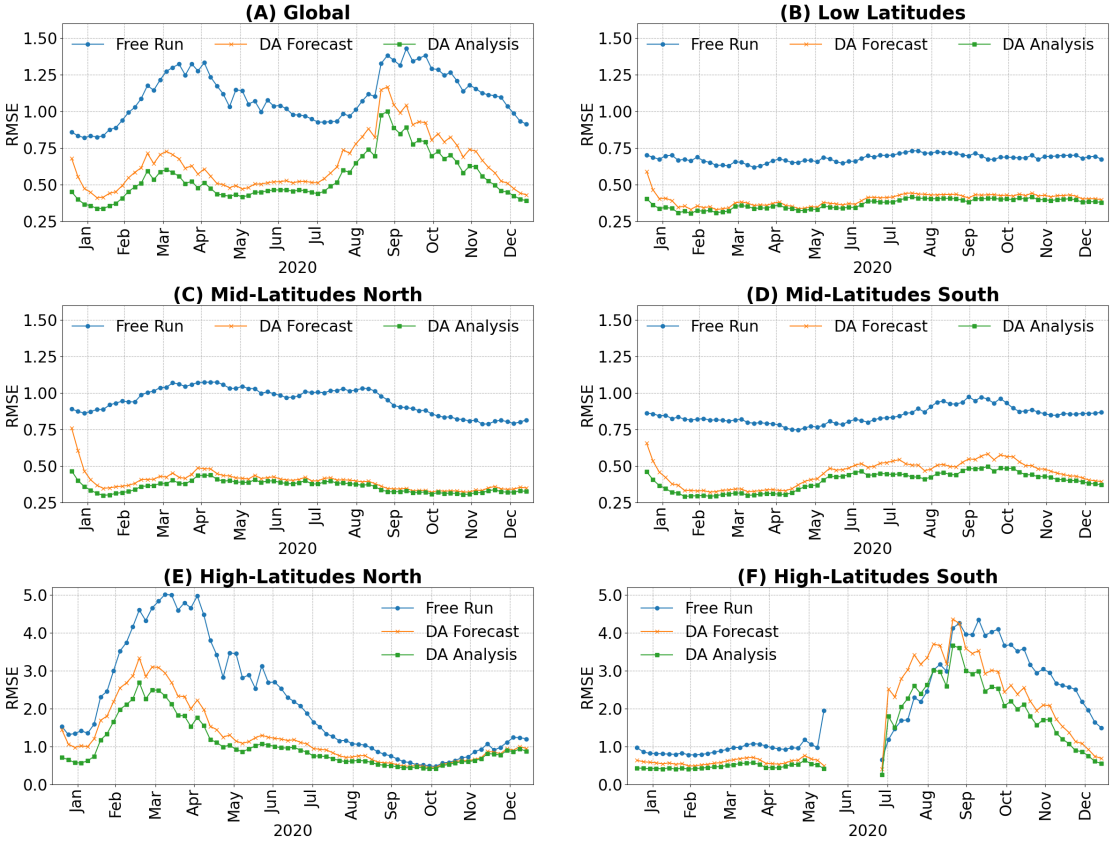

Figure 4.2 Comparison of area-weighted RMSE of log-transformed surface chlorophyll-a concentration relative to the OC-CCI data (A) for all available observations (Global); (B) from the 10°S–10°SN latitude (Low Latitude); (C) 10°N–50°N - (Mid-Latitude North); (D) 10°S–50°S (Mid-Latitude South); (E) North of 50°N (High Latitude North) and (F) South of 50°S (High Latitude South)

We evaluated the spatial distributions of the monthly mean of the logarithm of surface chlorophyll-a concentration for April and September (Figure 4.3). These two months chosen as the global area-weighted RMSEs are higher than the other months. We compare the ensemble mean of surface chlorophyll-a concentration simulated without DA (REF_FRE) and with DA (Analysis of JSPE) to observations. REF_FRE performed poorly with high positive bias in high latitudes. The JSPE experiment shows a better field with spatial pattern closer to the observations than the REF_FRE. However, in particular, in September, the model still overestimates the chlorophyll-a concentration compared to the observations.

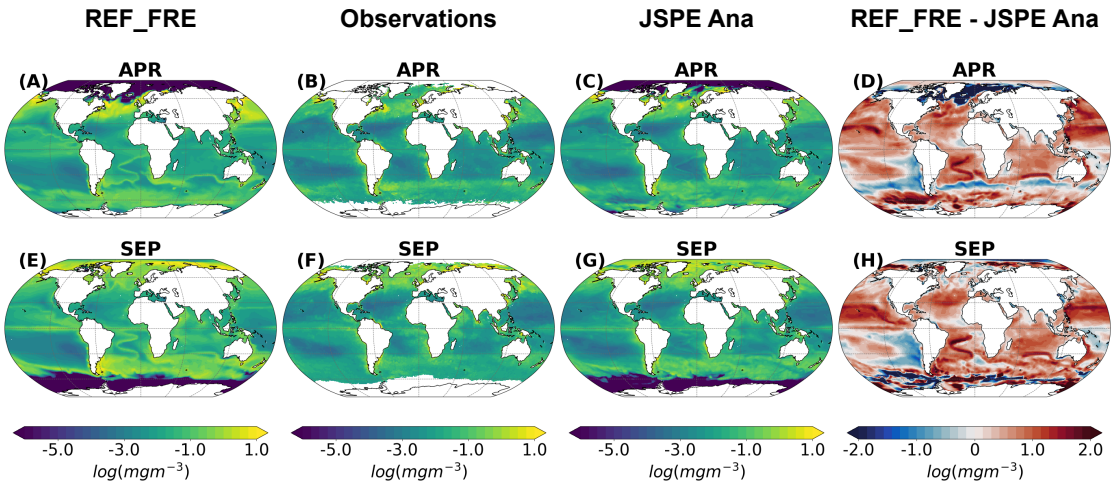

Figure 4.3 Monthly mean log-transformed surface chlorophyll-a concentrations for April 2020 (A-D) and September 2020 (E-H). From left to right: (REF_FRE); ESA OC-CCI data; JSPE analysis results and difference of JSPE analysis results from REF_FRE.

4.3.2 Parameter Estimation

This section discusses the estimated spatially varying BGC model process parameters. The DA estimates the parameters using their correlation with the total chlorophyll-a field (e.g., J. L. Anderson, 2001). The robust performance of the DA simulation compared to the free run for state estimation (Section 4.3.1) is partly due to the simultaneous optimization of the model parameters. In this section, we emphasize the spatial variability of the estimates of these parameter values. Figure 4.4 shows estimated parameter values in the global ocean for the nine parameters we considered for this study at the end of the first year of data assimilation. The global average, minimum, maximum, and standard deviation of spatially varying estimated parameters are presented in Table 3. The values of the BGC parameters vary in regions depending on the physical and BGC conditions naturally. All nine estimated parameters exhibit values larger and smaller than their default value, showing that DA optimizes the model's parameterization regionally with correlation to the observation.

Initial slope of the P-I curve of nanophytoplankton (α_{Nano}) and diatoms (α_{Dia})

The initial slope of the P-I curve (α) delineates the efficiency with which an organism conducts photosynthesis under limited light conditions by characterizing the relationship between photosynthetic rate and light intensity (Denman, 2003). The estimated values of α_{Nano} and α_{Dia} increase in most parts of the globe (Figure 4.4A and D) relative to their respective default values, and so do the global averages for both (Table 4.3).

A higher value of α indicates that a lower chlorophyll-a concentration is sufficient to achieve equivalent primary production under light-limited conditions. Consequently, the model predicts adequate phytoplankton production with reduced chlorophyll-a during winter when light is limited. However, to compensate for the negative model bias in the Subtropical South Pacific Ocean, the filter increased the values of α_{Nano} even though the light is not limited here. However, α_{Dia} has only slightly increased in this region, perhaps due to iron limitation diatom growth is limited thus not sensitive here. The Subarctic Atlantic Ocean is another region where the values of both α_{Nano} and α_{Dia} increased to compensate for where the REF_FRE produces low chlorophyll-a (Figure 4.3). On the other hand, the values of α_{Nano} decrease in the Subantarctic Zone of the Antarctic Circumpolar Current while the values of α_{Dia} increase in this region. In the coastal areas, the values of α_{Nano} increase in general, whereas the values α_{Dia} show no clear pattern of changes in coastal areas.
Compared to observations (see H. A. Bouman et al., 2018; Marañón & Holligan, 1999), the estimated values of α_{Nano} are higher than the maximum observed values in the Subtropical South Pacific Gyre, the South Atlantic, and the Barents Sea (Figure 4.4A). The values of α_{Dia} show no such extreme values; higher values are observed in the iron-limited South Pacific Ocean and the Barents Sea, though.

Maximum photosynthesis rate of nanophytoplankton (μ^{max}_{Nano}) and diatoms (μ^{max}_{Dia})

The maximum photosynthesis rate of phytoplankton (μ^{max}) defines the peak rate at which phytoplankton can transform inorganic carbon into organic matter through photosynthesis under optimal light and nutrient conditions (Denman, 2003). Unlike α_{Nano} and α_{Dia}, the values of μ^{max}_{Nano} and μ^{max}_{Dia} change in opposite directions – the global average of μ^{max}_{Nano} decreases from its default value, whereas that of μ^{max}_{Dia} increases (Table 4.3). Similarly, the spatial patterns of the estimated values of μ^{max}_{Nano} and μ^{max}_{Dia} show opposite signs – in those regions where the values of μ^{max}_{Nano} increase from its default value, the values of μ^{max}_{Dia} decrease from its default value, and vice versa (Figure 4.4B, E). Both nanophytoplankton and diatoms compete for similar resources, such as light and nutrients. The model has a competition term between nanophytoplankton and diatoms for a shared resource (Hauck et al., 2013), which might lead to an inverse relationship between their maximum photosynthesis rates. In general, the values of μ^{max}_{Nano} increase where the model highly underestimates the chlorophyll-a simulation, e.g., the Arctic Atlantic Ocean and the Subarctic Atlantic Ocean.

The maximum chlorophyll to nitrogen ratio in nanophytoplankton ($q^{Chl:Nmax}_{Nano}$) and diatoms ($q^{Chl:Nmax}_{Dia}$)

The maximum chlorophyll to nitrogen ratio ($q^{Chl:Nmax}$) defines the upper limit of chlorophyll-a that can be produced per unit of phytoplankton nitrogen, reflecting the

maximum chlorophyll content associated with specific nitrogen biomass in phytoplankton (Omta et al., 2017). The global spatial average values of $q_{Nano}^{Chl:Nmax}$ and $q_{Dia}^{Chl:Nmax}$ lower their default value (Table 4.3). The chlorophyll to nitrogen ratio reflects the ability of phytoplankton to utilize available nitrogen for growth and chlorophyll production. Therefore, the maximum Chl to nitrogen ratio indicates how efficiently the phytoplankton cells utilize nitrogen resources. A lower value of $q^{Chl:Nmax}$ implies that phytoplankton can produce less chlorophyll per unit of nitrogen than those of higher value. The filter reduces the values of $q_{Nano}^{Chl:Nmax}$ and $q_{Dia}^{Chl:Nmax}$ over the large part of the global ocean (Figure 4.4 C, F) to compensate for the overall overestimation of the surface chlorophyll-a simulation. However, the values of $q_{Nano}^{Chl:Nmax}$ are increased in the Subtropical Pacific Ocean, where the model underestimates the surface chlorophyll-a concentrations, whereas the values of $q_{Dia}^{Chl:Nmax}$ are not changed much in this region. Relatively less update of parameters related to diatoms in the Subtropical Pacific Ocean implies that diatom concentrations dominate less here, possibly because of iron deficiency. The values $q_{Dia}^{Chl:Nmax}$ show extreme in some regions, e.g., the Norwegian Sea, the Bellinghausen Sea, and the Amundsen Sea.

Chlorophyll degradation rate of nanophytoplanktons (d_{Nano}^{Chl}) and diatoms (d_{Dia}^{Chl})

The chlorophyll degradation rate (d^{Chl}) represents the rate at which chlorophyll is broken down or degraded, thus affecting the amount of chlorophyll available in phytoplankton, which in turn influences phytoplankton production. Though the global spatial average values of d_{Nano}^{Chl} and d_{Dia}^{Chl} are close to their default values (Table 4.3), they vary spatially two orders of magnitude (with 51% and 40% standard deviation of the global mean, respectively). The patterns of spatial variation of these two d_{Nano}^{Chl} and d_{Dia}^{Chl} are similar (Figure g, h) and directed by the model data misfit.

The maximum grazing rate of zooplankton (ξ)

ξ represents the maximum possible rate at which zooplankton can consume phytoplankton under ideal conditions – a measure of the grazing pressure zooplankton can exert on phytoplankton populations. The global average value ξ is higher than its default value (Table 4.3). A higher value of ξ can lead to a higher removal rate of phytoplankton from the system, thus decreasing the surface chlorophyll-a concentration and a lower of ξ leads to an increase in the surface chlorophyll-a concentration. The values of this parameter increase in a large part of the world's oceans to compansate the overestimation of surface chlorophyll-a by the model. The value decreased in the Arctic and Subarctic Atlantic Ocean, the East and West India Coast, the South Subtropical Convergence, and some parts of the Sub-Antarctic Water Ring. The dynamic range of estimated ξ values is quit high with values ranging from 0.12 to 20.34 $mmolNm^{-3}d^{-1}$ One possible interpretation for the resulting extensive range in ξ is that we did not adjust the grazing efficiency (γ),

which is highly sensitive to the surface chlorophyll-a simulation. Thus, a change in ξ would compensate for γ.

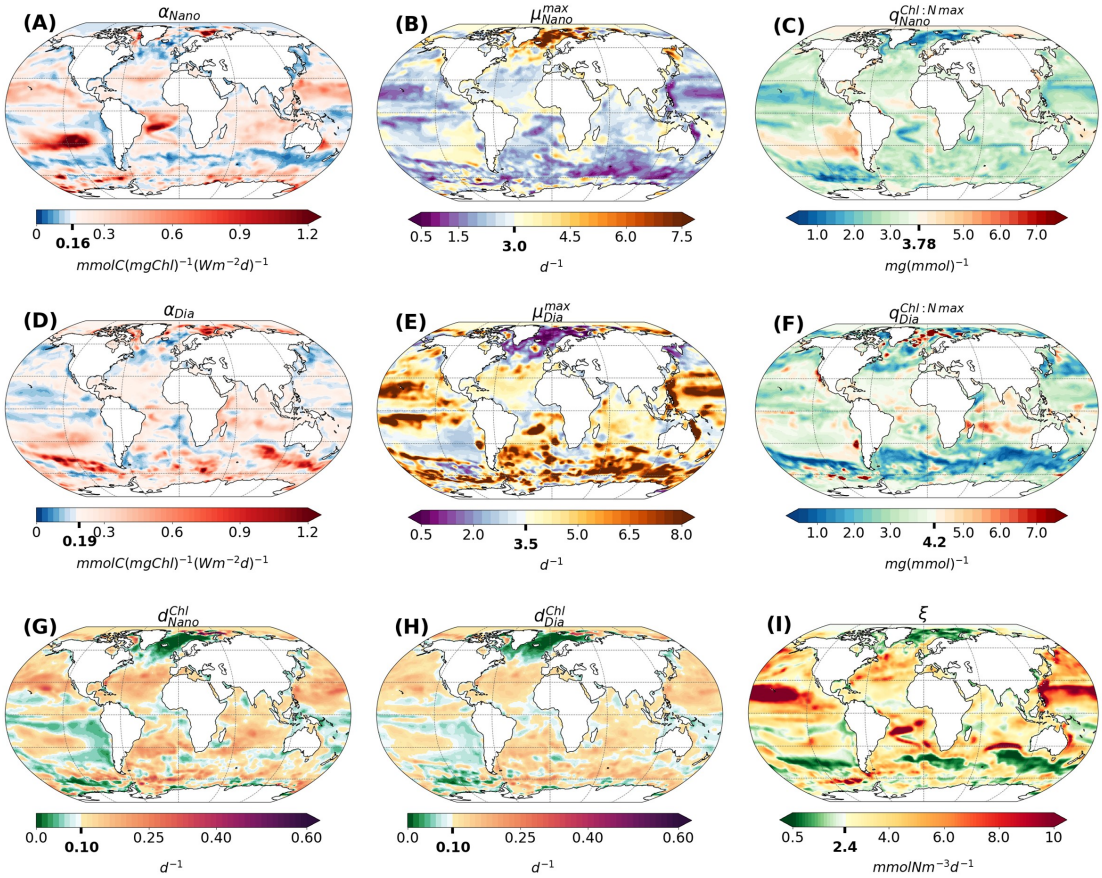

Figure 4.4 Estimated parameters values for initial slope of the Photosynthesis-irradiance curve of nanophytoplankton (A) and diatoms (D); maximum photosynthesis rate of nanophytoplankton (B) and diatoms (D); maximum chlorophyll to nitrogen ratio of nanophytoplankton (C) diatoms (F); Chl degradation rate nanophytoplankton (G) and diatoms (H); maximum grazing rate (I). The bold value indicated by the major tick mark on the color bar represents the default value.

The joint state-parameter estimation reduces the ensemble spread relative to the initial spread across all parameters. A spatial consistency is observed in the retrieved pattern values that align well with the spatial distribution of chlorophyll-a, though discrepancies persist. Small-scale noise is likely due to spurious correlations in our finite ensemble size of 40. Regions, where the estimation does not converge correspond to regions where the model exhibits deficiencies in simulating surface chlorophyll-a.

Table 4.3 The default value, global average, minimum, maximum and standard deviation (percentage relative to global average) of spatially varying estimated parameters.

	Parameter	Default value	Average value	Minimum value	Maximum value	Standard Deviation
1	α_{Nano}	0.14	0.23	0.009	2.4	0.17 (73%)
2	α_{Dia}	0.19	0.26	0.01	1.5	0.19 (73%)
3	μ^{max}_{Nano}	3.00	2.67	0.38	17.72	1.14 (43%)
4	μ^{max}_{Dia}	3.50	4.20	0.20	29.84	2.06 (49%)
5	$q^{Chl:Nmax}_{Nano}$	3.15	3.02	0.44	7.87	0.74 (24%)
6	$q^{Chl:Nmax}_{Dia}$	4.2	3.32	0.23	40.43	1.31 (31%)
7	d^{Chl}_{Nano}	0.10	0.107	0.001	0.98	0.055 (51%)
8	d^{Chl}_{Dia}	0.10	0.1007	0.001	0.43	0.04 (40%)
9	ξ	2.4	3.18	0.12	20.34	0.24 (62%)

4.3.3 Temporal evaluation along the Atlantic Ocean

To further elaborate, we monitored the time evolution of the estimated parameter values in 12 Longhurst provinces (Longhurst, 2007) along the Atlantic Ocean (see Figure 4.5). Most changes in the parameters occur during the bloom periods. In the low and mid-latitudes, most parameters reach more stable values by 30 DA cycles and show minor variability over time. However, as expected in the high latitudes, the parameters show more considerable temporal variability than in low and mid-latitudes.

The photosynthesis-irradiance α_{Nano} and α_{Dia} exhibit large temporal variability in the Polar provinces (Figure 4.5A, D), predominantly due to the latitudinal distribution of incident irradiance. In the Northern Hemisphere, heightened irradiance during the spring and summer months leads to decreased α_{Nano} and α_{Dia} values in the ARCT and SARC provinces. Conversely, during autumn, the values of both parameters continuously increase, surpassing their default values. They remain relatively stable for the remainder of the year. In the ANTA and SANT provinces, α_{Nano} and α_{Dia} consistently remain above their default values. In mid and low latitudes, most variations in these parameters occur during the initial cycles of DA experiments, after which they either stabilize or exhibit a discernible trend. Notably, α_{Nano} undergoes more pronounced changes than α_{Dia} in these mid and low-latitudinal provinces.

The opposite signs of chages in photosynthetic parameters μ^{max}_{Nano} and μ^{max}_{Dia} are also evedent in thier temporal evaluations (Figure 4.5A and D). Large updates in these parameters occur in ARCT and SARC provinces where the values of μ^{max}_{Nano} contineously icreased and the values of μ^{max}_{Dia} decreased from the begening of DA experiments untill the spring bloom then values for both parameter show steady. In the most of the provinces

Table 4.4 Code corresponding to Longhurst province, as defined by Longhurst (2007), included in the analysis.

Code	Province	Code	Province
ARCT	Atlantic Arctic	WTRA	Western Tropical Atlantic
SARC	Atlantic Subarctic	ETRA	Eastern Tropical Atlantic
NADR	North Atlantic Drift	SATL	South Atlantic Gyre
NASE	North Atlantic Subtropical Gyre East	SSTC	South Subtropical Convergence
NASW	North Atlantic Subtropical Gyre West	SANT	Subantarctic
NATR	North Atlantic Tropical Gyre	ANTA	Antarctic

the values of these parameters converges and not clear temporal variabilities are notice. The temporal evaluations of the photosynthetic parameters μ_{Nano}^{max} and μ_{Dia}^{max} reveal opposite trends in their changes (Figure 4.5B, E). In the ARCT and SARC provinces, there are substantial updates to these parameters: μ_{Nano}^{max} values consistently increase, while μ_{Dia}^{max} values decrease from the start of the DA experiments up to the spring bloom. Subsequently, the values for both parameters stabilize. In most provinces, the values of these parameters converge, and no distinct temporal variations are observed.
The $q_{Nano}^{Chl:Nmax}$ and $q_{Dia}^{Chl:Nmax}$ exhibit pronounced temporal variability, especially in the Polar provinces (Figure 4.5C and F). In most provinces, these values are consistently below their default levels. Thus, each province has lower values than default in the final estimates. Although both parameters deviate from their default values, they do not exhibit similar patterns of change.
The values of d_{Nano}^{Chl} and d_{Dia}^{Chl} exhibit similar trends over time. In most provinces examined, both parameters increase from their default values (Figure 4.5G and H). However, in the ARCT and SARC provinces, there is a significant reduction in their values. Provinces where d_{Nano}^{Chl} and d_{Dia}^{Chl} values increase also display temporal variability, with particularly elevated values observed during the spring and summer.
The grazing parameter ξ undergoes substantial updates during the initial DA cycles. ξ regulates phytoplankton biomass at the surface when phytoplankton concentration is high. Thus, To counteract the model's general overestimation of surface chlorophyll-a concentration, the values of ξ increase in most provinces to reduce phytoplankton concentration. Notable exceptions include the ARCT, SARC, SSTC, and SANT provinces. Despite these large updates, no discernible seasonal variability is observed.

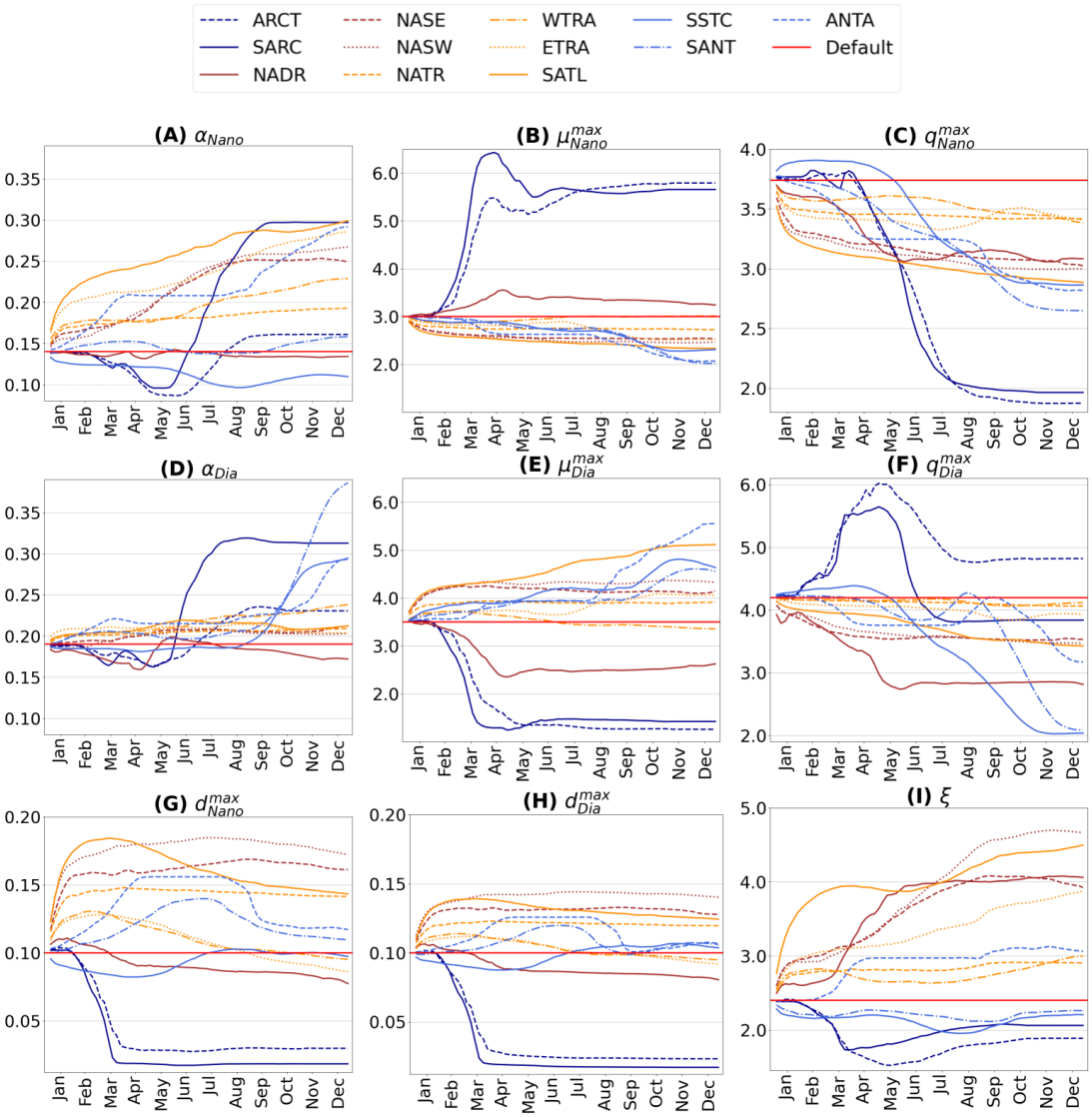

Figure 4.5 Temporal evaluation of average estimated parameter values across the 12 Longhurst provinces as listed in Table 4.4. The numbering of the subplots corresponds to that in Figure 4.4.

4.3.4 Model Run with Estimated Parameters

We verify the state accuracy of a single model forward run and an ensemble free run that uses the final parameter's estimates of experiments JSPE. We refer to them as ADJ_FRE and ADJ_REA, respectively. We compare the performance against the reference runs. This section presents the accuracy of the state variables in the reanalysis, which started in January 2019 and was run until December 2020 using spatially varying estimated parameters.

We first compare the annual average of chlorophyll-a concentrations obtained from both

simulations averaged from 2017 to 2021, with reference to OC-CCI averaged from the exact durations in Taylor diagrams (K. E. Taylor, 2001). The surface chlorophyll-a concentration simulated by the experiment ADJ_FRE outperforms the reference run (REF_FRE) with a 26% reduction of RMSE for the annual average of the surface chlorophyll-a concentrations from 2017 to 2021 (Figure 5). The correlation coefficient of the ADJ_FRE with OC-CCI data is much higher (0.73) than the correlation coefficient of the REF_FRE (0.52). Then, we compare the monthly average for April and October from 2017 to 2021, also with reference to OC-CCI monthly averaged data from the same durations as the spring in the northern and southern hemispheres, respectively.

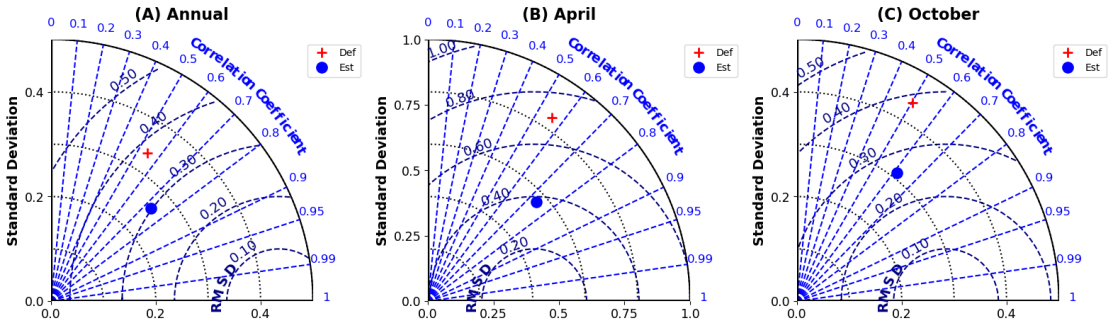

Figure 4.6 Taylor diagrams illustrating the comparison of surface chlorophyll-a concentration from model simulations with default parameters and estimated parameters against satellite observations for the period 2019-2021. The diagrams represent: (A) Annual mean, (B) Monthly mean for April, and (C) Monthly mean for October.

We evaluated the spatial distributions of the modeled vertically integrated NPP for default and estimated parameters and compared them with estimatesbased on satellite data , such as the updated carbon-based productivity model (CbPM, Westberry et al., 2008). CbPM uses spectrally resolved light attenuation based on a semi-analytical algorithm the Garver-Siegel-Maritorena (GSM, Betancur-Turizo et al., 2018). Over large parts of the global ocean, the vertically integrated NPP simulations agree reasonably with the observations. Nevertheless, there are regional differences. The misfits between the model simulations and satellite data-based estimates are large in high latitudes and coastal areas. Large deficiencies are particularly evident in coastal regions, which could be linked to model parameter estimation deficiencies or high uncertainty of satellite-data based NPP estimates in coastal water (see Westberry et al., 2008). The GSM algorithm used to estimate CbPM NPP tries to distinguish the optical signatures from phytoplankton, particles, and dissolved organic matter but still requires regional tuning in coastal regions, where non-biotic optically active material makes chlorophyll-a retrieval challenging.

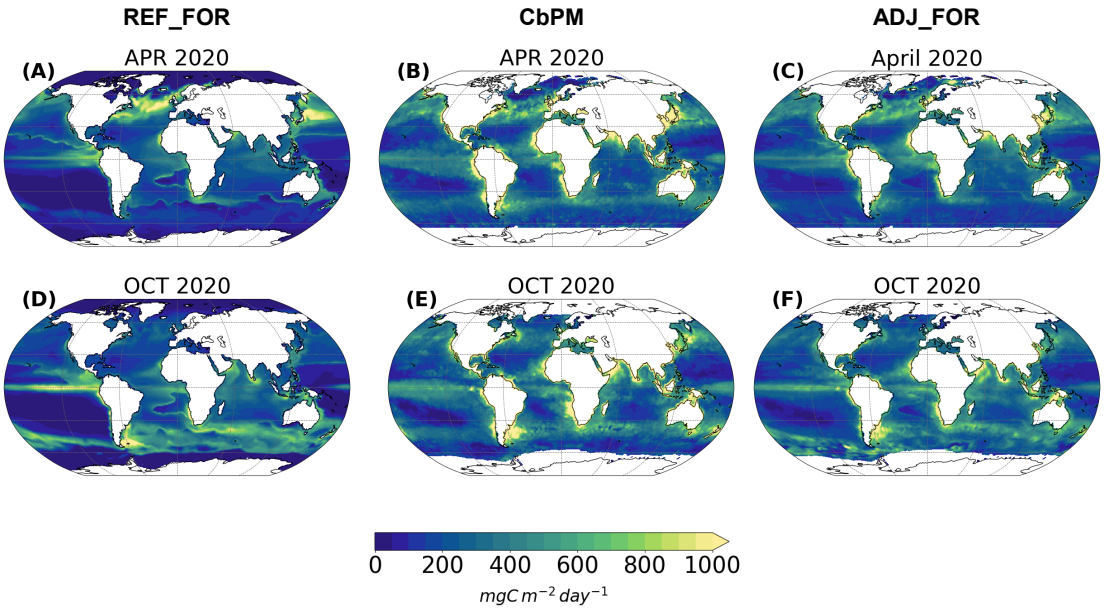

Figure 4.7 Monthly mean vertically Integrated NPP. The top row (A-C) is for April 2020, and the bottom (D-F) is for October 2020. The left column (A and D) is the reference simulation of a single model with DPVs (REF_FOR), the middle column (B and E) is for satellite-based estimation and the right column (C and F) is from the simulation of a single model with EPVs (ADJ_FOR).

4.4 Discussion

4.4.1 Subset of Parameters

In this study, we estimate the spatially varying values of nine parameters on a global scale using ocean color data assimilation. The number of parameters considered is comparable to other studies (e.g., Gharamti, Samuelsen, et al., 2017; H. H. Kim et al., 2021; Losa et al., 2004; Mamnun et al., 2022; Singh et al., 2022), which typically ranges from 3 to 15. Utilizing DA to estimate many BGC parameters may result in low predictive skills due to overfitting to observational noise (Friedrichs et al., 2007). The efficacy of parameter estimation depends on the sufficiency of available observations to accurately constrain the chosen parameters (Thacker, 1989). Directly correlating surface chlorophyll-a with phytoplankton biomass is challenging, given the variability and often ambiguous nature of the chlorophyll-to-biomass ratio. Even with a known chlorophyll to biomass ratio, satellite chlorophyll-a observations primarily inform parameters sensitive to surface chlorophyll-a. Nevertheless, several state variables other than surface chlorophyll-a might exhibit high sensitivity to the same parameters (Mamnun et al., 2023). Consequently, relying solely on satellite chlorophyll-a data for parameter estimation may leave these variables inadequately constrained. Relying on a singular observation type might be insufficient to differentiate between multiple viable parame-

ter combinations, exemplifying the underdetermination issue frequently encountered in BGC modeling (Ward et al., 2010).
We considered nine preselected parameters to align the model more closely with observational data, assuming that other BGC parameters do not significantly influence model uncertainty (Mamnun et al., 2023). Nonetheless, the current understanding of BGC parameter uncertainties and their interrelationships is inadequate for determining an optimal parameter subset. The outcomes of our analysis might be influenced by the specific parameters we chose to modify. Different parameter combinations could yield more accurate model predictions.
Analogous to the underdetermination problem, correlations between parameters can hinder the identification of a single optimal set of parameter values (Fiechter et al., 2011; Mamnun et al., 2022; Mattern et al., 2017). A notable manifestation of these parameter co-dependencies is the cancellation of uncertainties. In such cases, the model may align with available observations, not because each parameter value is optimal but because the uncertainties in correlated parameters offset each other. Therefore, individual parameter values may not be portable to other model configurations.

4.4.2 Spatial variation of estimated parameters

Allowing spatial variation in parameter values reduced the model data misfit with respect to both assimilated and independent data (section 3.3). However, this does not inherently validate the significance of these variations in relation to the foundational BGC processes. In this section, we aim to explore the spatial patterns of the estimated parameters concerning the primary environmental factors that dictate variability in these parameters and chlorophyll-a concentration.

Photosynthesis-irradiance parameters

The photosynthesis-irradiance parameters vary in response to various factors, from environmental to community composition (Bouman et al., 2018). Physical forcing governs nutrient availability, modulates the mean irradiance in the surface mixed layer, and critically influences phytoplankton cells' physiological performance (Carvalho et al., 2020). The estimated values of photosynthesis-irradiance parameters exhibited large spatial differences.
The values of α_{Nano} and α_{Dia} vary globally by two degrees of magnitude. This agrees with other global studies (see Bouman et al., 2018). The parameter values generally increased in high-latitude regions (Figures 4.4A and D). An increased value for the parameter α signifies enhanced photosynthetic efficiency of phytoplankton in a low-light environment. The parameter α is modulated by environmental variables that exhibit pronounced latitudinal variations, such as temperature and light availability (Harrison &

Platt, 1986). The upper ocean physical dynamics and their influence on temperature and light conditions critically shape the photosynthetic efficiency of marine phytoplankton in polar and temperate regions (H. Bouman et al., 2005; Harrison & Platt, 1986). Although large-scale shifts in the estimated α_{Nano} and α_{Dia} values are observed, temporal differences between seasons are only observed at higher latitudes.

In the oligotrophic Subtropical Pacific Ocean, the values α_{Nano} and α_{Dia} show increasing trends but never converge in the DA process. In these regions, the model consistently produces low nanophytoplankton chlorophyll-a concentration, mostly likely because of a limited supply of nutrients, thus negatively biased with observations. To compensate for the consistent biases, the filter raised the values of both α_{Nano} and α_{Dia} in the ocean basin. In contrast, the extreme values of α_{Nano} around 30°S of the basin indicates that the values of the parameter compensate for the uncertainty produced by other parameters or other components of the modeling system.

The estimated values of α_{Nano} and α_{Dia} in the oligotrophic North Atlantic were similar to the observations (see H. A. Bouman et al., 2018). The spatial pattern obtained in this study is also similar to Losa et al. (2004). For instance, some gradients of the values are observed. The values of α_{Nano} decrease with the increase of the latitude. Although the gradient for α_{Dia} is not prominent, it exhibits a similar pattern, i.e., the values increase from north to south. Similar spatial patterns were obtained by Losa et al. (2004). The values around the Bermuda Atlantic Time-series Study (BATS) agree with the value obtained by Mamnun et al. (2022) and Spitz et al. (2001).

A higher value of the maximum growth rate increases photosynthesis, thus increasing phytoplankton biomass. A higher phytoplankton growth rate will initially increase the productivity in these oligotrophic subtropical Pacific and subtropical Atlantic regions. However, the nutrient may be depleted over more extended periods (5 or more years) because there would be less supply of new nutrients below the euphotic zone. Subsequently, this condition leads to a reduction in the overall biological productivity.

There is generally a poor correlation between biomass and phytoplankton production in high latitudes (Platt et al., 1991). The relative uncoupling between the chlorophyll-a and the production distributions allowed the filter to make the parameters μ^{max}_{Nano} and μ^{max}_{Dia} highly variable over space. μ^{max}_{Nano} varied globally by a factor of ∼46 in this study (range: 0.38 to 17.72 d^{-1}) similar to observations (Marañón & Holligan, 1999). However, the μ^{max}_{Dia} variation was two degrees of magnitude, which is comparatively larger than reported in the observation (see H. A. Bouman et al., 2018). Diatoms have higher values of maximum photosynthesis rate depending on their size (Richardson et al., 2016). However, spatially varying estimates of this study show no indication of having higher values of μ^{max}_{Dia} compared to μ^{max}_{Nano}.

Spatiotemporal differences in the photosynthesis parameters μ^{max}_{Nano} and μ^{max}_{Dia} are likely driven by changes in oceanographic conditions (e.g., temperature, stratification, macro and micronutrient availability) (Geider et al., 1996) and in community structure and other biological processes that may consume cellular energy at the expense of carbon

fixation (Puxty et al., 2016). Cold water at high latitudes may limit the photosynthesis parameters μ_{Nano}^{max} and μ_{Dia}^{max} for carbon fixation (Smith Jr & Donaldson, 2015), which is reflected in the generally low values of these parameters in the boreal and austral polar regions (Figures 4.4B and E). Sea surface temperature (SST) can govern the variations in photosynthesis parameters (Behrenfeld & Falkowski, 1997a, 1997b; Harrison & Platt, 1980; Zaiss et al., 2021). However, in this study, the warm temperatures encountered in tropical latitudes were not accompanied by consistently elevated values of μ_{Nano}^{max} and μ_{Dia}^{max}. Similarly, Marañón and Holligan (1999) found no significant dependency of these parameters on SST. The lack of correlation between SST and maximum photosynthesis rate in the open ocean justified the latitudinal pattern of estimated parameter values in the current study.

Nutrient availability is the main factor controlling the large variability of photosynthesis parameters (Marañón & Holligan, 1999). The estimated photosynthesis parameters μ_{Nano}^{max} and μ_{Dia}^{max} in this study are correlated to the variations in the annual maximum mixed layer depth (MLD), which can be seen as a proxy for nutrient flux into the upper mixed layer. To delve deeper into the relationship between nutrient availability and photosynthesis parameters, we examined the model's annual maximum MLD for 2020. Figure 4.8 provides a visual representation of this analysis, with Figure 4.8A illustrating the maximum MLD and Figure 4.8B highlighting the month in which this maximum MLD occurred.

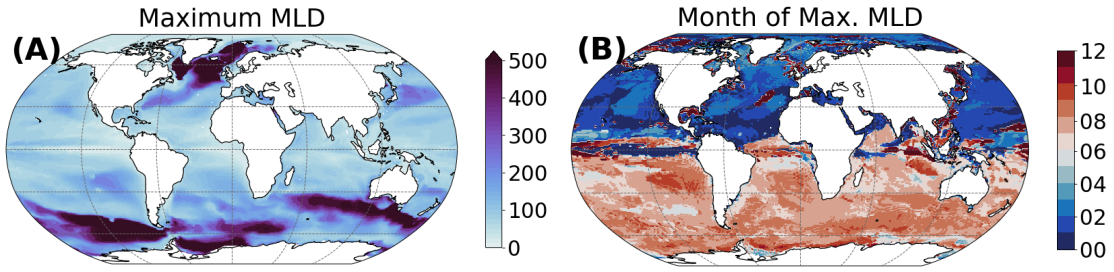

Figure 4.8 (A) Annual maximum MLD of MITgcm for 2020; and (B) The month of the year when maximum MLDs of MITgcm were found in 2020.

Moreover, there is an inverse relationship between temperature and nutrient supply in the open ocean (Sathyendranath et al., 1991). Thus, an increase in μ_{Nano}^{max} in association with the upwelling areas and lower values of μ_{Nano}^{max} were estimated in the southern central gyre compared to those in the northern central gyre, presumably reflecting the enhanced stability of the water column in the former. Deep MLD and strong convective mixing in the North Atlantic (Artic and Subarctic) Ocean in the MITgcm (Figure 4.8) result in high nutrient concentrations at the surface to increase the μ_{Nano}^{max} and thus increased phytoplankton concentration and surface chlorophyll-a. However, as the model chlorophyll-a concentrations are positively biased to minimize the model data misfit, the filter compensates for phytoplankton production by reducing μ_{Dia}^{max} and generating an inverse pattern of these two parameters estimates. Similar inverse patterns of up-

dates in the estimated values μ_{Nano}^{max} and μ_{Dia}^{max} were found at BATS by (Mamnun et al., 2022). In a large part of the Southern Ocean, annual maximum MLD goes deeper than 500m (Figure 4.8) before austral summer (Figure 4.8B); thus, the model simulates high chlorophyll-a concentration. As the filter does not know the joint uncertainty of parameter values to bring the model close to observation, the filter reduced the values of μ_{Nano}^{max}. Moreover, it is known that satellite observations underestimate chlorophyll-a concentration in the Southern Ocean (Johnson et al., 2013). In the regions of model deficits (e.g., Sub-Artic Atlantic), the filter estimated these two parameters (μ_{Nano}^{max} and μ_{Dia}^{max}) commonly considered unrealistic (see H. A. Bouman et al., 2018) until a reasonable agreement between observation and simulation is found.

Spatial variation in surface irradiance may also influence the latitudinal variation in the values of μ_{Nano}^{max} and μ_{Dia}^{max}. The combination of lower surface irradiances and deep convective mixing in high latitudes results in markedly lower light levels within the mixed layer, which may result in photoacclimation to lower light levels by modulating pigment content per cell and hence maximum photosynthesis rate (Cullen, 1982; Sathyendranath et al., 2009). However, the influences of the irradiance on the variability of parameters controlling the maximum photosynthesis rate are poorly understood (Marañón & Holligan, 1999). In this study, we have not found any indication that irradiance influences the spatial variation of μ_{Nano}^{max} and μ_{Dia}^{max}, which also agrees with the findings of Marañón and Holligan (1999). Moreover, culture studies have invoked viral infection as another potential source of variability poorly understood in natural marine systems (Puxty et al., 2016) and is not described in models.

Maximum Chlorophyll-to-nitrogen ratio

The variations of the maximum chlorophyll-to-nitrogen ratio ($q^{Chl:Nmax}$) in the open ocean are caused by an imbalance between the light absorption and energy demands for photosynthesis and biosynthesis in phytoplankton cells (Geider et al., 1996). $q^{Chl:Nmax}$ can also change because of variations in phytoplankton photoacclimation or physiological differences across phytoplankton groups, from a lower value for smaller species to a higher value for larger diatom cells (Geider et al., 1998). In the REcoM2, carbon-specific nitrogen assimilation is converted to chlorophyll units by multiplying by $q^{Chl:Nmax}$ for each phytoplankton class (Hauck et al., 2013). In our estimates, the $q_{Nano}^{Chl:Nmax}$ and $q_{Dia}^{Chl:Nmax}$ values increased in general to minimize overall positive bias in simulated chlorophyll-a concentration. However, the estimates of $q_{Nano}^{Chl:Nmax}$ and $q_{Dia}^{Chl:Nmax}$ show a relatively small degree of spatial variability compared to other parameters considered in this study (Table 4.3).

Growth irradiance significantly regulates $q^{Chl:Nmax}$ ratios (A. H. Taylor et al., 1997). The dependency of photoacclimation on light is pivotal for accurately predicting the stoichiometry of phytoplankton within light gradients (Álvarez et al., 2018). The photoacclimation term in the original model by Geider et al. (1998) ties chlorophyll syn-

thesis to the light saturation level of the photosynthetic apparatus. Specifically, when pigments absorb light in excess of what is utilized for photosynthesis, there is a downregulation in the synthesis of chlorophyll-a. According to this model, the reduction in light-harvesting complexes arises purely from dilution, given that the rate of chlorophyll synthesis decreases compared to carbon fixation. Notably, in REcoM2, in addition to the downregulated chlorophyll synthesis with $q_{Nano}^{Chl:Nmax}$ and $q_{Dia}^{Chl:Nmax}$, loss of chlorophyll from functional cells is described by a chlorophyll degradation rate.

Chlorophyll degradation rates

Constraining the chlorophyll degradation rates (d_{Nano}^{Chl} and d_{Dia}^{Chl}) presents a challenge in quota-based BGC models. The original model by (Geider et al., 1998) described photoacclimation over day-long timescales, but it lacks a term accounting for Chl degradation. This inclusion of the Chl degradation rate becomes particularly significant during low-growth periods in winter and at the lower reaches of the euphotic zone. Without a term for chlorophyll loss, which represents intricate processes in aging of photostressed cells, the carbon to chlorophyll ratios (C:Chl) in phytoplankton can become skewed.
Consequently, this parameter is often subjectively adjusted until a satisfactory alignment between observational data and model simulations is achieved. However, this approach might not be universally applicable across different BGC models. Interestingly, this parameter's broad spectrum of values can enhance model outcomes, mainly since it exhibits correlations with other parameters (Mamnun et al., 2022). Our estimation experiments yielded values varying by three orders of magnitude, with lower values going as low as 0.001. We consider our estimated' spatial variation of d_{Nano}^{Chl} and d_{Dia}^{Chl} as reasonable as they did not get extremely high. Replacing the rudimentary chlorophyll degradation model with a more detailed process-based depiction of photosystem functionality degradation can refine the modeled C:Chl ratios (Álvarez et al., 2018). However, little attention has been paid to that direction.

Maximum grazing rate of zooplankton

The estimated maximum grazing rate of zooplankton (ξ) shows sizeable spatial variability. Although zooplankton consists of a large variety of taxa, from unicellular flagellates to multicellular organisms, the version of REcoM2 we used describes only one generic zooplankton group, which is common in the majority of ocean BGC models (Séférian et al., 2020). Zooplankton grazing is the largest source of uncertainty in the ocean BGC models for generating climate projections (Laufkötter et al., 2015; Rohr et al., 2023). Zooplankton grazing influences carbon exchange, modulates surface phytoplankton biomass, and consequently governs biological production and nutrient uptake through photosynthesis. Incorporating a more intricate and complex representation of zooplankton grazing reduces biases in surface chlorophyll-a concentrations (Karakuş et al., 2022). Moreover,

in our estimation, we did not consider another sensitive grazing parameter, the grazing efficiency (γ) (Mamnun et al., 2023) because ξ and γ are highly correlated (Mamnun et al., 2022). Therefore, it is most likely that the ξ values were compensated for other beta and other grazing parameters.
The values of ξ are notably low in the Arctic and Subarctic Atlantic oceans (Figure 4.4I). During a spring bloom, the biomass of zooplankton trails behind the growth and accumulation due to the effects of temperature on zooplankton development (Daase et al., 2013; Søreide et al., 2010). As a result, there can be instances where phytoplankton and zooplankton exhibit either a negative correlation (e.g., when phytoplankton increases while zooplankton biomass is low or vice versa) or a positive correlation (e.g., when both populations are on the rise). These dynamics were evident in our study. In REcoM2, surface ocean phytoplankton biomass typically diminishes due to aggregated sinking or grazing, as the model does not include physiological mortality. During the spring bloom, the growth interplay between zooplankton and phytoplankton was more synchronized, mainly as much of the frontal structure had dissipated by then (Dong et al., 2021). Given the spatiotemporal fluctuations observed throughout the study, comprehending the intricate relationship between phytoplankton and zooplankton remains complex.
Reducing the value of ξ in the oligotrophic Subtropical South Pacific Ocean (Figure 4i), where the model underestimates chlorophyll-a (Figure 4.3), substantially increases the phytoplankton production in the simulations to cover the underestimation. Saito et al. (2005) also found that grazing parameters in this region are highly uncertain. In regions with strong upwelling and convective mixing, such as the Southern Ocean and the Tropical North Pacific, increasing the grazing rate substantially reduces surface chlorophyll-a concentration to minimize misfit with observations. The sensitivity studies with 1–D model configurations in the Tropical North Pacific Ocean (Chai et al., 2002; Dugdale et al., 2002) also agree. The filter increased the values of ξ around the BATS site, which agrees with the study with a 1–D model configuration of REcoM2 (Mamnun et al., 2022) and other previous studies (Doron et al., 2013; Losa et al., 2004). In situ measurements (Evelyn & Michael, 1998) also show that the grazer community consumes most of the production at this location. In addition, increases of ξ in the high-nutrient, low chlorophyll regions of the Southern Ocean suppress phytoplankton mass on the surface, thereby compensating for overestimated surface chlorophyll-a by the model.

4.4.3 Parameter compensation for other model deficiencies

In this study, we have focused exclusively on the uncertainties arising from BGC parameters. By treating only nine biological parameters as stochastic and by updating them to fit the observations, we do not account for the fact that model-data discrepancies are also caused by other sources of model error, such as the other biological parameters, parameters of the underlying physical model, physical forcing, boundary, and initial conditions as well as the functional form of the equations themselves. However, it is

critical to acknowledge that errors may also emanate from other components of coupled modeling systems, such as ocean physics and sea ice dynamics, atmospheric forcing, or inherent structural inadequacies in the model framework. While the model reasonably agrees with existing observations, this concordance may be because BGC parameter uncertainties offset imitations in other model components or structural uncertainties. Such compensatory errors pose significant challenges for future climate projections. However, they may yield plausible simulations for the present state, but they erode confidence in the model's predictive capability for future scenarios (Löptien & Dietze, 2019).
The free run consistently produces a thin line of elevated chlorophyll-a in the subtropical gyres, most visible in the Subtropical South Atlantic and Indian Ocean (Figure 4.3). The feature is not seen in satellite data, and DA analysis somewhat dissolved the line of elevated chlorophyll-a. Directly at the transition from iron to nitrogen limitation, neither of the two limitation terms is as low as in the centers of the limited regions. In the REcoM2 code, the co-limitation is calculated as a minimum of two limitation terms, so there is less limitation directly at the transition than in the equilibrium regions.
Although the values of chlorophyll-a in these features are relatively small and probably do not affect global biogeochemical cycles much, the parameter estimation process, responded to this model deficiency. This is particularly visible for the maximum chlorophyll to nitrogen ratio of nanophytoplankton and maximum grazing rate in Figure 4.4C and I. These parameters had larger changes in the transition regions to compensate for the elevated chlorophyll-a.
Whenever uncertainties from different sources compensate for each other, the ocean BGC model may yield reasonable outputs for the period for which the parameter estimation was implemented. However, this compensatory behavior compromises the model's utility for gaining mechanistic insights and being a reliable predictive instrument beyond that specific timeframe. This phenomenon is particularly concerning when considering slow climate BGC feedback mechanisms, which are inherently challenging to probe with current observations. A judicious strategy for model development would involve applying Occam's razor (Sober, 1981). This could be accomplished by restricting the number of BGC variables to only those essential and focusing on processes for which a well-founded conceptual or theoretical understanding of their climate sensitivity exists. Nevertheless, the optimal approach may vary depending on the specific scientific questions being addressed, introducing an element of subjectivity into the process.
In practice, when uncertainties beyond just model parameter uncertainties influence the parameter estimations, the outcomes of parameter estimates become indeterminate in their effectiveness. While compensating for these uncertainties can mitigate some deficits, it does not address all of them. This phenomenon was evident in Simon et al. (2015), where they conducted parameter estimation on a regional BGC model for the North Atlantic and Arctic Oceans. Furthermore, parameter estimates optimized for a specific location or regional scale can deteriorate model outcomes for other regions, as highlighted by (Friedrichs et al., 2007). This underscores the need for estimating

spatially varying BGC parameters.

4.5 Conclusion

We employed ensemble DA to estimate spatiotemporally varying values of nine uncertain parameters within a 3–D global ocean BGC model by assimilating satellite-derived surface chlorophyll-a concentrations. The estimated parameters are the initial slope of the P-I curve for nanophytoplankton and diatoms, the maximum photosynthesis rate of nanophytoplankton and diatoms, the maximum chlorophyll-to-nitrogen ratio for nanophytoplankton and diatoms, chlorophyll degradation rate of nanophytoplankton and diatoms, and the maximum grazing rate of zooplankton. Leveraging an EnKF, we adopt the augmented state vector approach, grounded in multivariate correlations between BGC parameters and observed state variables, i.e., surface chlorophyll-a concentration in this study. In addition to the chosen nine parameters, the DA updated eight model state variables, biomass content of carbon, nitrogen and calcium carbonate of nanophytoplankton, biomass content of carbon, nitrogen and silicate of diatoms, and chlorophyll-a concentration in nanophytoplankton and diatoms, which were used as the initial conditions for the next forecast cycle.

The resulting parameter estimates span a range above and below the default value, underscoring the efficacy of DA in enhancing the model's regional parameterization. Notably, simulations conducted with the spatially varying values of this optimized parameter set align more closely with observations compared to the reference simulation that employs spatially uniform default parameter values.

A notable, albeit anticipated, consequence of augmented-state parameter estimation is the filter's unpredictable use of the additional degrees of freedom. Although our primary objective is to achieve the best parameter estimates by minimizing its uncertainty, the DA process may inadvertently offset the uncertainty from other sources. This can result in suboptimal parameter estimates yet improved state estimates. Such parameter estimates, resulting from compensation of other uncertainties, restrict the portability of these estimates to a different model configuration or a different model.

While our results demonstrate the efficacy of the estimation method assimilating ocean color data, possible extensions and improvements of the method are numerous, and further developments of DA for different types of observations should be explored. The methodology evaluated in this study is not exclusive to the MITgcm-REcoM2 model and does not necessitate extensive inverse model developments. Thus, it can be adapted to other models, provided that the ensemble simulations, which describe the model's response to parameter uncertainty, are computationally viable. Our approach offers a valuable alternative for consideration in a research environment with multiple coexisting models and limited computational resources for expanding variable counts and calibrating parameters.

Chapter 5

Conclusion and Outlook

5.1 Conclusion

To improve our ability to predict climate and to asses the effects of climate change on ecosystems, accounting for the influence of the carbon cycle and how they relate to climate processes is fundamental. Ocean biogeochemical (BGC) models provide an integral tool for investigating ocean biogeochemistry and its effects on the carbon cycle. These models are highly uncertain in their parametrization. These uncertainties are unavoidable. Nonetheless, uncertainty quantification (UQ) of the BGC models can make the models more useful and mitigate discrepancies in the model outputs. UQ for ocean BGC models is used broadly to describe parameter sensitivity analyses and parameter estimation problems, including characterization of the uncertainty in the model fields and process parameters, specification of uncertainties in parameter estimates, and model parameterizations. In this dissertation, UQ methods were successfully applied to improve model predictions of an ocean BGC model, the Regulated Ecosystem Model Version 2 (REcoM2). The above sets the overall goal of this dissertation, focusing on identifying and quantifying uncertainties arising in ocean BGC models and obtaining improved parameters to reduce those uncertainties and yield improved model predictions. The dissertation provides two approaches toward reaching its goal:

a) Parameter sensitivity analyses aiming to evaluate the impact of parameter uncertainties on the variability model outputs and
b) Parameter estimation aiming to estimate the optimal parameter values given observational data.

Three interlinked but not mutually exclusive studies were carried out to address the uncertainties in ocean BGC models utilizing REcoM2. The first study focuses on sensitivity analysis to identify the process parameters most influential to model outputs. The second study delves into uncertainty quantification, employing ensemble data assimilation to estimate uncertain process parameters in two ocean sites for which observational time series data are available. The third study uses a global model setup to estimate spatially varying parameters by expanding the scope and applicability from a location-specific focus of the second study.

Study 1: Global sensitivity analysis (GSA) at two locations (BATS and DYFAMED) utilizing a simplified one-dimensional (1–D) model setup

Ocean BGC models contain numerous parameters, often exceeding the number of variables. The uncertainties in these parameters can lead to possibly significant uncertainty in the model outputs. To get reasonable model outputs, it is essential to calibrate the parameters in each application case using observational data, either manually or through optimization algorithms that minimize the misfit between simulations and available data. It is vital to prioritize the parameters that impact the uncertainty of model outputs the most. A GSA of REcoM2 was conducted to obtain insights into which model parameters most influence the uncertainty of an output quantity of interest.

Utilizing a 1–D configuration of the coupled MITgcm- REcoM2 model at two ocean time series stations, this study computed variance-based Sobol' indices (Sobol', 1993) of model parameters for chosen model outputs that are commonly considered for calibration and validation of ocean BGC models. The two stations are 1) the Bermuda Atlantic Time-series Study (BATS, Steinberg et al., 2001) in the North Atlantic and 2) the DYFAMED station (DYFAMED, J. C. Marty, 2002) in the Mediterranean Sea. Sobol' indices measure the relative contribution of individual input parameters to the variance of a model output or quantity of interest (QoI). In the dissertation, the focus was set on the first- and total-order Sobol' indices. The first-order index of a parameter measures the expected reduction in the variance of QoI if the parameter could be set as fixed value (Homma & Saltelli, 1996), thus leaving out the variability of QoI caused by interactions of the respective input parameter with others. The total-order index of an input parameter provides how much variance remains in the QoI if every parameter except the respective one could be set as fixed value (Homma & Saltelli, 1996), thus accounting for interactions with other input parameters.

The traditional local sensitivity methods can lead to inaccurate conclusions and can result in misconceptions about the influence of individual processes on model outcomes (Prieur et al., 2019). However, the local methods are typically preferred in practice because GSA is computationally expensive. A key takeaway from our study for future ocean BGC studies is the following:

The continual growth in computational resources, coupled with advancements in sensitivity measure estimation algorithms, has made it feasible to execute a GSA of a 1–D BGC model considering a large number of input parameters. Even resource-intensive indices like total-order Sobol' indices can be efficiently computed, particularly with a high-performing computer. However, it is noteworthy to mention that implementing such a GSA into a 3–D model is still out of reach.

The results of our GSA can be summarized as follows. The most important parameters for chlorophyll-a simulations are the cell quota chlorophyll to nitrogen ratio, ones related to grazing by zooplankton, chlorophyll degradation rate, and photosynthesis parameters. The most influential parameters for net primary production (NPP) predictions are photosynthesis, grazing parameters, cell quota carbon to nitrogen ratio, excretion of organic

carbon by phytoplankton, and zooplankton respiration. Export production and CO_2 flux are influenced mainly by the remineralization of nutrients and grazing by zooplankton. Overall, the sensitivity responses of most of the QoIs were similar between the two locations.

The primary output achieved by this GSA is a list of the most important BGC parameters that need to be quantified for the future. In the context of UQ for a model with many parameters, like ocean BGC models, GSA streamlines the optimization process by concentrating on those parameters. This study was the basis for selecting parameters for estimation with data assimilation in the subsequent projects (Study 3). Ranking of the most influential REcoM2 parameters could be useful for the optimization efforts of other models. However, we recommend a GSA before starting any parameter optimization study.

The added value of GSA lies in assisting modelers in comprehending the behavior of their models and pinpointing the most influential parameters. For example, the results of this study suggest that implementing multiple zooplankton function types in BGC models may be useful to improve chlorophyll-a and NPP prediction, provided that efforts are invested in estimating parameters characterizing the grazing in marine ecosystems. In addition to grazing, aggregation parameters account for phytoplankton mortality in REcoM2. The physiological mortality is not explicitly represented in the model. However, phytoplankton biomass (in terms of chlorophyll-a concentration and NPP) simulation of REcoM2 is not sensitive to the aggregation parameters, indicating that representing phytoplankton mortality as physiological mortality explicitly can improve the model outputs in oligotrophic regions. The GSA results also indicate that explicitly implementing heterotrophic bacteria in the model has the potential for better simulating the export production and CO_2 fluxes.

GSA can be invaluable for model reduction as it highlights essential parameters that cannot be held constant. Sobol' et al. (2007) argued that model reduction based on first-order Sobol' indices can lead to erroneous conclusions. The GSA carried out in this study also agrees the argument. The first-order Sobol' indices for the maximum nitrogen uptake, the minimum cell quota of nitrogen (C:N), and the cost of nitrogen biosynthesis were very low. However, these parameters could not be screened out due to their high total-order indices – strong interaction with other parameters.

The above insights gained from the GSA will be useful for future BGC modeling case studies, parameter estimation and optimization, and further development of BGC models. The methods presented in this study are broadly applicable to other ocean BGC models and other intricate modeling domains.

Study 2: Application of ensemble data assimilation to a 1–D model for parameter estimation

The values of the numerous parameters involved in ocean BGC models are poorly known. The available reference values were taken from laboratory experiments on single species or estimated with limited field data of a single field campaign. However, in the model, they are applied more broadly to describing whole classes of organisms and for all physical and biogeochemical contexts. Using the identical model setup as in the previous GSA experiments (Study 1), ten important BGC parameters were estimated by applying the ensemble data assimilation technique.

This study utilized an Ensemble Kalman Filter, the Error-Subspace Transform Kalman Filter (ESTKF; Nerger et al., 2012a), provided by the Parallel Data Assimilation Framework (PDAF; Nerger & Hiller, 2013) to assimilate satellite chlorophyll-a concentration data and in-situ observations of net primary production. This study used a 108-member ensemble. The varying model states (ensemble members) were generated by randomly perturbing the selected ten parameters, assuming a lognormal distribution with a relative variance of 0.25 for all the selected parameters. DA experiments were performed from October 1999 to December 2002 for BATS and from October 1997 to December 2000 for DYFAMED. The difference in the chosen period was caused by the availability of the in situ flask NPP data.

Consistent with previous studies (e.g., Gharamti, Samuelsen, et al., 2017; Mattern et al., 2010), our findings affirm that ensemble DA techniques effectively enhance parameter estimation in 1–D ocean BGC models, reducing the discrepancy between model predictions and data. Notable adjustments were observed in parameters related to phytoplankton photosynthesis rate, chlorophyll degradation, and grazing. Consequently, these parameter adjustments substantially improved model prediction, decreasing the Root Mean Square Error (RMSE) by up to 66% for surface chlorophyll-a and 56% for NPP relative to assimilated data. Compared to independent data, the RMSE was reduced by up to 43% for chlorophyll-a and 18% for NPP.

When satellite chlorophyll-a and in situ NPP data were assimilated simultaneously, the parameter estimation process yielded enhanced parameter values. Solely assimilating satellite chlorophyll-a data did not sufficiently refine the model, especially at the BATS station. In this case, the filter optimized the surface chlorophyll-a simulations. Solely assimilating satellite chlorophyll-a led to greater discrepancies between simulated and in situ NPP data. While surface chlorophyll-a simulations are sensitive to the chosen parameters, the surface chlorophyll-a observation might not encompass information for all parameters. Consequently, certain variables might remain inadequately defined by surface chlorophyll-a. This issue is known as the underdetermination problem in ocean BGC data assimilation (Ward et al., 2010).

The large discrepancies between the simulated and in situ NPP data at the BATS station could be attributed to the 14C methodology and the distribution of particles and organisms in the highly oligotrophic waters (Harris et al., 1989). While in situ NPP displayed

minimal seasonality during the study period, satellite-based estimates highlighted pronounced seasonal variations. Additionally, the in situ data exhibited greater variability, potentially stemming from measurement errors, suggesting substantial uncertainty in the in situ flask data measurements.
Analogs to the underdetermination problem parameter interdependencies are evident in ocean BGC models (see Tjiputra et al., 2007). This study also found that co-dependencies among parameters prevent the estimation of a unique optimal parameter set, indicating the necessity for additional conditions to achieve meaningful BGC parameter estimations.
In this study, parameter estimations resulted in distinct optimal parameter values for each of the locations of the experiment. Similar findings have been reported in previous studies, where BGC parameters estimated across various locations yielded differing values (e.g., Friedrichs et al., 2007; Gharamti, Tjiputra, et al., 2017; Schartau & Oschlies, 2003; Tjiputra et al., 2007). Such variations indicate that BGC parameters can exhibit significant spatial variability influenced by physical conditions and ecosystem contexts. Consequently, regional and global 3–D models would benefit from incorporating these spatially varying parameter values. This estimation method can be adapted for a 3–D model.

Study 3: Spatially varying parameters estimation in a 3–D global ocean model

Chapter 4 of this dissertation presents spatially and temporally varying parameter values in a 3–D global ocean model by assimilating Ocean Color Data. Nine parameters were chosen based on the GSA presented in Chapter 2. Each of the nine selected parameters was defined as a 2–D field for estimating spatially varying parameter values, which then was updated by leveraging cross covariances with satellite chlorophyll-a observations. This study utilized domain localization (Nerger et al., 2012a) of ESTKF also using PDAF. Each horizontal model grid point is considered a disjoint local domain in domain localization. Only observations with a distance smaller than a cut-off radius (localization radius) are considered for a given local domain. The parameter values were updated at each grid point with a distance-weighted influence of the observation within the localization radius.
The estimated parameters exhibit values larger and smaller than the default value, showing an effective impact of data assimilation on the model's parameterization regionally. The parameter values converge within six months in a large part of the globe. The model simulations with the set of estimated parameters are closer to the observations than the reference simulations using constant parameter values for surface chlorophyll-a concentration and vertically integrated NPP. However, estimated spatially varying parameter values lead to more extended spring bloom periods compared to the estimates from satellite observation.
The dynamic range of estimated parameter values was within the values reported from observations and other studies. The spatial variations of estimated parameter values

were similar to observed variations and explainable with our current understanding of the regional BGC process. We obtained a range of variation of about two orders of magnitude for the photosynthesis parameters, which agrees with the observed variability (H. A. Bouman et al., 2018). Platt et al. (1991) highlighted a weak correlation between biomass and production, particularly at high latitudes. This observation is further supported by Marañón and Holligan (1999), who extended this assertion to mid and low latitudes. The weak correlations between chlorophyll-a concentration and production distributions elucidate the limited enhancement in vertically integrated NPP relative to surface chlorophyll-a when incorporating estimated spatially varying parameter values.
Significant variability in the maximum grazing rate is primarily attributed to grazing pressure being the predominant source of uncertainty in REcOM2, as detailed in Chapter 2 (Mamnun et al., 2023). This observation aligns with the findings of Rohr et al. (2023), which identified similar patterns across numerous BGC models in Coupled Model Intercomparison Project Phase 6. Such variability implies that pronounced disparities in the magnitude of grazing parameters within models might dominate key qualitative differences in marine primary production, thereby influencing the dynamics of phytoplankton populations. This study indicates the potential benefits of refining the portrayal of zooplankton grazing in marine biogeochemical models, which could yield more accurate and consistent estimations of the marine carbon cycle.
An interesting, though not surprising, effect of joint state-parameter estimation is the filter's unpredictable use of the additional degrees of freedom. While our goal is to estimate the parameters to the best possible accuracy, the filter algorithm might compensate for model deficits instead, resulting in extreme parameter values but better state estimates.
Based on all findings, the UQ methods in this dissertation have been proven to apply well to the complex BGC model REcoM2. They are model-independent and, therefore, can be used for other models. While the parameter values derived from our study may not be directly transferable to other models, the insights gained can enhance the evaluation and refinement of predictions in general BGC models. This research underscores the potential advantages of incorporating spatially varying process parameters in regional and global 3–D BGC models.

5.2 Outlook

Sensitivity analysis evaluates the extent to which a model's outputs rely on its assumptions and input parameters. It addresses the balance between model complexity and interpretability, determining when the quality of its input parameters justifies its complexity. A prior sensitivity analysis was recommended as essential for modeling applications related to model quality (see Razavi et al., 2021). When a model is considered appropriate for a specific research question, conducting a sensitivity analysis is urged to be routine practice (see Saltelli et al., 2021). Notably, many ocean BGC modeling

studies either neglect this crucial step or fail to report it (Shimoda & Arhonditsis, 2016). The GSA detailed in this dissertation revealed that aggregation exhibits lower sensitivity than grazing, shedding light on the uncertainties associated with estimated aggregation parameters.

Additionally, we discerned that the sensitivities of photosynthesis parameters have minimal impact on chlorophyll-a simulations while interacting with other parameters. As such, they cannot be effectively constrained using surface chlorophyll-a observations when many parameters are considered concurrently. This sensitivity analysis proved invaluable for selecting target parameters to be estimated, streamlining our parameter estimation efforts on a limited number of parameters. Therefore, we advocate for modelers to conduct sensitivity analyses in all BGC modeling applications.

Ocean BGC models continue to be developed to include more details of the BGC processes, for example, incorporating advanced carbonate chemistry (Gürses et al., 2023), including additional nutrients (Tagliabue et al., 2018), and carbon pools (Polimene et al., 2018), adding additional model components (Ye et al., 2023) and including more ecological diversity and other trophic levels (e.g., Leles et al., 2018; Stock et al., 2017; Zakem et al., 2018). As BGC models become more complex (such as resolving more phytoplankton function types and nutrient pools) the parametric uncertainty will likely to increase (Figure 1.1). Simply developing satellite chlorophyll-a concentration-based DA systems may not be sufficient to capture all complexities. An outlook for future studies can be toward novel assimilation of ocean-color products (e.g., remote sensing reflectance, phytoplankton functional types, ocean carbon stocks) and in situ observation (e.g., BGC-ARGO) and observational constraints, and of the uncertainties of DA itself (e.g., applying nonlinear filters).

On the other hand, the evolution of model development could be tailored to accommodate novel observational products. For instance, as advancements in ocean color products occur, it might become evident that the determination of phytoplankton size distribution is more reliable than its function (Kostadinov et al., 2023). Should this be the case, prioritizing the simulation of size distribution in models is a beneficial avenue.

Given the relatively small number of studies that have addressed spatially varying parameter estimation, it is worthwhile to continue present approaches and try new ones. The methods menonstrated in this dissertation are well applicable to included more observation types into DA model. As satellite-derived chlorophyll-a concentration is highly uncertain (Zhang et al., 2022, and references therein) it is likely that the assimilation of less uncertain products, such as vertical attenuation at 490 nm or remote-sensing reflectance, is a worthwhile direction.

The spatially varying values of all parameters considered here were estimated reasonably well, as evidenced by the reduction in uncertasinties compared to when using uniform default values. Additionally, the spatial variations of these values align well with our understanding of BGC processes and are similar to observations. However, we observed that parameter estimates can sometimes compensate for model deficits. These compensations

of model deficits also affect state estimation, and the resulting parameter estimations become unpredictable. While compensating for specific model deficits can be advantageous, it is not universally beneficial. This phenomenon was distinctly highlighted in the study by Simon et al. (2015), who conducted joint state-parameter estimation on an ecosystem model for the North Atlantic and Arctic Oceans. Therefore, Future research should look into the effect of assimilating observation from different modeling components, especially the components where the model performs poorly.

When observations span multiple compartments of the earth system, such as the ocean, sea ice, and biogeochemistry, an approach known as weakly coupled data assimilation (WCDA; Penny & Hamill, 2017) is often employed. WCDA assimilates data independently in their respective components, with other model components dynamically adjusting to these changes during simulations. In contrast, strongly coupled data assimilation (SCDA; Penny & Hamill, 2017; Penny et al., 2019) allows for updates across model components. For state estimation, SCDA has been shown to surpass WCDA in performance (Goodliff et al., 2019; Tang et al., 2020, 2021; Yu et al., 2018). This outcome is attributed to its ability to enhance the dynamical consistency of initial conditions and broaden the influence of observations within their respective components. Singh et al. (2022) demonstrated the advantages of cross-compartment updates in SCDA through a twin experiment utilizing synthetic observations. Given these findings, it is imperative to explore further the effects of both WCDA and SCDA on parameter estimates within a realistic model using actual observations.

Bibliography

Albani, S., Mahowald, N. M., Perry, A. T., Scanza, R. A., Zender, C. S., Heavens, N. G., Maggi, V., Kok, J. F., & Otto-Bliesner, B. L. (2014). Improved dust representation in the Community Atmosphere Model. *Journal of Advances in Modeling Earth Systems*, *6*(3), 541–570. https://doi.org/10.1002/2013ms000279

Álvarez, E., Thoms, S., & Völker, C. (2018). Chlorophyll to Carbon Ratio Derived from a Global Ecosystem Model With Photodamage. *Global Biogeochemical Cycles*, *32*(5), 799–816. https://doi.org/10.1029/2017gb005850

Andersen, T. K., Bolding, K., Nielsen, A., Bruggeman, J., Jeppesen, E., & Trolle, D. (2021). How morphology shapes the parameter sensitivity of lake ecosystem models. *Environmental Modelling & Software*, *136*, 104945. https://doi.org/10.1016/j.envsoft.2020.104945

Anderson, J. L. (2001). An Ensemble Adjustment Kalman Filter for Data Assimilation. *Monthly Weather Review*, *129*(12), 2884–2903. https://doi.org/10.1175/1520-0493(2001)129<2884:AEAKFF>2.0.CO;2

Anderson, T. R. (1993). A Spectrally Averaged Model of Light Penetration and Photosynthesis. *Limnology and Oceanography*, *38*(7), 1403–1419. https://doi.org/10.4319/lo.1993.38.7.1403

Anderson, T. R. (2005). Plankton functional type modelling: Running before we can walk? *Journal of Plankton Research*, *27*(11), 1073–1081. https://doi.org/10.1093/plankt/fbi076

Anderson, T. R., Hessen, D. O., Mitra, A., Mayor, D. J., & Yool, A. (2013). Sensitivity of secondary production and export flux to choice of trophic transfer formulation in marine ecosystem models. *Journal of Marine Systems*, *125*, 41–53. https://doi.org/10.1016/j.jmarsys.2012.09.008

Andrews, O., Buitenhuis, E., Le Quere, C., & Suntharalingam, P. (2017). Biogeochemical modelling of dissolved oxygen in a changing ocean. *Philosophical Transactions of the Royal Society A*, *375*(2102), 20160328. https://doi.org/10.1098/rsta.2016.0328

Archibald, K. M., Siegel, D. A., & Doney, S. C. (2019). Modeling the Impact of Zooplankton Diel Vertical Migration on the Carbon Export Flux of the Biological Pump. *Global Biogeochemical Cycles*, *33*(2), 181–199. https://doi.org/10.1029/2018GB005983

Asch, M., Bocquet, M., & Nodet, M. (2016). *Data Assimilation: Methods, Algorithms, and Applications*. Society for Industrial and Applied Mathematics (SIAM). https://doi.org/10.1137/1.9781611974546

Aumont, O., Maury, O., Lefort, S., & Bopp, L. (2018). Evaluating the Potential Impacts of the Diurnal Vertical Migration by Marine Organisms on Marine Biogeochemistry. *Global Biogeochemical Cycles*, *32*(11), 1622–1643. https://doi.org/10.1029/2018GB005886

Bagniewski, W., Fennel, K., Perry, M. J., & D'Asaro, E. A. (2011). Optimizing models of the North Atlantic spring bloom using physical, chemical and bio-optical observations from a Lagrangian float. *Biogeosciences*, *8*(5), 1291–1307. https://doi.org/10.5194/bg-8-1291-2011

Baklouti, M., Faure, V., Pawlowski, L., & Sciandra, A. (2006). Investigation and sensitivity analysis of a mechanistic phytoplankton model implemented in a new modular numerical tool (Eco3M) dedicated to biogeochemical modelling. *Progress in Oceanography*, *71*(1), 34–58. https://doi.org/10.1016/j.pocean.2006.05.003

Barbieux, M., Uitz, J., Gentili, B., de Fommervault, O. P., Mignot, A., Poteau, A., Schmechtig, C., Taillandier, V., Leymarie, E., Penkerc'h, C., D'Ortenzio, F., Claustre, H., & Bricaud, A. (2019). Bio-optical characterization of subsurface chlorophyll maxima in the Mediterranean Sea from a Biogeochemical-Argo float database. *Biogeosciences*, *16*(6), 1321–1342. https://doi.org/10.5194/bg-16-1321-2019

Baretta, J. W., Ebenhöh, W., & Ruardij, P. (1995). The European regional seas ecosystem model, a complex marine ecosystem model. *Netherlands Journal of Sea Research*, *33*(3), 233–246. https://doi.org/10.1016/0077-7579(95)90047-0

BATS Team. (Last access: June 2022). http://bats.bios.edu/.

Behrenfeld, M. J., & Falkowski, P. G. (1997a). A consumer's guide to phytoplankton primary productivity models. *Limnology and Oceanography*, *42*(7), 1479–1491. https://doi.org/10.4319/lo.1997.42.7.1479

Behrenfeld, M. J., & Falkowski, P. G. (1997b). Photosynthetic rates derived from satellite-based chlorophyll concentration. *Limnology and Oceanography*, *42*(1), 1–20. https://doi.org/10.4319/lo.1997.42.1.0001

Behrenfeld, M. J., & Milligan, A. J. (2013). Photophysiological expressions of iron stress in phytoplankton. *Annual Review of Marine Science*, *5*, 217–46. https://doi.org/10.1146/annurev-marine-121211-172356

Betancur-Turizo, S., González-Silvera, A., Santamaría-del-Ángel, E., Tan, J., & Frouin, R. (2018). Evaluation of Semi-Analytical Algorithms to Retrieve Particulate and Dissolved Absorption Coefficients in Gulf of California Optically Complex Waters. *Remote Sensing*, *10*(9). https://doi.org/10.3390/rs10091443

Béthoux, J. P., Morin, P., Chaumery, C., Connan, O., Gentili, B., & Ruiz-Pino, D. (1998). Nutrients in the Mediterranean Sea, mass balance and statistical analysis of

concentrations with respect to environmental change. *Marine Chemistry*, *63*(1), 155–169. https://doi.org/10.1016/S0304-4203(98)00059-0

Bindoff, N., Cheung, W., Kairo, J., Arístegui, J., Guinder, V., Hallberg, R., Hilmi, N., Jiao, N., Karim, M., Levin, L., O'Donoghue, S., Purca Cuicapusa, S., Rinkevich, B., Suga, T., Tagliabue, A., & Williamson, P. (2019). Changing ocean, marine ecosystems, and dependent communities. In H.-O. Pörtner, D. Roberts, V. Masson-Delmotte, P. Zhai, M. Tignor, E. Poloczanska, K. Mintenbeck, A. Alegría, M. Nicolai, A. Okem, J. Petzold, B. Rama, & N. Weyer (Eds.), *The Ocean and Cryosphere in a Changing Climate: Special Report of the Intergovernmental Panel on Climate Change* (pp. 447–588). Cambridge University Press. https://doi.org/10.1017/9781009157964.007

Bopp, L., Resplandy, L., Orr, J. C., Doney, S. C., Dunne, J. P., Gehlen, M., Halloran, P., Heinze, C., Ilyina, T., Séférian, R., Tjiputra, J., & Vichi, M. (2013). Multiple stressors of ocean ecosystems in the 21^{st} century: projections with CMIP5 models. *Biogeosciences*, *10*(10), 6225–6245. https://doi.org/10.5194/bg-10-6225-2013

Bopp, L., Resplandy, L., Untersee, A., Le Mezo, P., & Kageyama, M. (2017). Ocean (de)oxygenation from the Last Glacial Maximum to the twenty-first century: insights from Earth System models. *Philosophical Transactions A*, *375*(2102). https://doi.org/10.1098/rsta.2016.0323

Bouman, H. A., Platt, T., Kraay, G. W., Sathyendranath, S., & Irwin, B. D. (2000). Bio-optical properties of the subtropical North Atlantic. I. Vertical variability. *Marine Ecology Progress Series*, *200*, 3–18. https://doi.org/10.3354/meps200003

Bouman, H. A., Platt, T., Doblin, M., Figueiras, F. G., Gudmundsson, K., Gudfinnsson, H. G., Huang, B., Hickman, A., Hiscock, M., Jackson, T., Lutz, V. A., Mélin, F., Rey, F., Pepin, P., Segura, V., Tilstone, G. H., van Dongen-Vogels, V., & Sathyendranath, S. (2018). Photosynthesis-irradiance parameters of marine phytoplankton: Synthesis of a global data set. *Earth System Science Data*, *10*(1), 251–266. https://doi.org/10.5194/essd-10-251-2018

Bouman, H., Platt, T., Sathyendranath, S., & Stuart, V. (2005). Dependence of light-saturated photosynthesis on temperature and community structure. *Deep Sea Research Part I: Oceanographic Research Papers*, *52*(7), 1284–1299. https://doi.org/10.1016/j.dsr.2005.01.008

Boyer, T. P., Garcia, H. E., Locarnini, R. A., Zweng, M. M., Mishonov, A. V., Reagan, J. R., Weathers, K. A., Baranova, O. K., Seidov, D., & Smolyar, I. V. (2018). World Ocean Atlas 2018. NOAA National Centers for Environmental Information. https://www.ncei.noaa.gov/products/world-ocean-atlas

Boyle, E. A., Anderson, R. F., Cutter, G. A., Fine, R., Jenkins, W. J., & Saito, M. (2015). Introduction to the U.S. GEOTRACES North Atlantic Transect (GA-03): USGT10 and USGT11 cruises. *Deep Sea Research Part II: Topical Studies in Oceanography*, *116*, 1–5. https://doi.org/10.1016/j.dsr2.2015.02.031

Bracis, C., Lehuta, S., Savina-Rolland, M., Travers-Trolet, M., & Girardin, R. (2020). Improving confidence in complex ecosystem models: The sensitivity analysis of an Atlantis ecosystem model. *Ecological Modelling*, *431*, 109133. https://doi.org/ARTN10913310.1016/j.ecolmodel.2020.109133

Brett, G. J., Whitt, D. B., Long, M. C., Bryan, F., Feloy, K., & Richards, K. J. (2021). Sensitivity of 21st-century projected ocean new production changes to idealized biogeochemical model structure. *Biogeosciences*, *18*(10), 3123–3145. https://doi.org/10.5194/bg-18-3123-2021

Broto, B., Bachoc, F., & Depecker, M. (2020). Variance Reduction for Estimation of Shapley Effects and Adaptation to Unknown Input Distribution. *SIAM/ASA Journal on Uncertainty Quantification*, *8*(2), 693–716. https://doi.org/10.1137/18M1234631

Brown, P. T., & Caldeira, K. (2017). Greater future global warming inferred from Earth's recent energy budget. *Nature*, *552*(7683), 45–50. https://doi.org/10.1038/nature24672

Campbell, J. W. (1995). The lognormal distribution as a model for bio-optical variability in the sea. *Journal of Geophysical Research*, *100*(C7), 13237–13254. https://doi.org/10.1029/95jc00458

Campin, J.-M., Heimbach, P., Losch, M., Forget, G., Adcroft, A., Menemenlis, D., Jahn, O., Hill, C., Scott, J., Mazloff, M., Fox-Kemper, B., Doddridge, E., Fenty, I., Bates, M., Smith, T., Eichmann, A., Lauderdale, J., Martin, T., Abernathey, R., … Deremble, B. (2023). MITgcm/MITgcm: checkpoint68n. https://doi.org/10.5281/zenodo.7621779

Carroll, D., Menemenlis, D., Adkins, J. F., Bowman, K. W., Brix, H., Dutkiewicz, S., Fenty, I., Gierach, M. M., Hill, C., Jahn, O., Landschützer, P., Lauderdale, J. M., Liu, J., Manizza, M., Naviaux, J. D., Rödenbeck, C., Schimel, D. S., Van der Stocken, T., & Zhang, H. (2020). The ECCO-Darwin Data-Assimilative Global Ocean Biogeochemistry Model: Estimates of Seasonal to Multidecadal Surface Ocean pCO_2 and Air-Sea CO_2 Flux. *Journal of Advances in Modeling Earth Systems*, *12*(10). https://doi.org/10.1029/2019ms001888

Casella, G., & Berger, R. L. (2002). *Statistical inference (second edition)*. Duxbury Press.

Chai, F., Dugdale, R. C., Peng, T. H., Wilkerson, F. P., & Barber, R. T. (2002). One-dimensional ecosystem model of the equatorial Pacific upwelling system. Part I: model development and silicon and nitrogen cycle. *Deep Sea Research Part II: Topical Studies in Oceanography*, *49*(13), 2713–2745. https://doi.org/10.1016/S0967-0645(02)00055-3

Chatterjee, S. (2020). A New Coefficient of Correlation. *Journal of the American Statistical Association*, *116*(536), 2009–2022. https://doi.org/10.1080/01621459.2020.1758115

Chenillat, F., Riviere, P., & Ohman, M. D. (2021). On the sensitivity of plankton ecosystem models to the formulation of zooplankton grazing. *PLoS One*, *16*(5), e0252033. https://doi.org/10.1371/journal.pone.0252033

Cheung, W. W. L., Lam, V. W. Y., Sarmiento, J. L., Kearney, K., Watson, R. E. G., Zeller, D., & Pauly, D. (2010). Large-scale redistribution of maximum fisheries catch potential in the global ocean under climate change. *Global Change Biology*, *16*(1), 24–35. https://doi.org/10.1111/j.1365-2486.2009.01995.x

Chien, C. T., Pahlow, M., Schartau, M., & Oschlies, A. (2020). Optimality-based non-Redfield plankton-ecosystem model (OPEM v1.1) in UVic-ESCM 2.9-Part 2: Sensitivity analysis and model calibration. *Geoscientific Model Development*, *13*(10), 4691–4712. https://doi.org/10.5194/gmd-13-4691-2020

Ciavatta, S., Brewin, R. J. W., Skakala, J., Polimene, L., de Mora, L., Artioli, Y., & Allen, J. I. (2018). Assimilation of Ocean-Color Plankton Functional Types to Improve Marine Ecosystem Simulations. *Journal of Geophysical Research-Oceans*, *123*(2), 834–854. https://doi.org/10.1002/2017jc013490

Ciavatta, S., Kay, S., Saux-Picart, S., Butenschon, M., & Allen, J. I. (2016). Decadal reanalysis of biogeochemical indicators and fluxes in the North West European shelf-sea ecosystem. *Journal of Geophysical Research-Oceans*, *121*(3), 1824–1845. https://doi.org/10.1002/2015jc011496

Ciavatta, S., Torres, R., Martinez-Vicente, V., Smyth, T., Dall'Olmo, G., Polimene, L., & Allen, J. I. (2014). Assimilation of remotely-sensed optical properties to improve marine biogeochemistry modelling. *Progress in Oceanography*, *127*, 74–95. https://doi.org/10.1016/j.pocean.2014.06.002

Coppola, L., Diamond, R. E., & Carval, T. (2021). Dyfamed observatory data. SEANOE. https://doi.org/10.17882/43749

Crisp, D., Dolman, H., Tanhua, T., McKinley, G. A., Hauck, J., Bastos, A., Sitch, S., Eggleston, S., & Aich, V. (2022). How well do we understand the land-ocean-atmosphere carbon cycle? *Reviews of Geophysics*, *60*(2). https://doi.org/10.1029/2021rg000736

Cullen, J. J. (1982). The Deep Chlorophyll Maximum: Comparing Vertical Profiles of Chlorophyll a. *Canadian Journal of Fisheries and Aquatic Sciences*, *39*(5), 791–803. https://doi.org/10.1139/f82-108

Daase, M., Falk-Petersen, S., Varpe, Darnis, G., Søreide, J. E., Wold, A., Leu, E., Berge, J., Philippe, B., & Fortier, L. (2013). Timing of reproductive events in the marine copepod Calanus glacialis: a pan-Arctic perspective. *Canadian Journal of Fisheries and Aquatic Sciences*, *70*(6), 871–884. https://doi.org/10.1139/cjfas-2012-0401

Daines, S. J., Clark, J. R., & Lenton, T. M. (2014). Multiple environmental controls on phytoplankton growth strategies determine adaptive responses of the N : P ratio. *Ecology Letters*, *17*(4), 414–425. https://doi.org/10.1111/ele.12239

Dee, D. P., Uppala, S. M., Simmons, A. J., Berrisford, P., Poli, P., Kobayashi, S., Andrae, U., Balmaseda, M. A., Balsamo, G., Bauer, P., Bechtold, P., Beljaars, A. C. M., van de Berg, L., Bidlot, J., Bormann, N., Delsol, C., Dragani, R., Fuentes, M., Geer, A. J., … Vitart, F. (2011). The ERA-Interim reanalysis: configuration and performance of the data assimilation system. *Quarterly Journal of the Royal Meteorological Society*, *137*(656). https://doi.org/10.1002/qj.828

de Fommervault, O. P., Migon, C., D'Ortenzio, F., Ribera d'Alcalà, M., & Coppola, L. (2015). Temporal variability of nutrient concentrations in the northwestern Mediterranean sea (DYFAMED time-series station). *Deep Sea Research Part I: Oceanographic Research Papers*, *100*, 1–12. https://doi.org/10.1016/j.dsr.2015.02.006

Denman, K. L. (2003). Modelling planktonic ecosystems: Parameterizing complexity. *Progress in Oceanography*, *57*(3-4), 429–452. https://doi.org/10.1016/S0079-6611(03)00109-5

Dong, H., Zhou, M., Hu, Z., Zhang, Z., Zhong, Y., Basedow, S. L., & Smith, W. O. (2021). Transport Barriers and the Retention of Calanus finmarchicus on the Lofoten Shelf in Early Spring. *Journal of Geophysical Research: Oceans*, *126*(8). https://doi.org/10.1029/2021jc017408

Doron, M., Brasseur, P., Brankart, J. M., Losa, S. N., & Melet, A. (2013). Stochastic estimation of biogeochemical parameters from Globcolour ocean colour satellite data in a North Atlantic 3D ocean coupled physical-biogeochemical model. *Journal of Marine Systems*, *117*, 81–95. https://doi.org/10.1016/j.jmarsys.2013.02.007

Dowd, M., Jones, E., & Parslow, J. (2014). A statistical overview and perspectives on data assimilation for marine biogeochemical models. *Environmetrics*, *25*(4), 203–213. https://doi.org/10.1002/env.2264

Droop, M. R. (1983). 25 Years of Algal Growth-Kinetics - a Personal View. *Botanica Marina*, *26*(3), 99–112. https://doi.org/DOI10.1515/botm.1983.26.3.99

Druon, J.-N., & Le Fèvre, J. (1999). Sensitivity of a pelagic ecosystem model to variations of process parameters within a realistic range. *Journal of Marine Systems*, *19*(1), 1–26. https://doi.org/10.1016/S0924-7963(98)00021-9

Dugdale, R. C., Barber, R. T., Chai, F., Peng, T. H., & Wilkerson, F. P. (2002). One-dimensional ecosystem model of the equatorial Pacific upwelling system. Part II: sensitivity analysis and comparison with JGOFS EqPac data. *Deep Sea Research Part II: Topical Studies in Oceanography*, *49*(13). https://doi.org/10.1016/S0967-0645(02)00056-5

DuRand, M. D., Olson, R. J., & Chisholm, S. W. (2001). Phytoplankton population dynamics at the Bermuda Atlantic Time-series station in the Sargasso Sea. *Deep-Sea Research Part II-Topical Studies in Oceanography*, *48*(8-9), 1983–2003. https://doi.org/10.1016/S0967-0645(00)00166-1

Eknes, M., & Evensen, G. (2002). An Ensemble Kalman filter with a 1-D marine ecosystem model. *Journal of Marine Systems*, *36*(1), 75–100. https://doi.org/10.1016/S0924-7963(02)00134-3

European Space Agency. (Last access: March 2023). https://www.oceancolour.org/.

Evelyn, J. L., & Michael, C. M. (1998). Microzooplankton herbivory and phytoplankton growth in the northwestern Sargasso Sea. *Aquatic Microbial Ecology*, *16*(2), 173–188. https://www.int-res.com/abstracts/ame/v16/n2/p173-188/

Evensen, G. (2003). The Ensemble Kalman Filter: theoretical formulation and practical implementation. *Ocean Dynamics*, *53*(4), 343–367. https://doi.org/10.1007/s10236-003-0036-9

Falkowski, P. G. (1981). Light-shade adaptation and assimilation numbers. *Journal of Plankton Research*, *3*(2), 203–216. https://doi.org/10.1093/plankt/3.2.203

Fasham, M. J. R., Ducklow, H. W., & McKelvie, S. M. (1990). A nitrogen-based model of plankton dynamics in the oceanic mixed layer. *Journal of Marine Research*, *48*(3), 591–639. https://doi.org/10.1357/002224090784984678

Fawcett, S. E., Lomas, M. W., Ward, B. B., & Sigman, D. M. (2014). The counterintuitive effect of summer-to-fall mixed layer deepening on eukaryotic new production in the Sargasso Sea. *Global Biogeochemical Cycles*, *28*(2), 86–102. https://doi.org/10.1002/2013gb004579

Feely, R. A., Doney, S. C., & Cooley, S. R. (2009). Ocean Acidification: Present Conditions and Future Changes in a High–CO_2 World. *Oceanography*, *22*, 37–47. https://doi.org/10.5670/oceanog.2009.95

Fennel, K., Gehlen, M., Brasseur, P., Brown, C. W., Ciavatta, S., Cossarini, G., Crise, A., Edwards, C. A., Ford, D., Friedrichs, M. A. M., Gregoire, M., Jones, E., Kim, H. C., Lamouroux, J., Murtugudde, R., Perruche, C., the GODAE OceanView Marine Ecosystem Analysis, & Team, P. T. (2019). Advancing Marine Biogeochemical and Ecosystem Reanalyses and Forecasts as Tools for Monitoring and Managing Ecosystem Health. *Frontiers in Marine Science*, *6*. https://doi.org/10.3389/fmars.2019.00089

Fennel, K., Losch, M., Schroter, J., & Wenzel, M. (2001). Testing a marine ecosystem model: Sensitivity analysis and parameter optimization. *Journal of Marine Systems*, *28*(1-2), 45–63. https://doi.org/10.1016/S0924-7963(00)00083-X

Fennel, K., & Boss, E. (2003). Subsurface maxima of phytoplankton and chlorophyll: Steady-state solutions from a simple model. *Limnology and Oceanography*, *48*(4), 1521–1534. https://doi.org/10.4319/lo.2003.48.4.1521

Fennel, K., Mattern, J. P., Doney, S. C., Bopp, L., Moore, A. M., Wang, B., & Yu, L. (2022). Ocean biogeochemical modelling. *Nature Reviews Methods Primers*, *2*(1). https://doi.org/10.1038/s43586-022-00154-2

Fiechter, J., Broquet, G., Moore, A. M., & Arango, H. G. (2011). A data assimilative, coupled physical-biological model for the Coastal Gulf of Alaska. *Dynamics of*

Atmospheres and Oceans, *52*(1-2), 95–118. https://doi.org/10.1016/j.dynatmoce.2011.01.002

Fiechter, J., Herbei, R., Leeds, W., Brown, J., Milliff, R., Wikle, C., Moore, A., & Powell, T. (2013). A Bayesian parameter estimation method applied to a marine ecosystem model for the coastal Gulf of Alaska. *Ecological Modelling*, *258*, 122–133. https://doi.org/10.1016/j.ecolmodel.2013.03.003

Flato, G., Marotzke, J., Abiodun, B., Braconnot, P., Chou, S., Collins, W., Cox, P., Driouech, F., Emori, S., Eyring, V., Forest, C., Gleckler, P., Guilyardi, E., Jakob, C., Kattsov, V., Reason, C., & Rummukainen, M. (2014). Evaluation of Climate Models. In T. F. Stocker, D. Qin, G.-K. Plattner, M. Tignor, S. K. Allen, J. Doschung, A. Nauels, Y. Xia, V. Bex, & P. M. Midgley (Eds.), *Climate Change 2013 - The Physical Science Basis: Working Group I Contribution to the Fifth Assessment Report of the Intergovernmental Panel on Climate Change* (pp. 741–866). Cambridge University Press. https://doi.org/10.1017/CBO9781107415324.020

Flato, G. M. (2011). Earth system models: An overview. *Wiley Interdisciplinary Reviews-Climate Change*, *2*(6), 783–800. https://doi.org/10.1002/wcc.148

Flynn, K. J., & McGillicuddy, D. J. (2018). Modeling Marine Harmful Algal Blooms: Current Status and Future Prospects. *Harmful Algal Blooms*, 115–134. https://doi.org/10.1002/9781118994672.ch3

Follows, M. J., Dutkiewicz, S., Grant, S., & Chisholm, S. W. (2007). Emergent biogeography of microbial communities in a model ocean. *Science*, *315*(5820), 1843–1846. https://doi.org/10.1126/science.1138544

Ford, D., & Barciela, R. (2017). Global marine biogeochemical reanalyses assimilating two different sets of merged ocean colour products. *Remote Sensing of Environment*, *203*, 40–54. https://doi.org/10.1016/j.rse.2017.03.040

Ford, D., Key, S., McEwan, R., Totterdell, I., & Gehlen, M. (2018). Marine Biogeochemical Modelling and Data Assimilation for Operational Forecasting, Reanalysis, and Climate Research. In E. P. Chassignet, A. Pascual, J. Tintore, & J. Verron (Eds.), *New frontiers in operational oceanography*.

Forget, G., Campin, J. M., Heimbach, P., Hill, C. N., Ponte, R. M., & Wunsch, C. (2015). ECCO version 4: an integrated framework for non-linear inverse modeling and global ocean state estimation. *Geoscientific Model Development*, *8*(10), 3071–3104. https://doi.org/10.5194/gmd-8-3071-2015

Franks, P. J. S. (2002). NPZ models of plankton dynamics: Their construction, coupling to physics, and application. *Journal of Oceanography*, *58*(2), 379–387. https://doi.org/10.1023/A:1015874028196

Franks, P. J. S. (2009). Planktonic ecosystem models: Perplexing parameterizations and a failure to fail. *Journal of Plankton Research*, *31*(11), 1299–1306. https://doi.org/10.1093/plankt/fbp069

Friedlingstein, P., O'Sullivan, M., Jones, M. W., Andrew, R. M., Gregor, L., Hauck, J., Le Quéré, C., Luijkx, I. T., Olsen, A., Peters, G. P., Peters, W., Pongratz, J., Schwingshackl, C., Sitch, S., Canadell, J. G., Ciais, P., Jackson, R. B., Alin, S. R., Alkama, R., … Wright, R., et al. (2022). Global Carbon Budget 2022. *Earth System Science Data*, *14*(11), 4811–4900. https://doi.org/10.5194/essd-14-4811-2022

Friedrichs, M. A. M. (2001). Assimilation of JGOFS EqPac and SeaWiFS data into a marine ecosystem model of the central equatorial Pacific Ocean. *Deep-Sea Research Part Ii-Topical Studies in Oceanography*, *49*(1-3), 289–319. https://doi.org/10.1016/s0967-0645(01)00104-7

Friedrichs, M. A. M., Dusenberry, J. A., Anderson, L. A., Armstrong, R. A., Chai, F., Christian, J. R., Doney, S. C., Dunne, J., Fujii, M., Hood, R., McGillicuddy, D. J., Moore, J. K., Schartau, M., Spitz, Y. H., & Wiggert, J. D. (2007). Assessment of skill and portability in regional marine biogeochemical models: Role of multiple planktonic groups. *Journal of Geophysical Research-Oceans*, *112*(C8). https://doi.org/10.1029/2006jc003852

Friedrichs, M. A. M., Hood, R. R., & Wiggert, J. D. (2006). Ecosystem model complexity versus physical forcing: Quantification of their relative impact with assimilated Arabian Sea data. *Deep-Sea Research Part II-Topical Studies in Oceanography*, *53*(5-7), 576–600. https://doi.org/10.1016/j.dsr2.2006.01.026

Gamboa, F., Gremaud, P., Klein, T., & Lagnoux, A. (2022). Global sensitivity analysis: A novel generation of mighty estimators based on rank statistics. *Bernoulli*, *28*(4), 2345–2374. https://doi.org/10.3150/21-BEJ1421

García, H. E., Weathers, K., Paver, C. R., Smolyar, I., Boyer, T. P., Locarnini, R. A., Zweng, M. M., Mishonov, A. V., Baranova, O. K., Seidov, D., & Reagan, J. R. (2019a). World Ocean Atlas 2018, Volume 3: Dissolved Oxygen, Apparent Oxygen Utilization, and Oxygen Saturation. A. Mishonov Technical Ed.; NOAA Atlas NESDIS 83.

García, H. E., Weathers, K., Paver, C. R., Smolyar, I., Boyer, T. P., Locarnini, R. A., Zweng, M. M., Mishonov, A. V., Baranova, O. K., Seidov, D., & Reagan, J. R. (2019b). World Ocean Atlas 2018, Volume 4: Dissolved Inorganic Nutrients (phosphate, nitrate and nitrate+nitrite, silicate). A. Mishonov Technical Ed.; NOAA Atlas NESDIS 84.

Gattuso, J.-P., Magnan, A. K., Bopp, L., Cheung, W. W. L., Duarte, C. M., Hinkel, J., McLeod, E., Micheli, F., Oschlies, A., Williamson, P., Billé, R., Chalastani, V. I., Gates, R. D., Irisson, J.-O., Middelburg, J. J., Pörtner, H.-O., & Rau, G. H. (2018). Ocean Solutions to Address Climate Change and Its Effects on Marine Ecosystems. *Frontiers in Marine Science*, *5*. https://doi.org/10.3389/fmars.2018.00337

Gehlen, M., Barciela, R., Bertino, L., Brasseur, P., Butenschon, M., Chai, F., Crise, A., Drillet, Y., Ford, D., Lavoie, D., Lehodey, P., Perruche, C., Samuelsen, A., &

Simon, E. (2015). Building the capacity for forecasting marine biogeochemistry and ecosystems: Recent advances and future developments. *Journal of Operational Oceanography*, *8*(sup1), S168–S187. https://doi.org/10.1080/1755876x.2015.1022350

Gehlen, M., Gangstø, R., Schneider, B., Bopp, L., Aumont, O., & Ethe, C. (2007). The fate of pelagic $CaCO_3$ production in a high CO_2 ocean: a model study [BG]. *Biogeosciences*, *4*(4), 505–519. https://doi.org/10.5194/bg-4-505-2007

Geider, R. J., & La Roche, J. (1994). The role of iron in phytoplankton photosynthesis, and the potential for iron-limitation of primary productivity in the sea. *Photosynthesis Research*, *39*(3), 275–301. https://doi.org/10.1007/BF00014588

Geider, R. J., MacIntyre, H. L., & Kana, T. M. (1996). A dynamic model of photoadaptation in phytoplankton. *Limnology and Oceanography*, *41*(1), 1–15. https://doi.org/10.4319/lo.1996.41.1.0001

Geider, R. J., MacIntyre, H. L., & Kana, T. M. (1997). Dynamic model of phytoplankton growth and acclimation: Responses of the balanced growth rate and the chlorophyll a:carbon ratio to light, nutrient-limitation and temperature. *Marine Ecology Progress Series*, *148*(1-3), 187–200. https://doi.org/DOI10.3354/meps148187

Geider, R. J., MacIntyre, H. L., & Kana, T. M. (1998). A dynamic regulatory model of phytoplanktonic acclimation to light, nutrients, and temperature. *Limnology and Oceanography*, *43*(4), 679–694. https://doi.org/10.4319/lo.1998.43.4.0679

Gharamti, M. E., Samuelsen, A., Bertino, L., Simon, E., Korosov, A., & Daewel, U. (2017). Online tuning of ocean biogeochemical model parameters using ensemble estimation techniques: Application to a one-dimensional model in the North Atlantic. *Journal of Marine Systems*, *168*, 1–16. https://doi.org/10.1016/j.jmarsys.2016.12.003

Gharamti, M. E., Tjiputra, J., Bethke, I., Samuelsen, A., Skjelvan, I., Bentsen, M., & Bertino, L. (2017). Ensemble data assimilation for ocean biogeochemical state and parameter estimation at different sites. *Ocean Modelling*, *112*, 65–89. https://doi.org/10.1016/j.ocemod.2017.02.006

Glen, G., & Isaacs, K. (2012). Estimating Sobol sensitivity indices using correlations. *Environmental Modelling & Software*, *37*, 157–166. https://doi.org/10.1016/j.envsoft.2012.03.014

Glover, D. M., Jenkins, W. J., & Doney, S. C. (2011). *Modeling Methods for Marine Science*. Cambridge University Press. https://doi.org/DOI:10.1017/CBO9780511975721

Goodliff, M., Bruening, T., Schwichtenberg, F., Li, X., Lindenthal, A., Lorkowski, I., & Nerger, L. (2019). Temperature assimilation into a coastal ocean-biogeochemical model: Assessment of weakly and strongly coupled data assimilation. *Ocean Dynamics*, *69*(10), 1217–1237. https://doi.org/10.1007/s10236-019-01299-7

Gregg, W. W. (2008). Assimilation of SeaWiFS ocean chlorophyll data into a three-dimensional global ocean model. *Journal of Marine Systems*, *69*(3-4), 205–225. https://doi.org/10.1016/j.jmarsys.2006.02.015

Gruber, N., Boyd, P. W., Frolicher, T. L., & Vogt, M. (2021). Biogeochemical extremes and compound events in the ocean. *Nature*, *600*(7889), 395–407. https://doi.org/10.1038/s41586-021-03981-7

Guieu, C., & Blain, S. (2013). Concentrations of total dissolved iron measured on water bottle samples during THALASSA cruise PROSOPE. https://doi.org/10.1594/PANGAEA.805278

Guillas, S., Rougier, J., Maute, A., Richmond, A. D., & Linkletter, C. D. (2009). Bayesian calibration of the Thermosphere-Ionosphere Electrodynamics General Circulation Model (TIE-GCM) [GMD]. *Geosci. Model Dev.*, *2*(2), 137–144. https://doi.org/10.5194/gmd-2-137-2009

Gupta, A. S., Muir, L. C., Brown, J. N., Phipps, S. J., Durack, P. J., Monselesan, D., & Wijffels, S. E. (2012). Climate Drift in the CMIP3 Models. *Journal of Climate*, *25*(13), 4621–4640. https://doi.org/10.1175/JCLI-D-11-00312.1

Gupta, H. V., & Razavi, S. (2018). Revisiting the basis of sensitivity analysis for dynamical Earth System Models. *Water Resources Research*, *54*(11), 8692–8717. https://doi.org/10.1029/2018wr022668

Gürses, Ö., Oziel, L., Karakuş, O., Sidorenko, D., Völker, C., Ye, Y., Zeising, M., Butzin, M., & Hauck, J. (2023). Ocean biogeochemistry in the coupled ocean-sea ice-biogeochemistry model FESOM2.1-REcoM3 [GMD]. *Geosci. Model Dev.*, *16*(16), 4883–4936. https://doi.org/10.5194/gmd-16-4883-2023

Gutknecht, E., Reffray, G., Mignot, A., Dabrowski, T., & Sotillo, M. G. (2019). Modelling the marine ecosystem of Iberia-Biscay-Ireland (IBI) European waters for CMEMS operational applications. *Ocean Science*, *15*(6), 1489–1516. https://doi.org/10.5194/os-15-1489-2019

Harris, G. P., Griffiths, F. B., & Thomas, D. P. (1989). Light and dark uptake and loss of ^{14}c: Methodological problems with productivity measurements in oceanic waters. *Hydrobiologia*, *173*(2), 95–105. https://doi.org/10.1007/bf00015519

Harrison, W. G., & Platt, T. (1980). Variations in assimilation number of coastal marine phyto-phytoplankton: Effects of environmental co-variates. *Journal of Plankton Research*, *2*(4), 249–260. https://doi.org/10.1093/plankt/2.4.249

Harrison, W. G., & Platt, T. (1986). Photosynthesis-irradiance relationships in polar and temperate phytoplankton populations. *Polar Biology*, *5*(3), 153–164. https://doi.org/10.1007/BF00441695

Hatje, V., Sarin, M., Sander, S. G., Omanović, D., Ramachandran, P., Völker, C., Barra, R. O., & Tagliabue, A. (2022). Emergent interactive effects of climate change and contaminants in coastal and ocean ecosystems. *Frontiers in Marine Science*, *9*. https://doi.org/10.3389/fmars.2022.936109

Hauck, J., Volker, C., Wang, T., Hoppema, M., Losch, M., & Wolf-Gladrow, D. A. (2013). Seasonally different carbon flux changes in the Southern Ocean in response to the southern annular mode. *Global Biogeochem Cycles*, *27*(4), 1236–1245. https://doi.org/10.1002/2013GB004600

Hauck, J., Zeising, M., Le Quéré, C., Gruber, N., Bakker, D. C. E., Bopp, L., Chau, T. T. T., Gürses, Ö., Ilyina, T., Landschützer, P., Lenton, A., Resplandy, L., Rödenbeck, C., Schwinger, J., & Séférian, R. (2020). Consistency and Challenges in the Ocean Carbon Sink Estimate for the Global Carbon Budget. *Frontiers in Marine Science*, *7*. https://doi.org/10.3389/fmars.2020.571720

Hauri, C., Gruber, N., Vogt, M., Doney, S. C., Feely, R. A., Lachkar, Z., Leinweber, A., McDonnell, A. M. P., Munnich, M., & Plattner, G. K. (2013). Spatiotemporal variability and long-term trends of ocean acidification in the California Current System [BG]. *Biogeosciences*, *10*(1), 193–216. https://doi.org/10.5194/bg-10-193-2013

Hauri, C., Schultz, C., Hedstrom, K., Danielson, S., Irving, B., Doney, S. C., Dussin, R., Curchitser, E. N., Hill, D. F., & Stock, C. A. (2020). A regional hindcast model simulating ecosystem dynamics, inorganic carbon chemistry, and ocean acidification in the Gulf of Alaska. *Biogeosciences*, *17*(14), 3837–3857. https://doi.org/10.5194/bg-17-3837-2020

Hauri, C., Pagès, R., McDonnell, A. M. P., Stuecker, M. F., Danielson, S. L., Hedstrom, K., Irving, B., Schultz, C., & Doney, S. C. (2021). Modulation of ocean acidification by decadal climate variability in the Gulf of Alaska. *Communications Earth & Environment*, *2*(1), 191. https://doi.org/10.1038/s43247-021-00254-z

Hawkins, E., Smith, R. S., Allison, L. C., Gregory, J. M., Woollings, T. J., Pohlmann, H., & de Cuevas, B. (2011). Bistability of the Atlantic overturning circulation in a global climate model and links to ocean freshwater transport. *Geophysical Research Letters*, *38*(10). https://doi.org/10.1029/2011GL047208

Herman, J., & Usher, W. (2017). SALib: An open-source python library for sensitivity analysis. *The Journal of Open Source Software*, *2*(9). https://doi.org/10.21105/joss.00097

Hersbach, H., Bell, B., Berrisford, P., Biavati, G., Horányi, A., Muñoz Sabater, J., Nicolas, J., Peubey, C., Radu, R., Rozum, I., Schepers, D., Simmons, A., Soci, C., Dee, D., & Thépaut, J.-N. (2018). ERA5 hourly data on single levels from 1979 to present. https://doi.org/10.24381/cds.adbb2d47

Hersbach, H., Bell, B., Berrisford, P., Hirahara, S., Horányi, A., Muñoz-Sabater, J., Nicolas, J., Peubey, C., Radu, R., Schepers, D., Simmons, A., Soci, C., Abdalla, S., Abellan, X., Balsamo, G., Bechtold, P., Biavati, G., Bidlot, J., Bonavita, M., … Thépaut, J.-N. (2020). The ERA5 global reanalysis. *Quarterly Journal of the Royal Meteorological Society*, *146*(730), 1999–2049. https://doi.org/10.1002/qj.3803

Hohn, S. (2009). *Coupling and decoupling of biogeochemical cycles in marine ecosystems* [Thesis]. Fachbereich 2 Biologie. https://elib.suub.uni-bremen.de/diss/docs/00011278.pdf

Homma, T., & Saltelli, A. (1996). Importance measures in global sensitivity analysis of nonlinear models. *Reliability Engineering & System Safety*, *52*(1), 1–17. https://doi.org/10.1016/0951-8320(96)00002-6

Hoshiba, Y., Hirata, T., Shigemitsu, M., Nakano, H., Hashioka, T., Masuda, Y., & Yamanaka, Y. (2018). Biological data assimilation for parameter estimation of a phytoplankton functional type model for the western North Pacific. *Ocean Science*, *14*(3), 371–386. https://doi.org/10.5194/os-14-371-2018

Hourdin, F., Mauritsen, T., Gettelman, A., Golaz, J. C., Balaji, V., Duan, Q. Y., Folini, D., Ji, D. Y., Klocke, D., Qian, Y., Rauser, F., Rio, C., Tomassini, L., Watanabe, M., & Williamson, D. (2017). The art and science of climate model tuning. *Bulletin of the American Meteorological Society*, *98*(3), 589–602. https://doi.org/10.1175/Bams-D-15-00135.1

Hu, J. T., Fennel, K., Mattern, J. P., & Wilkin, J. (2012). Data assimilation with a local Ensemble Kalman Filter applied to a three-dimensional biological model of the Middle Atlantic Bight. *Journal of Marine Systems*, *94*, 145–156. https://doi.org/10.1016/j.jmarsys.2011.11.016

Hu, L. Y., Zhao, Y., Liu, Y., Scheepens, C., & Bouchard, A. (2013). Updating multipoint simulations using the ensemble Kalman filter. *Computers& Geosciences*, *51*, 7–15. https://doi.org/10.1016/j.cageo.2012.08.020

Ilyina, T., Li, H., Spring, A., Müller, W. A., Bopp, L., Chikamoto, M. O., Danabasoglu, G., Dobrynin, M., Dunne, J., Fransner, F., Friedlingstein, P., Lee, W., Lovenduski, N. S., Merryfield, W. J., Mignot, J., Park, J. Y., Séférian, R., Sospedra-Alfonso, R., Watanabe, M., & Yeager, S. (2021). Predictable Variations of the Carbon Sinks and Atmospheric CO_2 Growth in a Multi-Model Framework. *Geophysical Research Letters*, *48*(6). https://doi.org/10.1029/2020gl090695

Ilyina, T., Six, K. D., Segschneider, J., Maier-Reimer, E., Li, H., & Núñez-Riboni, I. (2013). Global ocean biogeochemistry model HAMOCC: Model architecture and performance as component of the MPI-Earth system model in different CMIP5 experimental realizations. *Journal of Advances in Modeling Earth Systems*, *5*(2), 287–315. https://doi.org/10.1029/2012ms000178

Ilyina, T., Zeebe, R. E., Maier-Reimer, E., & Heinze, C. (2009). Early detection of ocean acidification effects on marine calcification. *Global Biogeochemical Cycles*, *23*(1). https://doi.org/10.1029/2008GB003278

Iooss, B., & Prieur, C. (2019). Shapley effects for sensitivity analysis with correlated inputs: Comparisons with Sobol' indices, numerical estimation and applications. *International Journal for Uncertainty Quantification*, *9*(5), 493–514. https://doi.org/10.1615/Int.J.UncertaintyQuantification.2019028372

Iooss, B., Da Veiga, S., Janon, A., & Pujol, G. (2022). *sensitivity: Global Sensitivity Analysis of Model Outputs, R package version 1.27.1* (tech. rep.). C-RAN. https://CRAN.R-project.org/package=sensitivity

Islam, A., & Karadogan, E. (2019). Sensitivity and uncertainty analysis of one-dimensional Tanaka and Liang-Rogers Shape Memory Alloy Constitutive Models. *Materials*, *12*(10). https://doi.org/10.3390/ma12101687

Iwanaga, T., Usher, W., & Herman, J. (2022). Toward SALib 2.0: Advancing the accessibility and interpretability of global sensitivity analyses. *Socio-Environmental Systems Modelling*, *4*, 18155. https://doi.org/10.18174/sesmo.18155

Jackson, G. A., Waite, A. M., & Boyd, P. W. (2005). Role of algal aggregation in vertical carbon export during SOIREE and in other low biomass environments. *Geophysical Research Letters*, *32*(13). https://doi.org/10.1029/2005gl023180

JGOFS. (1997). *Bermuda Atlantic Time-series Study (BATS) Methods* (Report). Joint Global Ocean Flux Study (JGOFS). http://bats.bios.edu/wp-content/uploads/2017/07/report_methods.pdf

Ji, X. L., Liu, G. M., Gao, S., & Wang, H. (2015). Parameter sensitivity study of the biogeochemical model in the China coastal seas. *Acta Oceanologica Sinica*, *34*(12), 51–60. https://doi.org/10.1007/s13131-015-0762-0

Johnson, R., Strutton, P. G., Wright, S. W., McMinn, A., & Meiners, K. M. (2013). Three improved satellite chlorophyll algorithms for the southern ocean. *Journal of Geophysical Research-Oceans*, *118*(7), 3694–3703. https://doi.org/10.1002/jgrc.20270

Jones, E. M., Baird, M. E., Mongin, M., Parslow, J., Skerratt, J., Lovell, J., Margvelashvili, N., Matear, R. J., Wild-Allen, K., Robson, B., Rizwi, F., Oke, P., King, E., Schroeder, T., Steven, A., & Taylor, J. (2016). Use of remote-sensing reflectance to constrain a data assimilating marine biogeochemical model of the Great Barrier Reef. *Biogeosciences*, *13*(23), 6441–6469. https://doi.org/10.5194/bg-13-6441-2016

Jones, V., Meador, T. B., Gogou, A., Migon, C., Penkman, K. E. H., Collins, M. J., & Repeta, D. J. (2013). Characterisation and dynamics of dissolved organic matter in the Northwestern Mediterranean Sea. *Progress in Oceanography*, *119*, 78–89. https://doi.org/10.1016/j.pocean.2013.06.007

Kaiser, M., Buklijas, T., & Gluckman, P. (2022). Models and Numbers: Representing the World or Imposing Order? *Perspectives on Science*, *30*(4), 525–548. https://doi.org/10.1162/posc_a_00373

Kalra, T. S., Aretxabaleta, A., Seshadri, P., Ganju, N. K., & Beudin, A. (2017). Sensitivity analysis of a coupled hydrodynamic-vegetation model using the effectively subsampled quadratures method (ESQM v5.2). *Geoscientific Model Development*, *10*(12), 4511–4523. https://doi.org/10.5194/gmd-10-4511-2017

Kane, A., Moulin, C., Thiria, S., Bopp, L., Berrada, M., Tagliabue, A., Crepon, M., Aumont, O., & Badran, F. (2011). Improving the parameters of a global ocean

biogeochemical model via variational assimilation of in situ data at five time series stations. *Journal of Geophysical Research – Oceans*, *116*(C6). https://doi.org/10.1029/2009jc006005

Karakuş, O., Völker, C., Iversen, M., Hagen, W., & Hauck, J. (2022). The Role of Zooplankton Grazing and Nutrient Recycling for Global Ocean Biogeochemistry and Phytoplankton Phenology. *Journal of Geophysical Research: Biogeosciences*, *127*(10). https://doi.org/10.1029/2022jg006798

Khatiwala, S., Tanhua, T., Mikaloff Fletcher, S., Gerber, M., Doney, S. C., Graven, H. D., Gruber, N., McKinley, G. A., Murata, A., Ríos, A. F., & Sabine, C. L. (2013). Global ocean storage of anthropogenic carbon. *Biogeosciences*, *10*(4), 2169–2191. https://doi.org/10.5194/bg-10-2169-2013

Kim, H. H., Luo, Y. W., Ducklow, H. W., Schofield, O. M., Steinberg, D. K., & Doney, S. C. (2021). WAP-1D-VAR v1.0: development and evaluation of a one-dimensional variational data assimilation model for the marine ecosystem along the West Antarctic Peninsula. *Geoscientific Model Development*, *14*(8), 4939–4975. https://doi.org/10.5194/gmd-14-4939-2021

Kim, Y., & Nakata, N. (2018). Geophysical inversion versus machine learning in inverse problems. *The Leading Edge*, *37*(12), 894–901. https://doi.org/10.1190/tle37120894.1

Kostadinov, T. S., Robertson Lain, L., Kong, C. E., Zhang, X., Maritorena, S., Bernard, S., Loisel, H., Jorge, D. S. F., Kochetkova, E., Roy, S., Jonsson, B., Martinez-Vicente, V., & Sathyendranath, S. (2023). Ocean color algorithm for the retrieval of the particle size distribution and carbon-based phytoplankton size classes using a two-component coated-sphere backscattering model [OS]. *Ocean Sci.*, *19*(3), 703–727. https://doi.org/10.5194/os-19-703-2023

Kovač, Ž., Platt, T., Sathyendranath, S., & Lomas, M. (2018). Extraction of photosynthesis parameters from time series measurements of in situ production: Bermuda Atlantic Time-Series Study. *Remote Sensing*, *10*(6), 915. https://doi.org/10.3390/rs10060915

Kriest, I., Oschlies, A., & Khatiwala, S. (2012). Sensitivity analysis of simple global marine biogeochemical models. *Global Biogeochemical Cycles*, *26*(2). https://doi.org/10.1029/2011gb004072

Krumhardt, K. M., Lovenduski, N. S., Long, M. C., Levy, M., Lindsay, K., Moore, J. K., & Nissen, C. (2019). Coccolithophore Growth and Calcification in an Acidified Ocean: Insights From Community Earth System Model Simulations. *Journal of Advances in Modeling Earth Systems*, *11*(5), 1418–1437. https://doi.org/10.1029/2018MS001483

Kucherenko, S., & Song, S. (2017). Different numerical estimators for main effect global sensitivity indices. *Reliability Engineering & System Safety*, *165*, 222–238. https://doi.org/10.1016/j.ress.2017.04.003

Kucherenko, S., Tarantola, S., & Annoni, P. (2012). Estimation of global sensitivity indices for models with dependent variables. *Computer Physics Communications*, *183*(4), 937–946. https://doi.org/10.1016/j.cpc.2011.12.020

Kucherenko, S., Feil, B., Shah, N., & Mauntz, W. (2011). The identification of model effective dimensions using global sensitivity analysis. *Reliability Engineering & System Safety*, *96*(4). https://doi.org/10.1016/j.ress.2010.11.003

Kvale, K. F., & Meissner, K. J. (2017). Primary production sensitivity to phytoplankton light attenuation parameter increases with transient forcing. *Biogeosciences*, *14*(20), 4767–4780. https://doi.org/10.5194/bg-14-4767-2017

Kwiatkowski, L., Torres, O., Bopp, L., Aumont, O., Chamberlain, M., Christian, J. R., Dunne, J. P., Gehlen, M., Ilyina, T., John, J. G., Lenton, A., Li, H. M., Lovenduski, N. S., Orr, J. C., Palmieri, J., Santana-Falcon, Y., Schwinger, J., Séférian, R., Stock, C. A., … Ziehn, T. (2020). Twenty-first century ocean warming, acidification, deoxygenation, and upper-ocean nutrient and primary production decline from CMIP6 model projections. *Biogeosciences*, *17*(13), 3439–3470. https://doi.org/10.5194/bg-17-3439-2020

Kwiatkowski, L., & Orr, J. C. (2018). Diverging seasonal extremes for ocean acidification during the twenty-first century. *Nature Climate Change*, *8*(2), 141–145. https://doi.org/10.1038/s41558-017-0054-0

Laiolo, L., Matear, R., Baird, M. E., Soja-Wozniak, M., & Doblin, M. A. (2018). Information content of in situ and remotely sensed chlorophyll-a: Learning from size-structured phytoplankton model. *Journal of Marine Systems*, *183*, 1–12. https://doi.org/10.1016/j.jmarsys.2018.03.005

Lam, V. W. Y., Cheung, W. W. L., Reygondeau, G., & Sumaila, U. R. (2016). Projected change in global fisheries revenues under climate change. *Scientific Reports*, *6*(1), 32607. https://doi.org/10.1038/srep32607

Large, W. G., & Yeager, S. G. (2008). The global climatology of an interannually varying air-sea flux data set. *Climate Dynamics*, *33*(2-3), 341–364. https://doi.org/10.1007/s00382-008-0441-3

Laufkötter, C., Vogt, M., Gruber, N., Aita-Noguchi, M., Aumont, O., Bopp, L., Buitenhuis, E., Doney, S. C., Dunne, J., Hashioka, T., Hauck, J., Hirata, T., John, J., Le Quèrè, C., Lima, I. D., Nakano, H., Séférian, R., Totterdell, I., Vichi, M., & Völker, C. (2015). Drivers and uncertainties of future global marine primary production in marine ecosystem models. *Biogeosciences*, *12*(23), 6955–6984. https://doi.org/10.5194/bg-12-6955-2015

Laufkötter, C., Vogt, M., Gruber, N., Aumont, O., Bopp, L., Doney, S. C., Dunne, J. P., Hauck, J., John, J. G., Lima, I. D., Séférian, R., & Völker, C. (2016). Projected decreases in future marine export production: The role of the carbon flux through the upper ocean ecosystem. *Biogeosciences*, *13*(13), 4023–4047. https://doi.org/10.5194/bg-13-4023-2016

Laurent, A., Fennel, K., Cai, W.-J., Huang, W.-J., Barbero, L., & Wanninkhof, R. (2017). Eutrophication-induced acidification of coastal waters in the northern Gulf of Mexico: Insights into origin and processes from a coupled physical-biogeochemical model. *Geophysical Research Letters*, *44*(2), 946–956. https://doi.org/10.1002/2016GL071881

Lauvset, S. K., Key, R. M., Olsen, A., van Heuven, S., Velo, A., Lin, X. H., Schirnick, C., Kozyr, A., Tanhua, T., Hoppema, M., Jutterstrom, S., Steinfeldt, R., Jeansson, E., Ishii, M., Perez, F. F., Suzuki, T., & Watelet, S. (2016). A new global interior ocean mapped climatology: The 1 degrees x 1 degrees GLODAP version 2. *Earth System Science Data*, *8*(2), 325–340. https://doi.org/10.5194/essd-8-325-2016

Lavoie, D., Lambert, N., Starr, M., Chassé, J., Riche, O., Le Clainche, Y., Azetsu-Scott, K., Béjaoui, B., Christian, J. R., & Gilbert, D. (2021). The gulf of St. Lawrence biogeochemical model: A modelling tool for fisheries and ocean management. *Frontiers in Marine Science*, *8*. https://doi.org/10.3389/fmars.2021.732269

Laws, E., Sakshaug, E., Babin, M., Dandonneau, Y., Falkowski, P., Geider, R., Legendre, L., Morel, A., Sondergaard, M., Takahashi, M., & Williams, P. J. l. (2002). Photosynthesis and Primary Productivity in Marine Ecosystems: Practical Aspects and Application of Techniques. http://ijgofs.whoi.edu/Publications/Report_Series/JGOFS_36.pdf

Le Quéré, C., Buitenhuis, E. T., Moriarty, R., Alvain, S., Aumont, O., Bopp, L., Chollet, S., Enright, C., Franklin, D. J., Geider, R. J., Harrison, S. P., Hirst, A. G., Larsen, S., Legendre, L., Platt, T., Prentice, I. C., Rivkin, R. B., Sailley, S., Sathyendranath, S., … Vallina, S. M. (2016). Role of zooplankton dynamics for Southern Ocean phytoplankton biomass and global biogeochemical cycles. *Biogeosciences*, *13*(14), 4111–4133. https://doi.org/10.5194/bg-13-4111-2016

Leles, S. G., Polimene, L., Bruggeman, J., Blackford, J., Ciavatta, S., Mitra, A., & Flynn, K. J. (2018). Modelling mixotrophic functional diversity and implications for ecosystem function. *Journal of Plankton Research*, *40*(6), 627–642. https://doi.org/10.1093/plankt/fby044

Levin, L. A. (2018). Manifestation, Drivers, and Emergence of Open Ocean Deoxygenation. *Annual Review of Marine Science*, *10*, 229–260. https://doi.org/10.1146/annurev-marine-121916-063359

Locarnini, R. A., Mishonov, A. V., Baranova, O. K., Boyer, T. P., Zweng, M. M., García, H. E., Reagan, J. R., Seidov, D., Weathers, K., Paver, C. R., & Smolyar, I. (2019). World Ocean Atlas 2018, Volume 1: Temperature. A. Mishonov Technical Ed.; NOAA Atlas NESDIS 81.

Longhurst, A. R. (2007). Chapter 7 - Provinces: The Secondary Compartments. In A. R. Longhurst (Ed.), *Ecological geography of the sea (second edition)* (pp. 103–114). Academic Press. https://doi.org/10.1016/B978-012455521-1/50008-5

Löptien, U., & Dietze, H. (2019). Reciprocal bias compensation and ensuing uncertainties in model-based climate projections: Pelagic biogeochemistry versus ocean mixing

[BG]. *Biogeosciences*, *16*(9), 1865–1881. https://doi.org/10.5194/bg-16-1865-2019

Losa, S. N., Kivman, G. A., & Ryabchenko, V. A. (2004). Weak constraint parameter estimation for a simple ocean ecosystem model: What can we learn about the model and data? *Journal of Marine Systems*, *45*(1). https://doi.org/10.1016/j.jmarsys.2003.08.005

Losch, M., Menemenlis, D., Campin, J. M., Heimbach, P., & Hill, C. (2010). On the formulation of sea-ice models. Part 1: Effects of different solver implementations and parameterizations. *Ocean Modelling*, *33*(1-2), 129–144. https://doi.org/10.1016/j.ocemod.2009.12.008

Losch, M., Schröter, M., Hohn, S., & Völker, C. (2008). High-resolution modelling of phytoplankton distribution and adaptation. In G. Münster, D. Wolf, & M. Kremer (Eds.), *Nic symposium 2008* (Vol. 39). John von Neumann Institute for Computing, Jülich. https://epic.awi.de/id/eprint/18337/1/Los2008a.pdf

Lotze, H. K., Tittensor, D. P., Bryndum-Buchholz, A., Eddy, T. D., Cheung, W. W. L., Galbraith, E. D., Barange, M., Barrier, N., Bianchi, D., Blanchard, J. L., Bopp, L., Büchner, M., Bulman, C. M., Carozza, D. A., Christensen, V., Coll, M., Dunne, J. P., Fulton, E. A., Jennings, S., … Worm, B. (2019). Global ensemble projections reveal trophic amplification of ocean biomass declines with climate change. *Proceedings of the National Academy of Sciences*, *116*(26), 12907–12912. https://doi.org/10.1073/pnas.1900194116

Loukos, H., Monfray, P., Bopp, L., & Lehodey, P. (2003). Potential changes in skipjack tuna (Katsuwonus pelamis) habitat from a global warming scenario: modelling approach and preliminary results. *Fisheries Oceanography*, *12*(4-5), 474–482. https://doi.org/10.1046/j.1365-2419.2003.00241.x

Makler-Pick, V., Gal, G., Gorfine, M., Hipsey, M. R., & Carmel, Y. (2011). Sensitivity analysis for complex ecological models - A new approach. *Environmental Modelling & Software*, *26*(2), 124–134. https://doi.org/10.1016/j.envsoft.2010.06.010

Malone, T. C., Pike, S. E., & Conley, D. J. (1993). Transient variations in phytoplankton productivity at the JGOFS Bermuda time series station. *Deep Sea Research Part I: Oceanographic Research Papers*, *40*(5), 903–924. https://doi.org/10.1016/0967-0637(93)90080-M

Mamnun, N., Völker, C., Vrekoussis, M., & Nerger, L. (2022). Uncertainties in ocean biogeochemical simulations: Application of ensemble data assimilation to a one-dimensional model. *Frontiers in Marine Science*, *9*, 980388. https://doi.org/10.3389/fmars.2022.984236

Mamnun, N., Völker, C., Krumscheid, S., Vrekoussis, M., & Nerger, L. (2023). Global sensitivity analysis of a one-dimensional ocean biogeochemical model. *SocioEnvironmental Systems Modelling*. https://doi.org/10.18174/sesmo.18613

Marañón, E., & Holligan, P. M. (1999). Photosynthetic parameters of phytoplankton from 50°N to 50°S in the Atlantic Ocean. *Marine Ecology Progress Series*, *176*, 191–203. https://doi.org/10.3354/meps176191

Marshall, J., Adcroft, A., Hill, C., Perelman, L., & Heisey, C. (1997). A finite-volume, incompressible Navier Stokes model for studies of the ocean on parallel computers. *Journal of Geophysical Research - Oceans*, *102*(C3), 5753–5766. https://doi.org/10.1029/96jc02775

Marshall, J., Hill, C., Perelman, L., & Adcroft, A. (1997). Hydrostatic, quasi-hydrostatic, and nonhydrostatic ocean modeling. *Journal of Geophysical Research - Oceans*, *102*(C3), 5733–5752. https://doi.org/10.1029/96JC02776

Martiny, A. C., Vrugt, J. A., Primeau, F. W., & Lomas, M. W. (2013). Regional variation in the particulate organic carbon to nitrogen ratio in the surface ocean. *Global Biogeochemical Cycles*, *27*(3), 723–731. https://doi.org/10.1002/gbc.20061

Marty, J. C. (2002). The DYFAMED time-series program (French-JGOFS). *Deep-Sea Research Part II -Topical Studies in Oceanography*, *49*(11), 1963–1964. https://doi.org/10.1016/S0967-0645(02)00021-8

Marty, J. C., & Chiaverini, J. (2010). Hydrological changes in the Ligurian Sea (NW Mediterranean, DYFAMED site) during 1995-2007 and biogeochemical consequences. *Biogeosciences*, *7*(7), 2117–2128. https://doi.org/10.5194/bg-7-2117-2010

Marty, J.-C., Garcia, N., & Raimbault, P. (2008). Phytoplankton dynamics and primary production under late summer conditions in the NW Mediterranean Sea. *Deep Sea Research Part I: Oceanographic Research Papers*, *55*(9), 1131–1149. https://doi.org/10.1016/j.dsr.2008.05.001

Mattern, J. P., Dowd, M., & Fennel, K. (2010). Sequential data assimilation applied to a physical-biological model for the Bermuda Atlantic time series station. *Journal of Marine Systems*, *79*(1-2), 144–156. https://doi.org/10.1016/j.jmarsys.2009.08.004

Mattern, J. P., & Edwards, C. A. (2017). Simple parameter estimation for complex models - Testing evolutionary techniques on 3-dimensional biogeochemical ocean models. *Journal of Marine Systems*, *165*, 139–152. https://doi.org/10.1016/j.jmarsys.2016.10.012

Mattern, J. P., Fennel, K., & Dowd, M. (2012). Estimating time-dependent parameters for a biological ocean model using an emulator approach. *Journal of Marine Systems*, *96-97*, 32–47. https://doi.org/10.1016/j.jmarsys.2012.01.015

Mattern, J. P., Fennel, K., & Dowd, M. (2013). Sensitivity and uncertainty analysis of model hypoxia estimates for the texas-louisiana shelf. *Journal of Geophysical Research - Oceans*, *118*(3), 1316–1332. https://doi.org/10.1002/jgrc.20130

Mattern, J. P., Fennel, K., & Dowd, M. (2014). Periodic time-dependent parameters improving forecasting abilities of biological ocean models. *Geophysical Research Letters*, *41*(19), 6848–6854. https://doi.org/10.1002/2014gl061178

Mattern, J. P., Song, H., Edwards, C. A., Moore, A. M., & Fiechter, J. (2017). Data assimilation of physical and chlorophyll-a observations in the California Current System using two biogeochemical models. *Ocean Modelling*, *109*, 55–71. https://doi.org/10.1016/j.ocemod.2016.12.002

Mayot, N., Nival, P., & Levy, M. (2020). Primary Production in the Ligurian Sea. In C. Migon, P. Nival, & A. Sciandra (Eds.), *The Mediterranean Sea in the era of Global Change 1: 30 years of multidisciplinary study of the Ligurian Sea* (pp. 139–164). Wiley-VCH GmbH. https://doi.org/10.1002/9781119706960.ch6

Mccave, I. N. (1984). Size spectra and aggregation of suspended particles in the deep ocean. *Deep-Sea Research Part a-Oceanographic Research Papers*, *31*(4), 329–352. https://doi.org/10.1016/0198-0149(84)90088-8

McDonald, C. P., Bennington, V., Urban, N. R., & McKinley, G. A. (2012). 1-D test-bed calibration of a 3-D Lake Superior biogeochemical model. *Ecological Modelling*, *225*, 115–126. https://doi.org/10.1016/j.ecolmodel.2011.11.021

McKinley, G. A., Pilcher, D. J., Fay, A. R., Lindsay, K., Long, M. C., & Lovenduski, N. S. (2016). Timescales for detection of trends in the ocean carbon sink. *Nature*, *530*(7591), 469–72. https://doi.org/10.1038/nature16958

Mignot, A., Claustre, H., Cossarini, G., D'Ortenzio, F., Gutknecht, E., Lamouroux, J., Lazzari, P., Perruche, C., Salon, S., Sauzède, R., Taillandier, V., & Teruzzi, A. (2023). Using machine learning and Biogeochemical-Argo (BGC-Argo) floats to assess biogeochemical models and optimize observing system design. *Biogeosciences*, *20*(7), 1405–1422. https://doi.org/10.5194/bg-20-1405-2023

Moradkhani, H., Hsu, K. L., Gupta, H., & Sorooshian, S. (2005). Uncertainty assessment of hydrologic model states and parameters: Sequential data assimilation using the particle filter. *Water Resources Research*, *41*(5). https://doi.org/10.1029/2004wr003604

Morris, M. D. (1991). Factorial sampling plans for preliminary computational experiments. *Technometrics*, *33*(2), 161–174. https://doi.org/10.2307/1269043

National Academies of Sciences, Engineering and Medicine. (2022). *A Research Strategy for Ocean-based Carbon Dioxide Removal and Sequestration*. The National Academies Press. https://doi.org/10.17226/26278

Natvik, L. J., & Evensen, G. (2003). Assimilation of ocean colour data into a biochemical model of the North Atlantic - Part 1. Data assimilation experiments. *Journal of Marine Systems*, *40*, 127–153. https://doi.org/10.1016/S0924-7963(03)00016-2

Nelson, D. M., & Brzezinski, M. A. (1997). Diatom growth and productivity in an oligo-trophic midocean gyre: A 3-yr record from the Sargasso Sea near Bermuda. *Limnology and Oceanography*, *42*(3), 473–486. https://doi.org/10.4319/lo.1997.42.3.0473

Nerger, L., & Gregg, W. W. (2007). Assimilation of SeaWiFS data into a global ocean-biogeochemical model using a local SEIK filter. *Journal of Marine Systems*, *68*(1-2), 237–254. https://doi.org/10.1016/j.jmarsys.2006.11.009

Nerger, L., & Gregg, W. W. (2008). Improving assimilation of SeaWiFS data by the application of bias correction with a local SEIK filter. *Journal of Marine Systems*, *73*(1-2), 87–102. https://doi.org/10.1016/j.jmarsys.2007.09.007

Nerger, L., & Hiller, W. (2013). Software for ensemble-based data assimilation systems – Implementation strategies and scalability. *Computers & Geosciences*, *55*, 110–118. https://doi.org/10.1016/j.cageo.2012.03.026

Nerger, L., Janjic, T., Schroter, J., & Hiller, W. (2012a). A regulated localization scheme for ensemble-based Kalman filters. *Quarterly Journal of the Royal Meteorological Society*, *138*(664), 802–812. https://doi.org/10.1002/qj.945

Nerger, L., Janjic, T., Schroter, J., & Hiller, W. (2012b). A Unification of Ensemble Square Root Kalman Filters. *Monthly Weather Review*, *140*(7), 2335–2345. https://doi.org/10.1175/Mwr-D-11-00102.1

Ökten, G., & Liu, Y. (2021). Randomized quasi-Monte Carlo methods in global sensitivity analysis. *Reliability Engineering & System Safety*, *210*, 107520. https://doi.org/10.1016/j.ress.2021.107520

Oliver, S., Cartis, C., Kriest, I., Tett, S. F. B., & Khatiwala, S. (2022). A derivative-free optimisation method for global ocean biogeochemical models. *Geoscientific Model Development*, *15*(9), 3537–3554. https://doi.org/10.5194/gmd-15-3537-2022

Olsen, A., Brown, K. R., Chierici, M., Johannessen, T., & Neill, C. (2008). Sea-surface CO_2 fugacity in the subpolar North Atlantic. *Biogeosciences*, *5*(2), 535–547. https://doi.org/10.5194/bg-5-535-2008

Omta, A. W., Talmy, D., Sher, D., Finkel, Z. V., Irwin, A. J., & Follows, M. J. (2017). Extracting phytoplankton physiological traits from batch and chemostat culture data. *Limnology and Oceanography: Methods*, *15*(5), 453–466. https://doi.org/10.1002/lom3.10172

O'Neill, R. V., DeAngelis, D. L., Pastor, J. J., Jackson, B. J., & Post, W. M. (1989). Multiple nutrient limitations in ecological models. *Ecological Modelling*, *46*(3-4), 147–163. https://doi.org/10.1016/0304-3800(89)90015-x

O'Neill, R. (1973). Error analysis of ecological models. W: Radionuclides in ecosystems.

Orr, J. C., Najjar, R. G., Aumont, O., Bopp, L., Bullister, J. L., Danabasoglu, G., Doney, S. C., Dunne, J. P., Dutay, J. C., Graven, H., Griffies, S. M., John, J. G., Joos, F., Levin, I., Lindsay, K., Matear, R. J., McKinley, G. A., Mouchet, A., Oschlies, A., … Yool, A. (2017). Biogeochemical protocols and diagnostics for the CMIP6 Ocean Model Intercomparison Project (OMIP). *Geoscientific Model Development*, *10*(6), 2169–2199. https://doi.org/10.5194/gmd-10-2169-2017

Oschlies, A., & Schartau, M. (2005). Basin-scale performance of a locally optimized marine ecosystem model. *Journal of Marine Research*, *63*(2), 335–358. https://doi.org/10.1357/0022240053693680

Oschlies, A., Brandt, P., Stramma, L., & Schmidtko, S. (2018). Drivers and mechanisms of ocean deoxygenation. *Nature Geoscience*, *11*(7), 467–473. https://doi.org/10.1038/s41561-018-0152-2

Owen, A. B., Dick, J., & Chen, S. (2014). Higher order Sobol' indices. *Information and Inference: A Journal of the IMA*, *3*(1), 59–81. https://doi.org/10.1093/imaiai/iau001

Owen, A. B., & Prieur, C. (2017). On Shapley value for measuring importance of dependent inputs. *SIAM/ASA Journal on Uncertainty Quantification*, *5*(1), 986–1002. https://doi.org/10.1137/16M1097717

Pathiraja, S., Moradkhani, H., Marshall, L., Sharma, A., & Geenens, G. (2018). Data-Driven Model Uncertainty Estimation in Hydrologic Data Assimilation. *Water Resources Research*, *54*(2), 1252–1280. https://doi.org/10.1002/2018wr022627

Pelc, J. S., Simon, E., Bertino, L., El Serafy, G., & Heemink, A. W. (2012). Application of model reduced 4D-Var to a 1D ecosystem model. *Ocean Modelling*, *57-58*, 43–58. https://doi.org/10.1016/j.ocemod.2012.09.003

Penny, S. G., Bach, E., Bhargava, K., Chang, C. .-., Da, C., Sun, L., & Yoshida, T. (2019). Strongly Coupled Data Assimilation in Multiscale Media: Experiments Using a Quasi-Geostrophic Coupled Model. *Journal of Advances in Modeling Earth Systems*, *11*(6), 1803–1829. https://doi.org/10.1029/2019ms001652

Penny, S. G., & Hamill, T. M. (2017). Coupled Data Assimilation for Integrated Earth System Analysis and Prediction. *Bulletin of the American Meteorological Society*, *98*(7), Es169–Es172. https://doi.org/10.1175/Bams-D-17-0036.1

Platt, T., Caverhill, C., & Sathyendranath, S. (1991). Basin-scale estimates of oceanic primary production by remote sensing: The North Atlantic. *Journal of Geophysical Research: Oceans*, *96*(C8), 15147–15159. https://doi.org/10.1029/91JC01118

Plischke, E., Borgonovo, E., & Smith, C. L. (2013). Global sensitivity measures from given data. *European Journal of Operational Research*, *226*(3), 536–550. https://doi.org/10.1016/j.ejor.2012.11.047

Polimene, L., Rivkin, R. B., Luo, Y.-W., Kwon, E. Y., Gehlen, M., Peña, M. A., Wang, N., Liang, Y., Kaartokallio, H., & Jiao, N. (2018). Modelling marine DOC degradation time scales. *National Science Review*, *5*(4), 468–474. https://doi.org/10.1093/nsr/nwy066

Popova, E. E., Coward, A. C., Nurser, G. A., de Cuevas, B., Fasham, M. J. R., & Anderson, T. R. (2006). Mechanisms controlling primary and new production in a global ecosystem model – part I: Validation of the biological simulation. *Ocean Science*, *2*(2), 249–266. https://doi.org/10.5194/os-2-249-2006

Pradhan, H. K., Völker, C., Losa, S. N., Bracher, A., & Nerger, L. (2019). Assimilation of Global Total Chlorophyll OC-CCI Data and Its Impact on Individual Phytoplankton Fields. *Journal of Geophysical Research - Oceans*, *124*(1), 470–490. https://doi.org/10.1029/2018jc014329

Pradhan, H. K., Völker, C., Losa, S. N., Bracher, A., & Nerger, L. (2020). Global Assimilation of Ocean-Color Data of Phytoplankton Functional Types: Impact of Different Data Sets. *Journal of Geophysical Research - Oceans*, *125*(2), e2019JC015586. https://doi.org/10.1029/2019JC015586

Prieur, C., Viry, L., Blayo, E., & Brankart, J. M. (2019). A global sensitivity analysis approach for marine biogeochemical modeling. *Ocean Modelling*, *139*, 101402. https://doi.org/10.1016/j.ocemod.2019.101402

Puxty, R. J., Millard, A. D., Evans, D. J., & Scanlan, D. J. (2016). Viruses Inhibit CO_2 Fixation in the Most Abundant Phototrophs on Earth. *Current Biology*, *26*(12), 1585–1589. https://doi.org/10.1016/j.cub.2016.04.036

Razavi, S., Jakeman, A., Saltelli, A., Prieur, C., Iooss, B., Borgonovo, E., Plischke, E., Lo Piano, S., Iwanaga, T., Becker, W., Tarantola, S., Guillaume, J. H. A., Jakeman, J., Gupta, H., Melillo, N., Rabitti, G., Chabridon, V., Duan, Q. Y., Sun, X. F., … Maier, H. R. (2021). The future of sensitivity analysis: An essential discipline for systems modeling and policy support. *Environmental Modelling & Software*, *137*, 104954. https://doi.org/10.1016/j.envsoft.2020.104954

Razavi, S., & Gupta, H. V. (2015). What do we mean by sensitivity analysis? the need for comprehensive characterization of "global" sensitivity in Earth and environmental systems models. *Water Resources Research*, *51*(5), 3070–3092. https://doi.org/10.1002/2014wr016527

Redfield, A. C. (1934). On the proportions of organic derivations in sea water and their relation to the composition of plankton. In R. Daniel (Ed.), *James johnstone memorial volume* (pp. 176–192). University Press of Liverpool.

Richardson, K., Bendtsen, J., Kragh, T., & Mousing, E. A. (2016). Constraining the Distribution of Photosynthetic Parameters in the Global Ocean. *Frontiers in Marine Science*, *3*. https://doi.org/10.3389/fmars.2016.00269

Rohr, T., Richardson, A. J., Lenton, A., Chamberlain, M. A., & Shadwick, E. H. (2023). Zooplankton grazing is the largest source of uncertainty for marine carbon cycling in CMIP6 models. *Communications Earth & Environment*, *4*(1). https://doi.org/10.1038/s43247-023-00871-w

Roy, S., Broomhead, D. S., Platt, T., Sathyendranath, S., & Ciavatta, S. (2012). Sequential variations of phytoplankton growth and mortality in an NPZ model: A remote-sensing-based assessment. *Journal of Marine Systems*, *92*(1), 16–29. https://doi.org/10.1016/j.jmarsys.2011.10.001

Rutherford, K., Fennel, K., Atamanchuk, D., Wallace, D., & Thomas, H. (2021). A modelling study of temporal and spatial pCO_2 variability on the biologically active and temperature-dominated Scotian Shelf [BG]. *Biogeosciences*, *18*(23), 6271–6286. https://doi.org/10.5194/bg-18-6271-2021

Saba, V. S., Friedrichs, M. A. M., Carr, M. E., Antoine, D., Armstrong, R. A., Asanuma, I., Aumont, O., Bates, N. R., Behrenfeld, M. J., Bennington, V., Bopp, L., Bruggeman, J., Buitenhuis, E. T., Church, M. J., Ciotti, A. M., Doney, S. C., Dowell, M., Dunne, J., Dutkiewicz, S., … Yool, A. (2010). Challenges of modeling depth-integrated marine primary productivity over multiple decades: A case study at BATS and HOT. *Global Biogeochemical Cycles*, *24*, GB3020. https://doi.org/10.1029/2009gb003655

Saito, H., Suzuki, K., Hinuma, A., Ota, T., Fukami, K., Kiyosawa, H., Saino, T., & Tsuda, A. (2005). Responses of microzooplankton to in situ iron fertilization in the western subarctic Pacific (SEEDS). *Progress in Oceanography*, *64*(2), 223–236. https://doi.org/10.1016/j.pocean.2005.02.010

Saltelli, A., & Funtowicz, S. (2014). When All Models Are Wrong. *Issues in Science and Technology*, *30*(02). https://issues.org/andrea/

Saltelli, A., Jakeman, A., Razavi, S., & Wu, Q. (2021). Sensitivity analysis: A discipline coming of age. *Environmental Modelling & Software*, *146*. https://doi.org/10.1016/j.envsoft.2021.105226

Saltelli, A., Ratto, M., Andres, T., Campolongo, F., Cariboni, J., Gatelli, D., Saisana, M., & Tarantola, S. (2008). *Global sensitivity analysis: The primer*. John Wiley & Sons.

Saltelli, A., Tarantola, S., Campolongo, F., & Ratto, M. (2004). *Sensitivity analysis in practice: A guide to assessing scientific models*. John Wiley & Sons Ltd.

Samuelsen, A., Hansen, C., & Wehde, H. (2015). Tuning and assessment of the HYCOM-NORWECOM V2.1 biogeochemical modeling system for the North Atlantic and Arctic oceans. *Geosci. Model Dev.*, *8*(7), 2187–2202. https://doi.org/10.5194/gmd-8-2187-2015

Sankar, S., Polimene, L., Marin, L., Menon, N. N., Samuelsen, A., Pastres, R., & Ciavatta, S. (2018). Sensitivity of the simulated Oxygen Minimum Zone to biogeochemical processes at an oligotrophic site in the Arabian Sea. *Ecological Modelling*, *372*, 12–23. https://doi.org/10.1016/j.ecolmodel.2018.01.016

Sathyendranath, S., Brewin, R. J. W., Brockmann, C., Brotas, V., Calton, B., Chuprin, A., Cipollini, P., Couto, A. B., Dingle, J., Doerffer, R., Donlon, C., Dowell, M., Farman, A., Grant, M., Groom, S., Horseman, A., Jackson, T., Krasemann, H., Lavender, S., … Platt, T. (2019). An Ocean-Colour Time Series for Use in Climate Studies: The Experience of the Ocean-Colour Climate Change Initiative (OC-CCI). *Sensors*, *19*(19), 4285. https://doi.org/10.3390/s19194285

Sathyendranath, S., Stuart, V., Nair, A., Oka, K., Nakane, T., Bouman, H., Forget, M. H., Maass, H., & Platt, T. (2009). Carbon-to-chlorophyll ratio and growth rate of phytoplankton in the sea. *Marine Ecology Progress Series*, *383*, 73–84. https://doi.org/10.3354/meps07998

Sathyendranath, S., Platt, T., Horne, E. P. W., Harrison, W. G., Ulloa, O., Outerbridge, R., & Hoepffner, N. (1991). Estimation of new production in the ocean by compound remote sensing. *Nature*, *353*(6340), 129–133. https://doi.org/10.1038/353129a0

Schartau, M., & Oschlies, A. (2003). Simultaneous data-based optimization of a 1D-ecosystem model at three locations in the North Atlantic: Part I - Method and parameter estimates. *Journal of Marine Research*, *61*(6), 765–793. https://doi.org/10.1357/002224003322981147

Schartau, M., Wallhead, P., Hemmings, J., Loptien, U., Kriest, I., Krishna, S., Ward, B. A., Slawig, T., & Oschlies, A. (2017). Reviews and syntheses: Parameter identification in marine planktonic ecosystem modelling. *Biogeosciences*, *14*(6), 1647–1701. https://doi.org/10.5194/bg-14-1647-2017

Schourup–Kristensen, V., Sidorenko, D., Wolf-Gladrow, D. A., & Völker, C. (2014). A skill assessment of the biogeochemical model recom2 coupled to the Finite Element Sea Ice-Ocean Model (FESOM 1.3). *Geoscientific Model Development*, *7*(6), 2769–2802. https://doi.org/10.5194/gmd-7-2769-2014

Scott, V., Kettle, H., & Merchant, C. J. (2011). Sensitivity analysis of an ocean carbon cycle model in the North Atlantic: An investigation of parameters affecting the air-sea CO_2 flux, primary production and export of detritus. *Ocean Science*, *7*(3), 405–419. https://doi.org/10.5194/os-7-405-2011

Séférian, R., Berthet, S., Yool, A., Palmieri, J., Bopp, L., Tagliabue, A., Kwiatkowski, L., Aumont, O., Christian, J., Dunne, J., Gehlen, M., Ilyina, T., John, J. G., Li, H., Long, M. C., Luo, J. Y., Nakano, H., Romanou, A., Schwinger, J., … Yamamoto, A. (2020). Tracking Improvement in Simulated Marine Biogeochemistry Between CMIP5 and CMIP6. *Current Climate Change Reports*, *6*(3), 95–119. https://doi.org/10.1007/s40641-020-00160-0

Sheikholeslami, R., Gharari, S., Papalexiou, S. M., & Clark, M. P. (2021). VISCOUS: A variance-based sensitivity analysis using copulas for efficient identification of dominant hydrological processes. *Water Resources Research*, *57*(7), e2020WR028435. https://doi.org/10.1029/2020WR028435

Shimoda, Y., & Arhonditsis, G. B. (2016). Phytoplankton functional type modelling: Running before we can walk? A critical evaluation of the current state of knowledge. *Ecological Modelling*, *320*, 29–43. https://doi.org/10.1016/j.ecolmodel.2015.08.029

Simon, E., Samuelsen, A., Bertino, L., & Dumont, D. (2012). Estimation of positive sum-to-one constrained zooplankton grazing preferences with the DEnKF: a twin experiment. *Ocean Science*, *8*(4), 587–602. https://doi.org/10.5194/os-8-587-2012

Simon, E., Samuelsen, A., Bertino, L., & Mouysset, S. (2015). Experiences in multiyear combined state-parameter estimation with an ecosystem model of the North Atlantic and Arctic Oceans using the Ensemble Kalman Filter. *Journal of Marine Systems*, *152*. https://doi.org/10.1016/j.jmarsys.2015.07.004

Singh, T., Counillon, F., Tjiputra, J., Wang, Y., & Gharamti, M. E. (2022). Estimation of Ocean Biogeochemical Parameters in an Earth System Model Using the Dual One Step Ahead Smoother: A Twin Experiment. *Frontiers in Marine Science*, *9*. https://doi.org/10.3389/fmars.2022.775394

Smith Jr, W. O., & Donaldson, K. (2015). Photosynthesis-irradiance responses in the Ross Sea, Antarctica: a meta-analysis [BG]. *Biogeosciences*, *12*(11), 3567–3577. https://doi.org/10.5194/bg-12-3567-2015

Sober, E. (1981). The Principle of Parsimony. *British Journal for the Philosophy of Science*, *32*(2), 145–156. https://doi.org/10.1093/bjps/32.2.145

Sobol, I. M. (1993). Sensitivity estimates for nonlinear mathematical model. *Mathematical Modeling and Computational Experiment*, *1*(4), 8.

Sobol', I. M. (2001). Global sensitivity indices for nonlinear mathematical models and their Monte Carlo estimates. *Mathematics and Computers in Simulation*, *55*(1-3), 271–280. https://doi.org/10.1016/S0378-4754(00)00270-6

Sobol', I. M., & Kucherenko, S. (2009). Derivative based global sensitivity measures and their link with global sensitivity indices. *Mathematics and Computers in Simulation*, *79*(10), 3009–3017. https://doi.org/10.1016/j.matcom.2009.01.023

Sobol', I. M., & Kucherenko, S. (2010). Derivative based global sensitivity measures. *Procedia - Social and Behavioral Sciences*, *2*(6), 7745–7746. https://doi.org/10.1016/j.sbspro.2010.05.208

Sobol', I. M., Tarantola, S., Gatelli, D., Kucherenko, S. S., & Mauntz, W. (2007). Estimating the approximation error when fixing unessential factors in global sensitivity analysis. *Reliability Engineering & System Safety*, *92*(7), 957–960. https://doi.org/10.1016/j.ress.2006.07.001

Song, H., Edwards, C. A., Moore, A. M., & Fiechter, J. (2016). Data assimilation in a coupled physical-biogeochemical model of the California Current System using an incremental lognormal 4-dimensional variational approach: Part 1-Model formulation and biological data assimilation twin experiments. *Ocean Modelling*, *106*, 131–145. https://doi.org/10.1016/j.ocemod.2016.04.001

Søreide, J. E., Leu, E. V. A., Berge, J., Graeve, M., & Falk-Petersen, S. (2010). Timing of blooms, algal food quality and Calanus glacialis reproduction and growth in a changing Arctic. *Global Change Biology*, no–no. https://doi.org/10.1111/j.1365-2486.2010.02175.x

Spitz, Y. H., Moisan, J. R., & Abbott, M. R. (2001). Configuring an ecosystem model using data from the Bermuda Atlantic Time Series (BATS). *Deep Sea Research Part II: Topical Studies in Oceanography*, *48*(8), 1733–1768. https://doi.org/10.1016/S0967-0645(00)00159-4

Steinberg, D. K., & Landry, M. R. (2017). Zooplankton and the ocean carbon cycle. *Annual Review of Marine Science*, *9*, 413–444. https://doi.org/10.1146/annurev-marine-010814-015924

Steinberg, D. K., Carlson, C. A., Bates, N. R., Johnson, R. J., Michaels, A. F., & Knap, A. H. (2001). Overview of the US JGOFS Bermuda Atlantic Time-series Study (BATS): A decade-scale look at ocean biology and biogeochemistry. *Deep Sea Research Part II: Topical Studies in Oceanography*, *48*(8-9), 1405–1447. https://doi.org/10.1016/s0967-0645(00)00148-x

St-Laurent, P., Friedrichs, M. A. M., Najjar, R. G., Martins, D. K., Herrmann, M., Miller, S. K., & Wilkin, J. (2017). Impacts of Atmospheric Nitrogen Deposition on Surface Waters of the Western North Atlantic Mitigated by Multiple Feedbacks.

Journal of Geophysical Research – Oceans, *122*(11), 8406–8426. https://doi.org/10.1002/2017jc013072

Stock, C. A., John, J. G., Rykaczewski, R. R., Asch, R. G., Cheung, W. W. L., Dunne, J. P., Friedland, K. D., Lam, V. W. Y., Sarmiento, J. L., & Watson, R. A. (2017). Reconciling fisheries catch and ocean productivity. *Proceedings of the National Academy of Sciences*, *114*(8), E1441–E1449. https://doi.org/10.1073/pnas.1610238114

Sweeney, E. N., McGillicuddy, D. J., & Buesseler, K. O. (2003). Biogeochemical impacts due to mesoscale eddy activity in the Sargasso Sea as measured at the Bermuda Atlantic Time-series Study (BATS). *Deep Sea Research Part II: Topical Studies in Oceanography*, *50*(22), 3017–3039. https://doi.org/10.1016/j.dsr2.2003.07.008

Tagliabue, A., Hawco, N. J., Bundy, R. M., Landing, W. M., Milne, A., Morton, P. L., & Saito, M. A. (2018). The Role of External Inputs and Internal Cycling in Shaping the Global Ocean Cobalt Distribution: Insights From the First Cobalt Biogeochemical Model. *Global Biogeochemical Cycles*, *32*(4), 594–616. https://doi.org/10.1002/2017GB005830

Tagliabue, A., Kwiatkowski, L., Bopp, L., Butenschön, M., Cheung, W., Lengaigne, M., & Vialard, J. (2021). Persistent Uncertainties in Ocean Net Primary Production Climate Change Projections at Regional Scales Raise Challenges for Assessing Impacts on Ecosystem Services. *Frontiers in Climate*, *3*. https://doi.org/10.3389/fclim.2021.738224

Tang, Q., Mu, L., Goessling, H. F., Semmler, T., & Nerger, L. (2021). Strongly Coupled Data Assimilation of Ocean Observations Into an Ocean-Atmosphere Model. *Geophysical Research Letters*, *48*(24). https://doi.org/10.1029/2021gl094941

Tang, Q., Mu, L. J., Sidorenko, D., Goessling, H., Semmler, T., & Nerger, L. (2020). Improving the ocean and atmosphere in a coupled ocean-atmosphere model by assimilating satellite sea-surface temperature and subsurface profile data. *Quarterly Journal of the Royal Meteorological Society*, *146*(733), 4014–4029. https://doi.org/10.1002/qj.3885

Tarantola, S., Gatelli, D., & Mara, T. A. (2006). Random balance designs for the estimation of first order global sensitivity indices. *Reliability Engineering & System Safety*, *91*(6), 717–727. https://doi.org/10.1016/j.ress.2005.06.003

Taylor, A. H., Geider, R. J., & Gilbert, F. J. H. (1997). Seasonal and latitudinal dependencies of phytoplankton carbon-to-chlorophyll a ratios: Results of a modelling study. *Marine Ecology Progress Series*, *152*, 51–66. https://www.int-res.com/abstracts/meps/v152/p51-66/

Taylor, K. E. (2001). Summarizing multiple aspects of model performance in a single diagram. *Journal of Geophysical Research-Atmospheres*, *106*(D7), 7183–7192. https://doi.org/10.1029/2000jd900719

Thacker, W. C. (1989). The role of the Hessian matrix in fitting models to measurements. *Journal of Geophysical Research: Oceans*, *94*(C5), 6177–6196. https://doi.org/10.1029/JC094iC05p06177

Thelen, M. C. B. (2021, April). *Quantication of Uncertainties and Determination of Sensitivities for Biogeochemical Ocean Simulation* [Master's thesis, RWTH Aachen University].

Tin, H. C., Lomas, M. W., & Ishizaka, J. (2016). Satellite-derived estimates of primary production during the Sargasso Sea winter/spring bloom: Integration of in-situ time-series data and ocean color remote sensing observations. *Regional Studies in Marine Science*, *3*, 131–143. https://doi.org/10.1016/j.rsma.2015.07.002

Tjiputra, J. F., Polzin, D., & Winguth, A. M. E. (2007). Assimilation of seasonal chlorophyll and nutrient data into an adjoint three-dimensional ocean carbon cycle model: Sensitivity analysis and ecosystem parameter optimization. *Global Biogeochemical Cycles*, *21*(1). https://doi.org/10.1029/2006gb002745

Tjiputra, J. F., & Winguth, A. M. E. (2008). Sensitivity of sea-to-air CO_2 flux to ecosystem parameters from an adjoint model. *Biogeosciences*, *5*(2), 615–630. https://doi.org/10.5194/bg-5-615-2008

Tommasi, D., Stock, C. A., Hobday, A. J., Methot, R., Kaplan, I. C., Eveson, J. P., Holsman, K., Miller, T. J., Gaichas, S., Gehlen, M., Pershing, A., Vecchi, G. A., Msadek, R., Delworth, T., Eakin, C. M., Haltuch, M. A., Séférian, R., Spillman, C. M., Hartog, J. R., … Werner, F. E. (2017). Managing living marine resources in a dynamic environment: The role of seasonal to decadal climate forecasts. *Progress in Oceanography*, *152*, 15–49. https://doi.org/10.1016/j.pocean.2016.12.011

Triantafyllou, G., Korres, G., Hoteit, I., Petihakis, G., & Banks, A. C. (2007). Assimilation of ocean colour data into a biogeochemical flux model of the eastern Mediterranean sea. *Ocean Science*, *3*(3), 397–410. https://doi.org/10.5194/os-3-397-2007

Tsujino, H., Urakawa, S., Nakano, H., Small, R. J., Kim, W. M., Yeager, S. G., Danabasoglu, G., Suzuki, T., Bamber, J. L., Bentsen, M., Boning, C. W., Bozec, A., Chassignet, E. P., Curchitser, E., Dias, F. B., Durack, P. J., Griffes, S. M., Harada, Y., Ilicak, M., … Yamazaki, D. (2018). JRA-55 based surface dataset for driving ocean-sea-ice models (JRA55-do). *Ocean Modelling*, *130*, 79–139. https://doi.org/10.1016/j.ocemod.2018.07.002

Turner, M. G., & Gardner, R. H. (2015). Introduction to models. In M. G. Turner & R. H. Gardner (Eds.), *Landscape Ecology in Theory and Practice* (pp. 63–95). Springer New York. https://doi.org/10.1007/978-1-4939-2794-4_3

Vancoppenolle, M., Bopp, L., Madec, G., Dunne, J., Ilyina, T., Halloran, P. R., & Steiner, N. (2013). Future Arctic Ocean primary productivity from CMIP5 simulations: Uncertain outcome, but consistent mechanisms. *Global Biogeochemical Cycles*, *27*(3), 605–619. https://doi.org/10.1002/gbc.20055

van Rossum, G., & the Python development team. (2022). The Python Language Reference; Release 3.9.16.

Vetra-Carvalho, S., Van Leeuwen, P. J., Nerger, L., Barth, A., Altaf, M. U., Brasseur, P., Kirchgessner, P., & Beckers, J. M. (2018). State-of-the-art stochastic data assimilation methods for high-dimensional non-gaussian problems. *Tellus Series a-Dynamic Meteorology and Oceanography*, *70*(1). https://doi.org/10.1080/16000870.2018.1445364

Völker, C., & Tagliabue, A. (2015). Modeling organic iron-binding ligands in a three-dimensional biogeochemical ocean model. *Marine Chemistry*, *173*, 67–77. https://doi.org/10.1016/j.marchem.2014.11.008

Wagener, T., & Pianosi, F. (2019). What has global sensitivity analysis ever done for us? A systematic review to support scientific advancement and to inform policy-making in earth system modelling. *Earth-Science Reviews*, *194*, 1–18. https://doi.org/10.1016/j.earscirev.2019.04.006

Wang, S., Flipo, N., & Romary, T. (2018). Time-dependent global sensitivity analysis of the C-RIVE biogeochemical model in contrasted hydrological and trophic contexts. *Water Research*, *144*, 341–355. https://doi.org/10.1016/j.watres.2018.07.033

Ward, B. A., Dutkiewicz, S., Jahn, O., & Follows, M. J. (2012). A size-structured food-web model for the global ocean. *Limnology and Oceanography*, *57*(6), 1877–1891. https://doi.org/10.4319/lo.2012.57.6.1877

Ward, B. A., Friedrichs, M. A. M., Anderson, T. R., & Oschlies, A. (2010). Parameter optimisation techniques and the problem of underdetermination in marine biogeochemical models. *Journal of Marine Systems*, *81*(1-2), 34–43. https://doi.org/10.1016/j.jmarsys.2009.12.005

Ward, B. A., Schartau, M., Oschlies, A., Martin, A. P., Follows, M. J., & Anderson, T. R. (2013). When is a biogeochemical model too complex? Objective model reduction and selection for North Atlantic time-series sites. *Progress in Oceanography*, *116*, 49–65. https://doi.org/10.1016/j.pocean.2013.06.002

Westberry, T., Behrenfeld, M. J., Siegel, D. A., & Boss, E. (2008). Carbon-based primary productivity modeling with vertically resolved photoacclimation. *Global Biogeochemical Cycles*, *22*(2). https://doi.org/10.1029/2007gb003078

White, A. E., Letelier, R. M., Whitmire, A. L., Barone, B., Bidigare, R. R., Church, M. J., & Karl, D. M. (2015). Phenology of particle size distributions and primary productivity in the North Pacific subtropical gyre (Station ALOHA). *J Geophys Res Oceans*, *120*(11), 7381–7399. https://doi.org/10.1002/2015JC010897

Xiao, Y., & Friedrichs, M. A. M. (2014a). The assimilation of satellite-derived data into a one-dimensional lower trophic level marine ecosystem model. *Journal of Geophysical Research - Oceans*, *119*(4), 2691–2712. https://doi.org/10.1002/2013jc009433

Xiao, Y., & Friedrichs, M. A. M. (2014b). Using biogeochemical data assimilation to assess the relative skill of multiple ecosystem models in the Mid-Atlantic Bight: effects of increasing the complexity of the planktonic food web. *Biogeosciences*, *11*(11), 3015–3030. https://doi.org/10.5194/bg-11-3015-2014

Xu, M., Liu, Y., Zhao, Z., Fu, K., & Lv, X. (2022). Advancing parameter estimation with Characteristic Finite Difference Method (CFDM) for a marine ecosystem model by assimilating satellite observations: Spatial distributions. *Frontiers in Marine Science*, *9*. https://doi.org/10.3389/fmars.2022.997537

Ye, Y., Munhoven, G., Köhler, P., Butzin, M., Hauck, J., Gürses, Ö., & Völker, C. (2023). FESOM2.1-REcoM3-MEDUSA2: an ocean-sea ice-biogeochemistry model coupled to a sediment model. *Geoscientific Model Development Discussion*, *2023*, 1–26. https://doi.org/10.5194/gmd-2023-181

Yu, L. Q., Fennel, K., Bertino, L., El Gharamti, M., & Thompson, K. R. (2018). Insights on multivariate updates of physical and biogeochemical ocean variables using an Ensemble Kalman Filter and an idealized model of upwelling. *Ocean Modelling*, *126*, 13–28. https://doi.org/10.1016/j.ocemod.2018.04.005

Zaiss, J., Boyd, P. W., Doney, S. C., Havenhand, J. N., & Levine, N. M. (2021). Impact of Lagrangian Sea Surface Temperature Variability on Southern Ocean Phytoplankton Community Growth Rates. *Global Biogeochemical Cycles*, *35*(8). https://doi.org/10.1029/2020gb006880

Zakem, E. J., Al-Haj, A., Church, M. J., van Dijken, G. L., Dutkiewicz, S., Foster, S. Q., Fulweiler, R. W., Mills, M. M., & Follows, M. J. (2018). Ecological control of nitrite in the upper ocean. *Nature Communications*, *9*(1), 1206. https://doi.org/10.1038/s41467-018-03553-w

Zhang, M., Ibrahim, A., Franz, B. A., Ahmad, Z., & Sayer, A. M. (2022). Estimating pixel-level uncertainty in ocean color retrievals from MODIS. *Optics Express*, *30*(17), 31415–31438. https://doi.org/10.1364/OE.460735

Zhao, L., Wei, H., Xu, Y., & Feng, S. (2005). An adjoint data assimilation approach for estimating parameters in a three-dimensional ecosystem model. *Ecological Modelling*, *186*(2), 235–250. https://doi.org/10.1016/j.ecolmodel.2005.01.017

Zweng, M. M., Reagan, J. R., Seidov, D., Boyer, T. P., Locarnini, R. A., García, H. E., Mishonov, A. V., Baranova, O. K., Weathers, K., Paver, C. R., & Smolyar, I. (2019). World Ocean Atlas 2018, Volume 2: Salinity. A. Mishonov Technical Ed.; NOAA Atlas NESDIS 82.

Appendix A

Appendices

A.1 List of tracers simulated by the Regulated Ecosystem Model 2 (REcoM2)

Table A.1 Tracers simulated by REcoM2

SL	Tracer	Unit
1	Dissolved Inorganic Nitrogen	mmol m^{-3}
2	Dissolved Inorganic Carbon	mmol m^{-3}
3	Total Alkalinity	mmol m^{-3}
4	Biomass content of Nitrogen in nanoplankton	mmol m^{-3}
5	Biomass content of Carbon in nanoplankton	mmol m^{-3}
6	Chlorophyll-a concentration of nanoplankton	mg m^{-3}
7	Nitrogen content of detritus	mmol m^{-3}
8	Carbon content of detritus	mmol m^{-3}
9	Biomass content of Nitrogen in heterotrophic zooplankton	mmol m^{-3}
10	Biomass content of carbon in heterotrophic zooplankton	mmol m^{-3}
11	Dissolved organic Nitrogen	mmol m^{-3}
12	Extra-cellular organic Carbon	mmol m^{-3}
13	Biomass content of Nitrogen in Diatoms	mmol m^{-3}
14	Biomass content of Carbon in diatoms	mmol m^{-3}
15	Chlorophyll-a concentration of diatoms	mg m^{-3}

16	Biomass content of Silicate in diatoms	mmol m^{-3}
17	Dissolved inorganic Silicate	mmol m^{-3}
18	Dissolved Iron	mmol m^{-3}
20	Dissolved oxygen	mmol m^{-3}
21	Biomass content of calcium carbonate in phytoplankton	mmol m^{-3}
22	Content of calcium carbonate in detritus	mmol m^{-3}

A.2 List of Parameters in the Regulated Ecosystem Model 2 (REcoM2)

Table A.2 REcoM2 parameters, their Symbol, unit, and default value

SL	**Parameter**	**Symbol**	**Unit**	**Value**
1	Default temperature	T_{ref}	Kelvin	188.15
2	Chlorophyll-a specific attenuation coefficient	α_{CHL}	$m^{-1}(mgCHL)^{-1}$	0.03
3	Light attenuation coefficient	K_W	m^{-1}	0.04
4	Nanophytoplankton half-saturation for nitrogen uptake	K^N_{Nano}	$mmolNm^{-3}$	0.55
5	Diatom half-saturation for nitrogen uptake	K^N_{Dia}	$mmolNm^{-3}$	1.0
6	Diatom half-saturation for silicate uptake	K^{Si}_{Dia}	$mmolSim^{-3}$	4.0
7	Nanophytoplankton half-saturation for iron uptake	K^{Fe}_{Nano}	$mmolFem^{-3}$	0.02
8	Diatom half-saturation for iron uptake	K^{Fe}_{Dia}	$mmolFem^{-3}$	0.12
9	Nanophytoplankton nitrogen to carbon uptake ratio	σ^N_{Nano}	$molN(molC)^{-1}$	0.20
10	Diatom nitrogen to carbon uptake ratio	σ^N_{Dia}	$molN(molC)^{-1}$	0.20
11	Diatom silicate to carbon uptake ratio	σ^{Si}_{Dia}	$molSi(molC)^{-1}$	0.20
12	Nanophytoplankton maximum nitrogen uptake	V^{Nmax}_{Nano}	dimensionless	0.7
13	Diatom maximum nitrogen uptake	V^{Nmax}_{Dia}	dimensionless	0.7
14	Iron scavenging rate	K^{Scav}_{Fe}	$(mmolCm^{-3})^{-1}$	0.0156
15	Nanophytoplankton initial slope of P-I curve	α_{Nano}	$mmolC(mgChl)^{-1}$	0.14
16	Diatom initial slope of P-I curve	α_{Dia}	$mmolC(mgChl)^{-1}$	0.19

17	Nanophytoplankton maximum photosynthesis rate	μ_{Nano}^{max}	d^{-1}	3.0
18	Diatom maximum photosynthesis rate	μ_{Dia}^{max}	d^{-1}	3.5
19	Redfield ratio of carbon and nitrogen	$q_{Redfield}^{C:N}$	$molC(molN)^{-1}$	6.625
20	Nanophytoplankton iron to nitrogen ratio	$q_{Nano}^{Fe:N}$	$molFe(molN)^{-1}$	0.033
21	Diatom iron to nitrogen ratio	$q_{Dia}^{Fe:N}$	$molFe(molN)^{-1}$	0.033
22	Calcite production ratio	Ψ	dimensionless	0.01
23	Nanophytoplankton minimum cell quota of nitrogen	$q_{Nano}^{N:Cmin}$	$molN(molC)^{-1}$	0.04
24	Nanophytoplankton Maximum cell quota of nitrogen	$q_{Nano}^{N:Cmax}$	$molN(molC)^{-1}$	0.20
25	Diatom minimum cell quota of nitrogen (N:C)	$q_{Dia}^{N:Cmin}$	$molN(molC)^{-1}$	0.04
26	Diatom maximum cell quota of nitrogen (N:C)	$q_{Dia}^{N:Cmax}$	$molN(molC)^{-1}$	0.20
27	Diatom minimum cell quota of silica	$q_{Dia}^{Si:Cmin}$	$molSi(molC)^{-1}$	0.04
28	Diatom maximum cell quota of silica	$q_{Dia}^{Si:Cmax}$	$molSi(molC)^{-1}$	0.80
29	Nanophytoplankton maximum of chlorophyll to nitrogen ratio	$q_{Nano}^{CHL:Nmax}$	$mgCHL(mmolN)^{-1}$	3.78
30	Diatom maximum of chlorophyll to nitrogen ratio	$q_{Dia}^{CHL:Nmax}$	$gCHL(molN)^{-1}$	4.2
31	Diatom minimum silica to nitrogen ratio	$q_{Dia}^{Si:Nmin}$	$molSi(molN)^{-1}$	0.30
32	Nanophytoplankton maintenance respiration rate	η_{Nano}	d^{-1}	0.01
33	Diatom maintenance respiration rate	η_{Dia}	d^{-1}	0.01
34	Nanophytoplankton cost of nitrogen biosynthesis	ζ_{Nano}^{N}	$molC(molN)^{-1}$	2.33

35	Diatom cost of nitrogen biosynthesis	ζ_{Dia}^{N}	$molC(molN)^{-1}$	2.33
36	Diatom cost of silica biosynthesis	ζ_{Dia}^{Si}	$molSi(molN)^{-1}$	0.5
37	Nanophytoplankton chlorophyll degradation rate	d_{Nano}^{CHL}	d^{-1}	0.1
38	Diatom chlorophyll degradation rate	d_{Dia}^{CHL}	d^{-1}	0.1
39	Nanophytoplankton excretion rate of carbon	ϵ_{Nano}^{C}	d^{-1}	0.05
40	Diatom excretion rate of carbon	ϵ_{Dia}^{C}	d^{-1}	0.05
41	Nanophytoplankton excretion rate of nitrogen	ϵ_{Nano}^{N}	d^{-1}	0.05
42	Diatom excretion rate of nitrogen	ϵ_{Dia}^{N}	d^{-1}	0.05
43	Maximum grazing rate by zooplankton	ξ	$mmolNm^{-3}d^{-1}$	2.4
44	Grazing efficiency of zooplankton	γ	dimensionless	0.4
45	Half-saturation constant for grazing	ϕ	$(mmolNm^{-3})^2$	0.35
46	Phytoplankton specific aggregation rate	φ_{Phy}	$(mmolNm^{-3})^{-1}$	0.015
47	Detritus specific aggregation rate	φ_{Det}	$(mmolNm^{-3})^{-1}$	0.165
48	Time-scale for restoring towards Redfield	K_{het}	d^{-1}	0.01
49	Quadratic mortality rate of zooplankton	m_{het}	$(mmolNm^{-3})^{-1}$	0.05
50	Zooplankton carbon excretion rate	ϵ_{Het}^{C}	d^{-1}	0.15
51	Zooplankton nitrogen excretion rate	ϵ_{Het}^{N}	d^{-1}	0.15
52	PON degradation rate of detritus	ρPON	d^{-1}	0.165
53	POC degradation rate of detritus	ρPOC	d^{-1}	0.15
54	Maximum silicate dissolution rate	ρSi	d^{-1}	0.02

55	Detritus sinking velocity	V_{Det}^{Sink}	d^{-1}	20.0
56	Stickiness for polysaccharides to polysaccharides	φ_{PCHO}	$(mmolCm^{-3})^{-1}$	0.0075
57	Stickiness for TEP to polysaccharides	φ_{TEP}	$(mgm^{-3})^{-1}$	-1.240
58	Total ligand concentration of iron	L_T	$\mu molm^{-3}$	1.0
59	Ligand stability constant of iron	K_FeL	$m^3\mu mol^{-1}$	200
60	Dissolved organic nitrogen remineralization rate	ρDON	d^{-1}	0.11
61	Dissolved organic carbon remineralization rate	ρDOC	d^{-1}	0.10
62	Extracellular organic carbon remineralization rate	ρEOC	d^{-1}	0.10
63	Benthos iron to nitrogen ration	$q_{Nano}^{Fe:N}$	$molFe(molN)^{-1}$	0.33
64	Particulate organic carbon degradation rate in sediment	d^C	d^{-1}	0.005
65	Particulate organic nitrogen degradation rate in sediment	d^N	d^{-1}	0.005
66	Silicate degradation rate in sediment	d^Si	d^{-1}	0.005
67	Calcium carbonate degradation rate in sediment	d^{CaCO_3}	d^{-1}	0.005
68	Linear slope of Arrhenius function	Ae	Kelvin	4500

A.3 Figures of first-order Sobol' indices

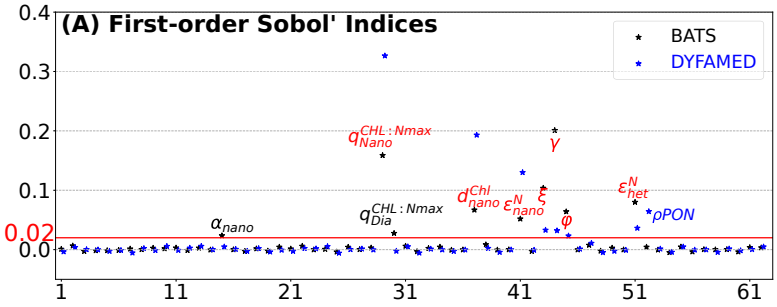

Figure A.1 First-order Sobol' indices regarding mean surface total chlorophyll-a (surf_totchl) for all 63 parameters. For parameters which the first-order Sobol' indices are greater than the threshold value at both stations are written in red, at only BATS in black, and at only DYFAMED in blue. For a description of the parameters, see Appendix A. The x-axis labels are the serial no. of parameters in Appendix A.2.

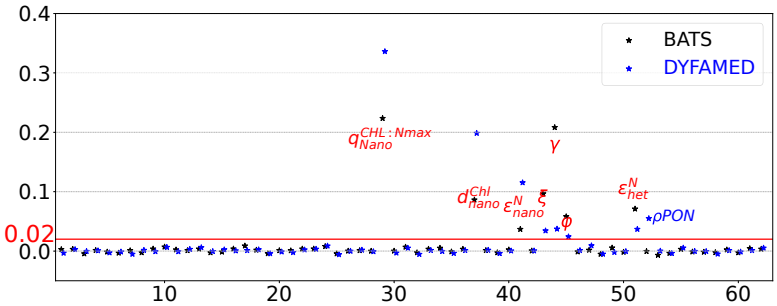

Figure A.2 First-order Sobol' indices regarding mean surface nanophytoplankton chlorophyll-a (SURF_NANOCHL) for all 63 parameters. The legends and text color are analogous to Figure A.1.

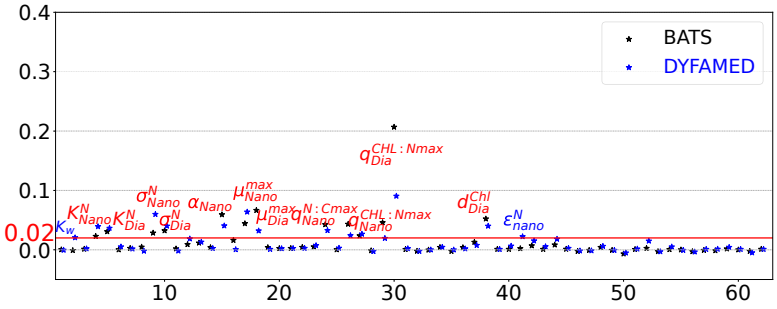

Figure A.3 First-order Sobol' indices regarding mean surface diatom chlorophyll-a (SURF_DIACHL) for all 63 parameters. The legends and text color are analogous to Figure A.1.

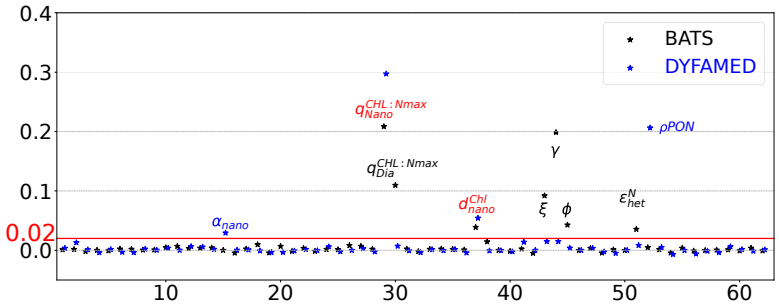

Figure A.4 First-order Sobol' indices regarding annual peak surface total chlorophyll-a (MBP_TOTCHL) for all 63 parameters. The legends and text color are analogous to Figure A.1.

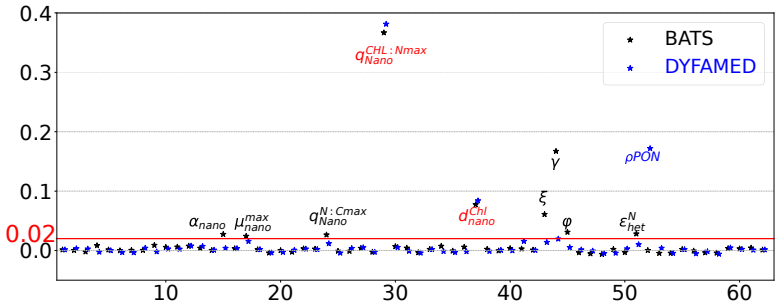

Figure A.5 First-order Sobol' indices regarding annual peak surface nanophytoplankton chlorophyll-a (MBP_NANOCHL) for all 63 parameters. The legends and text color are analogous to Figure A.1.

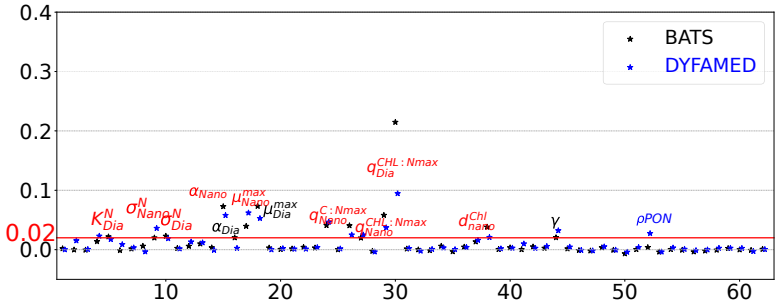

Figure A.6 First-order Sobol' indices regarding annual peak surface diatom chlorophyll-a (MBP_DIACHL) for all 63 parameters. The legends and text color are analogous to Figure A.1.

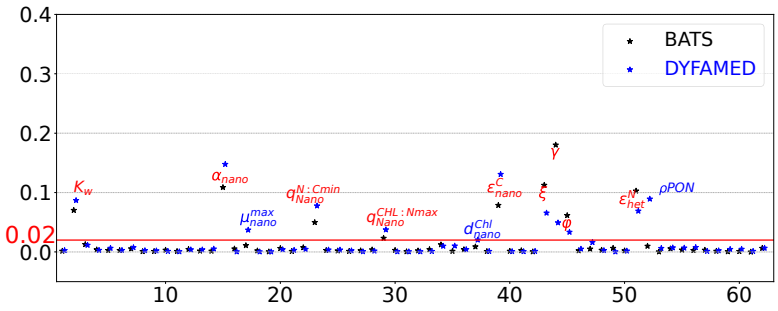

Figure A.7 First-order Sobol' indices regarding mean net primary production (TOTNPP) for all 63 parameters. The legends and text color are analogous to Figure A.1.

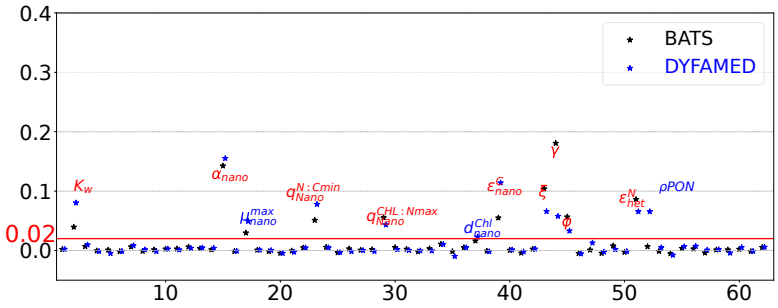

Figure A.8 First-order Sobol' indices regarding mean nanophytoplankton NPP (NANONPP) for all 63 parameters. The legends and text color are analogous to Figure A.1.

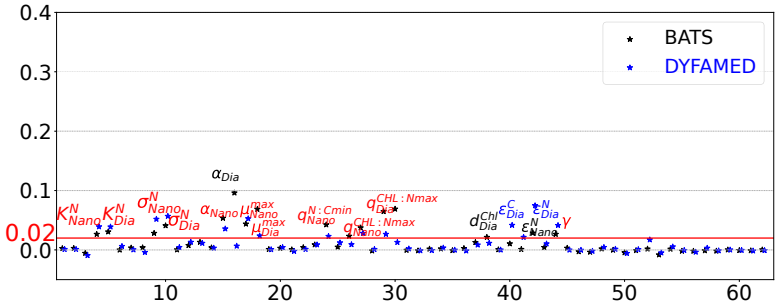

Figure A.9 First-order Sobol' indices regarding the mean diatom NPP (DIANPP) for all 63 parameters. The legends and text color are analogous to Figure A.1.

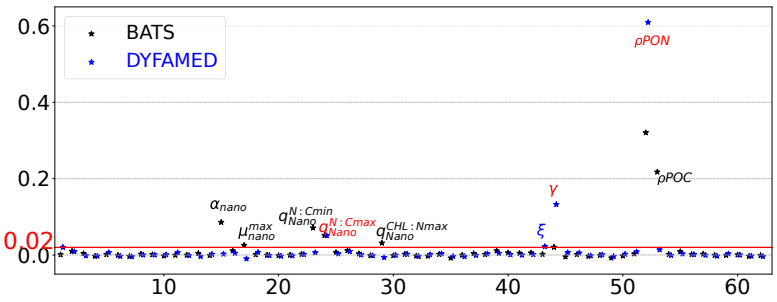

Figure A.10 First-order Sobol' indices regarding the mean export production of carbon (EXPORTP) for all 63 parameters. The legends and text color are analogous to Figure A.1.

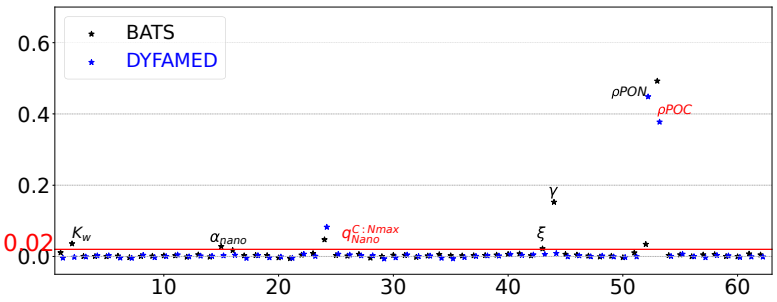

Figure A.11 First-order Sobol' indices regarding the mean surface flux of CO_2 (CO_2FLUX) for all 63 parameters. The legends and text color are analogous to Figure A.1.

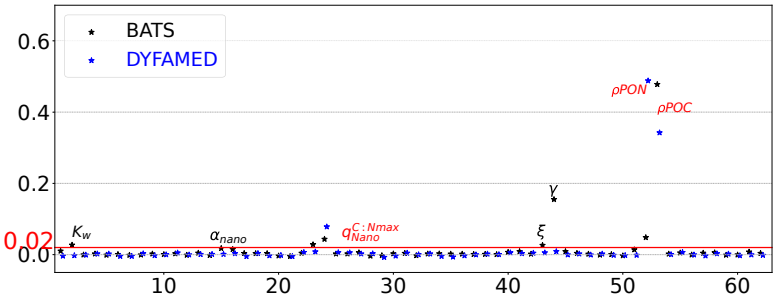

Figure A.12 First-order Sobol' indices regarding the mean partial pressure of CO_2 (pCO_2) for all 63 parameters. The legends and text color are analogous to Figure A.1.

A.4 Figures of ensemble evaluation of parameter estimates

A.4.1 Satellite chlorophyll-a only assimilation

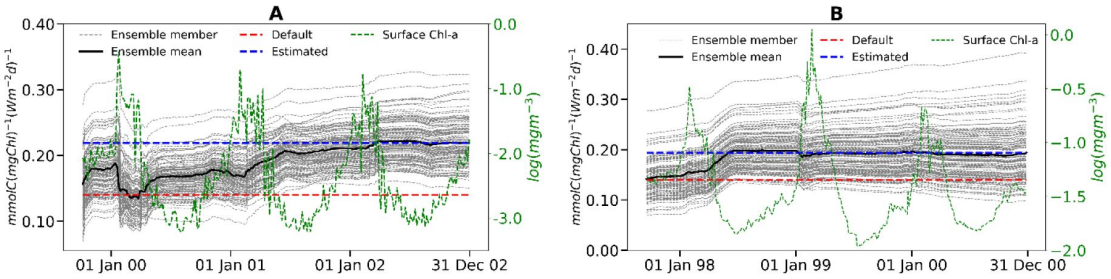

Figure A.13 Evaluation of nanoplankton initial slope of the P-I curve (α_{Nano}) at A) BATS and B) DYFAMED for satellite chlorophyll-a only assimilation. Gray dashed lines represent ensemble members and the black solid line shows associated ensemble means. The default and estimated values are shown as dashed lines (red for default and blue for estimated). The green dashed line is the surface chlorophyll-a concentration from the assimilation run with the y-axis value on the right-hand side.

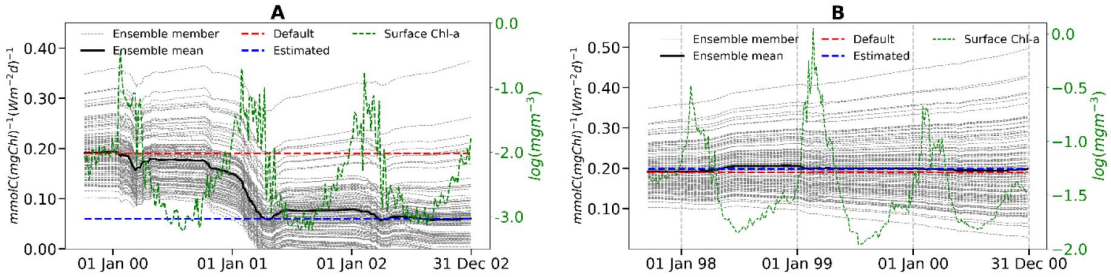

Figure A.14 Evaluation of diatoms initial slope of the P-I curve (α_{Dia}) at A) BATS and B) DYFAMED analogous to Figure A.13.

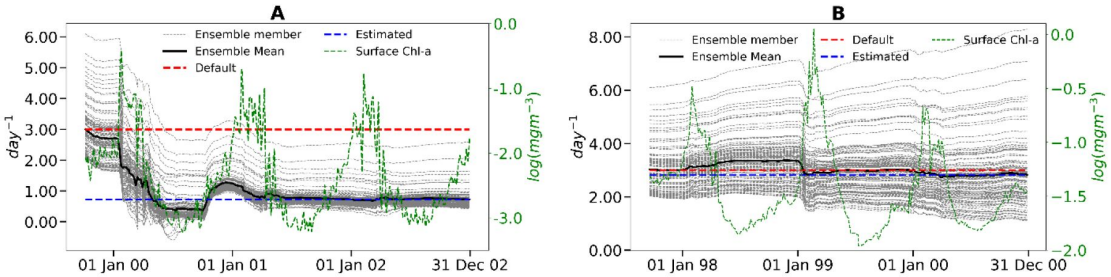

Figure A.15 Evaluation of nanoplankton maximum photosynthesis rate (μ^{max}_{Nano}) at A) BATS and B) DYFAMED analogous to Figure A.13.

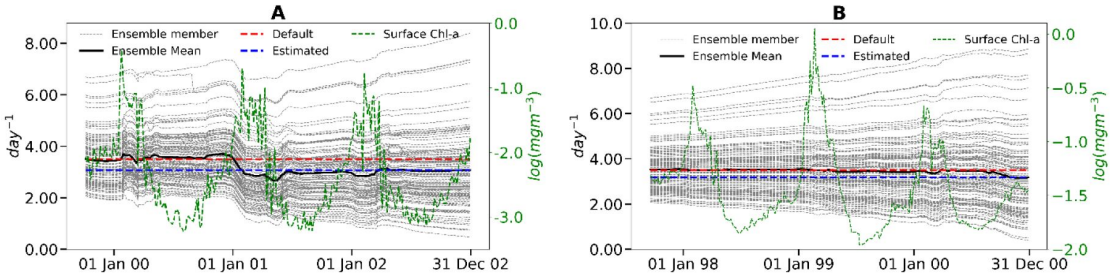

Figure A.16 Evaluation of diatoms maximum photosynthesis rate (μ_{Dia}^{max}) at A) BATS and B) DYFAMED analogous to Figure A.13.

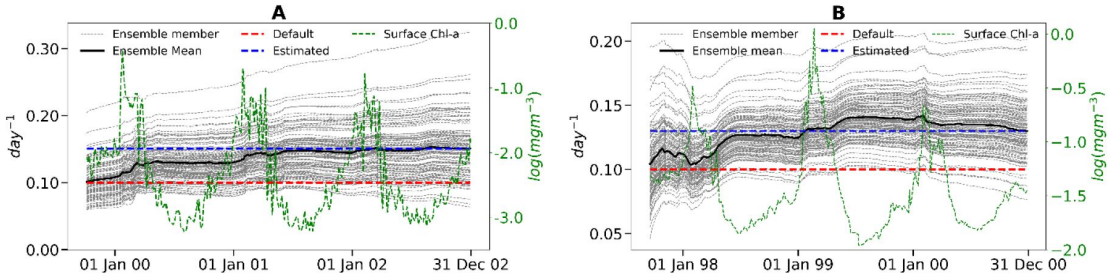

Figure A.17 Evaluation of nanoplankton chlorophyll degradation rate (d_{Nano}^{CHL}) at A) BATS and B) DYFAMED analogous to Figure A.13.

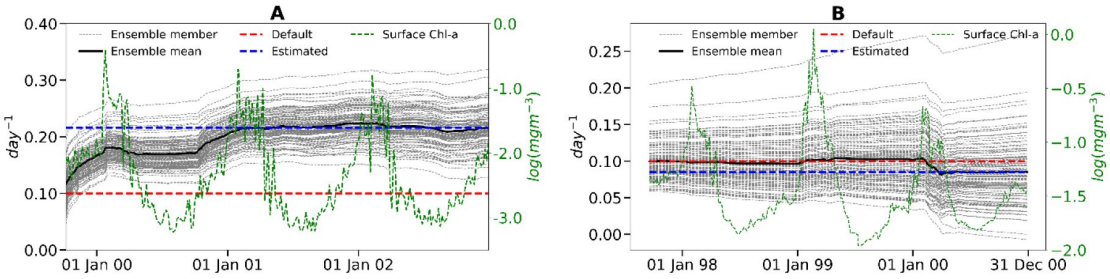

Figure A.18 Evaluation of diatoms chlorophyll degradation rate (d_{Dia}^{CHL}) at A) BATS and B) DYFAMED analogous to Figure A.13.

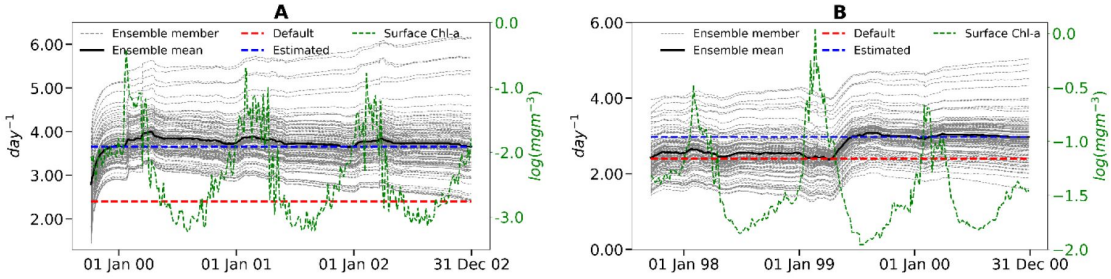

Figure A.19 Evaluation of maximum grazing rate (ξ) at A) BATS and B) DYFAMED analogous to Figure A.13.

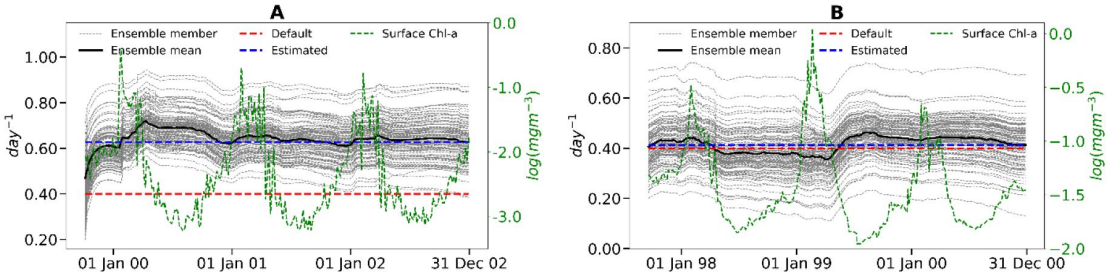

Figure A.20 Evaluation of grazing efficiency (γ) at A) BATS and B) DYFAMED analogous to Figure A.13.

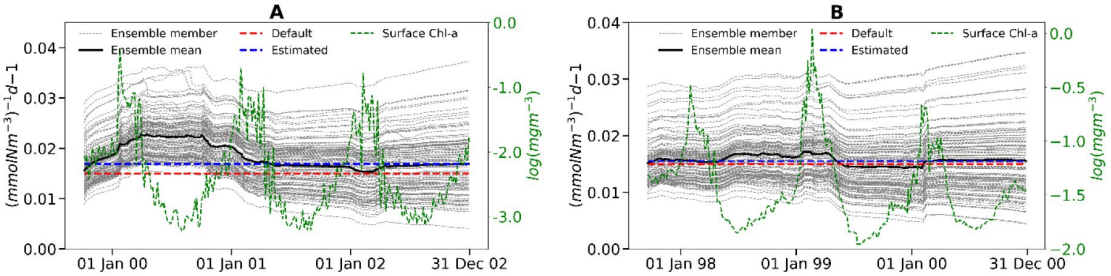

Figure A.21 Evaluation of phytoplankton specific aggregation rate (Φ_{Phy}) at A) BATS and B) DYFAMED analogous to Figure A.13.

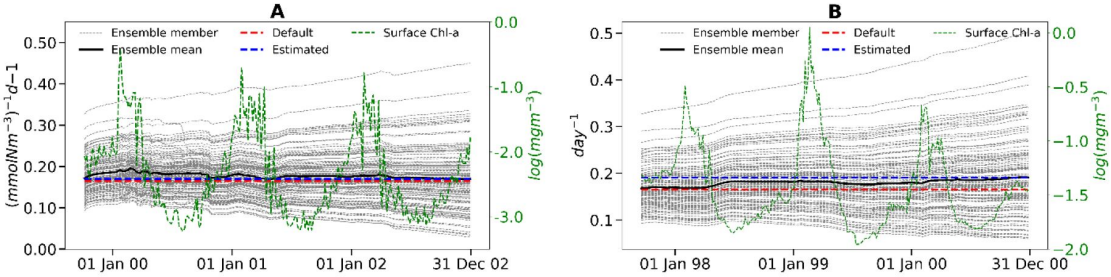

Figure A.22 Evaluation of detritus specific aggregation rate (Φ_{Det}) at A) BATS and B) DYFAMED analogous to Figure A.13.

A.4.2 Simultaneous assimilation of satellite chlorophyll-a and in-situ NPP

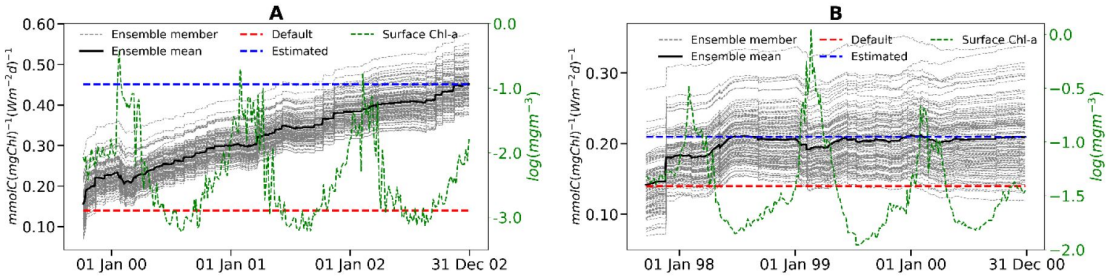

Figure A.23 Evaluation of nanoplankton initial slope of the P-I curve (α_{Nano}) at A) BATS and B) DYFAMED simultaneous assimilation of satellite chlorophyll-a and in-situ NPP. Gray dashed lines represent ensemble members and the black solid line shows associated ensemble means. The default and estimated values are shown as dashed lines (red for default and blue for estimated). The green dashed line is the surface chlorophyll-a concentration from the assimilation run with the y-axis value on the right-hand side.

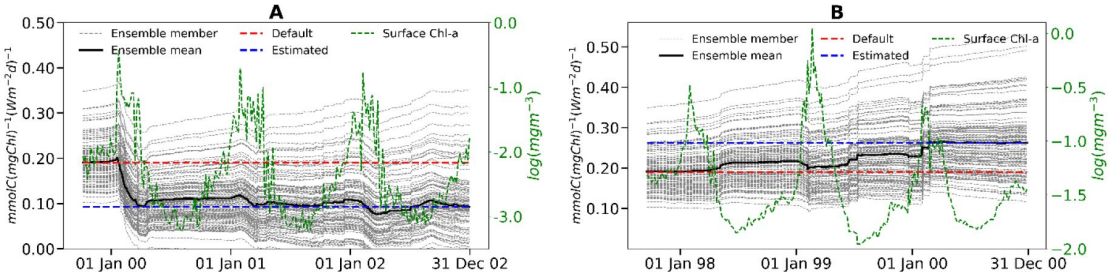

Figure A.24 Evaluation of diatoms initial slope of the P-I curve (α_{Dia}) at A) BATS and B) DYFAMED analogous to Figure A.23.

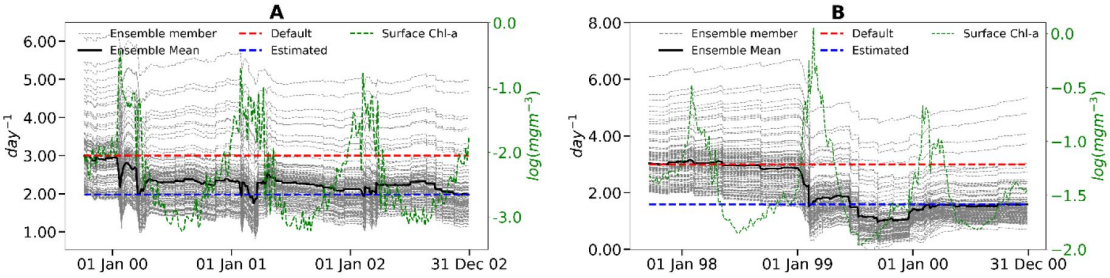

Figure A.25 Evaluation of nanoplankton maximum photosynthesis rate (μ^{max}_{Nano}) at A) BATS and B) DYFAMED analogous to Figure A.23.

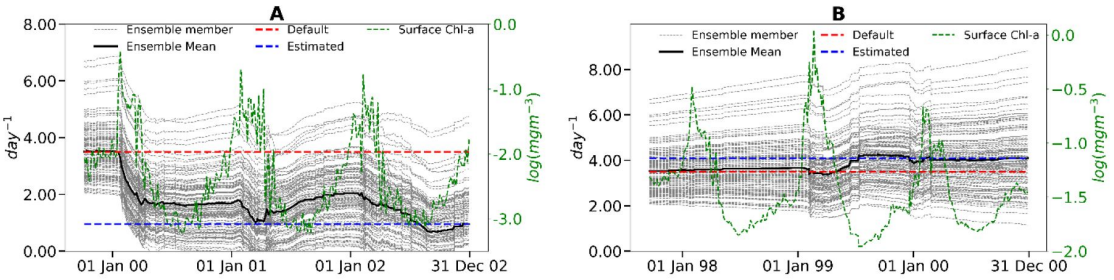

Figure A.26 Evaluation of diatoms maximum photosynthesis rate (μ_{Dia}^{max}) at A) BATS and B) DYFAMED analogous to Figure A.23.

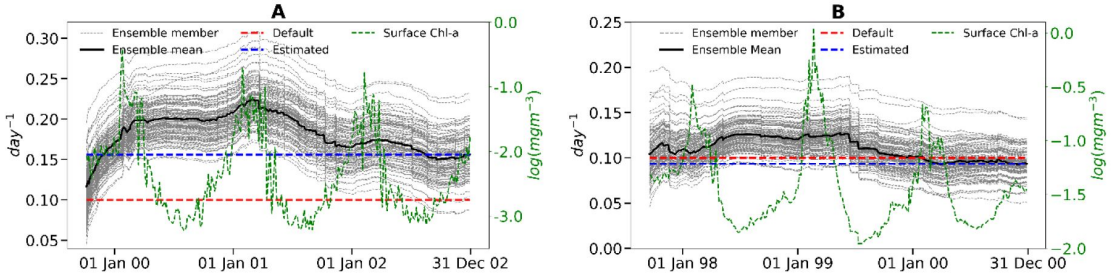

Figure A.27 Evaluation of nanoplankton chlorophyll degradation rate (d_{Nano}^{CHL}) at A) BATS and B) DYFAMED analogous to Figure A.23.

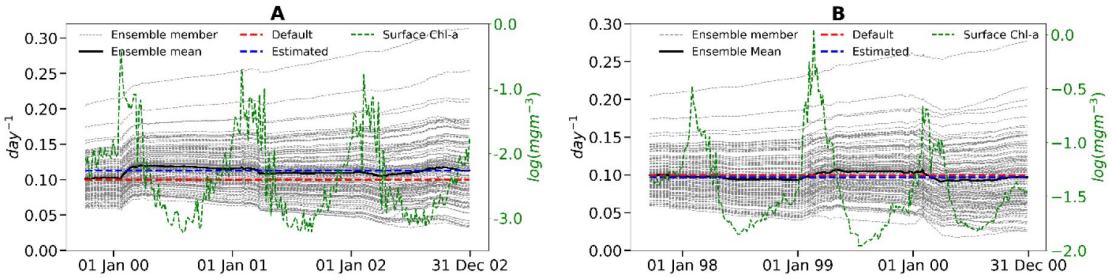

Figure A.28 Evaluation of diatoms chlorophyll degradation rate (d_{Dia}^{CHL}) at A) BATS and B) DYFAMED analogous to Figure A.23.

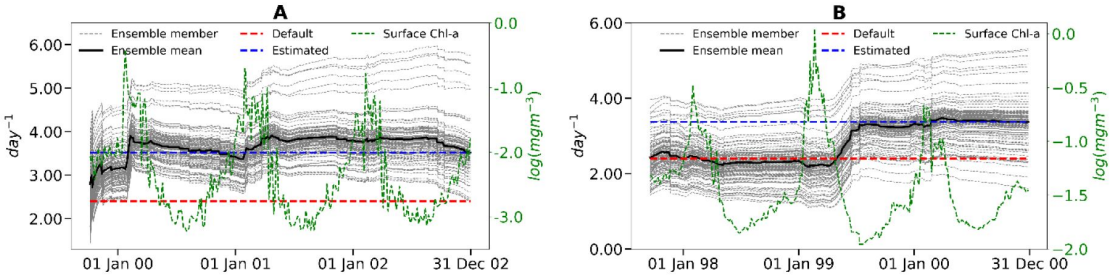

Figure A.29 Evaluation of maximum grazing rate (ξ) at A) BATS and B) DYFAMED analogous to Figure A.23.

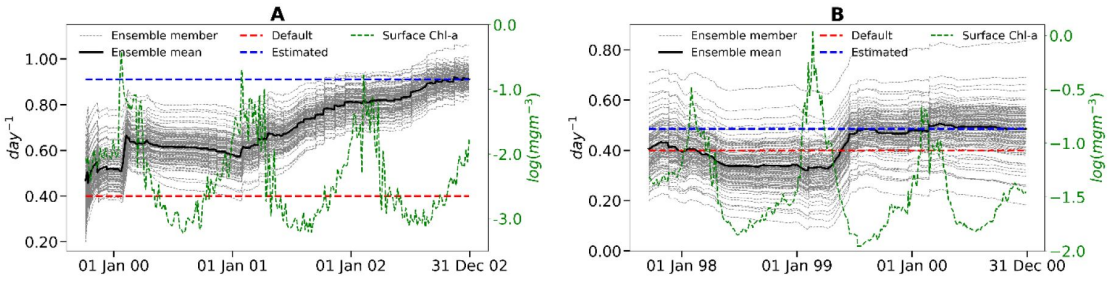

Figure A.30 Evaluation of grazing efficiency (γ) at A) BATS and B) DYFAMED analogous to Figure A.23.

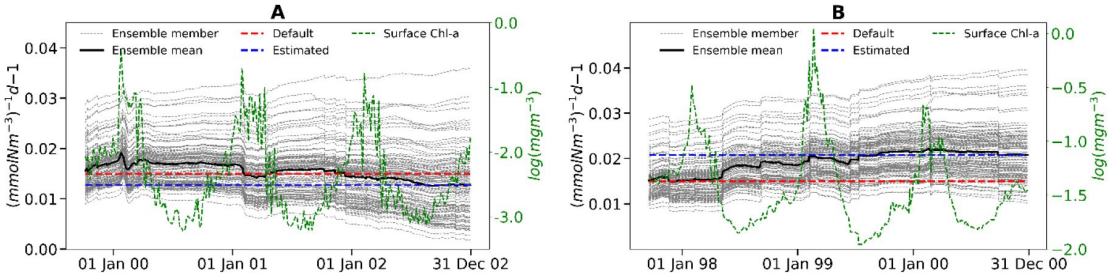

Figure A.31 Evaluation of phytoplankton specific aggregation rate (Φ_{Phy}) at A) BATS and B) DYFAMED analogous to Figure A.23.

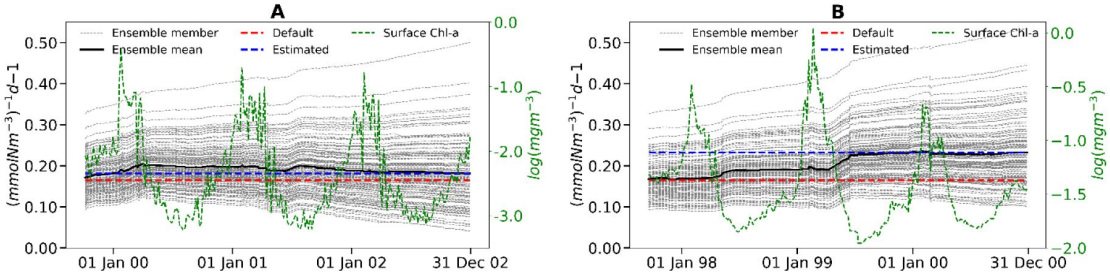

Figure A.32 Evaluation of detritus specific aggregation rate (Φ_{Det}) at A) BATS and B) DYFAMED analogous to Figure A.23.